THE KAROO SUPERGROUP (TRIASSIC-JURASSIC), SEYCHELLES : SEDIMENTOLOGY, PROVENANCE AND DIAGENESIS OF A TERRESTRIAL SUCCESSION AND COMPARISONS WITH MARGINAL SEDIMENTS FROM ELK POINT GROUP (DEVONIAN), ALBERTA, CANADA

Mohit Khanna

A Thesis Submitted for the Degree of PhD
at the
University of St Andrews

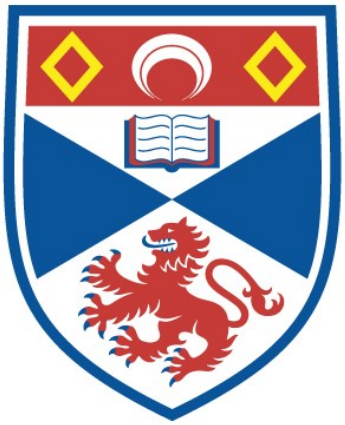

1992

THE KAROO SUPERGROUP (TRIASSIC-JURASSIC), SEYCHELLES

Sedimentology, Provenance & Diagenesis of a Terrestrial Succession and comparisons with Marginal Sediments from Elk Point Group (Devonian), Alberta, Canada

by

Mohit Khanna,
B.Sc(Hons), M.Sc(spl)

A thesis submitted for the award of
Doctor of Philosophy

University of St Andrews
September 1991

ProQuest LLC.
789 East Eisenhower Parkway
P.O. Box 1346
Ann Arbor, MI 48106 – 1346

DECLARATION FOR THE DEGREE OF Ph.D.

I *Mohit Khanna* hereby certify that this thesis has been composed by myself, that it is a record of my own work, and that it has not been accepted in partial or complete fulfillment of any other degree of professional qualification.

Signed. Dated 30/9/91

I *Mohit Khanna* was admitted to the faculty of Science of the University of St Andrews under Ordinance General No 12 on Jan 28, 1988 and as a candidate for the degree of Ph.D. on 29 Sept. 1988

Signed Dated 30/9/91

I hereby certify that *Mohit Khanna* has fulfilled the conditions of the Resolution and Regulations appropriate to the Degree of Ph.D.

Signature of Supervisor Dated 30/9/91

THESIS COPYRIGHT DECLARATION

A. UNRESTRICTED:

In submitting this thesis to the University of St Andrews I understand that I am giving permission for it to be made available for use in accordance with the regulations of the University Library for the time being in force, subject to any copyright vested in the work not being affected thereby. I also understand that the title and abstract will be published, and that a copy of work may be made and supplied to any bona fide library or research worker.

B. RESTRICTED:

In submitting this thesis to the University of St Andrews I wish access to it to be subject to the following conditions:

for a period of 0 years (maximum 5) from the date of submission, the thesis shall be

(a) with held for use

(b) ~~made available for use only with consent of the head or chairman of the department in which the work was carried out.~~

(Delete one clause)

I understand, however, that the title and abstract of the thesis will be published during this period of restricted access; and that after the expiry of this period the thesis will be made available for use in accordance with the regulations of the University Library for the time being in force, subject to any copyright in the work not being affected thereby, and a copy of the work may be made and supplied to any bona fide library or research worker.

Declaration:

I wish to exercise option *Ba* of the above options.

Signed..

Dated..30/9/91

ABSTRACT

THE KAROO SUPERGROUP (TRIASSIC-JURASSIC), SEYCHELLES: Sedimentology, Provenance & Diagenesis of a Terrestrial Succession and comparisons with Marginal Sediments from Elk Point Group (Devonian), Alberta, Canada

Mohit Khanna
University of St Andrews

The offshore Karoo Supergroup (+2 km thick) of the Seychelles has been divided into five members based mainly on sandstone/mudstone development as revealed by wireline logs and lithological samples. The four lower members are characterized by thick sandstones with minor mudstones and the lowest member distinguished by the presence of occasional bands of lignite; the topmost member has thick mudstones as well as thick sandstones. Members 2 and 3, and 4 and 5 form two upward-fining megacycles in which members 2 and 4 have coarser-grained pebbly, sandstones while the sandstones of 3 and 5 are medium and fine-grained. The sediments are fluvial in origin, possibly *braid plain* except for the uppermost member which may have formed under a *meandering system*.

Paleogeographic reconstruction invokes a source area in north-east Madagascar shedding debris eastwards towards the Seychelles which at that time (pre-mid-Jurassic) lay between Madagascar to the west, and India to the east. Burial curves are presented from considerations of sediment thickness and texture, structure, including the positions of unconformities and diagenesis as an aid in assessing oil potential. With possible source rocks in overlying marine sediments, hydrocarbon generation may have occurred in late Mesozoic and early Tertiary. Migration could possibly have taken place into fault-juxtaposed Karoo sandstones.

For comparative purposes petrographic features of samples from the Elk Point Group Alberta, Canada were studied. This Devonian sequence comprises marginal and marine sediments including carbonates and evaporites, but the sandstones studied come from marginal deltaic deposits.

Sandstones studied are remarkably similar in both original composition and diagenetic history. Primary mineralogy was determined by similar source areas - predominantly granitic with minor metamorphic and volcanic components. Despite being

deposited in different sedimentary environments both groups show extensive diagenesis involving dissolution of feldspars and lithoclasts, precipitation of quartz, and a second phase of dissolution of feldspar, lithoclasts and quartz. Kaolinite is the dominating clay in the sandstones of Karoo Supergroup up to depths of 10,000 ft, while illite prevails over other clays in the sequence between 10,000-12,500 ft. Illite and chlorite are present in the Elk Point Group; kaolinite is absent. The last stage of cementation in Elk Point sandstones was anhydrite precipitation during Cretaceous times. Precipitation of authigenic cements ended with the formation of carbonates in Karoo sandstones. Cementation, especially by quartz appears to have considerably reduced porosity in many places in both the successions. In both the study areas early diagenesis was controlled by meteoric waters while burial and marine influence are responsible for later diagenetic episodes.

The presence of illite and chlorite against kaolinite in the Elk Point Group is due to greater depths of burial than Karoo sandstones. Presence of evaporitic environments lead to the formation of anhydrite in the sandstones of Elk Point Group, while feldspar overgrowths are formed as a result of retention of pore-fluids due to the formation of a closed system controlled by marine flooding surfaces.

ACKNOWLEDGEMENTS

This project could not have been carried out and completed without the assistance and co-operation of numerous people, to whom I am greatly indebted.

I would particularly like to thank Professor Ken Walton, as my supervisor of studies, for his stimulating supervision, encouragement and support during this work and critical review of the manuscript. His experience, guidance and insight were nothing short of outstanding.

A special word of thanks are extended to Dr John McManus for his sincere advice and helpful discussions.

To Mr Guy Morel, Chairman and Mr. Surya N. Khanna, Managing Director, Seychelles National Oil Company and Dr Monzer Shawa of Shawa Geoconsultants, Calgary, I am more deeply indebted than can be adequately expressed, for supplying me with subsurface samples and other material during the course of my study.

This thesis was produced at University of St Andrews, where I am indebted to a great many individuals in the Department of Geography & Geology and in particular in the Division of Geology. Financial support provided by the Committee of Vice-Chancellors and Principals of the Universities in U.K. in form of an Overseas Research Award, Research Fellowship from the university and a maintenance grant from Sir Ernest Cassel Memorial Trust is gratefully acknowledged. Thanks are also extended to Dr G W Whittington, Chairman of the Department, for his support in organization of some of the financial resources. Technical assistance is also gratefully acknowledged, and I am especially thankful to Jim Allen for his photographic skills, Mr C B Bremner of Reprographic services for scanning a lot of my diagrams, Donald Herd for Electron Micro-probe, Sandy Edwards and Irwin for SEM, Angus Calder for XRD and XRF analysis and Andy Mackie for thin section preparation and most of the day to day technical assistance. It is a pleasure to acknowledge the help of Mrs Jean Galloway and Stuart Harvey for administrative assistance. The project has without doubt benefited from the friendly and communicative attitude of majority of staff and students.

A great deal of invaluable co-operation was provided by the staff of SURRC, East Kilbride. Grateful thanks are extended to Tony Fallick, Adrian Boyace and Paul for invaluable help and discussions during the course of isotope analysis.

Constant motivation and enlightening discussions with Abhilasha have undoubtedly benefitted this work.

It is my pleasure to record sincere appreciation for my parents, brother and other family members for their constant encouragement throughout my studies. Invaluable were the discussions with my father and I thank my mother for her understanding and relentless support.

CONTENTS

LIST OF FIGURES

LIST OF TABLES

LIST OF PLATES

Karoo Supergroup

CHAPTER1: INTRODUCTION

(with 4 figures)

1.1 AIMS AND OBJECTIVES:

An ability to assess the relationships between varied types of evidence is demanded by the nature of work performed by many professionals in the petroleum and mining industry and those engaged in projects for government surveys, especially, if the area is a potential hydrocarbon reservoir. Such studies provide the basis for an improved evaluation of the economic potential of the regions.

Modern trends in stratigraphical studies require an understanding of many diverse geological specialities including sedimentology, geochemistry, sequence stratigraphy, the documentation of eustatic sea level changes and the impact of plate tectonics. Such enormous advances have contributed significantly to our understanding of depositional histories.

On a specific level the study of diagenesis in rocks has academic interest involving consideration of provenance, tectonic setting, depositional environment, rock fluid interactions, amongst other factors. It is also of fundamental importance to the petroleum industry in affecting location and exploitation of reservoirs.

A comprehensive multidisciplinary sedimentological study to establish the provenance and diagenetic history, stratigraphy and models of sedimentation of the largely unexplored Karoo Supergroup (Triassic-Jurassic) of Seychelles (Fig. 1.1) was the primary objective of this research project. However, during the course of the study a paleogeographic reconstruction of 'Karoo times' and a burial history locating diagenetic events in space and time were also developed.

Another objective of the project was to compare the diagenesis of the terrestrial Karoo succession with the marginal marine Elk Point Group (Devonian) of Alberta, Canada (Fig. 1.2) in order to see the similarities/contrasts in the diagenesis of sandstones from different depositional environments.

1.2 AREAS OF INVESTIGATION:

1.2.1 The Karoo Supergroup:

The stratigraphic succession of the western shelf of the Seychelles has been established on the basis of three wells drilled in 1980-81 and the structures of the area revealed by seismic investigations (Khanna & Pillay, 1988). The three wells are situated on the western shelf between 100 and 150 km west of the island of Mahe (Fig 1.1). Two of the three wells, Seagull Shoals-1 and Reith Bank-1 penetrated Karoo rocks (Fig 1.3). Like other Karoo sediments in

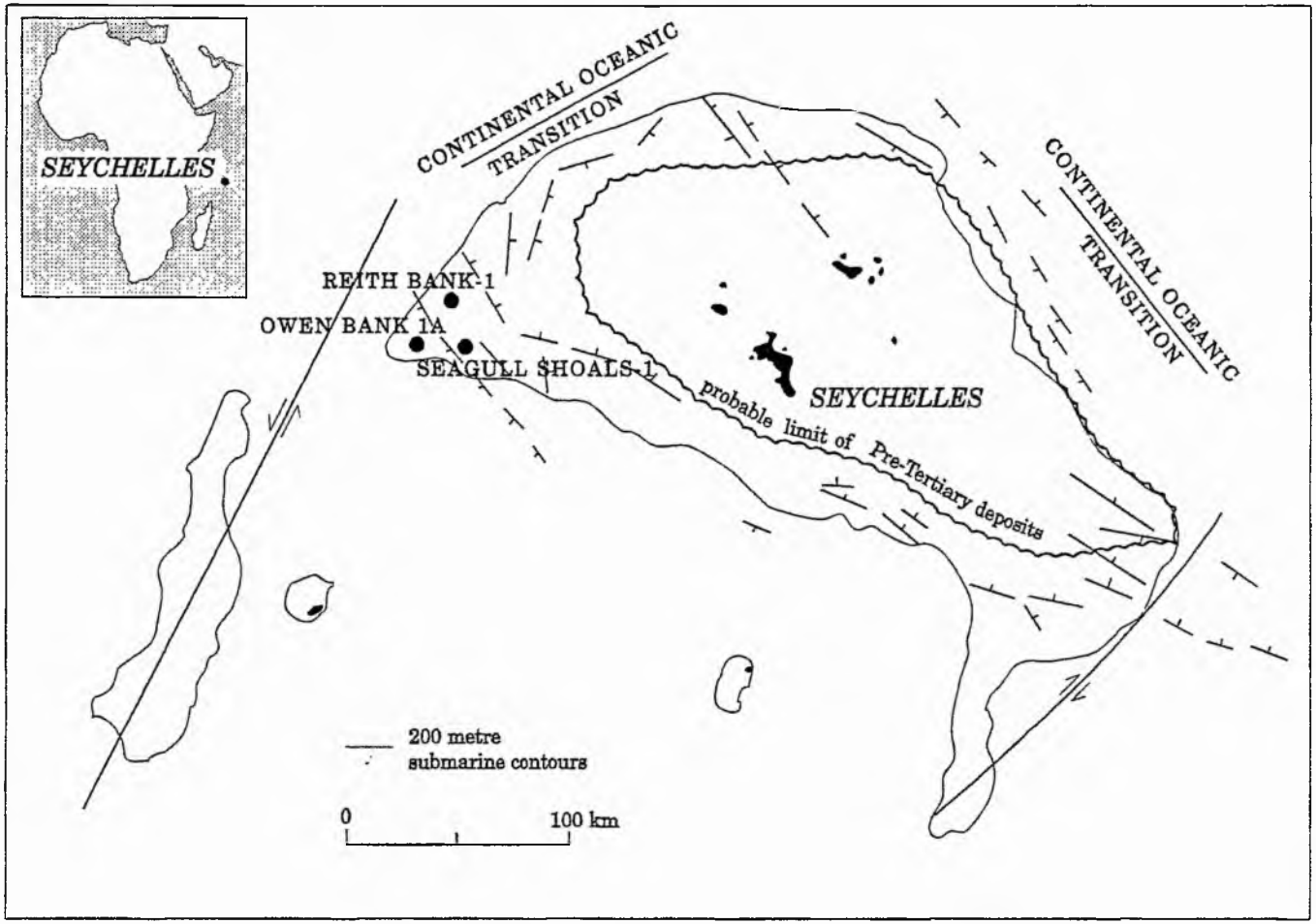

Fig. 1.1 Sketch map of the Seychelles area showing the location of three well, Seagull Shoals-1, Reith Bank-1 and Owen Bank-1A (based on Khanna & Pillay, 1986).

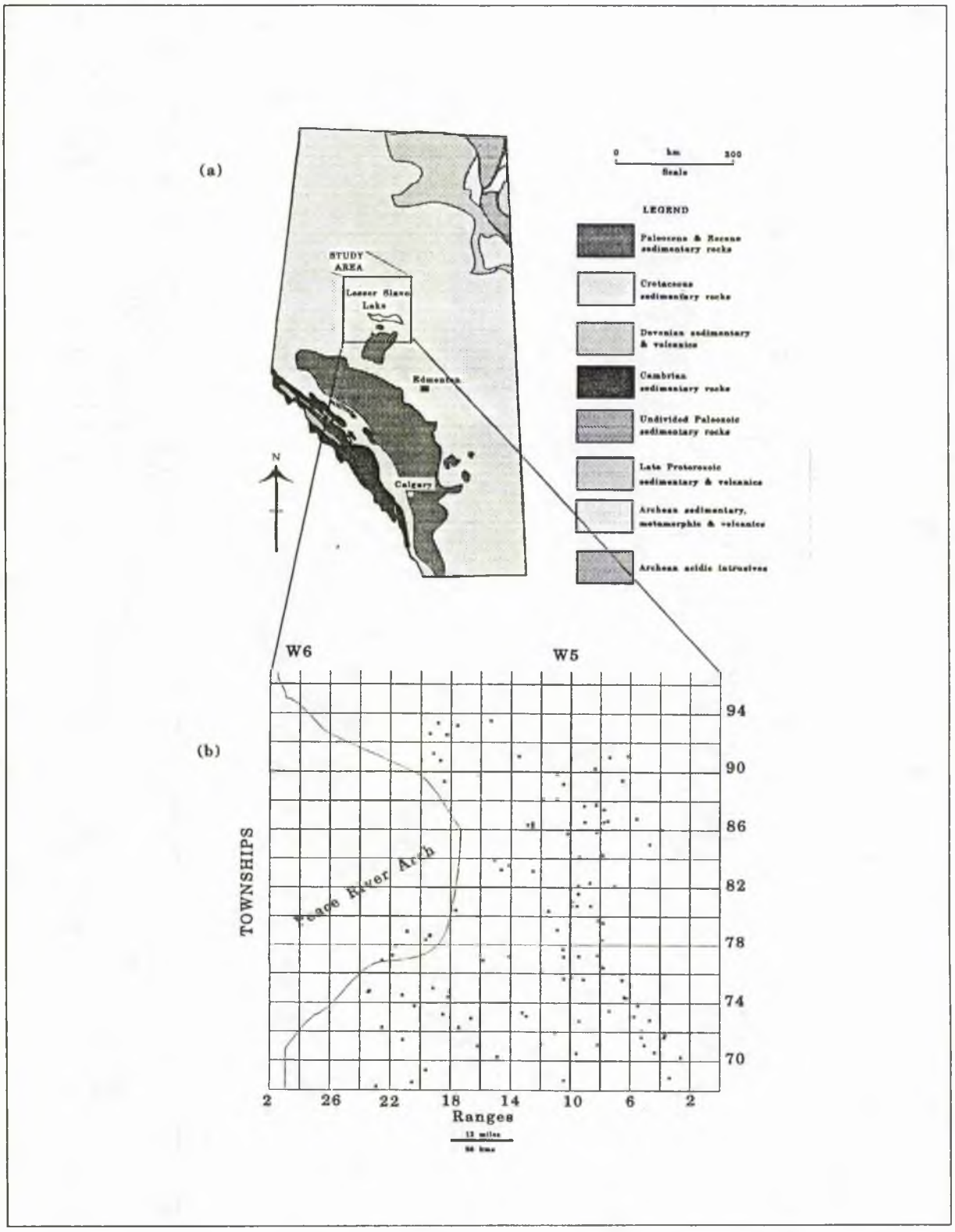

Fig. 1.2 Location map of Elk Point study area in Alberta, Canada. (a) Geological Map of Alberta with the study area marked by a box (Map redrawn from Grayston *et al.*, 1964). (b) Map showing distribution of wells from which samples were obtained on national grid system of Canada.

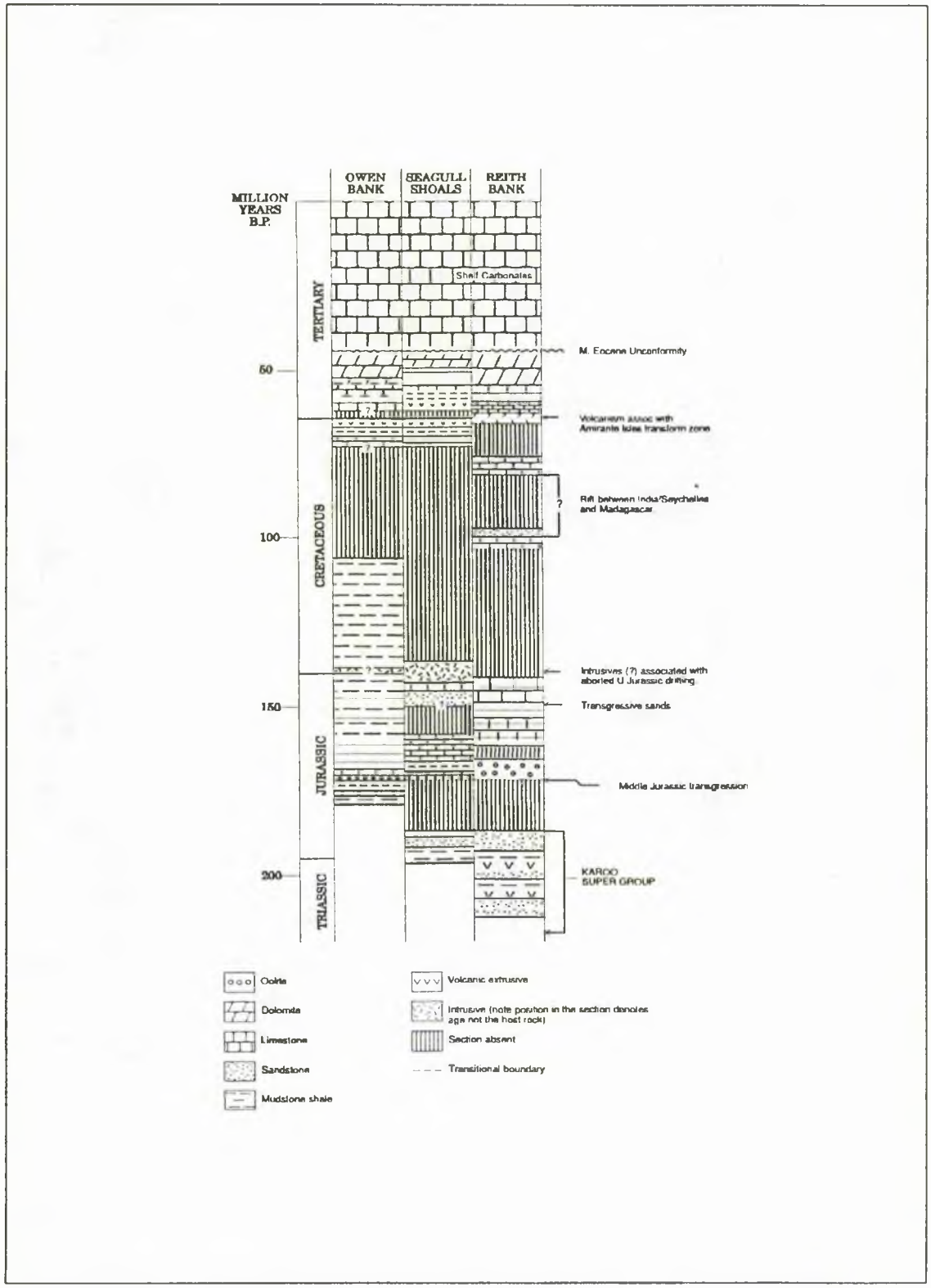

Fig. 1.3 Stratigraphic successions, Western Shelf, Seychelles (modified from Khanna & Pillay, 1986).

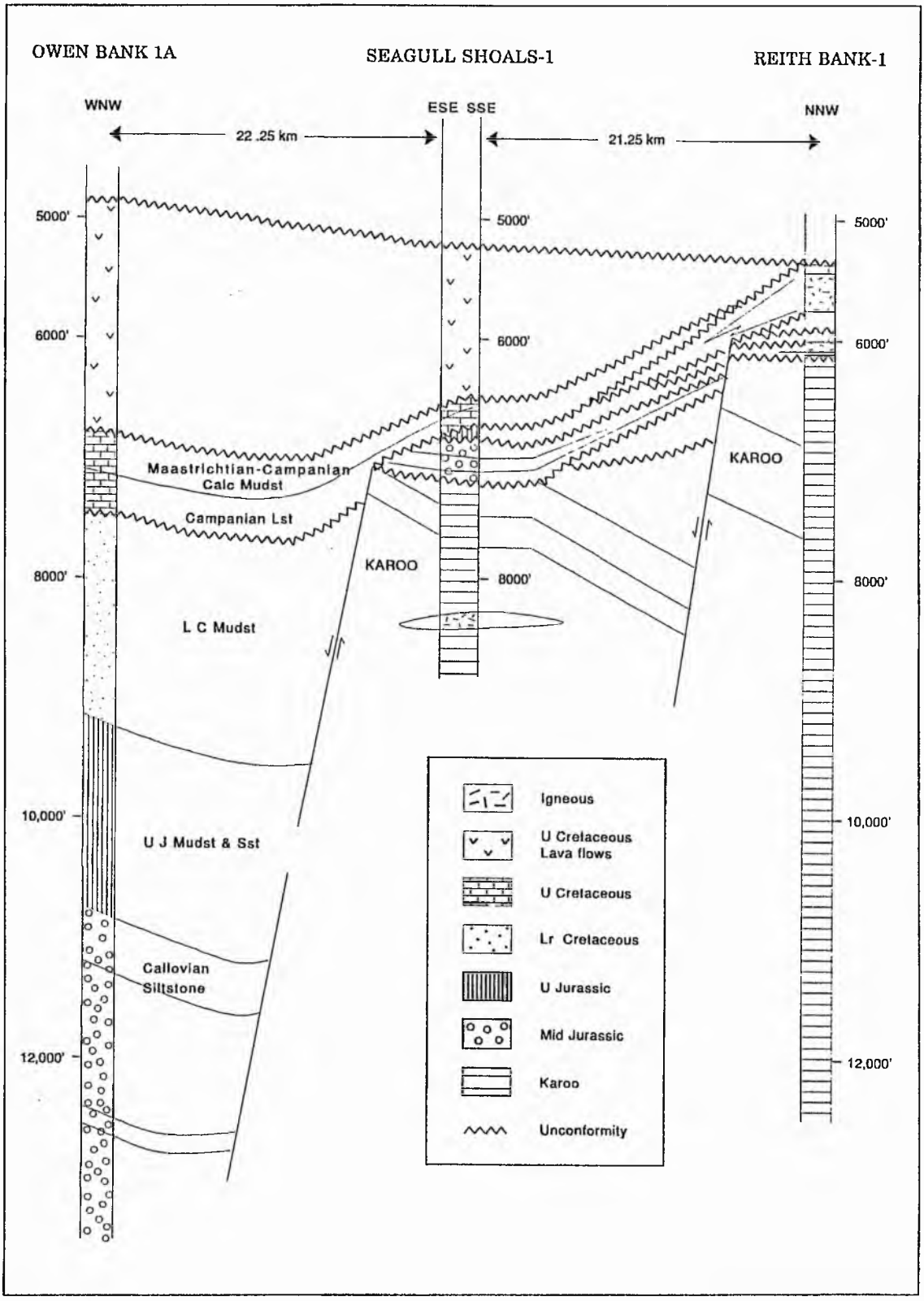

Fig. 1.4 Structural-stratigraphic correlation of the three Seychelles wells (modified from Nopec as., 1985).

Africa, those in the Seychelles were described as being mainly of fluvial-lacustrine origin. Over 6,000 ft of the Supergroup were revealed in Reith Bank but granitic basement was not reached. The third well, Owen Bank-1A recovered only younger rocks although traversing more than 14,000 ft. The sedimentary successions dip westwards and thicken in the same direction with an inner area (Fig 1.1) which remained uncovered by pre-Tertiary sediments. Subsidence, producing thicker sediments to the west, was punctuated by block faulting (Fig 1.4). Thus the down faulted Owen Bank-1A area has thick Jurassic and Cretaceous successions. Relative uplift of the Seagull Shoals-1 and Reith Bank-1 resulted in thinner sequences interrupted by unconformities.

1.2.2 The Elk Point Group:

The Elk Point Group of the study area is distributed over a wide, largely unexplored region. The area extends from Township 68 to Township 94 and from Range 2 west of the 5th Meridian to the Peace River Arch (a hilly source area during Elk Point times) and covers a surface area of approximately 20,000 sq kms (Fig. 1.2).

The Elk Point Group forms the basal unit of the Devonian System in western Canada and rests directly on the eroded Lower Paleozoic or Precambrian strata. It consists of a sequence of evaporite, carbonate and clastic rocks. The Elk Point Group is overlain by the carbonates and shales of the Upper Devonian formations.

In the study area, the group contains a cyclic sequence of sandstones and shales. The succession comprises four units with sandstones; basal Granite Wash lithology followed by Chinchaga, Keg River, Muskeg and Watt Mountain Formations in the upward succession.

The oil potential of the group is greater than any other reservoir in Western Canada (Shawa, 1987a, 1987b). The presence of excellent porosity trends coupled with the wide distribution of oil shown over the entire general area greatly enhance the oil potential of these sandstone reservoir units (Shawa, *op. cit.*).

1.3 DATA BASE:

1.3.1 Karoo Supergoup:

The Seychelles National Oil Company (SNOC) has provided material relating to the three wells drilled by AMOCO viz. Seagull Shoals-1, Owen Bank-1A and Reith Bank-1. Details of these materials are listed in Appendix 1.

As well as a variety of logs there are reports by Mineralogy Inc., Nopec a.s., Robertson Research International and Seychelles National Oil Company's geologists. The present study is

based on these reports for tectonics and lithological description of cores. Small cuttings of conventional and side wall cores were used for petrographic analyses. Thin sections produced by Robertson Research International were also made available.

1.3.2 Elk Point Group:

Shawa Geoconsultants of Calgary have provided small cuttings of conventional core samples and logs for the wells drilled in this area. Details are provided in Appendix 1.

1.4 TECHNIQUES:

The techniques which have been used are (Appendix 3);

1.4.1 Thin section microscopy:

Samples were chosen to prepare thin sections of sandstones, siltstones and shales. These were impregnated with blue-stained araldite to prevent disintegration and assess the porosity. The sections were also stained with Alizarin Red-S and Potassium Ferricyanide to allow recognition of carbonates.

1.4.2 Scanning electron microscopy:

Samples were mounted on stubs to be studied under the scanning electron microscope (SEM). This study was used to understand the texture and nature of clays and other components of the rock. Some EDX spectra were taken to help in identification of various components.

1.4.3 X-ray diffraction:

Samples were analysed by X-ray diffraction especially for the identification of clays.

1.4.4 Electron microprobe analysis:

Polished sections of sandstones have been prepared and used to analyse the composition and structure of cements and overgrowths on feldspars.

1.4.5 Cathodoluminescence Microscopy:

The sections used for Electron Microprobe studies were also used for luminescence studies.

1.4.6. Determination of fluid inclusions:

Samples with good inclusions were selected for study of fluid inclusions in quartz overgrowths and carbonate cements to determine composition and the temperature and salinity of the pore waters at the time of the formation of the cements.

1.4.7 Isotope analysis:

Isotope analysis was restricted to cements from sandstones of Elk point Group. Carbon and oxygen isotope analysis was carried out on carbonate cements, and sulphur isotopes were studied for anhydrite.

1.4.8 Assessment of logs:

Gamma ray, sonic, bulk density and computer-processed logs have been used to infer sequences of lithologies for the Karoo Supergroup. For the Elk Point Group gamma-ray, sonic and lithological logs have been used.

1.5 PRESENTATION OF DATA:

Results of the present investigations are presented in two separate sections. Section I deals with the sedimentology, petrology, diagenesis, burial history and paleogeography of the Karoo Supergroup while Section II discusses the petrology and diagenesis of the Elk Point Group, along with comparisons of diagenesis of the two successions.

SECTION I

CHAPTER 2: GENERAL GEOLOGY

(with 9 figures)

2.1. GEOLOGICAL LITERATURE:

Charles Darwin in 1842 was the first to work on the coral reefs of Seychelles. Velain (1879) published the petrographic descriptions of igneous rocks of Mahe and adjacent islands. Bauer (1898), Dupont (1907, 1916, 1928) and Fryer (1911) considered the rise of the reef islands to be due to the general lowering of sea-level in the late Miocene times. Gardiner (1906) envisaged an island connection between Africa and the Seychelles and Chargos and the Maldives archipelago via Madagascar. Baker (1963) has given a detailed geological account of Seychelles along with the geological maps, stratigraphy and economic geology based on the field work, while Francis *et al* (1966) attempted a correlation with East Africa, on the basis of seismic refraction work. Some aspects of the geology of Seychelles have been discussed by Anon (1908, 1911), Reed (1949), Frankel & Kent (1964), Baker & Miller (1963), Frankel (1969), and Meyer (1980). Khanna & Pillay (1986, 1987 & 1988) have summarised the geotectonic evolution of the Seychelles basin with emphasis on petroleum prospects. Walton & Khanna (1990) have proposed a sedimentation model for the Karoo, along with the paleogeographic reconstructions of Jurassic time. Khanna & Walton (1990) have discussed the petrological details, provenance and diagenetic history of Karoo sandstones.

2.2. REGIONAL GEOLOGICAL SETTING:

Seychelles had been an Indian Ocean analogue of the South Sea Islands and have long been a fascination for geologists and oceanographers for the study of drift and rifting. The granitic outcrops, however, pose some problems. The granites of Mahe and its adjoining islands (except Silhoutte and North Island, which are Paleocene) are about 600 Ma old and are usually found on major continental land masses. As such, the Seychelles Banks is often referred to as a "micro-continent". These granites, constitute a large portion of the basement of East Africa and Malagasy, and are intruded by dolerite dykes. Normal oceanic crust is represented between Seychelles and Africa and the exact distribution of granite and oceanic crust is not yet known (Khanna & Pillay, 1986).

In the present world wide plate kinematic pattern, the Seychelles lies within the Somali Plate, which is attached to the African Plate along the Mozambique Fracture Zone and the Rift Valley System on the main land (Fig. 2.1).

The northern limit of the Somali Plate is marked by the Shera Ridge and the Carlsberg Ridge which are separated by a lateral

displacement zone known as the Owen Fracture Zone. To the east and south the Somali Plate is bounded by two active spreading axes; the Mid Indian Ridge and the South West Indian Ridge.

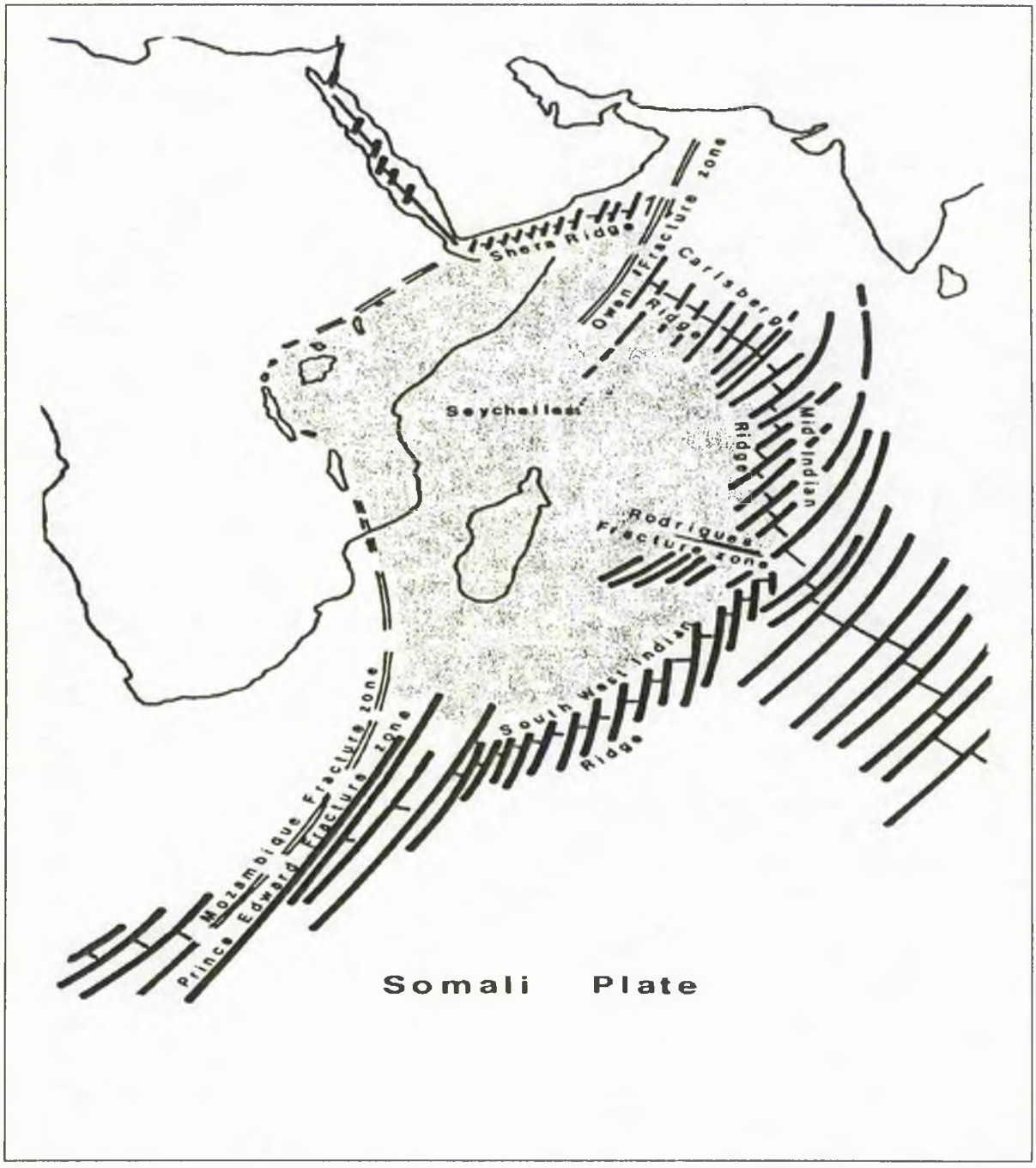

Fig. 2.1 The Somalia plate (stippled area marks the boundary of the plate) (modified after Nopec a.s., 1985).

The junction between these two ridges is located east of the Reunion and is transected by the east west trending Rodrigues Fracture Zone. (Fig. 2.1).

The break-up of Gondwana Land is the critical element in the analysis of the continental plate elements in and around the Indian Ocean. Royer (1990), using plate kinematic reconstructions based on the seafloor tectonic fabric and the crustal age has shown that the evolution of the Indian Ocean after the break-up of Gondwana in the Late Jurassic can be summarised in 3 main spreading phases. Prior to the three spreading phases a phase of continental extension started in Late Triassic-Early Jurassic (240-160 Ma).

Around 160 Ma (chron 25), the break-up of eastern (South America, Africa and Arabia) and western (Madagascar, Seychelles, India, Antarctica and Australia) Gondwana (Royer, 1990) was signalled by the extension of the extensive Karoo (Forster, 1975) and Ferrar basalts (Kyle *et al*, 1981) during the Early Triassic; however, the oldest oceanic crust in the Somali and Mozambique basins is Middle Jurassic in age (M25, 157 Ma; Seagoufin & Patriat, 1981). Rabinowitz *et al*, (1983) have deciphered magnetic anomalies of the western Somali Basin. Accordingly, the Africa-Madagascar separation began at the end of the Jurassic quiet zone (approximately 153 million years ago) and continued at least up to the anomaly M9 (approximately 121 million years ago). The Africa-Madagascar separation was thus initiated at about the same time as the breakup of Gondwana Land and the separation of North-America from Africa (Fig. 2.2). It appears that the Seychelles continental block formed part of Madagascar during the opening of the Somali Basin. Around 115 Ma seafloor spreading stopped in the Somali Basin (Royer, 1990).

The break-up between India and Madagascar was initiated around 95 Ma, opening up the Mascarene Basin with associated volcanism concentrated along transform faults (Fig. 2.2). In the Late Cretaceous-Early Tertiary the spreading centre in the Mascarene Basin jumped northward to a location between India and the Seychelles (A 28, 65 Ma; Schlich, 1982). As a result of this ridge jump, the Seychelles was transferred to the African plate and the proximity of the spreading axis to the margin of India may have triggered the eruption of the Deccan traps at about 65 Ma (chron 31) (Fig. 2.2) (Scotese *et al*, 1988; Royer, 1990).

During the Paleocene, India separated from the Seychelles and moved northward (Fig. 2.2). At this time the granites of Silhoutte and

North Island came into existence and since then the Seychelles microcontinent has been stable.

Seismic lines in Seychelles continuing into deep waters off the southern Main Shelf and Fortune Bank areas indicate that the pre-Tertiary

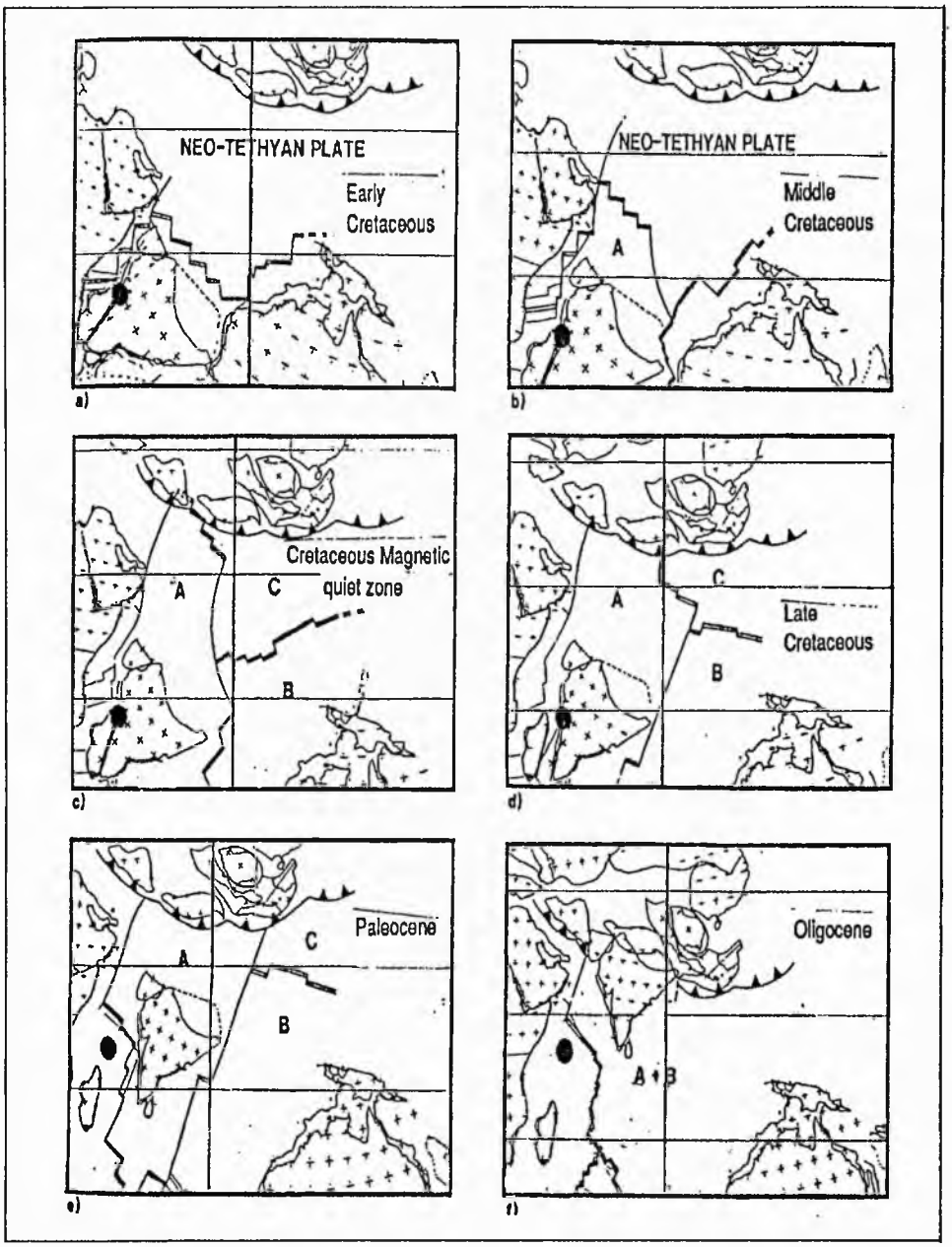

Fig. 2.2 Hypothetical plate boundaries in the Tethys during the Mesozoic and Cenozoic. Blackened circle represents position of Seychelles. a) Early Cretaceous (chron M17), b) Middle-Cretaceous (chron M0), c) Cretaceous magnetic quiet zone, d) Late Cretaceous (chron 34), e) Paleocene (chron 29), f) Oligocene (chron 15). (modified after Scotese et al, 1988).

sedimentary sequence continues to thicken south of the shelf edge. The southern extent of this deep sedimentary basin is not clearly known.

2.3. GEOLOGICAL EVOLUTION:

It is generally agreed (see Kent, 1974; Kamenkaye, 1978) that the earliest sediments in East Africa belong to the cycle of Karoo deposition (continental sediments like the Gondwana deposits, ranging in age from Permo-Carboniferous to Jurassic), occurring in basins from South Africa to Kenya and further across to Madagascar. These are regarded as the earliest sediments in the Seychelles Banks.

Further deposition in the Liassic (Lower Jurassic) initiated marine conditions with the deposition of marine shales. Karoo deposits are bounded by faults, contemporaneous with deposition (Kent, 1974). Thus, in general, the Seychelles basin was tectonically controlled by faulting which continued up to the early Jurassic. Subsequently, however, the basin underwent minor episodes of faulting or rejuvenation of the pre-existing faults, upheavals and alternate transgression and regressions. The basin appears to have remained stable with carbonate deposition in the shelf and formation of coralline islands during the Tertiary times that virtually gave rise to the Seychelles Archipelago as we see it today.

2.4. TECTONIC ELEMENTS OF SEYCHELLES:

The map (Fig 2.3, 2.4) is a composite model on the basis of the results proposed by aeromagnetic survey in 1983 and the seismic interpretation (unpublished reports of S.N.O.C.).

Several tectonic phases are evident:

2.4.1 <u>Pre-Jurassic, Karoo Faults</u>:

These faults are not easily identified as many faults have been reactivated during the Jurassic.

2.4.2 <u>Middle-late Jurassic rift margin</u>:

The rotated fault grabens of the western shelf are typical of continental margins and show strong similarities with the Viking Graben in the North Sea.

The fault trend is NW-SE with the Owen Bank-1A well on the graben side and the wells Reith Bank-1 and Seagull Shoals-1 on the graben flank (Fig. 1.1, 2.4).

The Jurassic rift margin is cut by Late Cretaceous transform faults off the shelf to the north-west where a transition to oceanic crust appears to occur (Fig. 2.4). To the south-east the faulted margins appear to continue in the deeper

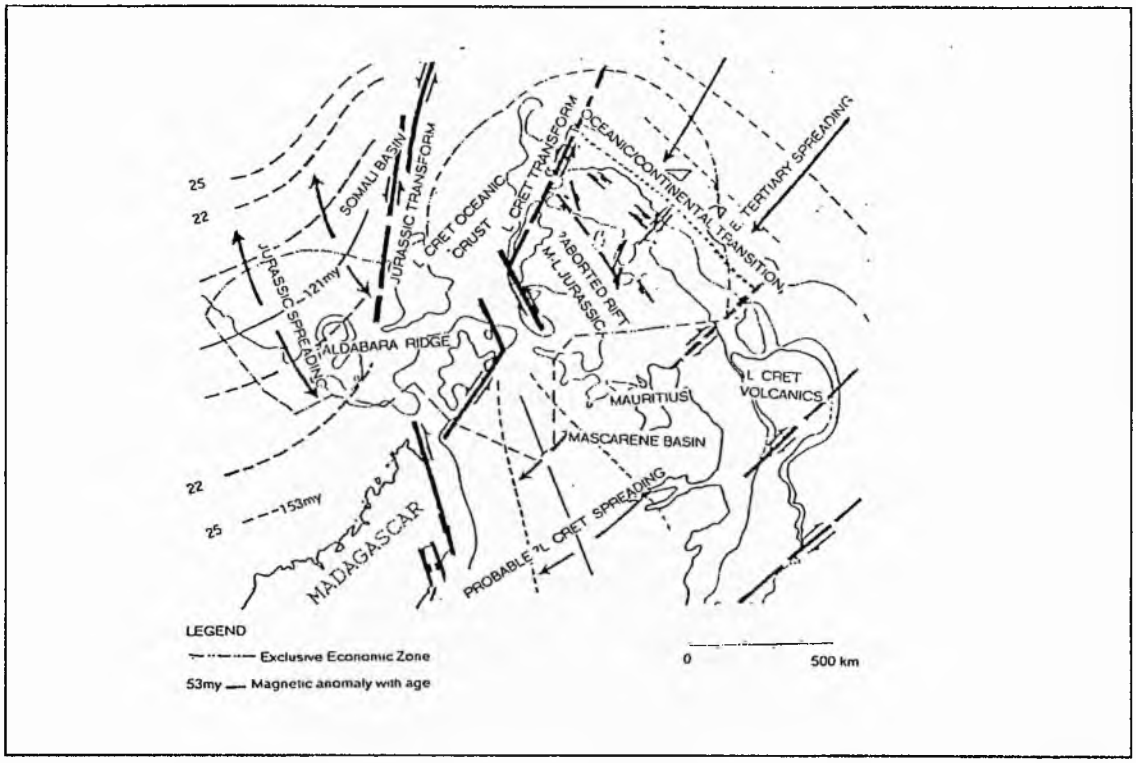

Fig. 2.3 Major tectonic elements of the Seychelles area (after Nopec a.s, 1985).

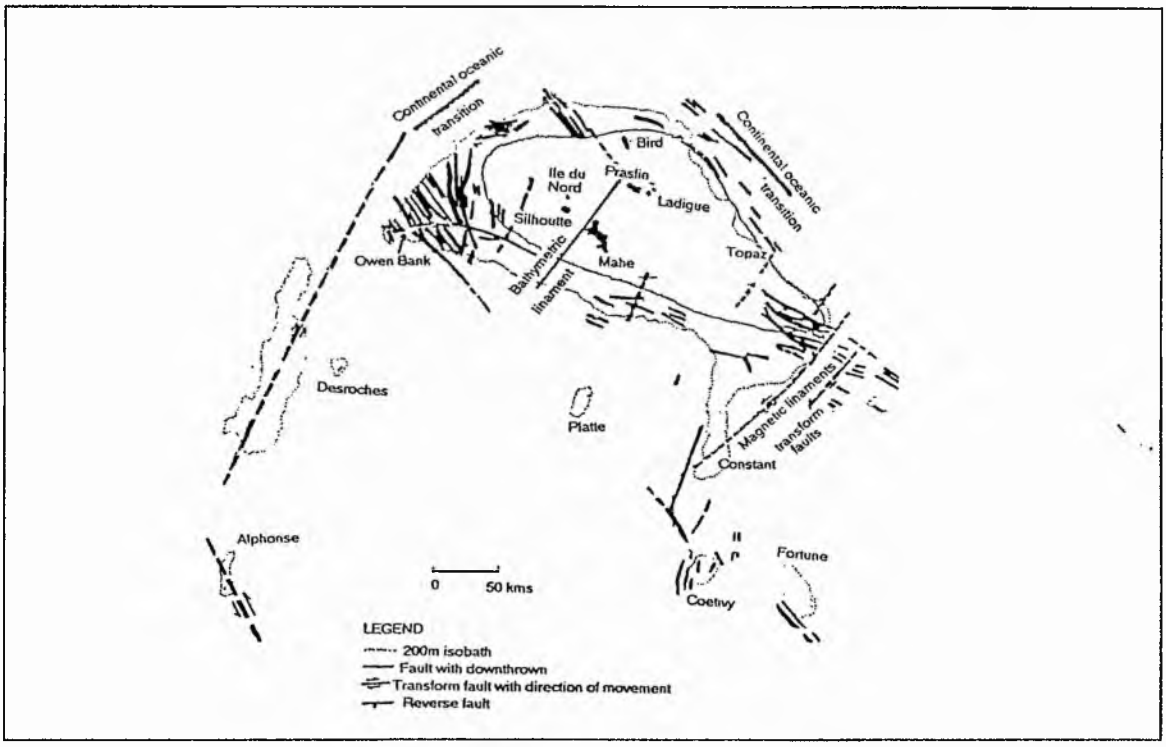

Fig. 2.4 Regional tectonic map (after Nopec as, 1985).

strata, but the evidence is weak. It may well be intersected by Late Cretaceous or younger transform faults which are known to cross the Seychelles-Mascarene ridge.

2.4.3 Late Cretaceous faulting:

Some of the deep Jurassic normal faults on the western shelf were slightly reactivated during the Late Cretaceous to Paleocene time.

The origin of widespread volcanic activity during the Maastrichtian is thought to be associated with northeast-southwest transform fractures, located mainly west of the present shelf (Fig. 2.4).

Constant Bank, Coetivy Bank and Fortune Bank, are clearly fault bounded along the western margins (Fig. 2.4). The age of these faults is difficult to determine, but they are assumed to be Cretaceous to perhaps Early Tertiary in age.

2.4.4 Tertiary faulting:

Tertiary Faulting is fairly widespread and well defined, with faults trending WNW to ESE, sub-parallel to the Carlsberg spreading axis. The north-east margin of the shelf is characterised by normal rift faulting during the Tertiary.

One distinct Tertiary tectonic feature is evident on the Topaz Bank, where the crest of the deep basement dome collapsed during the Early Tertiary (Fig. 2.4). A series of normal faults defines a graben complex along the axis of the basement high. Some of the faults show slight compressional reversals at a later stage of the Tertiary.

A similar feature is evident in the Bird area (Fig. 2.4) and one is tempted to suggest that a continuous horst/graben complex exists along the crest of the basement high. Praslin and La Digue are located on this trend (Fig. 2.4).

A series of compressional structures is found on the south flank of the basement high in the Topaz Bank area.

The compression pulse is seen partly as reversal of older down-to-the-south faults, partly as very mild folding of the Early Tertiary strata above old fault scarps.

The "fold axis" is perpendicular to the possible transform faults associated with the Indian Ocean spreading during the Tertiary. The compression pulse is therefore inferred to be as a result of Tertiary wrench movements.

Middle-Late Tertiary time is characterised by a stable tectonic regime. Minor synsedimentary faulting related to the steep margins of the Seychelles Banks are observed, but no major movements are identified.

The Paleocene to Eocene age of the granites of Ile de Nord (60 Ma) and Silhoutte (63 Ma) (Fig. 2.4) (Stephens, 1990) makes it plausible to link the development of these massifs to the Carlsberg Rifting stage with its associated transform fracture zones.

2.5. REGIONAL BASIN DEVELOPMENT:

The Seychelles area was associated with the depositional regime of Madagascar and East Africa until the Late Jurassic, and still associated with Madagascar until the Cretaceous, hence, the geology of the African Mainland and of Madagascar is of immediate relevance to the Seychelles.

2.5.1. Basement:

The granites and gneisose granites of Mahe have been dated 683-713 +/- 19 Ma (Rb-Sr) (Suwa *et al*, 1983), well correlated with the time of major magmatic activity in the Mozambique Belt.

2.5.2. Karoo:

In East Africa the oldest deposits over the basement are the Late Carboniferous to Early Jurassic continental deposits ranging in thickness from 100 to 5000m. Karoo deposits occur from South Africa to Kenya and probably into Somalia. The Karoo Super-group is also found in

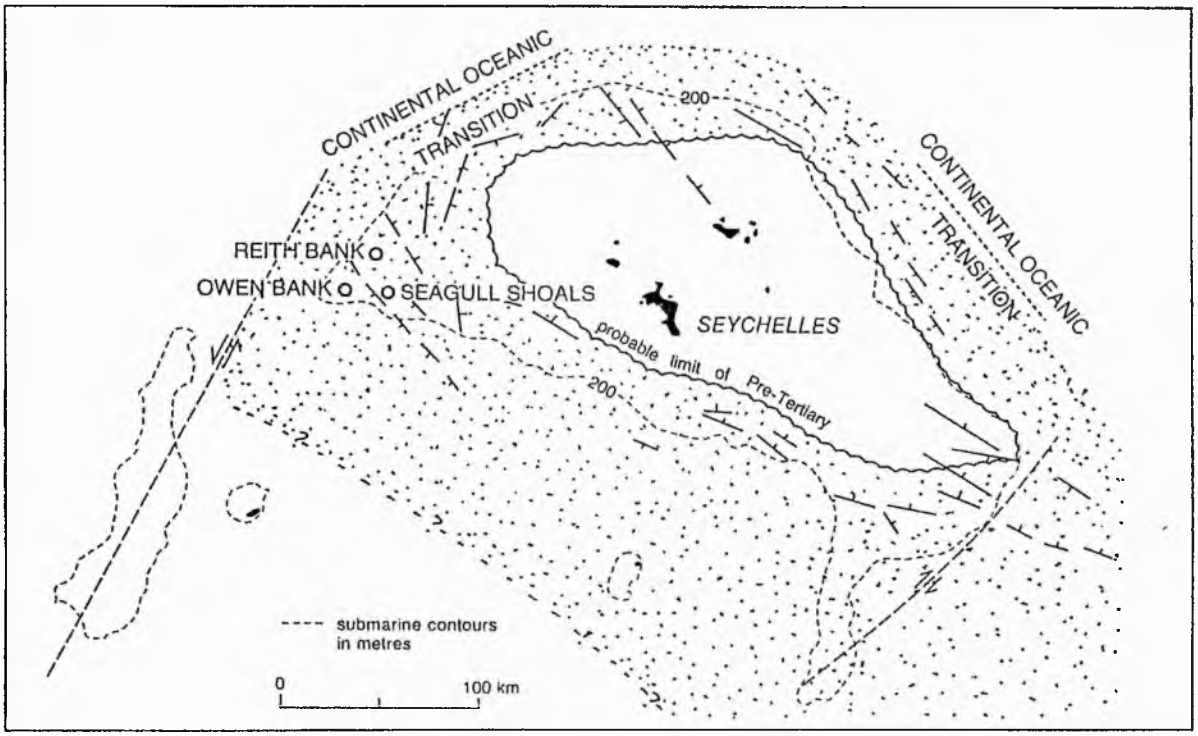

Fig. 2.5 Possible Karoo distribution in the Seychelles area (after Nopec a.s, 1985).

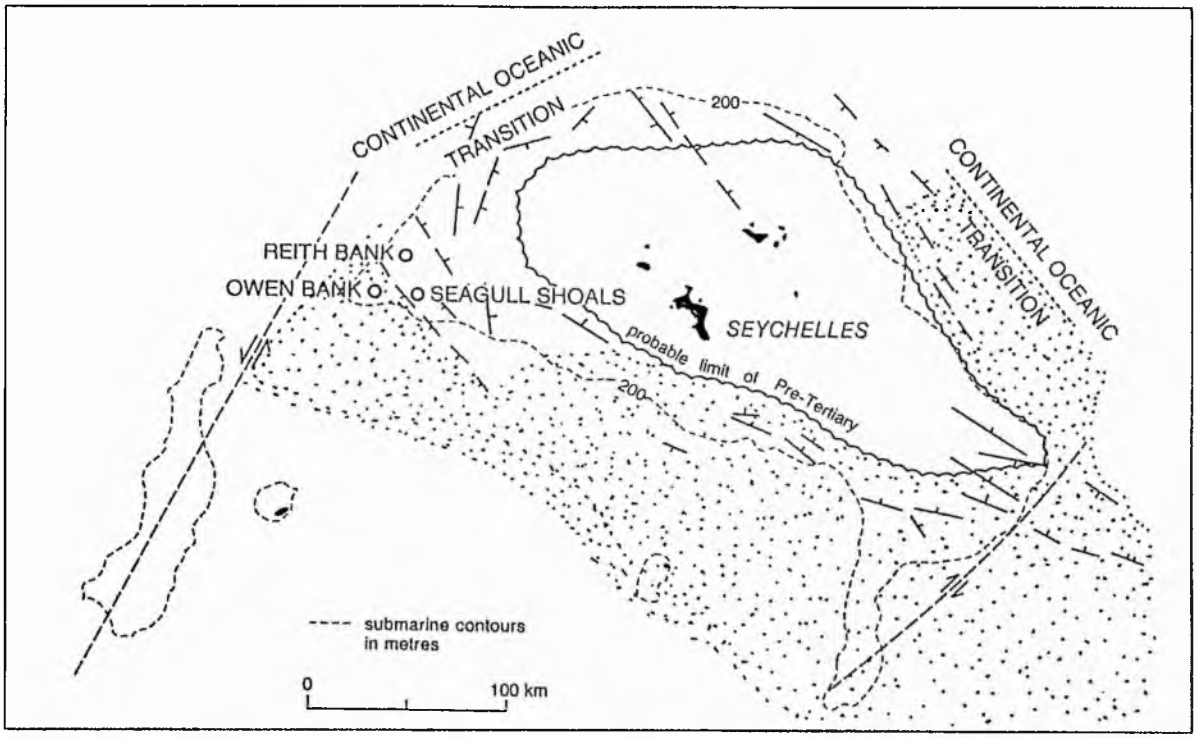

Fig. 2.6 Possible distribution of Marine Middle-Upper Jurassic and Lower Cretaceous sediments (after Nopec a.s, 1985).

Madagascar and in two wells drilled on the Seychelles western shelf (Fig. 2.5).

2.5.3. Marine Jurassic:

The continental Karoo sediments were transgressed in the Early Jurassic with the deposition of argillaceous carbonates (Fig. 2.6). The transgression is recognised in Seychelles, where continental Karoo strata are overlain by marine deposits of Early Jurassic age.

2.5.4. Cretaceous:

A mixture of marine sandstones, carbonates and shales is present in the Lower Cretaceous (Fig. 2.7). The Morondova basin in Madagascar shows all the stages, with the lower deposits made of alternation of limestone and sandstone, while thick basaltic lavas overlie the Cretaceous sequence.

The volcanic sequences found in Seychelles are probably of Late Cretaceous in age.

2.5.5. Tertiary:

The Seychelles main shelf has been tectonically quiet since Early Paleocene, and gentle subsidence gave rise to the deposition of thick shelf carbonates (Fig. 2.8). This depositional

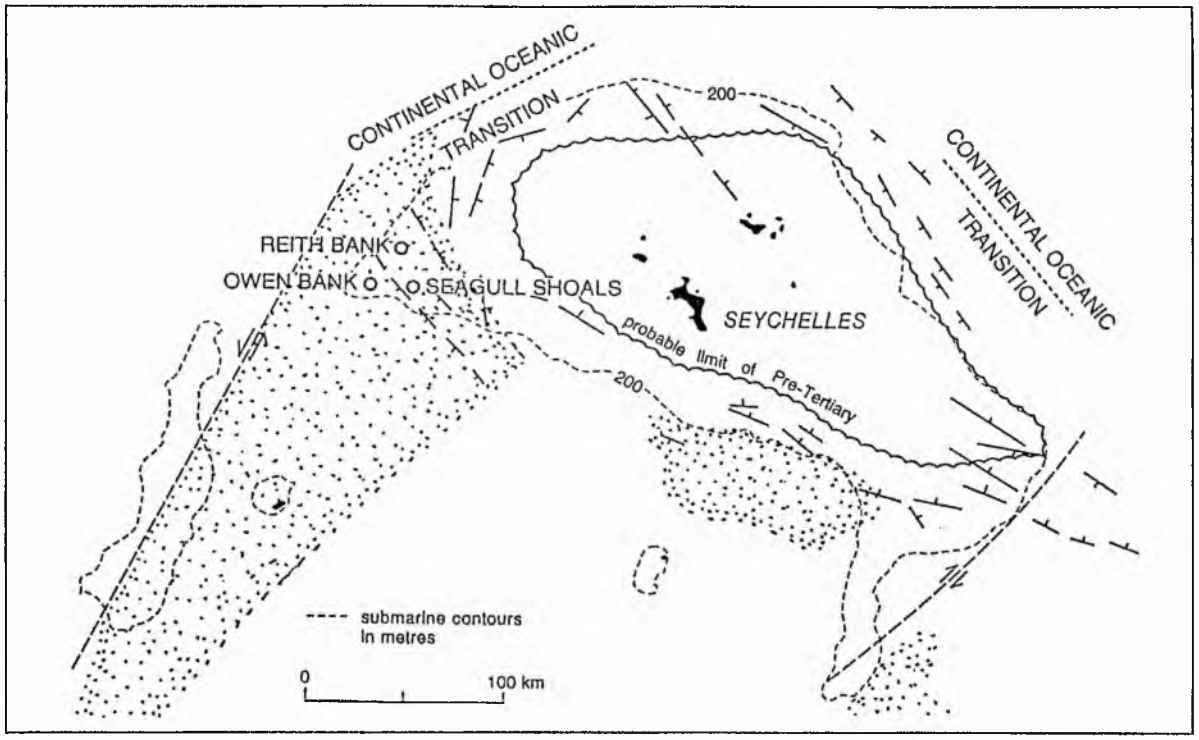

Fig. 2.7 Concentrations of Upper Cretaceous basalts in the Seychelles area (after Nopec a.s, 1985).

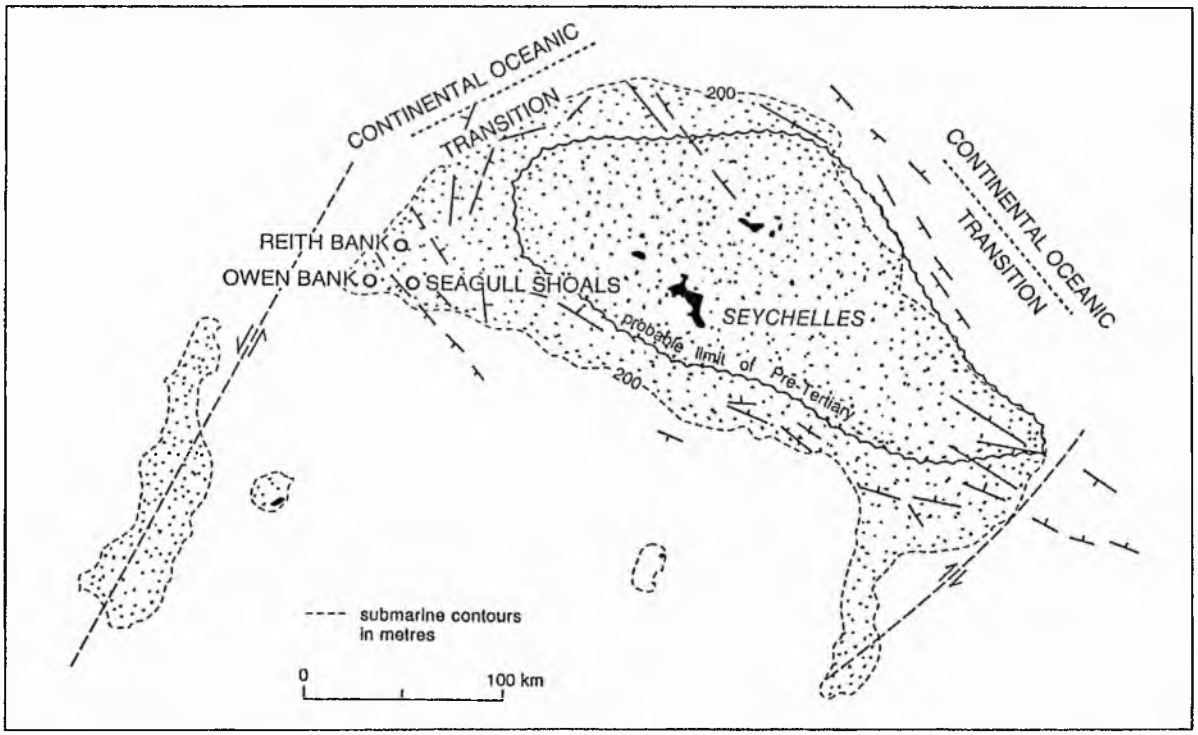

Fig. 2.8 Eocene to Recent shelf carbonate distribution (after Nopec a.s, 1985).

regime has continued to the present day.

2.6. GENERAL LITHOSTRATIGRAPHIC DESCRIPTION:

A generalised cross-section of the lithostratigraphic units of the Western Main Shelf (after Nopec a.s., 1985) is shown in Fig. 2.9.

2.6.1. Tertiary shelf carbonates:

Carbonate deposition dominated the Tertiary period. In the Eocene and Oligocene, minor sand stringers are indicated with shallow water carbonates. The approximate thickness in the three wells is 5,000 ft.

2.6.2. Upper Cretaceous volcanics (Maastrictian-Danian):

Basalt flows, tuffs and ashflows make up the volcanic interval varying between a few hundred feet to several thousand feet.

2.6.3. Lower Cretaceous/Upper Jurassic arenaceous limestones:

Inner shelf carbonates and mudstones dominate this interval, with rare sandstone stringers up to 35 ft thick. The whole sequence is thicker to the south. Owen Bank-1A penetrated 3700 ft while Seagull Shoals-1 and Reith Bank-1 penetrated only a few hundred feet.

2.6.4. Middle Jurassic calcareous sequence:

This sequence consists of mudstones and shales in the Owen Bank-1A well, with rare thin stringers of fine sandstone.

An arenaceous development of this sequence in structurally higher positions is clearly demonstrated by Seagull Shoals-1.

An oolitic limestone formed during the marine Jurassic transgression is present in all the three wells.

2.6.5. Middle-Lower Jurassic sequence:

The thick marine sequence found in Owen Bank-1A consists of argillaceous sediments with internal slump and load structures. This sequence is absent in the structurally higher wells, Reith Bank-1 and Seagull Shoals-1.

2.6.6. Karoo Supergroup:

A Karoo sequence consisting of interbedded sandstones and mudstones is present in Seagull Shoals-1 and Reith Bank-1. This sequence is believed to be fluvial and lacustrine.

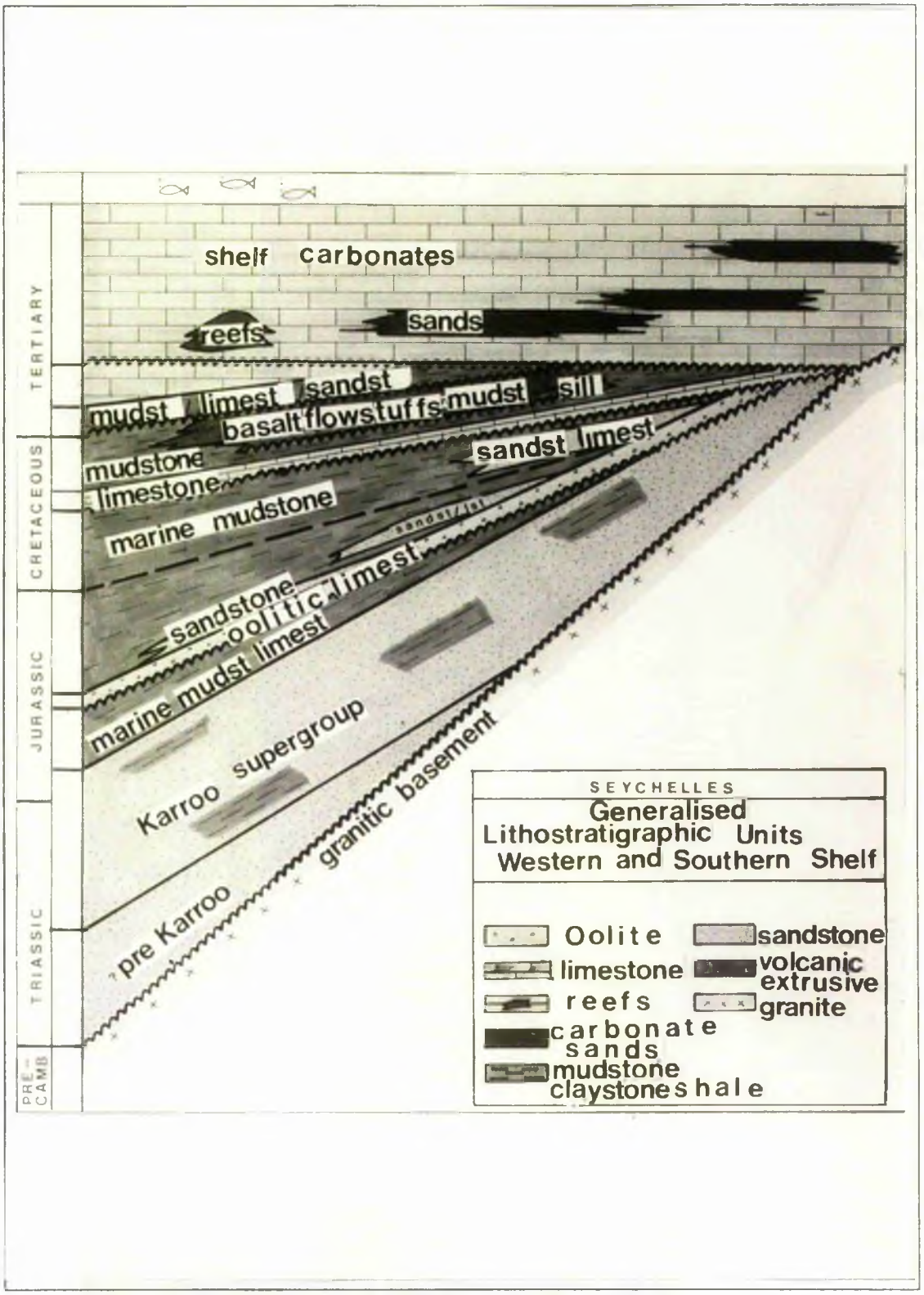

Fig. 2.9 General lithostratigraphic succession in the Seychelles area (after, Khanna & Pillay, 1986).

CHAPTER 3: LITHOLOGICAL SUCCESSION

(with 14 figures and 4 tables)

3.1 METHODOLOGY:

The interpretation of the lithological succession of Karoo Supergroup of Seychelles is based on wireline logs substantiated by petrographical studies of side wall and conventional cores, and well completion reports (Robertson Research International, 1981a, 1981b). The petrophysical logs supplied by Seychelles National Oil Company (Appendix I) comprised SP curve-gamma ray log, Resistivity log, Neutron log, Continuous Dipmeter and CORIBAND logs which have been widely used elsewhere in interpretation of lithology and identification of sedimentary environments (Doveton, 1986; Serra, 1985, 1986; Schlumberger, 1989; Rider, 1986).

3.1.1. Spontaneous Potential-gamma ray log:

The spontaneous potential (SP) and gamma-ray (GR) logs are subsurface measurements of radically different physical properties of a rock. The SP sonde records the strength of intrinsic electromotive forces within the borehole; the gamma-ray device counts the level of natural gamma radiation emanating from formations in the borehole wall. Nearly all rocks exhibit some natural radioactivity and the amount depends on the concentration of potassium, thorium, and uranium. Both the SP curve and GR log are generally recorded in Track 1 (left track) of the log.

The SP and GR logs are used to differentiate porous from nonporous rocks, define bed boundaries and allow correlation, give a qualitative indication of bed shaliness, aid in lithology identification; SP curves help in the determination of formation water resistivity, R_w; GR logs help in determining deposits of radioactive minerals and define the concentrations of potassium, thorium and uranium (Schlumberger, 1989).

The SP curve is more or less a straight line opposite the shales, called the *shale baseline.* Opposite permeable formations, the curve shows deflections from the shale baseline reaching a constant deflection against the thick beds defining a *sand line.* The shale baseline is usually fairly well defined on the SP log, however, sometimes a shift occurs whenever formation waters of different salinities are separated by a shale bed (Schlumberger, 1989).

The GR log is used quantitatively to calculate shale volume while qualitatively it is used to correlate and identify facies and different lithologies (Rider, 1986). The criteria to define a shale baseline using the GR follows similar principle as the SP log. The GR log is particularly useful for defining shale beds when the SP is

distorted or featureless, or when it cannot be recorded (Schlumberger, 1989).

3.1.2. Resistivity logs:

A resistivity log from a borehole represents a composite measurement of resistivities of rock-forming minerals and fluid and gaseous phases within the pore spaces. Resistivity logs are most important for hydrocarbon exploration. The resistivity of a formation is one of the geophysical properties and can be used for the interpretation of lithology, texture, facies, over pressure and source rock characteristics (Rider, 1986). Resistivity logs are used for correlation and help indicate gross lithology.

3.1.3. Porosity logs:

Sonic, density, or the neutron logs are used to investigate the porosity of a formation. Formation porosity, fluid and matrix affect the tool response for the devices used for log measurement. "... if the fluid and matrix effects are known or can be determined, the tool response can be related to porosity. Therefore, these devices are often referred to as porosity logs" (Schlumberger, 1989).

All the three logging techniques have a very shallow depth of penetration- only a few inches or less.

The sonic log is a recording of the time (t) required for a sound wave to traverse 1 ft of formation. This time is dependent upon porosity, when lithology is known.

Density logs are primarily used as porosity logs, but other uses are identification of minerals in evaporite deposits, detection of gas, evaluation of shaly sands and complex lithologies. The density tool consists of a source of gamma rays (e.g., cesium-137) which radiate into the formation and interact with the electron clouds of the atoms they encounter by Compton Scattering and photo-electric effect (Schlumberger, 1989). As a result there is a reduction in gamma ray flux which is measured and is proportional to the electron density of the formation. These measurements are then converted into bulk density of the formations through simple atomic theory (Rider, 1986; Schlumberger, 1989).

Neutron logs are used primarily for identification of porous formations and determination of their porosity. Hydrogen amounts present in the formation are used for the measurements. "...Thus, in clean formations whose pores are filled with water or oil, the neutron log reflects the amount of liquid-filled

porosity" (Schlumberger, 1989). The neutron tool contains a source of high-energy neutrons which radiate spherically into the adjacent formation. These neutrons experience a progressive reduction in energy due to collisions with nuclei of other atoms they encounter with a significant loss due to collision with a nucleus of similar mass. Hydrogen atoms are the primary cause for this reduction in energy. Ultimately, each neutron is reduced in energy to a thermal state, at which point it is captured by a nucleus and capture gamma rays are emitted. A tool measures the quantity of slow neutrons or the capture gamma rays. The reduction in the neutron flux is mainly a function of hydrogen concentration within the formations which can be equated with the pore fluid fraction of a typical lithology, thus giving the porosity of the formation (Rider, 1986; Schlumberger, 1989).

3.1.4. Computer processed logs- SARABAND® and CORIBAND®:

Computer processed logs are composite logs developed to determine water and hydrocarbon saturation in the formations using a combination of density, neutron, deep resistivity, microresistivity and GR logs. The Saraband and Coriband programs were designed by Schlumberger to perform these computations for sand-shale and complex (as encountered in carbonate and/or evaporite) sequences respectively (Schlumberger, 1989). Since, these are "...computer programs, advantage can be taken of the many features and capabilities of the computer to improve and expand the basic computations" (Schlumberger, 1989). Both the programs make extensive use of neutron-density crossplots.

The Saraband program uses a silt-shale-sand model while the Coriband program is a general interpretation method for mixed carbonate and clastic lithologies.

3.1.5. Dipmeter logs:

The dipmeter is a logging device to measure the orientation of bedding planes and other features within a borehole. A four-arm dipmeter device had been used for measurements in the Seychelles wells, while CLUSTER® processing was used for the presentation of the data. "..In CLUSTER processing, various combinations of three of the four microresistivity dipmeters curves are used to calculate a group of possible dip planes at a given depth" (Schlumberger, 1989).

The presentation of dip as a "tadpole" plot and a colour convention is used by log analyst to separate tadpole clusters as;

Green- dips with common azimuth and essentially constant dip,

Red- dips with common azimuth and increasing dip with depth, and

Blue- dips with common azimuth and decreasing dip with depth.

The head of a tadpole gives the amount of dip, while the tail gives the dip direction.

3.2. LITHOLOGY:

The upper boundary of the Karoo Supergroup, taken at the appearance of marine sediments, occurs at 7295 ft and 6150 ft respectively in Seagull Shoals-1 and Reith Bank-1. In neither well was the base achieved, 1670 ft being penetrated in Seagull Shoals-1 and 6500 ft at Reith Bank-1.

At Seagull Shoals the Karoo Supergroup consists of thickly bedded sandstones and mudstones. The sandstones range from very fine grained to coarse grained, while the mudstones vary in colour from dark grey to medium brown. A microgabbro intrusive, present from 8460 to 8435 ft (Fig. 3.2), has been helpful in dating. A latest Jurassic to earliest Cretaceous age has been assigned to this intrusive (Robertson Research International, 1981b) which implies an earlier age for the host rock. Biostratigraphic dating can only give a tentative Middle to Early Jurassic age for this interval (*op. cit.*).

At Reith Bank the Karoo sequence consists of interbedded sandstones and mudstones. The sandstones are very variable in grain size ranging from very fine grained to pebble grade. The mudstones vary from brownish-grey to greyish-green in colour and are generally silty. Volcanic glasses or felsites occur at intervals through the sequence (Table 3.1), and are thought to represent welded tuffs or ignimbrites. Biostratigraphy indicates an age not older than Early Jurassic down to 7100 ft (Robertson Research International, 1981a). Definite Triassic forms (*Patinosporites densus* and *Camarosporites secatus*) are present below 9300 ft (*op.cit.*).

Wireline logs have been widely used for the interpretation of lithology with the view that no single log can precisely define the different lithologies. A combination of gamma-ray, sonic, resistivity and .. bulk density along with CORIBAND® gave a reliable tool of differentiating various lithologies. A critical analysis of gamma-ray log shape has been discussed by Rider (1990).

Gamma-ray tool is based on the uranium, thorium and potassium radioactivity in the sediments. These elements are present

especially in clays and shales can be picked out by their high response. In addition the presence of clays ("shaliness") in sandstones can be detected by increased GR response and this may be taken as representing a decrease in grain-size. Interpretation on these lines is hazardous given the presence of k-feldspar. Petrographic analysis of side wall and conventional cores was therefore used as a control to check the validity of gamma-ray as an indicator of "shaliness". It was also seen that in Reith Bank-1 where below 12,000 ft feldspar content increases in sandstones (Khanna & Walton, 1990), gamma-ray curve did not behave abnormally and distinct sandstone and mudstone bands were identified.

The succession of 6500 ft in Reith Bank-1 has been divided into five members on the basis of grain-size and sandstone/mudstone ratios, derived from wireline logs and samples. (Table 3.1 & Figs. 3.1-3.8).

The five members group into three megacycles, which individually form fining upwards sequences, although only the upper, finer member of megacycle I is represented.

The entire succession of Seagull Shoals-1 (1670 ft) is believed to be the upper fine grained member of a megacycle. In terms of the arrangement of sandstones and mudstones this

Table 3.1 Lithological characteristics of the five members of the Karoo Supergroup, Reith Bank-1 (S,M-arithmetic mean thicknesses of sandstones and mudstones).

Member	Depth	Lithology	Description	Megacycle
5	6140-7680 ft	Thick sandstones & thick mudstones. S-47 ft M-35 ft S/M 1.5	Fine or medium grained sandstones, ocassionally coarse. Felsites at 7406-7435 ft.	III
4	7680-8812 ft	Thick sandstones & thin mudstones. S-82 ft M-13 ft S/M 7.7	Coarse grained sandstones Felsites at 8050-8090 ft.	III
3	8812-9837 ft	Sandstones are generally thinner than below. Thin mudstones S-36 ft M-9 ft S/M 4.0	Fine to medium grained sandstones	II
2	9837-11,190 ft	Thick sandstones, becoming thicker sands below (up to 100 ft). S-37 ft M-9 ft S/M 4.1	Coarse grained locally conglomeratic Basalt at 10,452 ft.	II
1	11,190-12,500 ft	Thick sandstones & thin mudstones. S-47 ft M-13 ft S/M 3.7	Fine grained or very fine with one (~100 ft) coarse grained interval. Occasional lignite or carbonaceous horizons	I

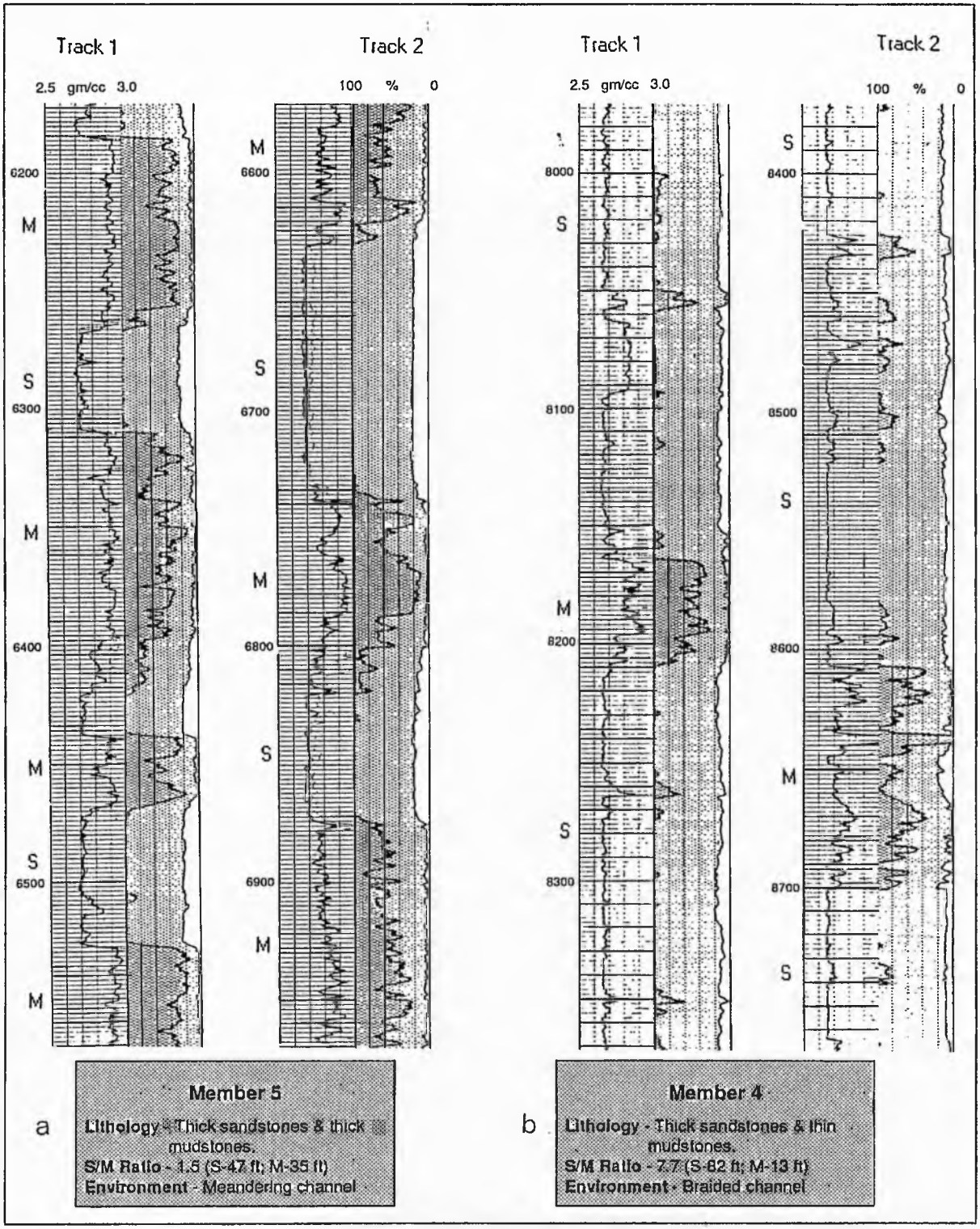

Fig. 3.1 Log presentation from computed CORIBAND® (Schlumberger, 1989) results illustrating sandstone-mudstone development in a) Member 5 and b) Member 4, Reith Bank-1 well. Mudstones (M) notably well developed in Member 5 contrasting with the dominance of sandstones (S) in Member 4. Track 1-Average grain density, Track 2-Formation analysis by volume; dark ornament- clay, light ornament- non-clay solids, blank- porosity. S, M-arithmetic mean thicknesses of sandstones and mudstones. (The figure is an extract from the original CORIBAND log of Reith Bank-1 well provided by Seychelles National Oil Company.)

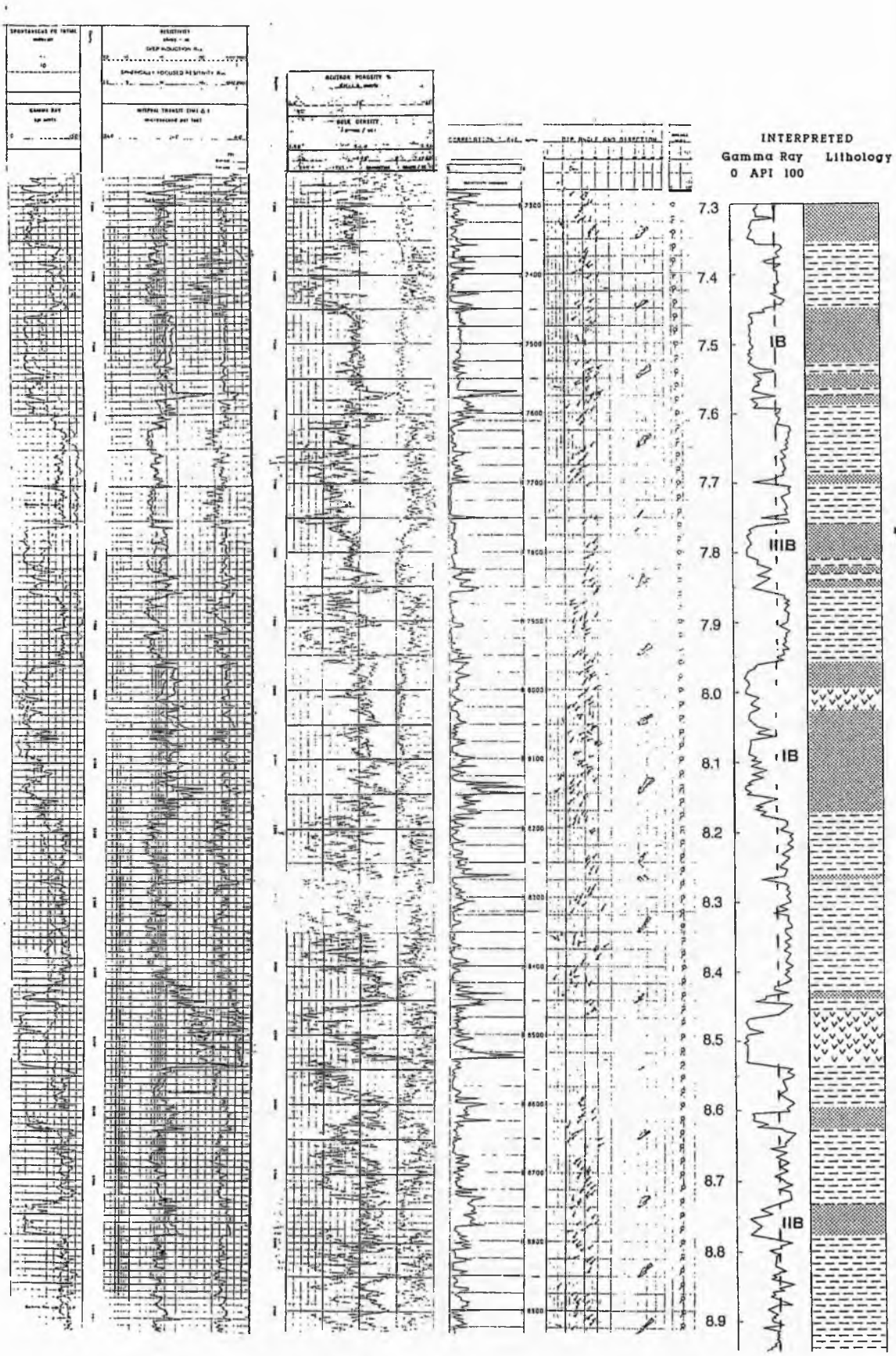

Fig. 3.2 Log responses and interpreted lithology of Karoo succession at Seagull Shoals-1 showing SP, Gamma-ray, Re and Sonic in cloumn 1; Neutron Porosity and Bulk Density in column 2; Dipmeter plot from cluster program in column 3; 4 presents interpreted lithology from wireline logs substantiated from well completion reports and side wall and conve core descriptions and petrographical analysis. Examples of Coarsening upwards sequence-CU, Fining upwards sequen Blocky sequence-B. Sandstone types (IB, IIB IIIB) discussed in Fig. 3.9. Depth on interpreted lithology x1000 ft.. Dotted gamma-ray track shows the shale base-line. (Source for wire line logs: Seychelles National Oil Company).

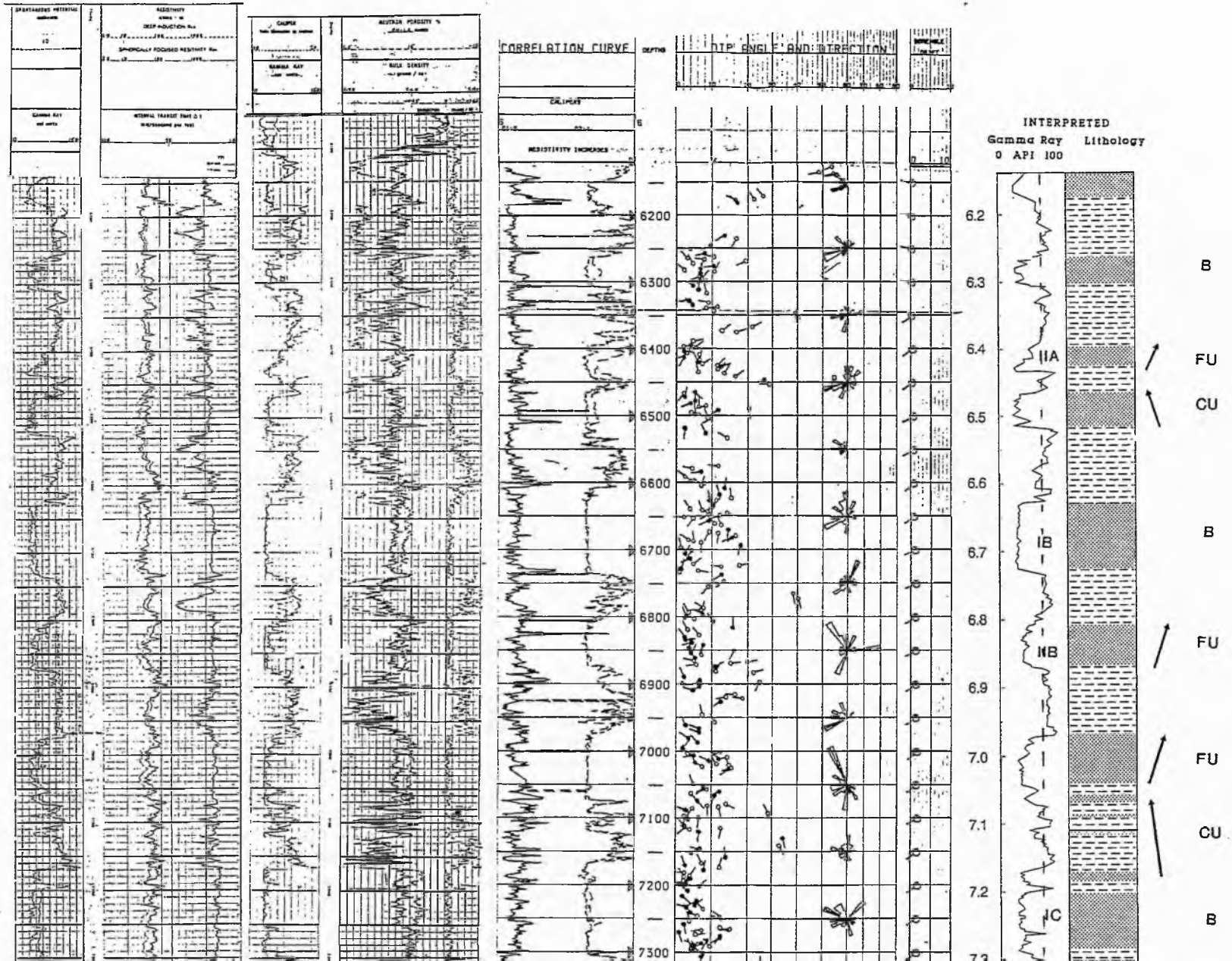
CORRELATION CURVE
DEPTH
DIP ANGLE AND DIRECTION
INTERPRETED
Gamma Ray
0 API 100
Lithology
6200
6300
6400
6500
6600
6700
6800
6900
7000
7100
7200
7300
6.2
6.3
6.4
6.5
6.6
6.7
6.8
6.9
7.0
7.1
7.2
IIA
IIB
IIC
B
FU
CU
B
FU
FU
CU
B

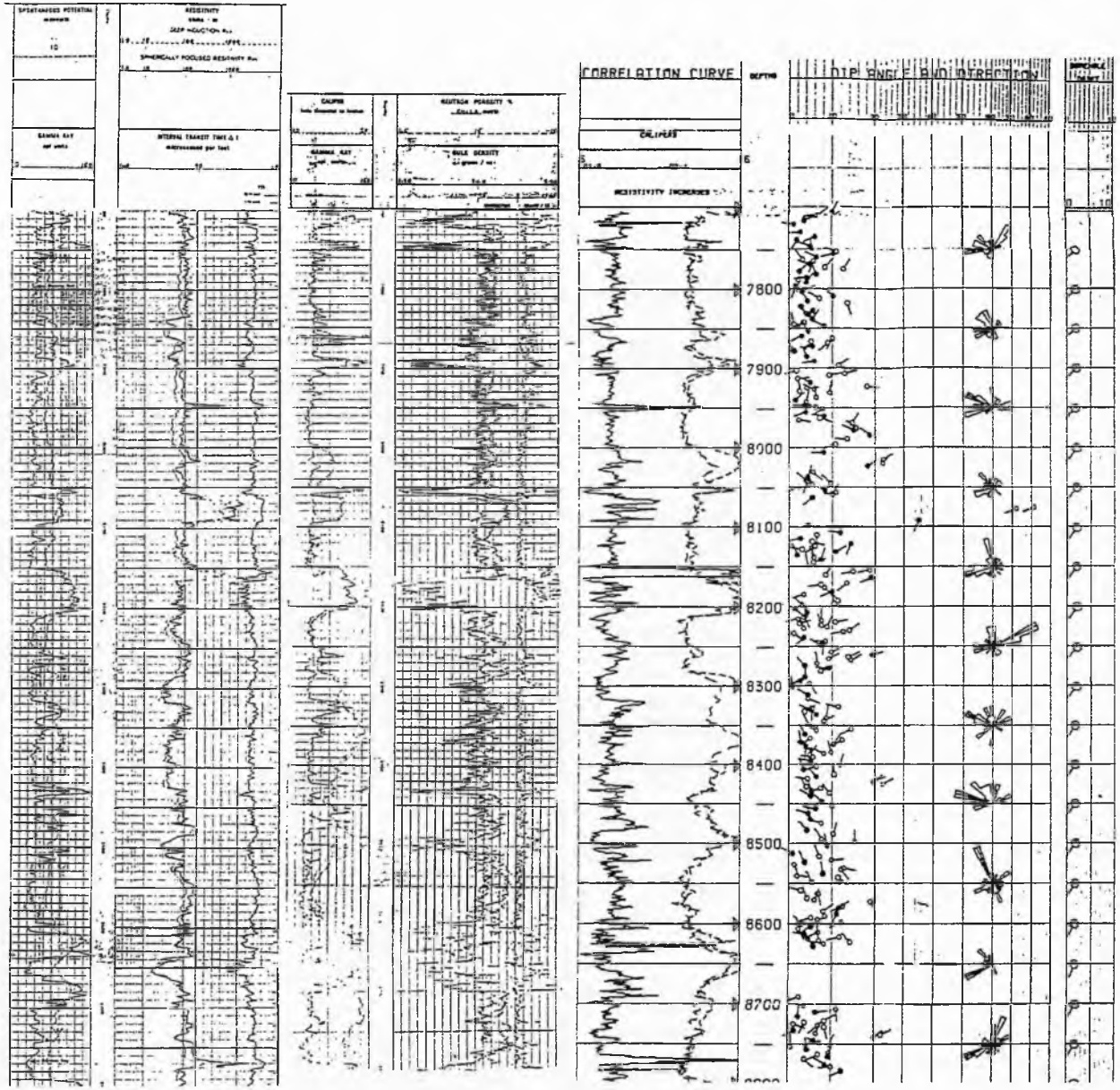
CORRELATION CURVE
DIP ANGLE AND DIRECTION
7800
7900
8000
8100
8200
8300
8400
8500
8600
8700

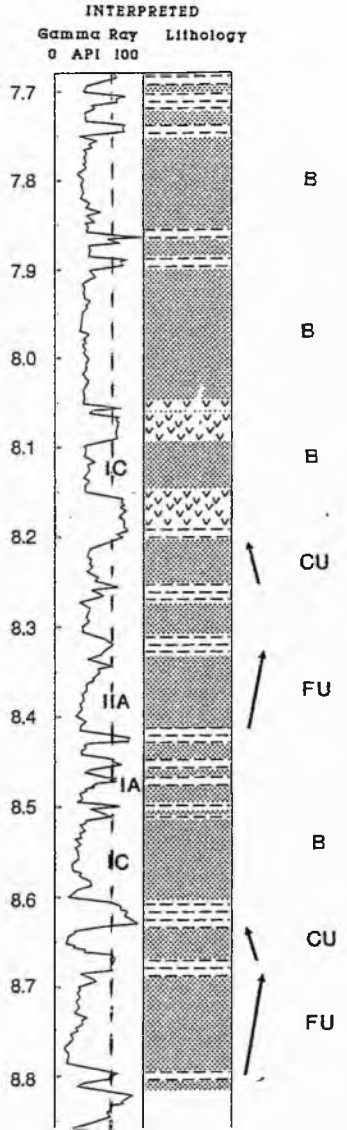
INTERPRETED
Gamma Ray Lithology
0 API 100
7.7
7.8
7.9
8.0
8.1
8.2
8.3
8.4
8.5
8.6
8.7
8.8
IC
IIA
IA
IC
B
B
B
CU
FU
B
CU
FU

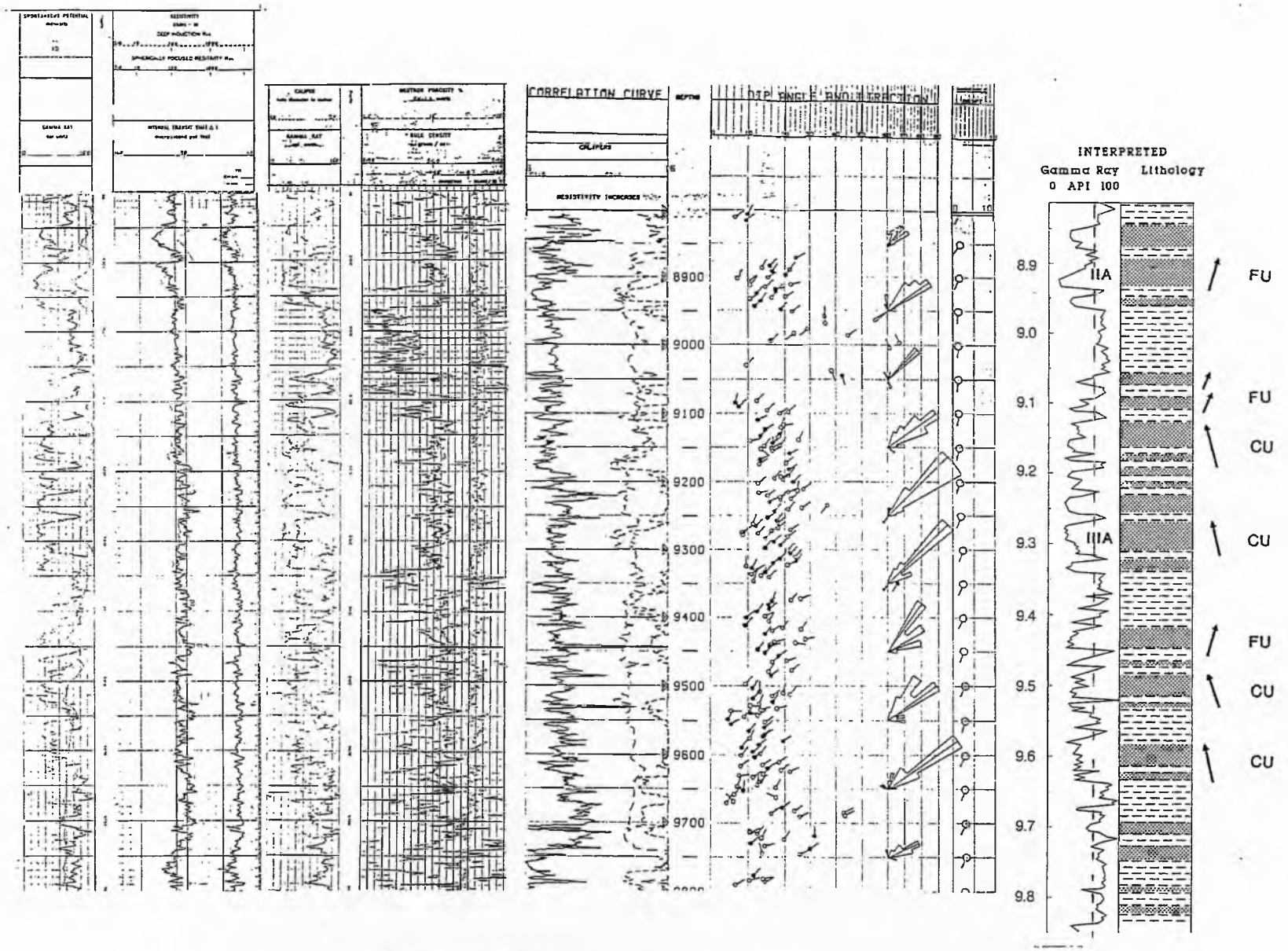

Fig. 3.5 Log responses and interpreted lithology of Karoo succession of Member 3 at Reith Bank-1 showing SP, Gamma-ray, Resistivity and Sonic in column 1; Caliper, Gamma-ray, Neutron Porosity and Bulk Density in column 2; Dipmeter plot from cluster program in column 3; Column 4 presents interpreted lithology from wireline logs substantiated from well completion

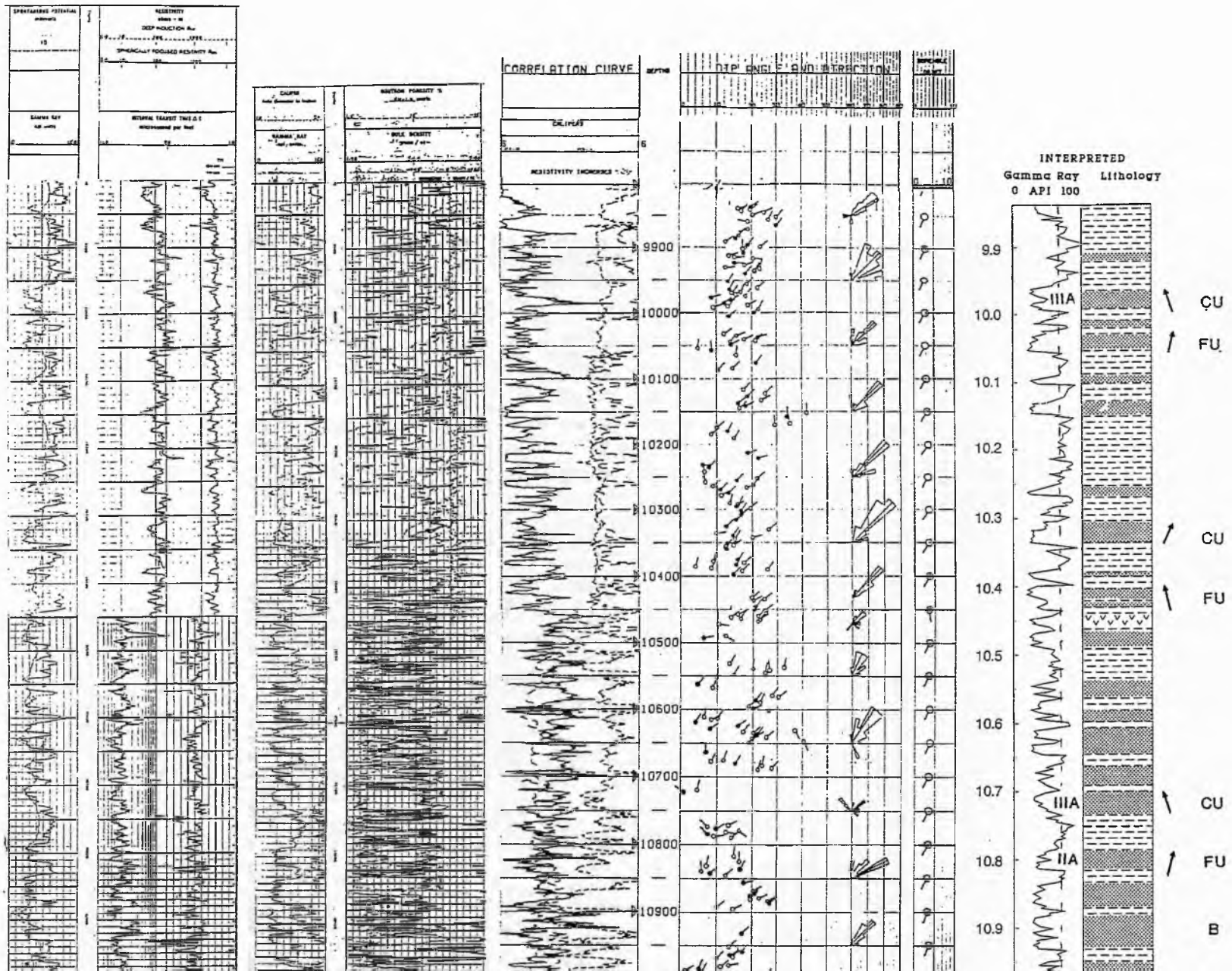
CORRELATION CURVE
DIP ANGLE AND DIRECTION
INTERPRETED
Gamma Ray Lithology
0 API 100
9900
10000
10100
10200
10300
10400
10500
10600
10700
10800
10900
9.9
10.0
10.1
10.2
10.3
10.4
10.5
10.6
10.7
10.8
10.9
IIIA
IIIA
IIA
CU
FU
CU
FU
CU
FU
B

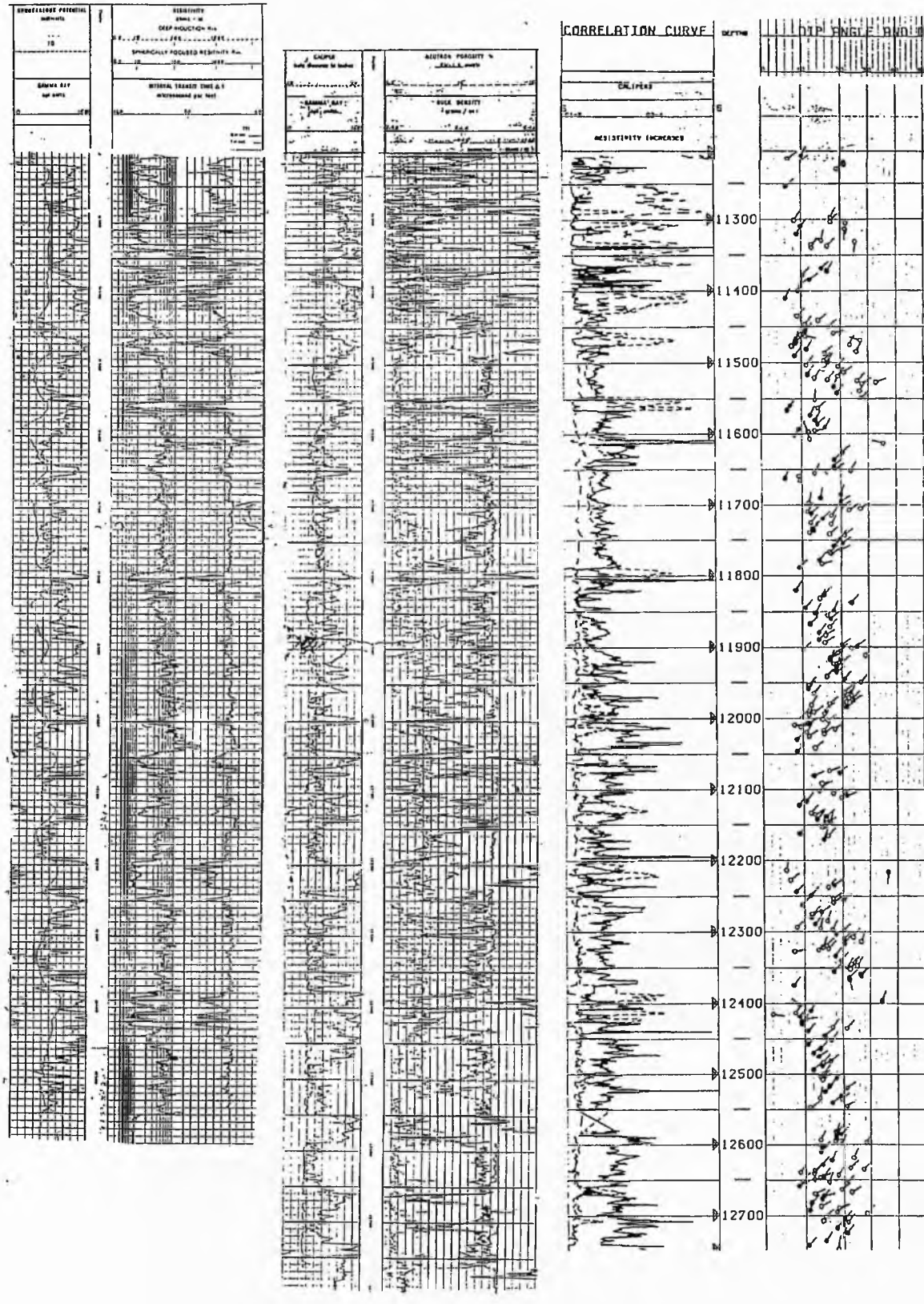

Fig. 3.7 Log responses and interpreted lithology of Karoo succession of Member 1 at Rei
Resistivity and Sonic in column 1; Caliper, Gamma-ray, Neutron Porosity and Bulk Dens
cluster program in column 3; Column 4 presents interpreted lithology from wireline logs
reports and side wall and conventional core descriptions and petrographical analysis.
sequence-CU, Fining upwards sequence-FU, Blocky sequence-B. Sandstone types (IB,
interpreted lithology x1000 ft.. Dotted line on gamma-ray track shows the shale base-line. (
National Oil Company).

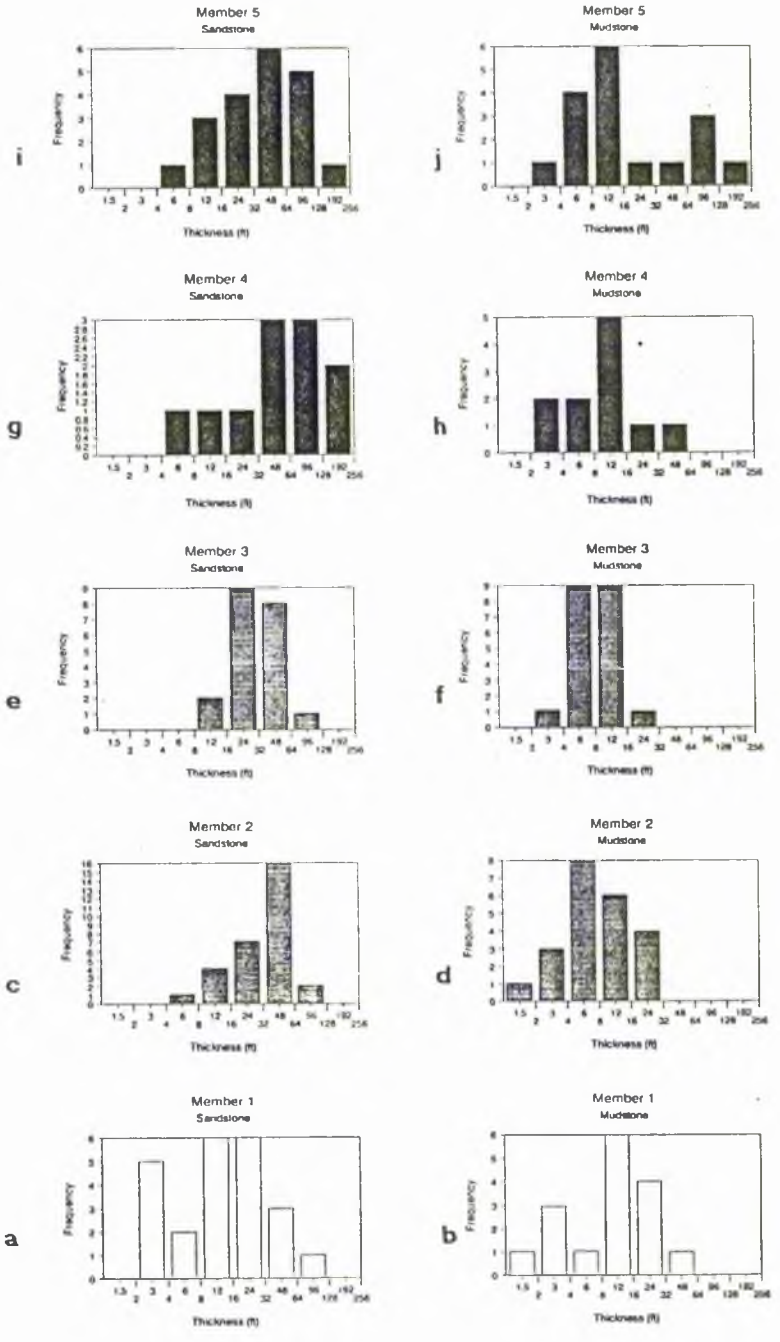

Fig. 3.8 Histograms showing thickness frequencies of sandstones and mudstones in Reith Bank-1 Karoo Supergroup. The thickness has been calculated from the petrophysical logs (gamma-ray, resistivity, sonic and CORIBAND®).
Thinnest sandstone units: 2-4 ft (a) Thinnest mudstone units: 1-2 ft (b, d)
Thickest sandstone units: 128-256 ft. (g, i) Thickest mudstone units: 128-256 ft (j)
Maximum number of sandstone units (35) are 32-64 ft thick, while only 3 are above 128 ft in thickness. Majority of mudstones (32) are 8-16 ft thick.

whole sequence of the Seagull Shoals-1 correlates with that of the uppermost member (6140-7680 ft) of Reith Bank-1 (Fig. 3.2, 3.3, Table 3.1).

3.2.1. Stratigraphic divisions:

Member 1 (11,190-12,500 ft) is made up predominantly of fine grained sandstones, siltstones and mudstones with one coarse-grained interval (Table 3.1). The sorting of the sandstones is generally good and usually better than those of the succeeding members. In colour they tend to be mostly grey, except for the lower beds which are pink. Thicknesses of the sandstone and mudstone show a wider range than other members with a greater number of thin (2-4 ft) and fewer thick (64-256 ft) beds[1] (Fig. 3.8). Interbedded mudstones are grey or brown like higher members but a distinguishing feature is the presence of dark or olive grey and even some even blackish beds. The last are carbonaceous and when plant material becomes dominant they are lignite horizons. Member 1 is taken to represent the upper, fine-grained portion of a megacycle.

It is suggested that Members 2 and 3 comprise a second megacycle. Member 2 (9837-11,190 ft) has thick coarse grained, locally conglomeratic horizons. The sandstones tend to be pinkish grey in colour, or white. They are often slightly argillaceous. Mudstones are usually silty, greyish red or greyish green or mottled in these two shades. The sandstones (S) are much thicker than the interbeds (M) in both Members 2 and 3 which have similar S/M ratios (Table 3.1). Member 3 (8812-9837 ft) has sandstones which are finer grained; they tend to be slightly thinner and mostly pinkish grey although some are mottled by brownish iron staining. The mudstones of Member 3 are mottled greyish red and greyish green with some purple and yellow. Overall the megacycle shows an upward fining in grain-size.

Member 4 (7680-8812 ft) shows a return to coarse and very coarse-grained sedimentation with very thick sandstones, thin mudstones and a high S/M ratio. Sandstones are white, greyish in pink or brown shades; mudstones are greyish-brown or -red. This lower member of the third megacycle passes up into the finer grained Member 5 (6140-7680 ft), which is distinguished by having thick mudstone beds as well as thick sandstones. These relations mean that the S/M ratio in this member is the lowest in the Supergroup at 1.5. The sandstones are mostly light grey or yellowish grey with a few pinkish grey in the lowest beds; mudstones are brownish or

[1]The term 'beds' is informally used here to represent bodies picked out from log responses and limited by precision of the techniques (thus a sand bed may have clay partings) and not as per the classification of bed, lamina... etc. when thicknesses can be determined in detail.

greenish grey above with some mottled below. A unique feature of this member is a conglomeratic horizon 30 ft thick between depths 6810 and 6840 ft.

3.2.2. Stratigraphic age:

The paucity of fossils makes the stratigraphic age of the members uncertain. Palynological evidence led Robertson Research International (1980, 1981a, 1981b) to regard the sequence down to 9300 ft i.e., Members 5,4 and the upper part of Member 3 as ?Middle Jurassic-?Late Triassic. In particular *Callialasporites dampieri* is cited as evidence of sediments down to 7100 ft as being younger than Early Jurassic. In the absence of evidence the whole interval 6152-9300 ft could be Early Jurassic. Non-marine palynomorphs occur below 9300 ft. The top of the Late Triassic, Norian sequence at 9300 ft is indicated by *Patinosporites densus* while below 10,010 ft *Camarosporites secatus* suggests a possible Carnian age for the lower beds to 10,890 ft. This lowest part of Member 2 together with Member 1 is richer in palynomorphs which are typical of Middle as well as Late Triassic. A few Permian forms were taken to be reworked from Permian sediments (Robertson Research International, 1980, 1981a, 1981b). Comparasion with the Madagascar sequence (see section 3.3.2.) may indicate a Permian age.

3.2.3. Sandstone types:

The nature of the Karoo sandstones and their development relative to mudstones have been analysed from wireline logs (Gamma ray, SP, Resistivity, Neutron, Density and Sonic as well as Dipmeter and CORIBAND^{R}). Sandstones, as recorded by wire line logs have been classified into seven types (Walton & Khanna, 1990) (Fig. 3.9, 3.10, Table 3.2).

Type I includes those sands with symmetrical curves. Type IA comprise thin beds with a simple symmetrical shape. IB and IC are thicker beds with an extended, cylindrical shape; IB has sharp margins and IC graded margins. Type II is the well known bell-shaped curve produced by the upward-fining sandstones. IIA is the simple bell; IIB has an extended section, a sharp base and a graded top. Type III sands coarsen upwards with IIIA, a simple funnel shape and IIIB extended with a cylindrical section. With the exception of type IA virtually all the curves are serrated i.e., the sandstones are multi-storey with fine-grained interbeds or partings.

On this basis it appears (Table 3.2, Fig. 3.10) that,

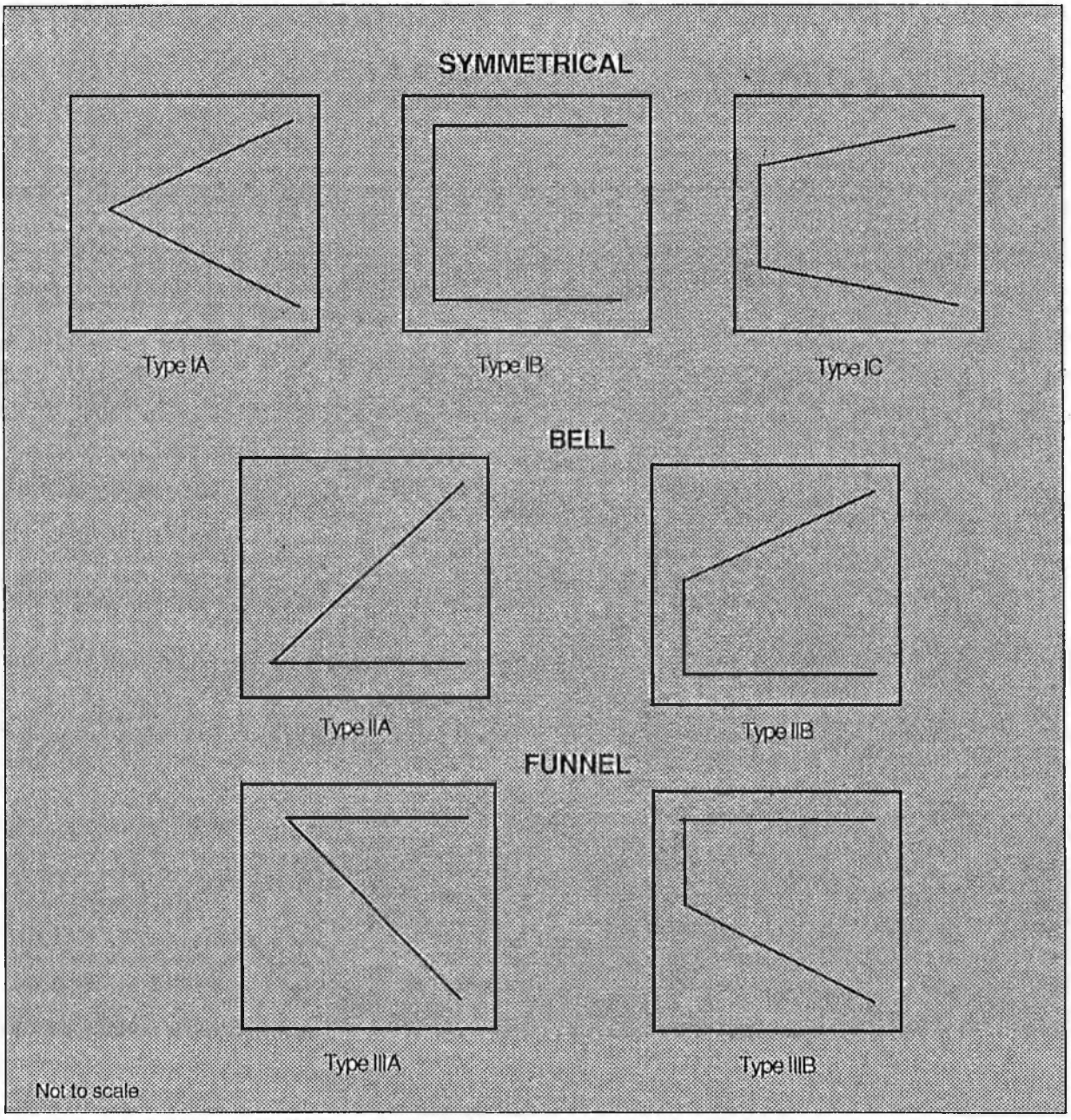

Fig. 3.9 Diagrammatic representation of wire-line curve indicating vertical grain-size changes in Karoo sandstones. IA-Symmetrical; IB-Symmetrical extended with sharp contacts (cylindrical); IC-Symmetrical, extended with graded upper and lower contacts; IIA-Simple bell-shaped curve - upward fining (UF); IIB-Extended bell-shaped curve - sharp lower contact, graded upper contact; IIIA-Simple, funnel-shaped curve, upward coarsening (UC); IIIB-Extended funnel-shaped curve, upward coarsening graded lower contact, sharp upper contact. Real log examples are given in Figs. 3.2-3.7.

i. overall a majority of sandstone types show upward fining (UF-42) or upward coarsening (UC-33)

ii. of the UF and UC the former are more frequent (UF/UC=1.27).

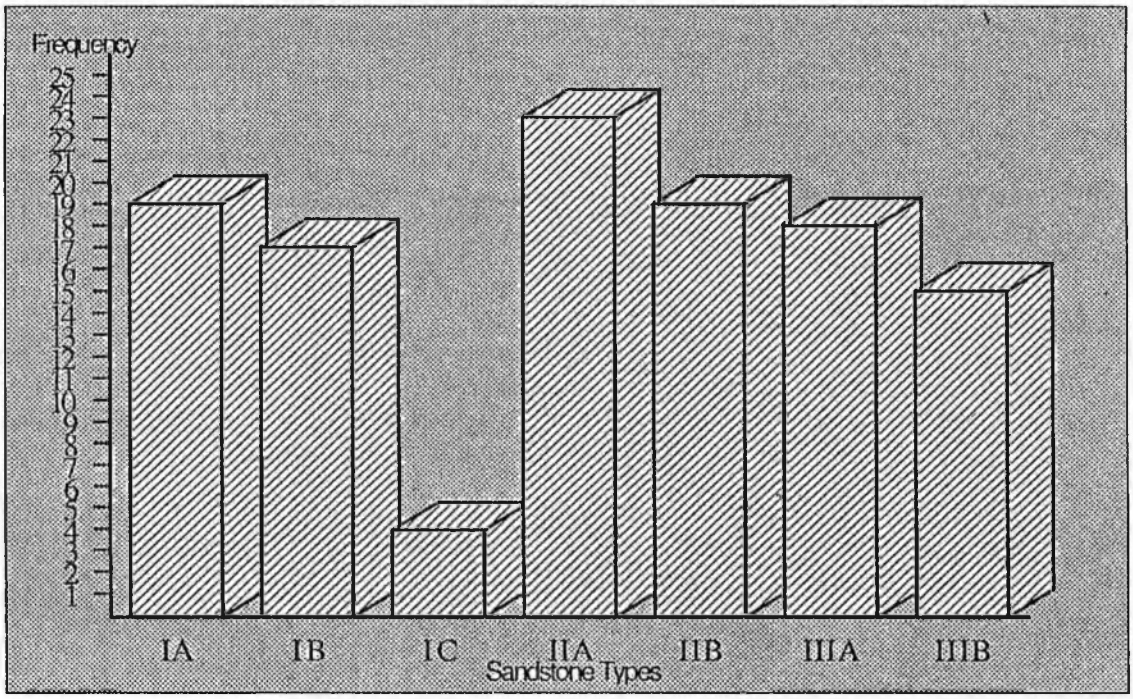

Fig. 3.10 Histogram showing frequency of sandstone types in Karoo sequence, Reith Bank-1 (Types in Fig. 3.9).

iii. amongst type I, sharp contacts are more frequent than gradational.

Some slight differences emerge when sandstones from the five members are compared (Table 3.2). Members 1 and 3 have distinctly more UF than UC. Both 2 and 4 have proportionately high numbers of cylindrical curves (IB- 7 and 5 respectively).

Table 3.2 Distribution of Karoo sandstone types based on the shape of gamma-ray curve (Types illustrated in Fig. 3.4).

Member	Bell					Funnel		Bell: Funnel
	IA	IB	IC	IIA	IIB	IIIA	IIIB	
5	5	2	-	2	4	1	4	6:5
4	-	5	-	1	2	3	1	3:4
3	4	3	1	8	3	3	3	11:6
2	5	7	3	7	4	6	5	11:11
1	5	-	-	5	6	5	2	11:7
Total	19	17	4	23	19	18	15	

3.2.4. Sandstone structures and paleocurrents:

Continuous dipmeter logs (four-arm) were examined for the Karoo sections between 6300 and 12,500 ft for Reith Bank-1 and between 7300 and 8900 ft in Seagull Shoals-1. Structural dip, read from shale-sandstone contacts, is 14° in Seagull Shoals-1 and 8° in Reith Bank-1, for the lower part of the sequence, both in a north-easterly direction (Figs. 3.2-3.7, 3.11). Between 6600 and 8800 ft in Reith Bank-1 dip tadpoles show a subhorizontal dips giving rise to

an angular difference of up to 14° which may be interpreted as an angular unconformity at 8800 ft. This unconformity has not been commented on in previous publications (Khanna & Pillay, 1986; Walton & Khanna, 1990) and this boundary is not reflected in lithological categories.

After these regional structural dips are removed from the observed dips within sandstones, orientations in Seagull Shoals-1 and the lower part of Reith Bank-1 are remarkably constant. A north-easterly dip of bedding is paralleled by a similar orientation of what is interpreted to be cross-bedding although local structural effects can not be entirely dismissed. The range of azimuths is generally restricted to 90° or less. Amongst the Reith Bank-1 sandstones, orientations vary with modes from SW or SSW (Table 3.3). Some minor variations occur. In Members 1, 2 and 5 of Reith Bank-1 a minor mode comes from the NW or NNW while in Seagull Shoals-1 a few readings are from the SE. A constant range of azimuths less than 90° is seen for sandstones below 8800 ft in Reith Bank-1, but between 6600 ft and 8800 ft a considerably wider spread of azimuth is seen (Figs. 3.2-3.7).

Individual structures picked out by red (successive dips increase progressively with depth and keep about the same azimuth) and blue units (successive dip decrease progressively with depth and keep about the same azimuth) occur at all stratigraphic levels (Table 3.3). If these do represent sedimentation features then the red units probably occur as channel fills and the blue as cross-lamination and bedding developed by dunes, or more likely by bars (Schlumberger, 1989). The former are more numerous in Member 5 and Seagull Shoals-1 sandstones while the latter tend to dominate in lower members in Reith Bank-1.

Table 3.3 Red and Blue units in Reith Bank-1 and Seagull Shoals-1 sandstones. (red-dip increases down section; blue-dip increases up section).

Well	Frequency of Units		Modal Direction	
	Red	Blue	Major	Minor
Seagull Shoals-1	10	5	SSW	SE
Reith Bank-1				
Member5	21	14	SW	NW
Member4	9	13	SSW	
Member3	11	9	SSW	
Member2	2	9	SW	WNW
Member1	8	10	SW	NW

Modal directions point to persistent currents from a south-westerly azimuth as read from the present position of the Seychelles for depths greater than 8800 ft in Reith Bank-1 while varying azimuths in all directions are seen for 6600-8800 ft. The minor occurrences of currents normal to the mode might reflect lateral filling of channels. Wider spreads of up to 180° have been suggested by Serra (1985) to be due to

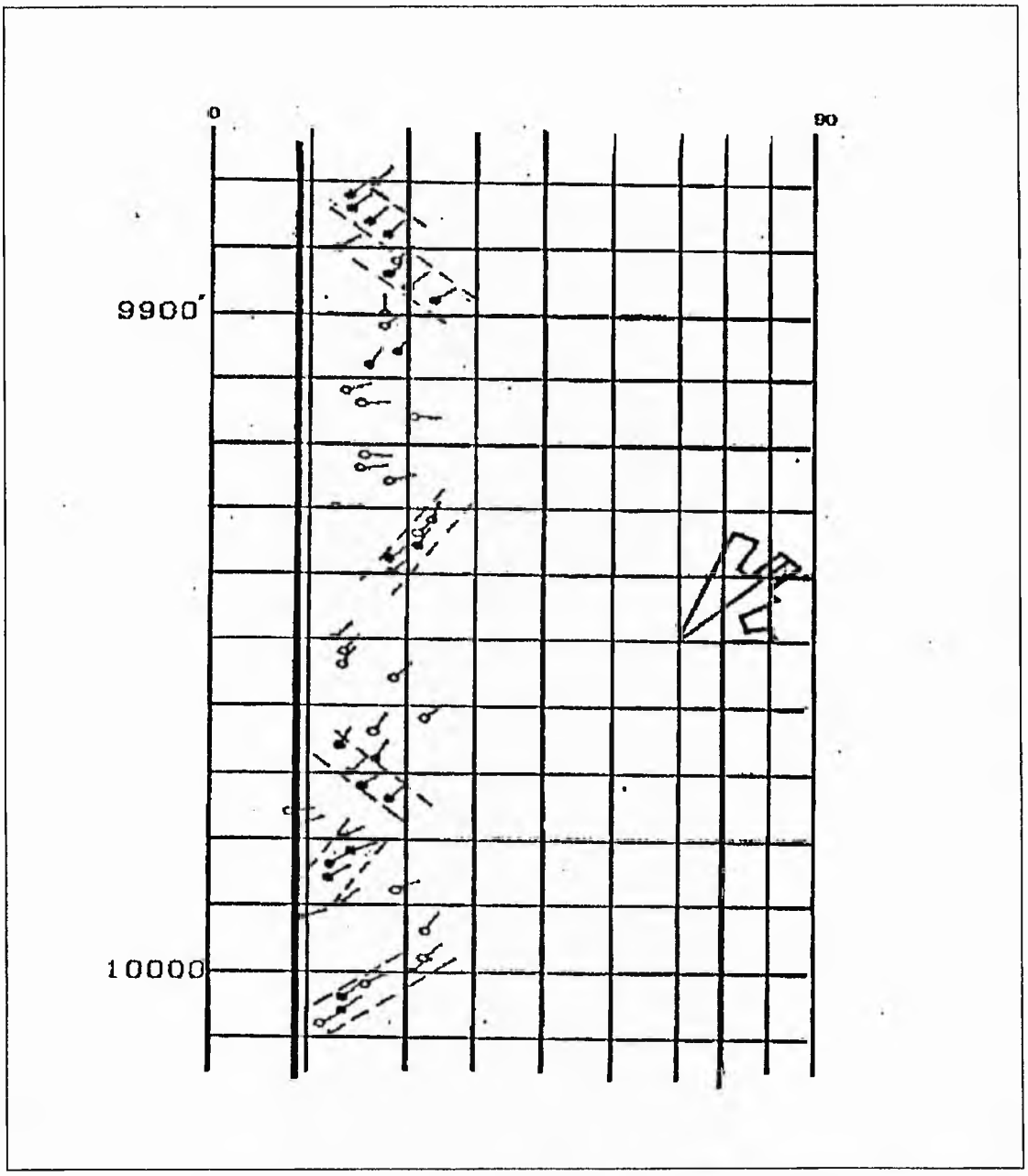

Fig. 3.11. Portion of Reith Bank-1 CLUSTER[R] program dipmeter profile (from 4-arm tool) illustrating dip directions and sedimentary structures picked out by red and blue units. Tectonic dip (8°) in solid line; The blank tadpoles are not definitive; Blackened tadpoles have been used to decipher blue and red units. Blue units: successive dips decrease progressively with depth and keep about the same azimuth; Red units: successive dips increase progressively with depth and keep about the same azimuth. The rosette gives the general direction of dip for tadpoles in the depth covering the diagram; each vertical line is 10°. (Source of dipmeter log: Seychelles National Oil Company).

"..orientations of cross bed dips as a response to trough shapes and variability of current flow".

3.3. DEPOSITIONAL ENVIRONMENT:

The sediments are clearly terrestrial in that the only fossils are non-marine, notably

palynomorphs. The common reddish or brown and mottled colours also point to frequent oxidising conditions associated with non-marine environments. Of possible terrestrial environments, proximal alluvial fan sites are unlikely in the general absence of conglomeratic beds; more than a solitary example of a possible mud flow would be expected in near-source areas. Sites further distant are indicated. The high S/M ratios and the mixture of non-graded, upward fining and upward coarsening sequences and sandstones with variable dips (Figs. 3.2-3.7) of members 1 to 4 suggest braided rivers on an alluvial plain below a fan (Fig. 3.12).

The persistent almost unimodal azimuths for the dips between 8800-12,000 ft in Reith Bank-1 might connote an aeolian deposit. However, the blue unit of aeolian deposits are more steep (angles of 30°) and their tails taper over long distances (Glennie, *pers. comm*, 1991; Serra, 1985) features not seen amongst the blue units of the Karoo sandstones. Aeolian deposits also show low radioactivity on gamma-ray (Serra, 1985) in contrast to the gamma-ray values for Karoo sandstones. Hence, the possibility of aeolian deposition of Karoo sequence between depths of 8800-12,000 ft at Reith Bank-1 is ruled out. Grain surface textures under scanning electron microscope would have further aided in

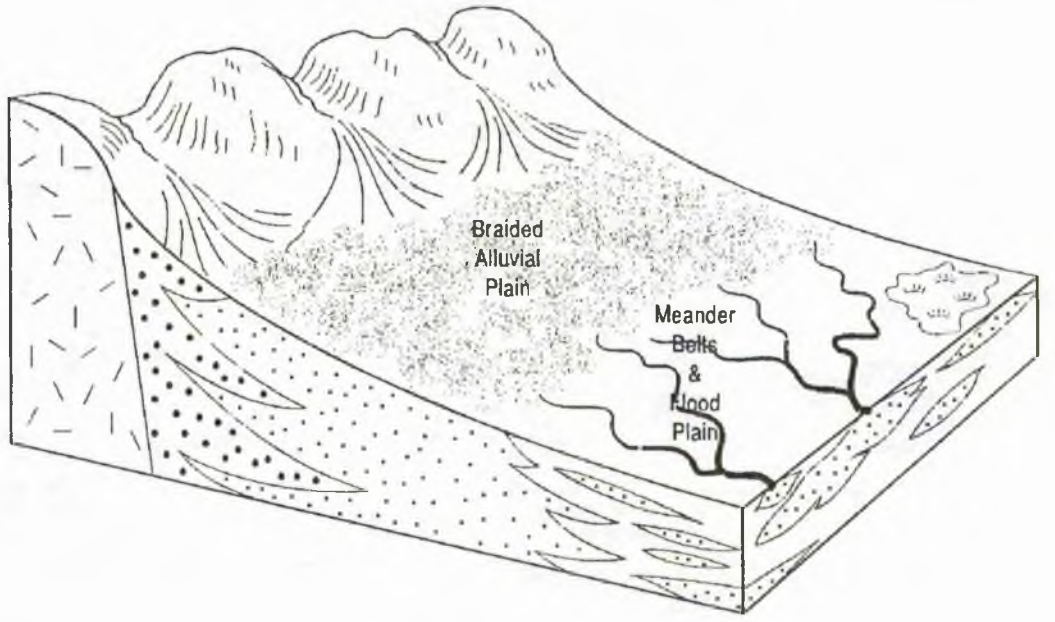

Fig. 3.12 Depositional model for Karoo sandstones. Members 2 and ?4, proximal alluvial plain; Members 1 and 3, distal alluvial plain; Member 5 and ?4, meander belt and flood plain.

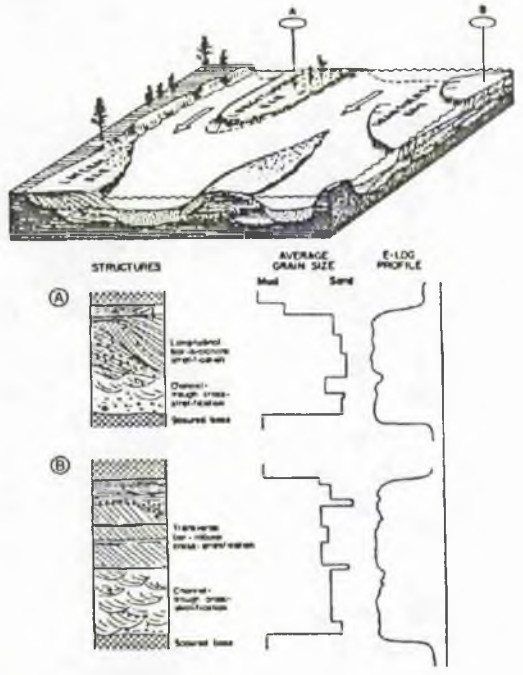

Fig. 3.13 Generalised depositional model, vertical sequences of grain size and sedimentary structures, and SP log profiles produced by a low sinuosity, braided channel. Sequence A is dominated by migration of a gravelly longitudinal bar. Sequence B shows deposition of successive transverse bar cross-bed sets upon a braided channel fill (from Galloway & Hobday, 1983).

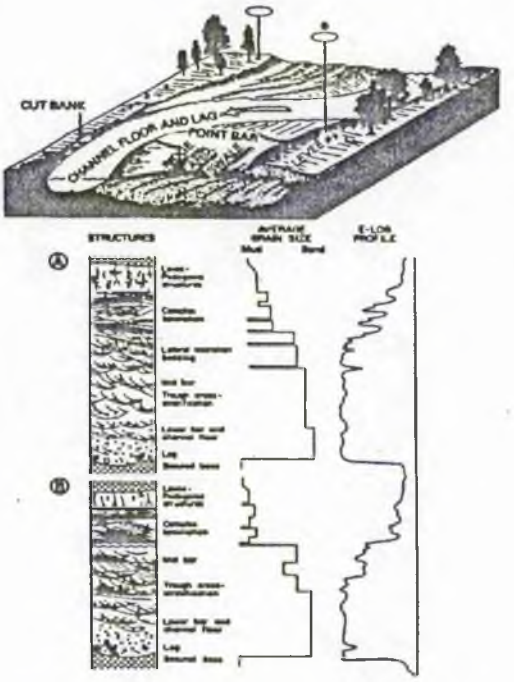

Fig. 3.14 Generalised depositional model, vertical sequences of grain size and sedimentary structures, and SP log profiles of a meander belt produced by a high sinuosity channel. Sequence A illustrates a complete fining upwards sequence typical of the mid- or downstream point bar. Sequence B shows the truncated vertical sequence commonly found in the upstream end of the bar (from Galloway & Hobday, 1983).

differentiating aeolian from fluvial conditions of deposition had intense diagenesis not taken place (see chapter 4).

A comparable sequence in the Karoo Supergroup of Southern Africa has S/M ratios of around 4.5 in proximal areas (estimated from diagrams in Turner, 1983) close to the Reith Bank-1 figures. Member 5 on the other hand has well separated sandstones and mudstones and a S/M ratio of 1.5. This suggests a change in conditions, evidently more distal deposition, perhaps within a meander belt.

The abrupt basal contacts of sands on dipmeter profiles are possibily related to erosional scoured surfaces. The cylindrical shapes of sand bodies as exhibited by wireline logs are characteristic of braided channels and their numbers are higher in Members 1-4 than in Member 5 (Table 3.2). Fining upwards sequence of meandering and braided channel sands often have a bell gamma-ray profile (Serra, 1985; Rider, 1990). The classic generalised depositional models (Fig. 3.13, 3.14) of Galloway & Hobday (1983) bring out these features very well.

The sinuosity and number of channels increased upwards greatly with Member 4 giving a greater spread of current azimuths. The graphical logging technique, though an excellent tool for facies analysis (Miall, 1984), is not of immense use in the study of architectural elements (Miall, 1985). Hence, no attempt has been made to apply the idea of architectural element analysis.

The lignites and carbonaceous shales of Member 1 might be taken to denote swamps associated with ponds of restricted size developed between successive levees of migrating channels. If these had any significant depths and permanence the swamps would have developed with predominantly upward-coarsening sequences. The relative scarcity of such upward coarsening sequences suggests that the sediments are overbank deposits formed in flood-plain areas.

The Molteno Formation in southern Africa has sands derived from highland sources some 100 km distant and some spread as far as 400 km across the basin (Turner, 1983). Paleogeographic considerations (see chapter 5) constrain estimates of the spread of the sands found in Reith Bank-1. For Member 1 topography may have been subdued and gravel fans restricted to say 20 km. Only on one occasion, drainage switching and/or climatic change, produced coarse sands. Rejuvenation of the source area would have increased the gravel spread to say 50 km or more and the coarse sands of Member 2 were deposited. Retreat of the source area, by erosion, brought on the more distal facies of Member 3. Renewed tectonic uplift caused a return to coarse sands in Member 4 with a subsequent reversion to fine-grain in Member 5. But conditions for the final member differed from those of the Member 3. Continued erosion and source retreat, perhaps accompanied by basin movements, leading to reduced slopes, produced a finer calibre of load, and perhaps the formation of meander-belts.

The distal nature of Member 5 is further reinforced by the incoming of marine conditions at the top of the Karoo succession. One feature which is not consistent with the interpretation of Seagull Shoal's Karoo as meander belt sediments is the dip log record which does not show the wide spread of sedimentary dips as shown by Member 5. However, Serra (1985) has suggested that not all meandering deposits show scattered dips on a dip log.

34. CORRELATION:

3.4.1. Regional Correlation:

The Karoo extends from its type area in South Africa to Kenya; it is also found in Madagscar and probably in Somalia, and is thought to be continental in origin. Studies based on stratigraphy, structure and tectonics of the conjugate East African and Madagascan margins have shown that the predominantly continental Karoo sediments do contain many marine intervals (Coffin, 1990). In South Africa the Karoo has been divided into lithological groups as Dwyka, Ecca, Beaufort and Stromberg. The Ecca Group of the northern Karoo basin in South Africa is marine-fluvio-deltaic in origin consisting of an argillaceous succession lying between the glacial sediments of the Dwyka Formation and the fluvial Beaufort Group (Van Vuuren, 1987).

The Adrigat Formation of North Somalia is fluvial in origin (as indicated by the absence of forams and microfossils) and has been taken to be Karoo equivalent (Nopec a.s., 1985). It consists of interbedded quartzitic sandstones and carbonaceous shales with calcareous and marly material. These strata are clearly different from the overlying marine carbonate strata of probably Jurassic age (*op. cit.*).

In Southern Somalia the Karoo includes mainly quartzose and "quartzitic" sandstone, nearly 120m thick, overlain by nearly 600m of dark shale with quartzitic streaks (Beltrandi & Pyre, 1973).

Karoo has also been reported from northern Malawi and Yemane (1987) has shown that the lower Beaufort (though upper Permian in age) along with the similar sequence in South Africa, to be lacustrine. The Karoo sediments here comprise glacial rudites, coal measures and lutites to calcilutites and carbonates (*op. cit.*).

Adrigat lithology is also reported from the Somalia-Ethiopia border, where its base is placed at the highest occurrence of red beds (Nopec a.s., 1985).

In Northern Kenya, the Karoo equivalent is the Mansa Guda group, lying between the basement and Jurassic carbonates (Ayers, 1952). The lithology is largely cross-bedded sandstone and conglomerate, about 600m thick with an unconformity/disconformity at the top (Joubert, 1960).

In coastal Kenya the Karoo has been divided into lower and upper parts (Walters & Linton, 1973). The lower portion contains thick feldspathic carbonaceous sandstone between thick shale beds, while the upper is dominated by sandstones completely barren of fossils.

In Tanzania, the base of the Karoo is marked by a basal conglomerate, while the rest

has been divided into two sandstone units separated by a siltstone with plant and reptile remains (Kent *et al*, 1971).

The Karoo group (or its equivalent) is best developed in the Morondova Basin along the Mozambique channel in Madagascar. The sediments range in age from Upper Carboniferous to Middle Jurassic and can be divided into the Sakoa series, the Sakamena series and the Isalo series (Ravelson *et al*, 1990). The three are separated from each other by angular unconformities.

3.4.2. Seychelles-Madagascar Correlation:

The Seagull Shoals-1 sequence is readily correlated with Member 5 of Reith Bank-1. In both localities the Karoo succession below marine Jurassic sediments comprises thick sandstones and mudstones. By coincidence both sequences are of similar (~1600 ft) thickness but individual sandstone horizons are not easily traced from one well to the other.

Wider lithological correlation is also possible (Table 3.4). In Madagascar basal tillites are followed in upward succession by a sequence containing coal horizons. This compares, further afield with coal-bearing measures lying above the Dwyka tillites in the type Karoo locality in southern Africa, where coarse-grained feldspathic sandstones are found in the upper part of the Supergroup (Ravelson *et al*, 1990).

Taking Member 1, Reith Bank-1 to be the correlative of the Madagascar coal-bearing sequence would suggest that glaciogenic or related sediments would occur lower down. Reith Bank-1 well may have penetrated almost all of the local Karoo succession. This might be the case since Robertson Research International (1981a) reported Permian palynomorphs from Member 1. However, the Permian forms were regarded as derived and the in-situ forms taken to be no older than Middle or Late Triassic; if this be valid then the lignite horizons of Member 1 represent a similar but much younger environment than the coal measures of southern Africa and Madagascar.

Table 3.4 Karoo correlation chart showing correlation of Seychelles Karoo succession with South Africa. and Madagascar. Member 5 and 4 together form megacycle III, Member 3 and 2 form megacycle II, while Member 1 is the remnant of megacycle I.

Age		Southern Africa (Smith, 1990)		Madagascar (Morondova Basin) (Ravelson et al, 1990)			Seychelles (Walton & Khanna, 1990)
J	L			Marine Transgression			
U							Member
R					III		5
A	M					Terrestrial	
S					II	Sandstones	4
S		Stromberg	Basalts, Terrestrial	Isalo Group		and mudstones	
I	E	Group	sandstones and	(up to 10,000'			3
C			mudstones	in wells)	I	Marine sandstone	
						and shales with	2
T	L	Beaufort	Fluvio-lacustrine			bituminous	
R		Group	sandstones and			sandstones	1
I				Sakamena		Sandstones and	
A	M			Group		mudstones	?
S				(up to 3000'			
S				in wells)			
I	E						
C							
P							
E		Ecca	Sandstones,	Sakoa		Red sandstones	
R	L	Group	shales and coal	Group		and mudstones.	
M			measures	(up to 6000')		Black shales and	
I						coal measures	
A							
N	E						
CARB		Dwyka Tillite		Tillite			

CHAPTER 4: PETROLOGY & DIAGENESIS

(with 28 figures, 5 tables and 35 plates)

The aim of this chapter is to study the petrological details of the sandstones in order to determine their probable sources as well as their depositional and diagenetic history.

4.1. METHODOLOGY:

Thirteen core samples from Seagull Shoals-1 and 28 from Reith Bank-1 were studied as thin sections under optical microscope and scanning electron microscope (SEM). Energy-dispersive elemental analysis (EDAX) was routinely used to study the composition of specific minerals under SEM. The sections were impregnated with blue araldite and stained for carbonates with alizarin red S and potassium ferricyanide. No potassium feldspar stain was used. Analysis on clays was carried out using the X-ray diffraction (XRD) on 9 samples from Seagull Shoals-1 and 17 samples from Reith Bank-1. Fifty two thin sections from Reith Bank-1 were made available by Robertsons Research Ltd. for this study. These sections were neither impreganted with blue araldite nor stained for carbonates. They were studied under the optical microscope. Modal analysis was carried out by point counting 300 points per section ensuring that nothing was counted more than once. Modal analysis for a four variable plot of the nature of the quartz grains in the populations in Karoo sandstones from Reith Bank-1 well was carried out by point counting 100 points per section. The samples selected for the analysis were 0.25-0.50 mm in grain-size and are largely quartzose as suggested by Basu (1985). The samples did not show any evidence of tectonic strain, which might induce ambiguous results (Basu, *pers. comm.*, 1991).

Four samples from Seagull Shoals and seven from Reith Bank-1 were also studied as polished sections using the back-scattered electron (BSE) imaging mode of the electron micro-probe. Quantitative analyses were made of cements, clays and feldspars. The same sections were studied using a cold cathode luminescence microscope to determine cementation histories and provenance of the sandstones.

Reflected light was used to differentiate between various iron oxides and sulphides.

Twenty five samples were selected for whole rock geochemical analysis. The criteria for sample selection were based on the availability of sufficient amounts by weight rather than any particular depth consideration.

4.2. PETROGRAPHY:

4.2.1. Texture:

The grain-size of the sandstones examined varies from fine to very coarse with scattered pebbles (Plates 4.1, 4.2). The samples from the upper part of Reith Bank-1A well have a variable sorting from poor to good with very coarse samples showing poor sorting, while the relatively finer ones show moderate to good sorting. The coarse-grained samples from Seagull Shoals-1 and below 10,000 ft in Reith Bank-1A are moderately sorted, sometimes bi-modal with predominantly larger grains and a finer ground. Assessment of original shape is virtually impossible, the quartz having syntaxial overgrowths and often the feldspars having been corroded. Where original shapes are seen, quartz grains tend to be sub-angular or sub-rounded and feldspars angular.

Overgrowths have also obscured the original nature of the packing but the amount of quartz cement suggests that the coarser sediments were deposited as loosely packed open frameworks with little interstitial matrix. All the finer-grained samples have abundant clay. The sandstones examined exhibit tight packing with some quartz mosaics (Plate 4.3).

Macro-porosity (interparticle, i.e. between particles), is low, usually less than 10%. Primary porosity has been reduced not only by quartz but also by carbonate cement and authigenic clays (Plates 4.4-4.6). Rarely primary pores can be seen. Those pores which remain tend to have triangular or polygonal shapes bounded by overgrowth faces (Plate 4.5). The post-depositional leaching of feldspars and lithoclasts have given rise to secondary porosity. Secondary porosity created in such a way produced redistributional secondary (RDS) porosity (Giles & de Boer, 1990) resulting in oversized pores but these have generally been filled by carbonate and/or clay. The preserved pores show reduced intergranular to enlarged intergranular and oversized pore textures of Schmidt & McDonald (1979). Fracture pore textures (*op. cit.*) are also present in the samples but it is not always possible to distinguish original fractures from those produced by sample collection and section preparation.

Within the clay-filled pores some secondary microporosity is retained amongst the clay crystals. Some corroded feldspars are skeletal and provide further microporosity (intraparticle or within particle porosity) (Plate 4.4). As viewed in thin section both micro- and macropores seem to be poorly interconnected.

Low porosities as seen in thin sections may not be the whole story, however, higher

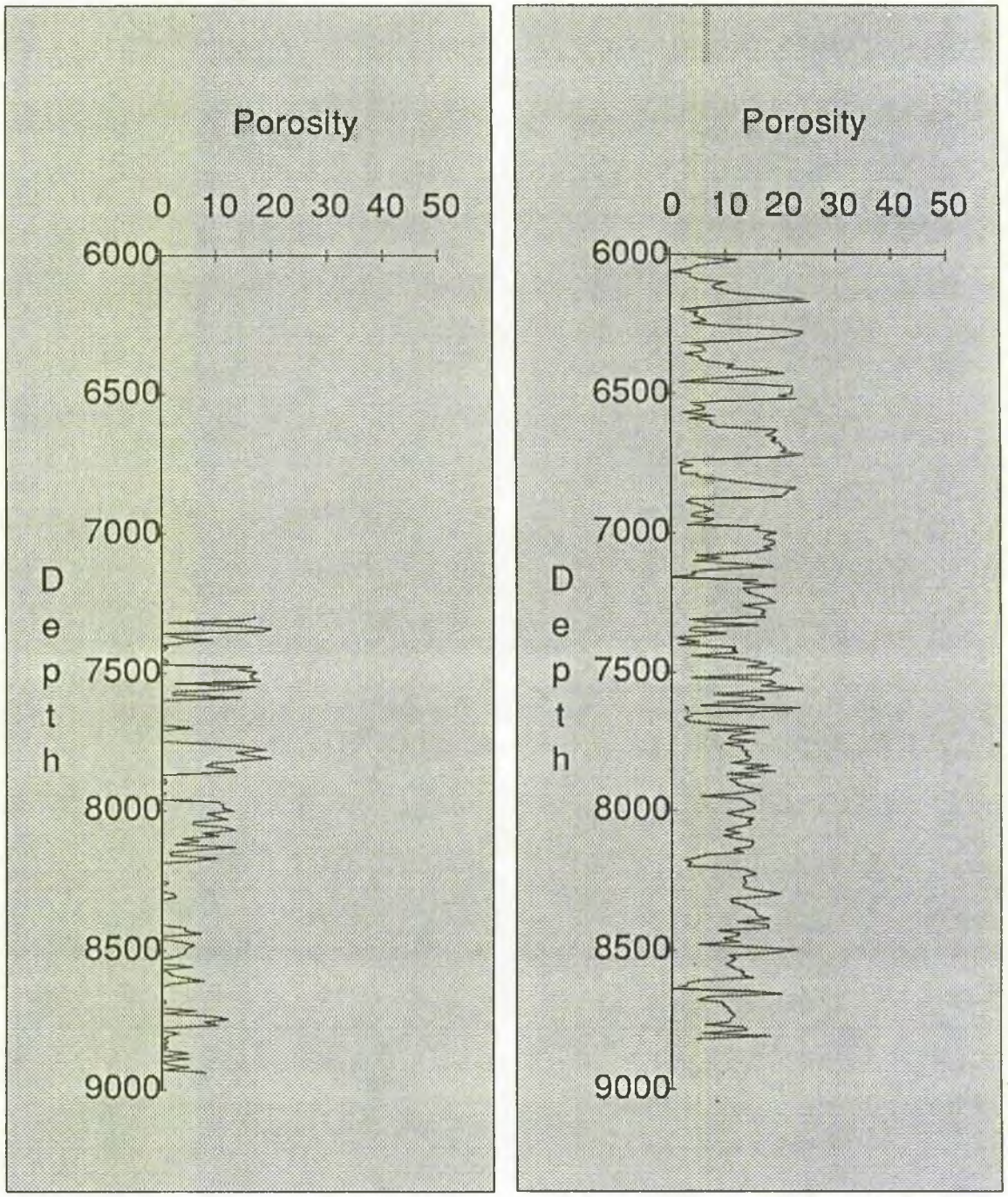

Fig. 4.1 Porosity variation with depth (ft) in (a) Seagull Shoals-1, and (b) Reith Bank-1 wells. The values are obtained from the computer processed information data of Schlumberger for depths between 7300 & 9000 ft for Seagull Shoals-1 and 6000 & 9000 ft for Reith Bank-1 wells. The sample points are chosen at 10 ft intervals. It can be seen that there are horizons with porosity values up to 20% alternating with values as low as 0-less than 1% in both the wells.

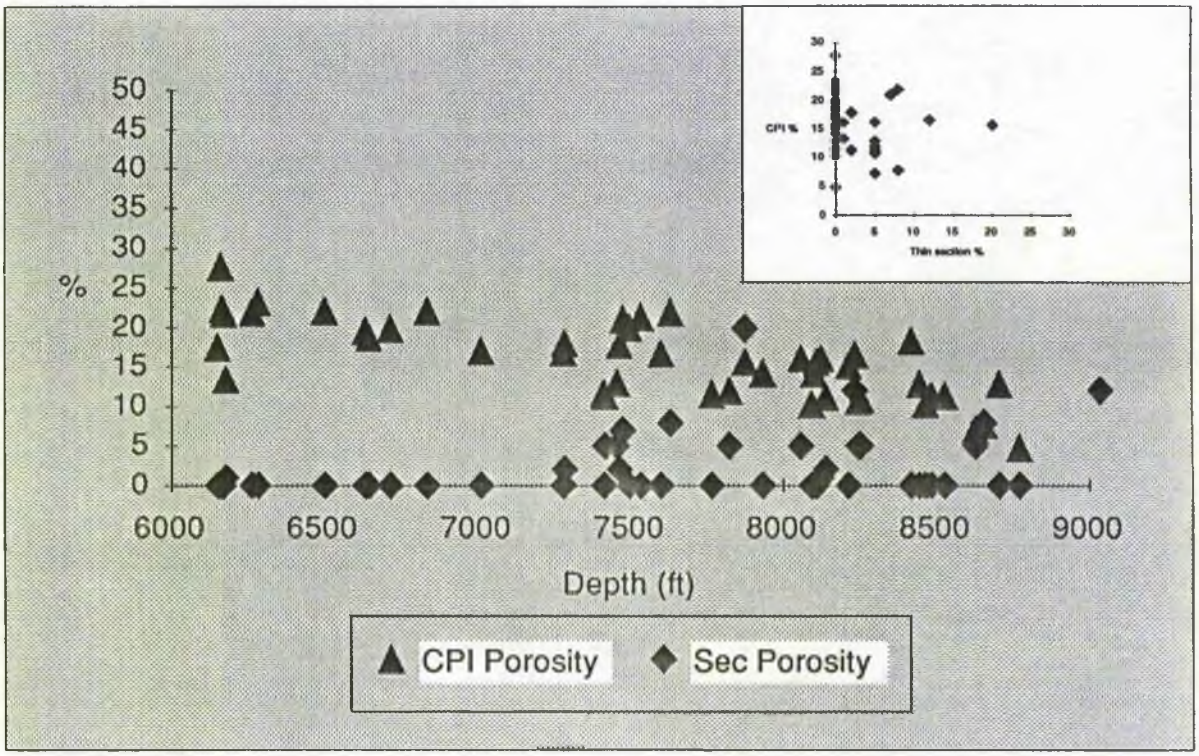

Fig. 4.2 Variation of porosity with depth (ft) for Reith Bank-1 well. CPI porosity: values are taken from the computer processed information, whereas total thin section (Sec) Porosity values are obtained from representative modal analysis of porosity in thin sections. Inset shows a cross plot between total porosity obtained from modal analysis in thin sections against CPI porosity. No distinct trend can be seen.

values, around 20% are indicated at various horizons (Fig. 4.1, 4.2) by petrophysical logs and flow tests at between 6152-6182 ft; 8060-8090 ft; 8545-8575 ft & 9235-9255 ft, have yielded significant flow rates. The apparent lack of porosity visible in thin sections contrasts with significant flow rates measured by drill stem tests. Microporosity associated with kaolinite may contribute to the permeability, and flow rates may be enhanced by fracturing both of sandstones and mudstones. However, it is not always possible to distinguish original fractures from those produced by sample collection and thin-section preparation. Another possibility is that cemented and uncemented zones alternate in the sandstones (Fig. 4.1) and only cemented samples were obtained (Fig. 4.2).

4.2.2. Mineralogical Composition:

Primary components consist of grains of quartz, feldspar, mica (Plates 4.1-4.4), clays and scarce heavy minerals such as zircon, tourmaline, garnet and opaques; lithoclasts are also present but rare in all but the coarsest

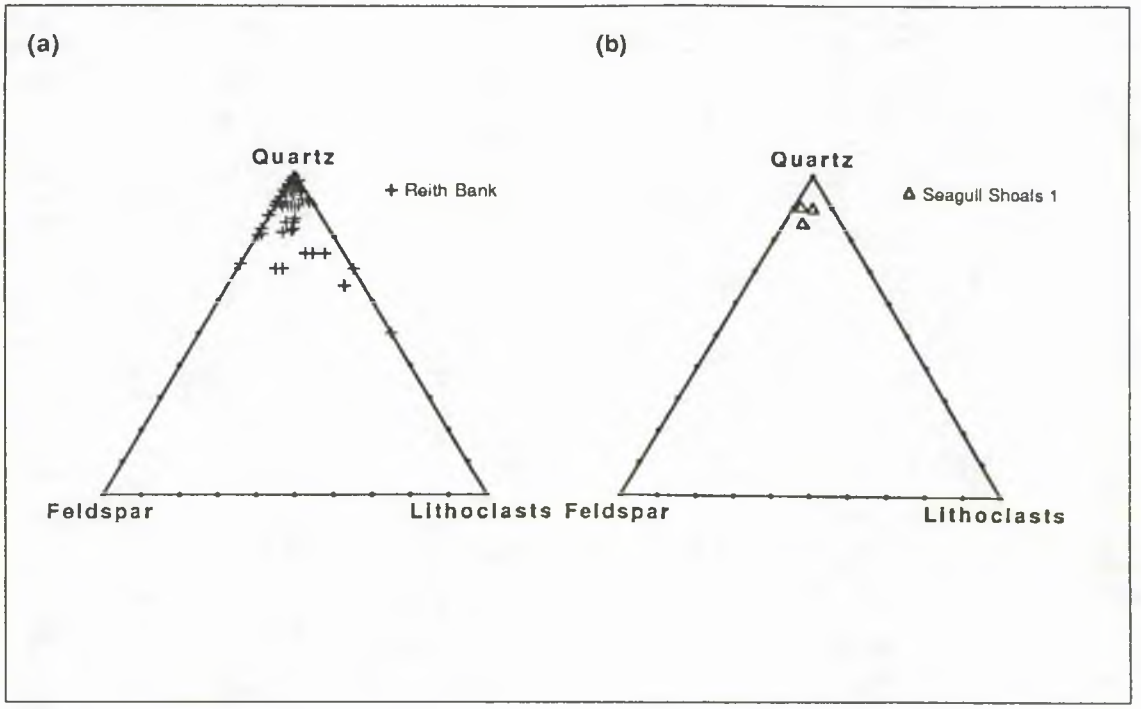

Fig. 4.3 Q-F-L plot for Karoo sandstones from (a) Reith Bank-1, and (b) Seagull Shoals-1 wells. Each corner represents 100%.

conglomeratic sandstones (Table 4.1). The sandstones classify as arenite and feldspathic arenite (Fig 4.3).

Authigenic components are silica (mostly as overgrowths but also as tiny authigenic crystals) clays, carbonates and opaques.

4.2.2.1. Quartz:

Quartz grains are predominantly monocrystalline with non-undulose extinction. Modal analysis on monocrystalline low extinction, monocrystalline undulose extinction and polycrystalline grains with less than 4 units and more than 4 units show that the grains are largely monocrystalline and have extinction angles of less than 5 degrees (Fig. 4.4). The analysis was

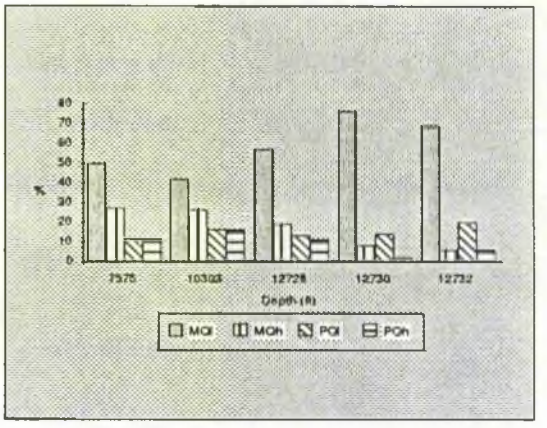

Fig. 4.4 Modal analysis of monocrystalline low extinction (MQl), monocrystalline undulose extinction (MQh) and polycrystalline grains with less than 4 units (PQl) and more than 4 units (PQh) showing higher percentage of MQl grains in Reith Bank-1 well.

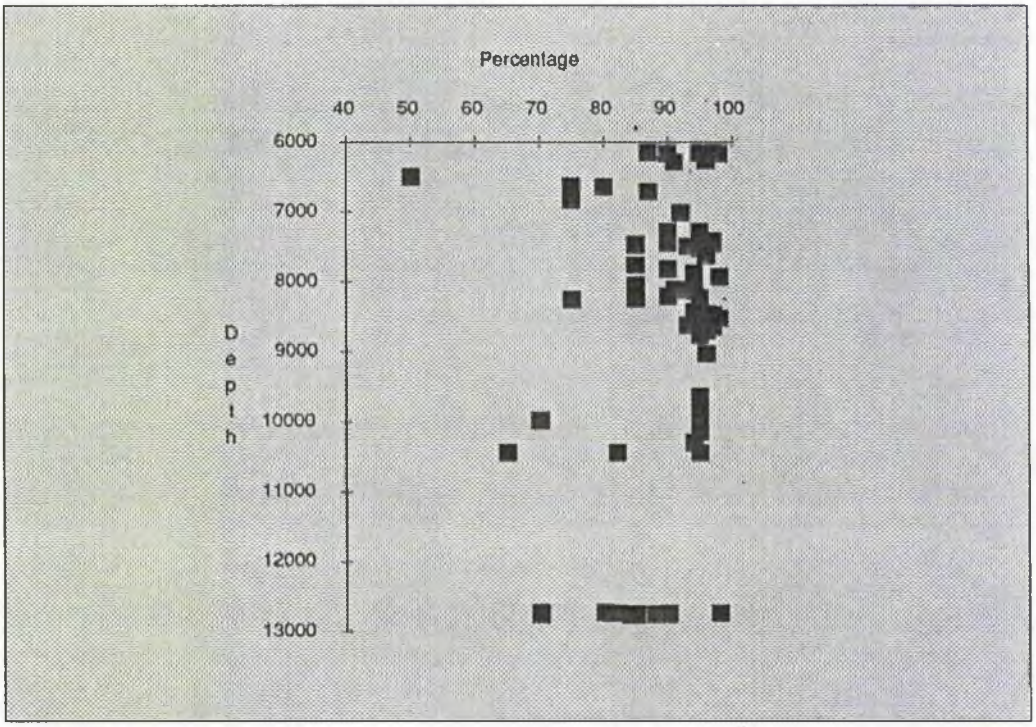

Fig. 4.5 Quartz distribution in grain percentage of rock with depth (ft) in Reith Bank-1 well. Point count data (300 points) displayed graphically.

restricted to only five samples because of the grain-size restriction of 0.25-0.50mm as discussed earlier.

Under cathodoluminescence quartz glowed in violet and brown colours, but no overgrowth patterns could be picked out (Plates 4.7, 4.8).

Polycrystalline clasts are usually coarse-grained with few units; occasionally they are quartzitic with many small, sutured, elongate crystals showing undulose extinction (Plates 4.3, 4.9).

With overgrowths, the quartz percentage varies from 50% to 80% of the whole rock (Fig 4.5). Samples which show a lower percentage of quartz have higher amounts of lithoclasts/feldspar.

4.2.2.2. Feldspars**:**

Feldspars comprise plagioclase, orthoclase and microcline, in that order of abundance with the last very rare (Plates 4.1-4.3, 4.9, 4.10). The plagioclase is usually oligoclase-andesine. Grains are commonly altered and this varies from a slight dustiness, through grains with kaolinite or micaceous clays developed, to skeletal grains. Feldspars luminesced in a bright blue colour under cathodoluminescence (Plate 4.8). They account for less than 10% in most samples except for

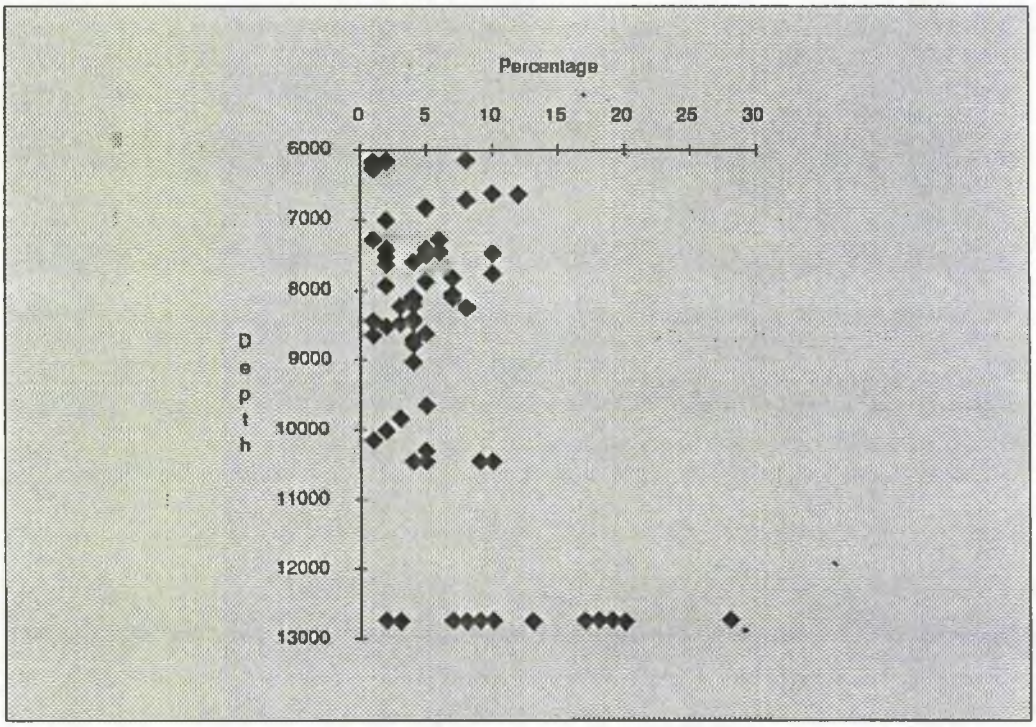

Fig. 4.6 Feldspar distribution in grain percentage of rock with depth (ft) in Reith Bank-1 well. Point count data (300 points) displayed graphically.

those from below 12,000 ft in the Reith Bank-1 well where the sandstones may contain as much as 25% of feldspar (Fig 4.6).

4.2.2.3. Mica:

Mica content is controlled by grain size. Abundant in the finer samples, it is represented by only one or two flakes in the coarser grains. Both white and brown mica occur with the latter prominent although, usually degraded, in fine-grained sandstones (Fig 4.7).

4.2.2.4. Lithoclasts:

Lithoclasts account for less than 5% of the rock, except at conglomeratic levels, where they reach up to 50%. They comprise the coarser quartz-feldspar types along with fine-grained altered feldspathic and quartz-feldspar porphyry, volcanogenic fragments (Fig 4.8).

4.2.2.5. Cements and clays:

Silica, as overgrowths, is the most abundant authigenic mineral although it is impossible to measure its actual amount by optical microscopy. Occasional 'dust lines' around original grains reveal thick overgrowth rims (Plates 4.9, 4.10). Coalescing overgrowths have straight, slightly curved or stepped boundaries with some triple points. Occasionally a strongly convex boundary suggests some pressure

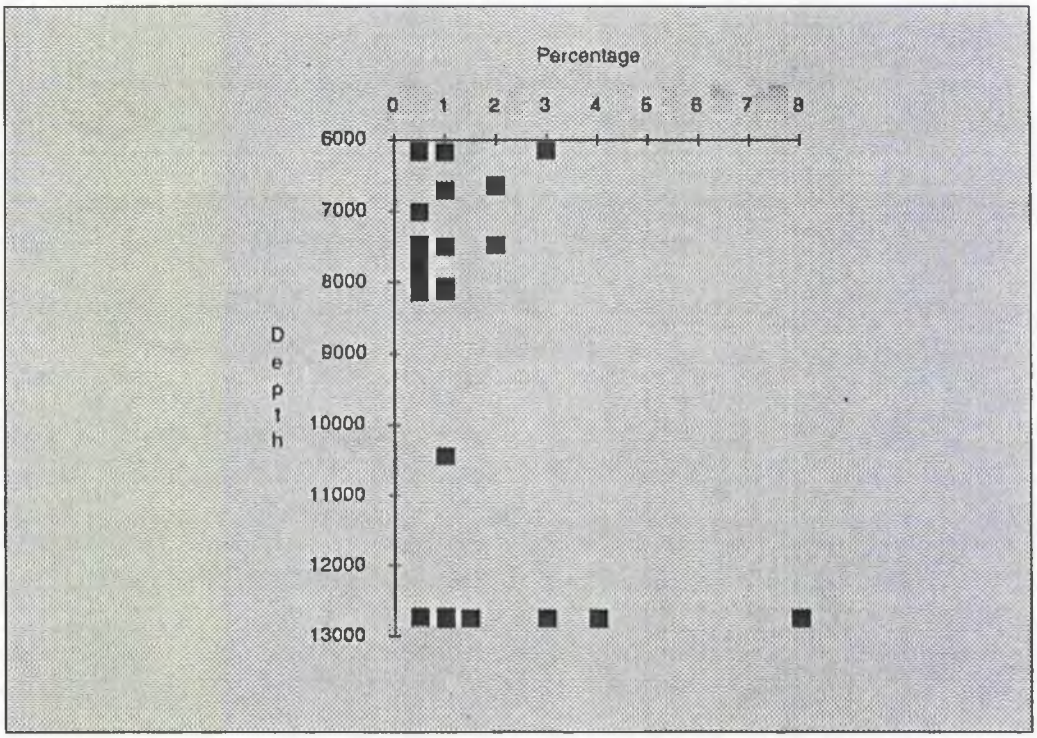

Fig. 4.7 Mica distribution in grain percentage of rock with depth (ft) in Reith Bank-1 well. Point count data (300 points) displayed graphically.

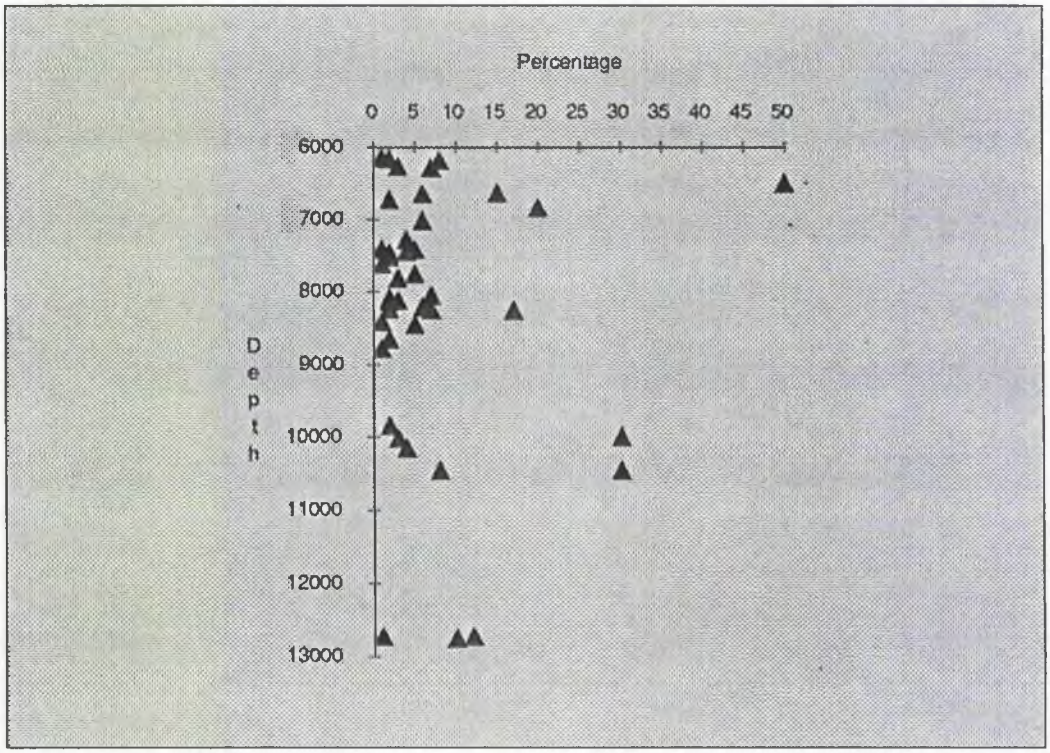

Fig. 4.8 Lithoclasts distribution in grain percentage of rock with depth (ft) in Reith Bank-1 well. Point count data (300 points) displayed graphically.

solution but this is a minor feature. Overgrowth has penetrated and filled interstices amongst quartz and feldspar grains as well as forming scalloped boundaries with corroded feldspars. Many areas of some thin sections are entirely occupied by coalescing grains forming non-porous quartz mosaics of grains and cement. These mosaics can often be subdivided into an aggregate of coarser or finer units. As well as the overgrowths, though scarce in amount, quartz also forms small euhedral crystals (<40u) amongst clays. Preliminary results from fluid inclusions present along the dust-lines indicate a temperature of 100°C.

Clay is very common (Table 4.2; Plates 4.4, 4.6, 4.9); indeed it is often so abundant, especially in fine-grained samples, that SEM analysis is rendered very difficult; grains are obscured and the only texture visible is one of a felted nature formed by anastomosing clay flakes. Most of this clay is detrital illite. Authigenic illite, illite-smectite, kaolinite and chlorite also occur (Plates 4.4, 4.6, 4.10, 4.11-4.13, 4.15, 4.16; Figs. 4.9-4.11). In the finer grained sandstones the clays may reach 30% of the rock. In coarser samples the proportion is usually less than 10%. Illite occurs in most samples, kaolinite is restricted to Seagull Shoals-1, and Members 4 & 5 of Reith Bank-1, while chlorite is confined largely to Member 1 of Reith Bank-1.

Illite occurs as flakes or fibres in three modes of occurrence; as seams or fringes between grains (especially in finer-grained samples) (Plates. 4.11, 4.14); as flakes within partially altered feldspars; and in aggregates with or without chlorite (Plate 4.16). The aggregates have a similar size to associated clasts and therefore probably represent replaced or removed silicates or rock fragments. Authigenic illite has a typical 'hairy' form and mixed layer illite-smectite, occurring in Seagull Shoals-1 and Reith Bank-1 (in depths below 12,000 ft) has its usual honeycomb texture.

Chlorite forms distinct fringes (up to 60um) to grains in Reith Bank-1 samples in the interval 12,726 ft to 12,755 ft. It also forms aggregates either singly or in intimate association with illite. Some chlorite present in upper members is detrital, occurring partly as degenerating flakes and partly formed from degenerated biotite, rather than fringes.

In Seagull Shoals-1 samples, kaolinite fills pores, many of which have been enlarged by corrosion and removal of primary grains (Plates 4..4-4.6, 4.14, 4.15). Its characteristic 'books' (up to 20um long) are made up of pseudohexagonal crystals, 15um to 20um in diameter and 0.1um

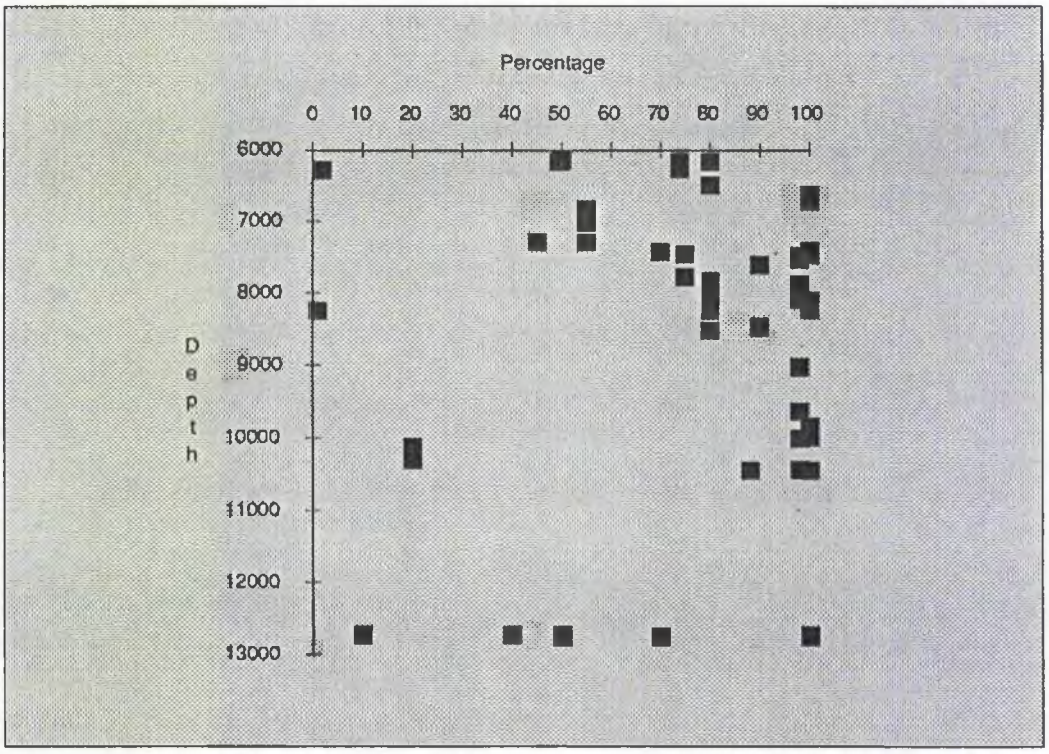

Fig. 4.9 Illite distribution in the clay fraction of rocks with depth (ft) in Reith Bank-1 well. Modal analysis data displayed graphically.

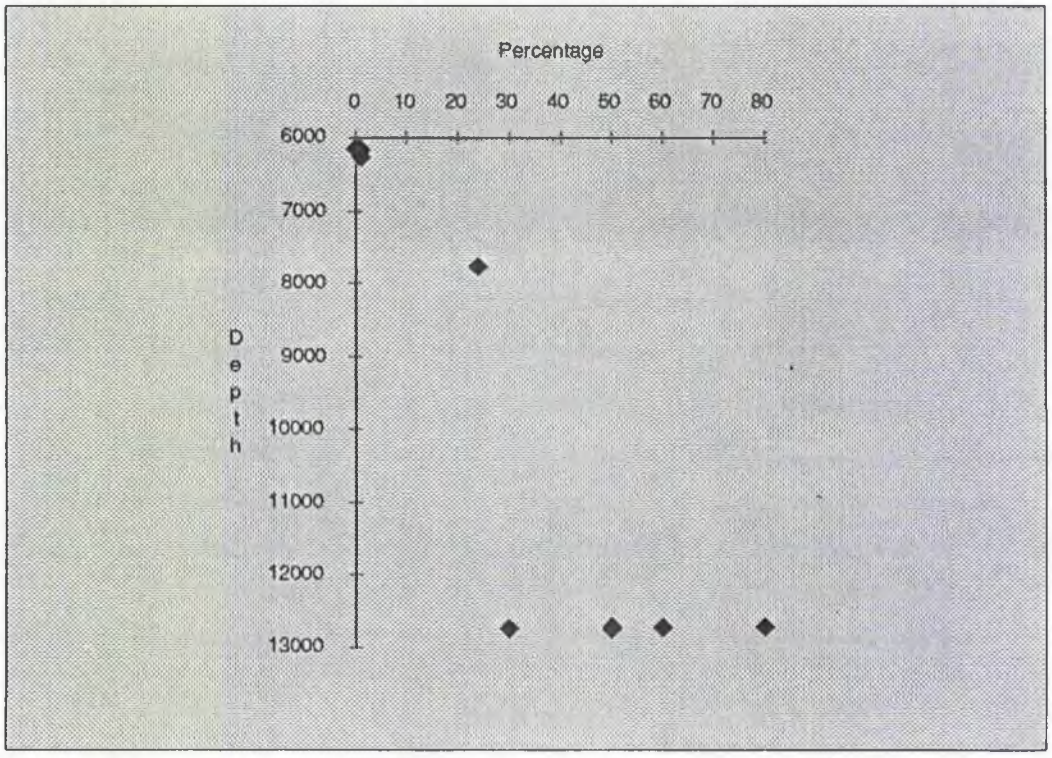

Fig. 4.10 Chlorite distribution in the clay fraction of rocks with depth (ft) in Reith Bank-1 well. Modal analysis data displayed graphically.

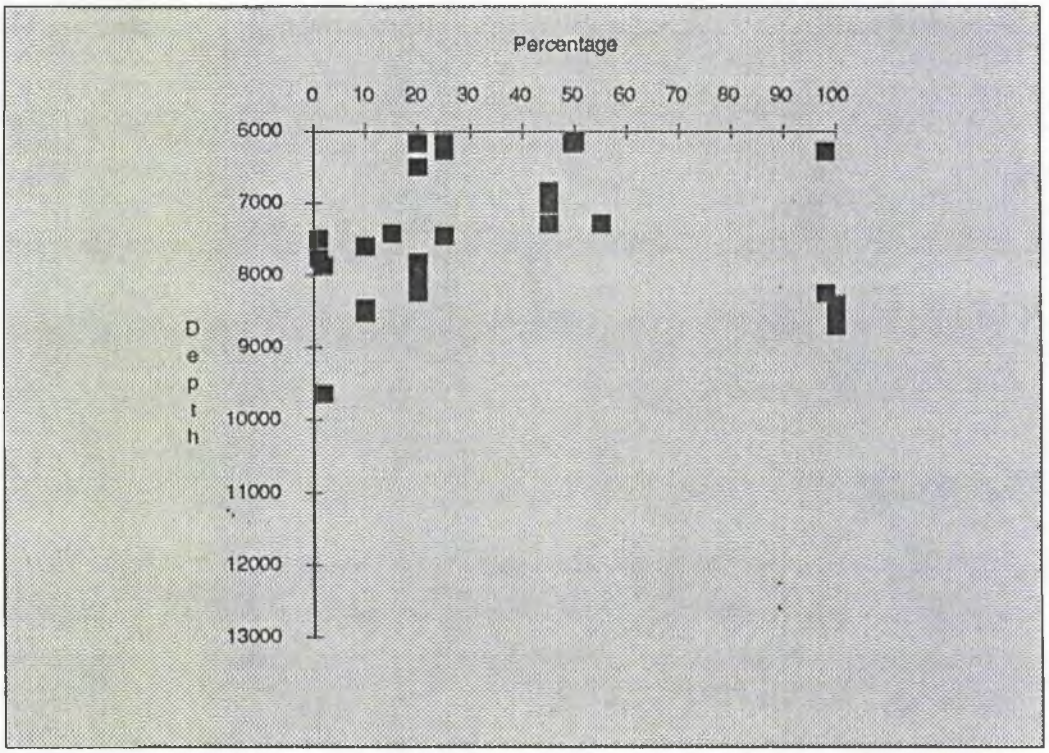

Fig. 4.11 Kaolinite distribution in the clay fraction of rocks with depth (ft) in Reith Bank-1 well. Modal analysis data displayed graphically.

thick.

Carbonate occurs in almost every sample in small amounts, usually less than 10% but exceptionally up to 50%. It forms in large (<2 mm) widely spaced patches which are made up of coarse-grained, sometimes poikilotopic crystals up to 1 mm across (Plates 4.17-4.20). The patches are often larger than the grains making up the sand. Evidently primary constituents have been removed and replaced- processes which are also indicated by corrosion especially of feldspars but also, to a lesser extent, of quartz (Plates 4.17, 4.18). Sometimes the carbonate even penetrates and cuts across quartz grains (Plate 4.20).

Other coarse-grained carbonate fills remnant angular pores margined by quartz overgrowth faces. Occasionally well formed, but smaller rhombs are found (Plates 4.21, 4.22). The carbonate stains blue in the thin section indicating that it is ferroan dolomite (Plates 4.28, 4.29). This is confirmed under SEM which has also revealed occasional coarse-grained calcite rather than dolomite (Plates 4.21, 4.22). Due to high percentage of manganese in carbonate luminescence colours of carbonate are bright orange (Plates 4.23, 4.24). Some patches of bright and faint glows could be identified, suggesting some form of zonation.

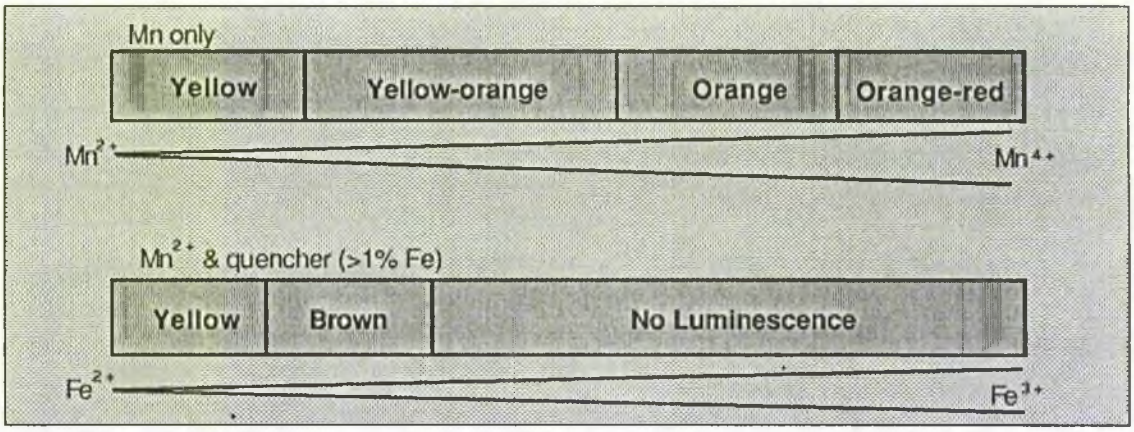

Fig. 4.12 Relationship of cathodoluminescence colours of calcite and valence state of manganese and iron. (from Matter & Ramseyer, 1985 based on data by Amieux, 1982 and Schrank & Friedman, 1975).

Yellow to orange-red changes in luminescence colours in calcite cements of the Karoo sandstones are also due to amounts of Mg^{2+} activator or the valence state of manganese (Fig. 4.12) (Matter & Ramseyer,1985).

Sommer (1972) has shown that yellow or red luminescences of dolomite are due to the presence of Mn^{2+} in Ca^{2+} or Mg^{2+} sites. Since, the dolomite cement in the Karoo sandstones shows luminescence in yellow it can be said that Mn^{2+} is present in Ca^{2+} sites which is confirmed in probe results, as discussed later.

The carbonate shows a complex pattern, however, broadly two stages can be seen in Seagull Shoals-1 and Reith Bank-1, with a possible third stage existing in the Reith Bank-1 samples (Plates 4.25-4.30; Figs. 4.13, 4.14). Across a large area of carbonate (Plates 4.26, 4.27) the strongly zoned peripheral portion tends to have a lower proportion of iron (Fig 4.14) relative to the central (later) portion. In addition there is internally a complicated boundary between darker and lighter grey which suggests a dissolution phase before the final precipitation of dolomite enriched in iron relative to magnesium. Due to the dissolution phase the iron rich dolomite also precipitated towards the outer margins around the peripheral zones (Plate 4.26). The rhombs by contrast, show the early zoned phase in the core passing out to lighter tones without any discontinuity (Plate 4.28). If the darker zones were contemporaneous with the early zones of the anhedral carbonate then the rhombs were unaffected by the phase of dissolution.

The first-stage carbonate shows well formed zones and has a lower content of iron than the second stage (Plates 4.26, 4.27; Fig.

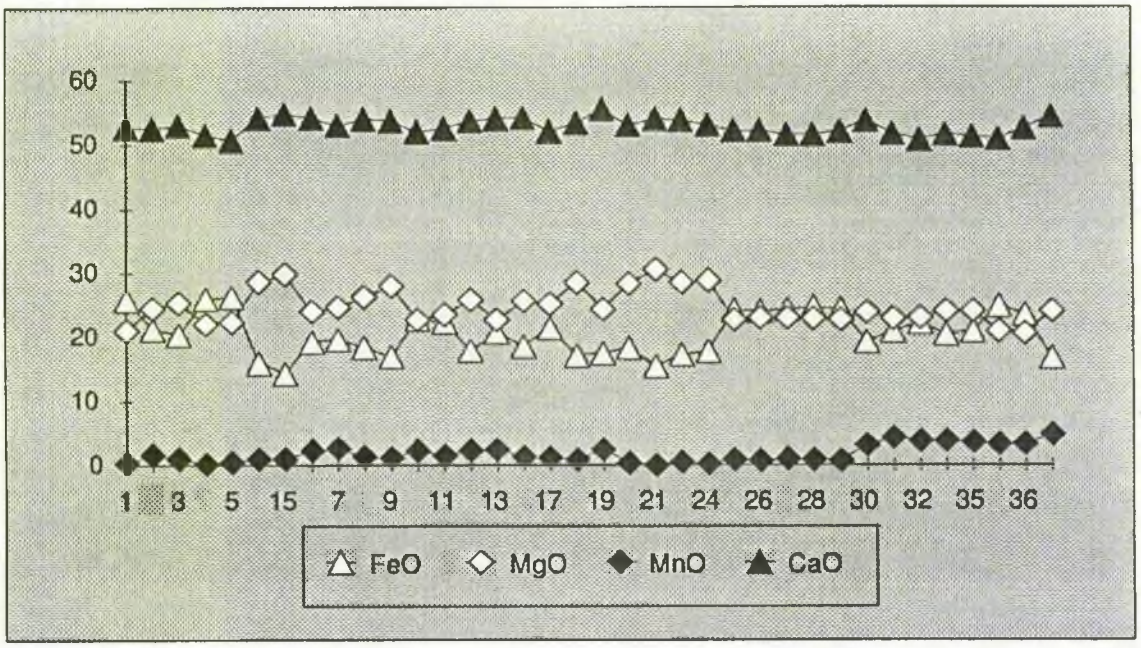

Fig. 4.13 Oscillatory zonation in carbonate cement (c.f. plate 4.26). Spot analysis of ferroan-dolomite from Rim (near origin of graph) to centre. The numbers correspond to the spot sites where analysis was carried out and refer to Plate 4.26. Spots 2-3, 6-9, 12, 14-16, 18-24 fall under stage I, while spots 4-5, 10-11, 13, 17, 25-36 fall under stage II carbonates. No attempt has been made to show gradation from rim to centre.

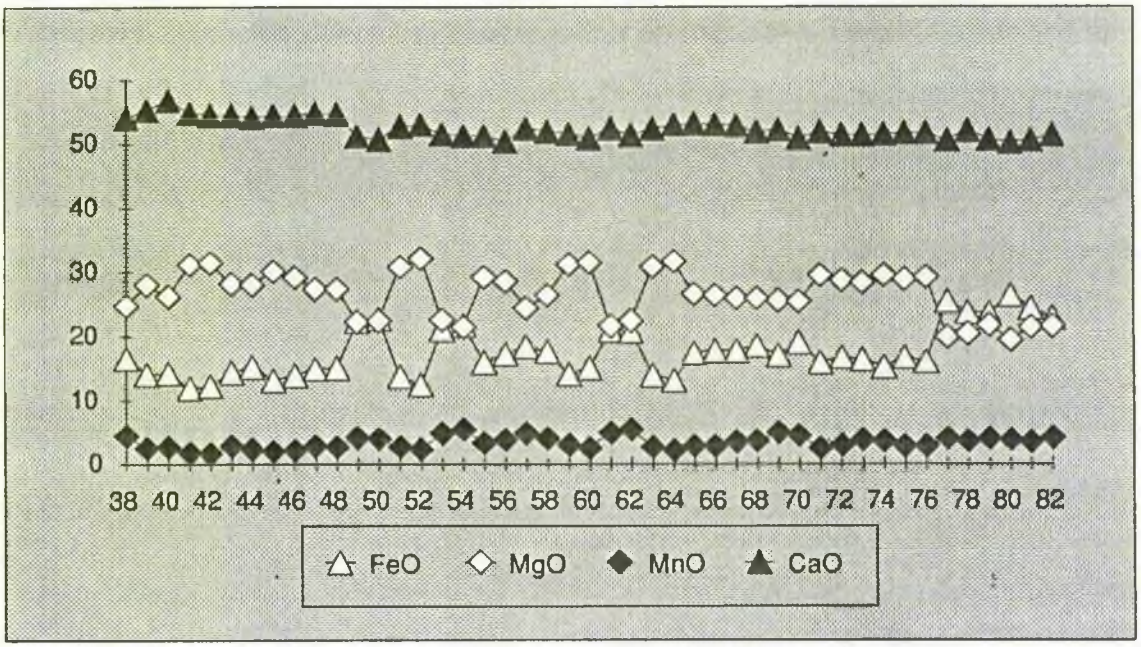

Fig. 4.14 Oscillatory zonation in carbonate cement (c.f. plate 4.27). Spot analysis of ferroan-dolomite from Rim (near origin of graph) to centre. The numbers correspond to the spot sites where analysis was carried out and refer to Plate 4.27. Spots 38-47, 51-52, 55-60, 63-76 fall under stage I, while spots 48-50, 53-54, 61-62, 77-82 fall under stage II carbonates. No attempt has been made to show gradation from rim to centre.

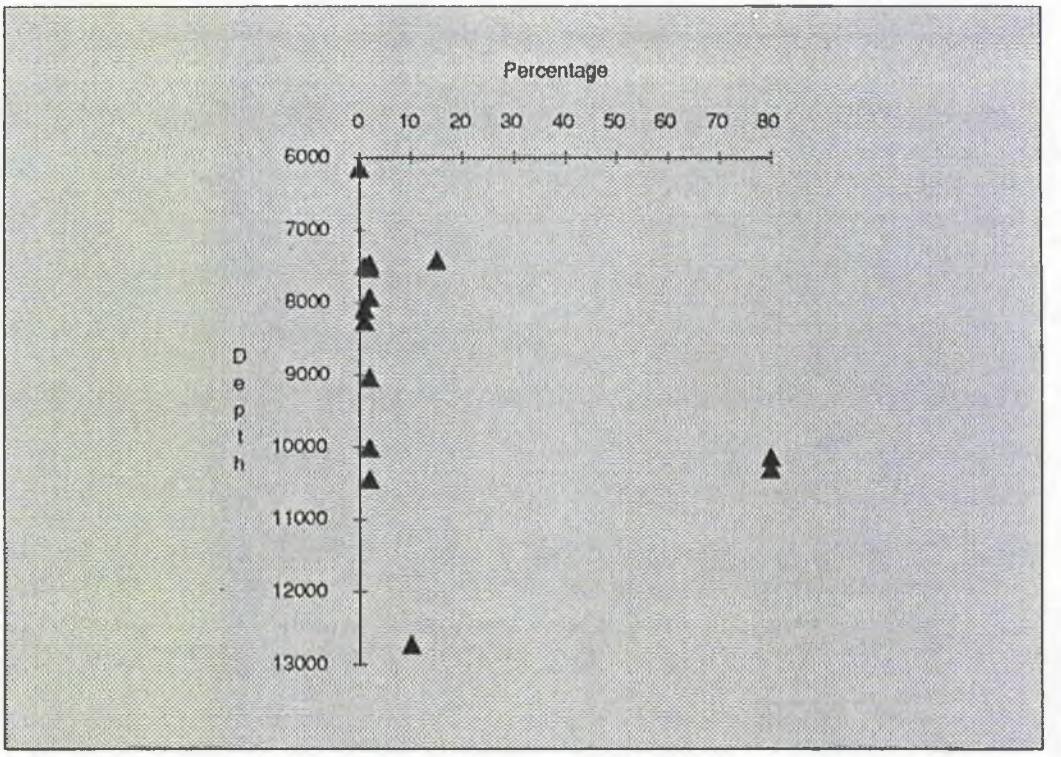

Fig. 4.15 Hematite distribution in the clay fraction of rocks with depth (ft) in Reith Bank-1 well. Modal analysis data displayed graphically.

4.13, 4.14). First stage FeO content varies between 11.89% and 25.86% with MgO lying between 21.12% and 32.12%. CaO is stable between 50.62% and 56.88%. MnO is seen to generally compensate for the lower values of CaO i.e., it is inversely proportional to the latter.

In the second stage the content of FeO and MgO is greatly enhanced, while that of CaO has dropped (Figs. 4.13, 4.14). FeO percentage varies between 21.05 and 26.4, which is higher than the first stage. MgO lies between 21.39% and 22.41%, with the upper limit of MgO falling considerably in contrast to the first stage. CaO percentage varies between 50.22 and 52.07 % and follows a similar trend as MnO which precisely substitutes for lower percentage of the former. The limits of MnO are between 3.5% and 5.48% (Fig. 4.13, 4.14).

Tiny crystals of pyrite are widely dispersed though never abundant. Hematite sometimes occurs as opaque patches filling in the pores (Fig. 4.15). Both hematite and pyrite were not found to occur in the same sample and their occurence is thought to be due to the effect of oxidation and reduction in a local environment.

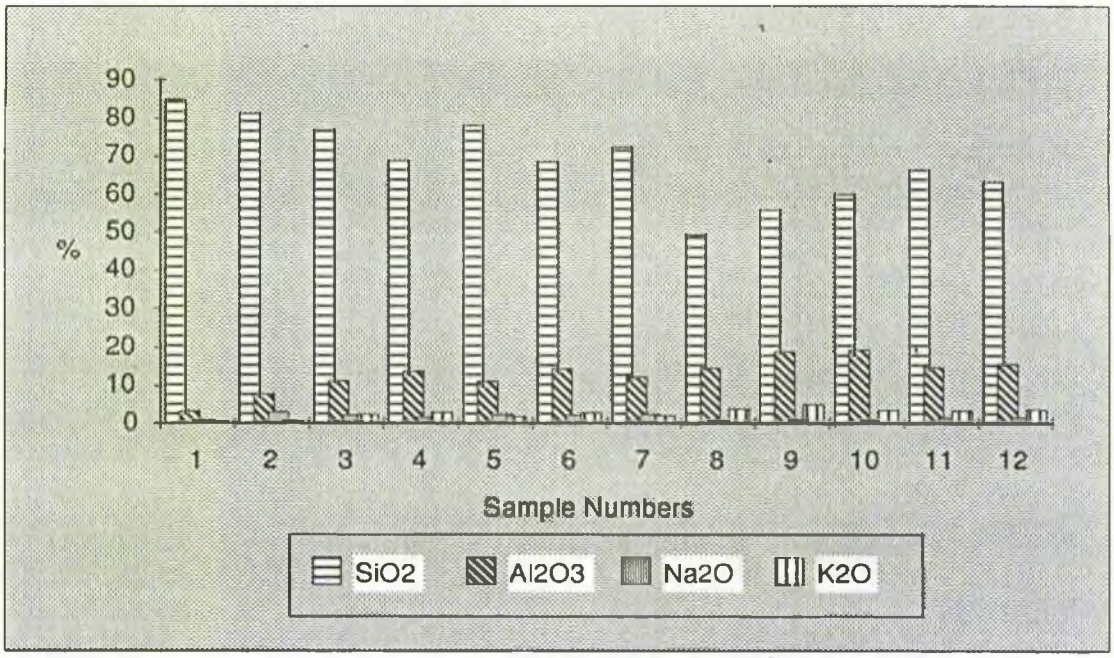

Fig. 4.16 Distribution of SiO_2, Al_2O_3, Na_2O & K_2O in samples from Reith Bank-1 well.

4.3. GEOCHEMISTRY:

Whole rock geochemical analyses have been carried out on 18 samples from Reith Bank-1 and 7 from Seagull Shoals-1. Five samples from Reith Bank-1 and five from Seagull Shoals-1 were fine grained (mudstones). The results are presented in this section (Table 4.3 & 4.4).

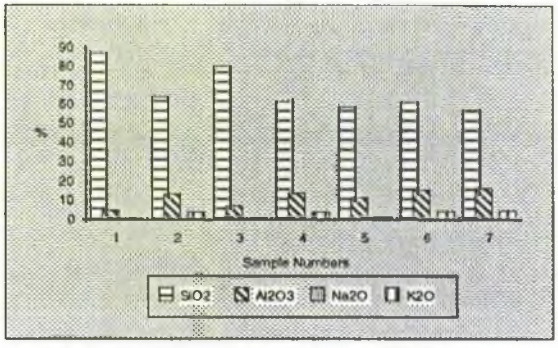

Fig. 4.17 Distribution of SiO_2, Al_2O_3, Na_2O & K_2O in samples from Seagull Shoals-1 well.

In section 4.2.2.1 it was shown that quartz grains and silica overgrowths formed 50-80% of the rock as seen in thin sections. The chemically determined SiO_2 percentage in Reith Bank-1 sediments ranged from 49% to 85% (Fig. 4.16). in the Seagull Shoals-1 samples it varied from 57% to 87% (Fig. 4.17). The percentage is much higher in sandstone samples than those from those from the mudstones (Table 4.3, 4.4). This variation is due to greater amounts of quartz and feldspar in sandstones than in the mudstones, where some of the SiO_2 is contributed from clays. The variation of SIO_2 with Al_2O_3 and K_2O is antipathetic for all the samples

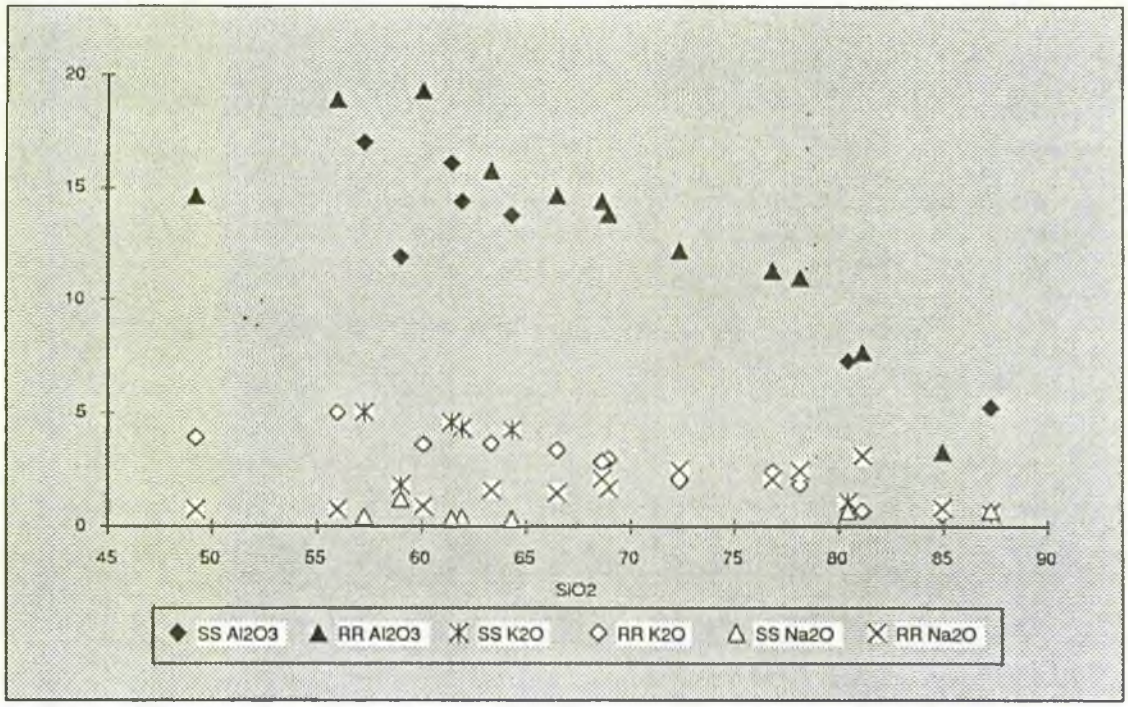

Fig. 4.18 SiO_2 plotted against Al_2O_3 and K_2O for samples from Reith Bank-1 (RR) and Seagull Shoals-1 (SS) well. The general trend being inverse relationship between SiO_2 and Al_2O_3 and SiO_2 and K_2O.

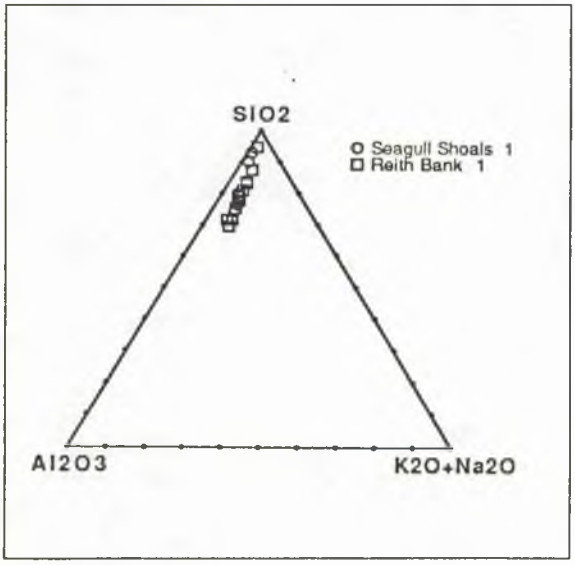

Fig. 4.19 SiO_2-Al_2O_3-(K_2O+Na_2O) plot for samples from Reith Bank-1 and Seagull Shoals-1 well. Each corner represents 100%.

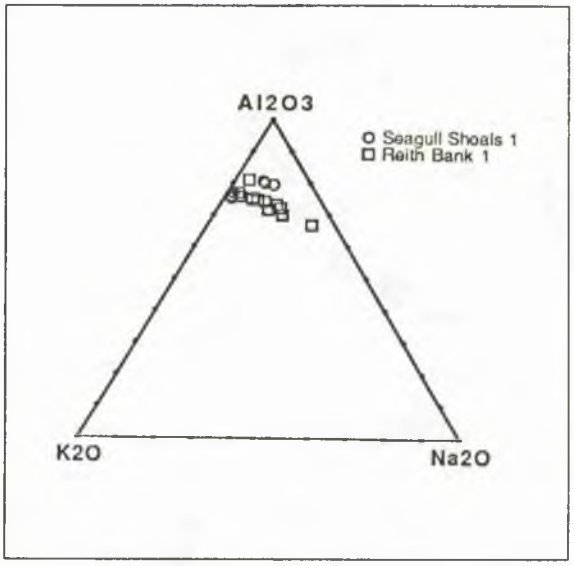

Fig. 4.20 Al_2O_3-K_2O+Na_2O plot for samples from Reith Bank-1 and Seagull Shoals-1 well. Each corner represents 100%.

(Fig. 4.18). In the SiO_2-Al_2O_3-(K_2O+Na_2O) plot most of the samples plot near the SiO_2-Al_2O_3 axis (Fig. 4.19), with the SiO_2 content determined essentially by the quartz (including overgrowths), feldspar and clays, and Al_2O_3 by the feldspar and clay contents.

Feldspars present in the samples also contribute towards the SiO_2 and Al_2O_3 along with Na_2O and K_2O. The values of Na_2O are less than 1% for the sandstones from depths above 10,500 ft, while for deeper samples the Na_2O content approaches 2.5%. There is a wide variation of Na_2O amongst the mudstones. The K_2O content follows the same trend as the Na_2O, with values of less than 1% for sandstones above 10,500 ft and between 1.5 and 3% for deeper sandstones. For the mudstones of Reith Bank-1 K_2O values lie above 3.3% but the figures are much more variable from Seagull Shoals-1 (1.1-5.0). The K_2O/Na_2O ratios of sandstones are generally low (0.2-1.8) but they are much higher in the mudstones, less variable at Reith Bank-1 (2.3-6.7) than at Seagull Shoals-1 (1.5-13.4). In Figure 4.20 all points lie near the Al_2O_3 corner along the Al_2O_3-K_2O line.

The variation in the values of Na_2O, K_2O and the ratio between K_2O and Na_2O suggest increasing percentages of feldspar with depth (c.f. section 4.2.2.2). This reflect source variations in the detrital grains now forming the sandstones or may be due to greater amounts of feldspar leaching at shallower depths. Higher values of the ratio K_2O/Na_2O can be due to clays and orthoclase feldspar (Fig. 4.20). Higher amounts of K_2O in the mudstones is due to the greater proportions of clay such as illite occuring in the mudstones (Table 4.2).

Amongst the Reith Bank-1 sandstone samples Al_2O_3 is greater in the samples from depths below 12700 ft but this increase is believed to be due to greater amounts of feldspars in the deeper samples as shown by petrographical analysis (c.f. section 4.2.2.2).

TiO_2 varies between 0.06 and 1.02% (Table 4.3, 4.4). Heavy minerals like rutile and entrapment of titanium in chlorites account for such values since no ilmenite was found.

High values of Fe_2O_3 (Table 4.3, 4.4; Fig. 4.21 & 4.22 are associated with carbonates, chlorite and hematite. The MgO/CaO ratios of 0-7 in Seagull Shoals-1 and 0.5-9 in Reith Bank-1 (Table 4.3, 4.4; Fig. 4.21 & 4.22) suggest large amounts of dolomite with some calcite. The higher proportions of magnesium and iron would also arise from chlorite. MnO values for the samples are generally below 0.05% and are derived from carbonates. A high percentage of manganese has been detected in carbonate

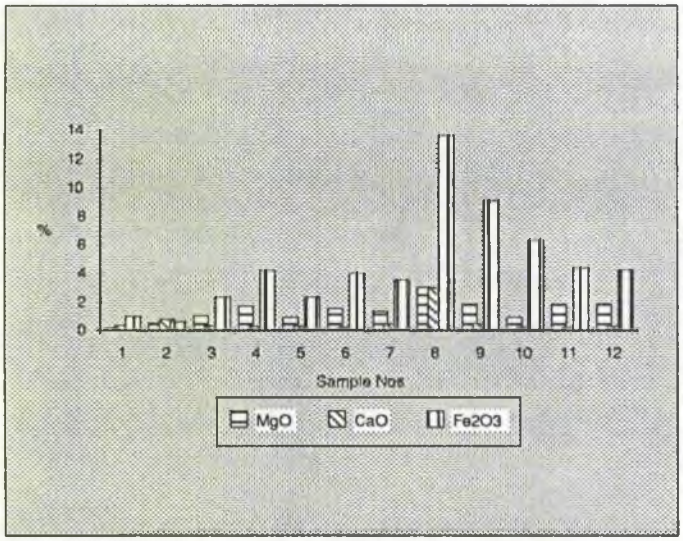

Fig. 4.21 MgO, CaO and Fe_2O_3 distributionin samples from Seagull Shoals-1 well.

cements using spot analysis by microprobe (section 4.1.2.5).

4.4. PROVENANCE:

Mineral composition points to a provenance dominated by acid plutonic rocks with both k-feldspar and sodic plagioclase. Some contributions were made by a metamorphic complex and volcanics. Cathodoluminescence colours from quartz (Plates 4.7, 4.8) suggest igneous and metamorphic origins.

Quartz falls under blue-violet (mauve) and violet class of luminescent quartz of Matter & Ramsay (1985). Since these colours are from detrital grains and not from quartz phenocrysts in volcanic rocks (which also show the same colour due to early

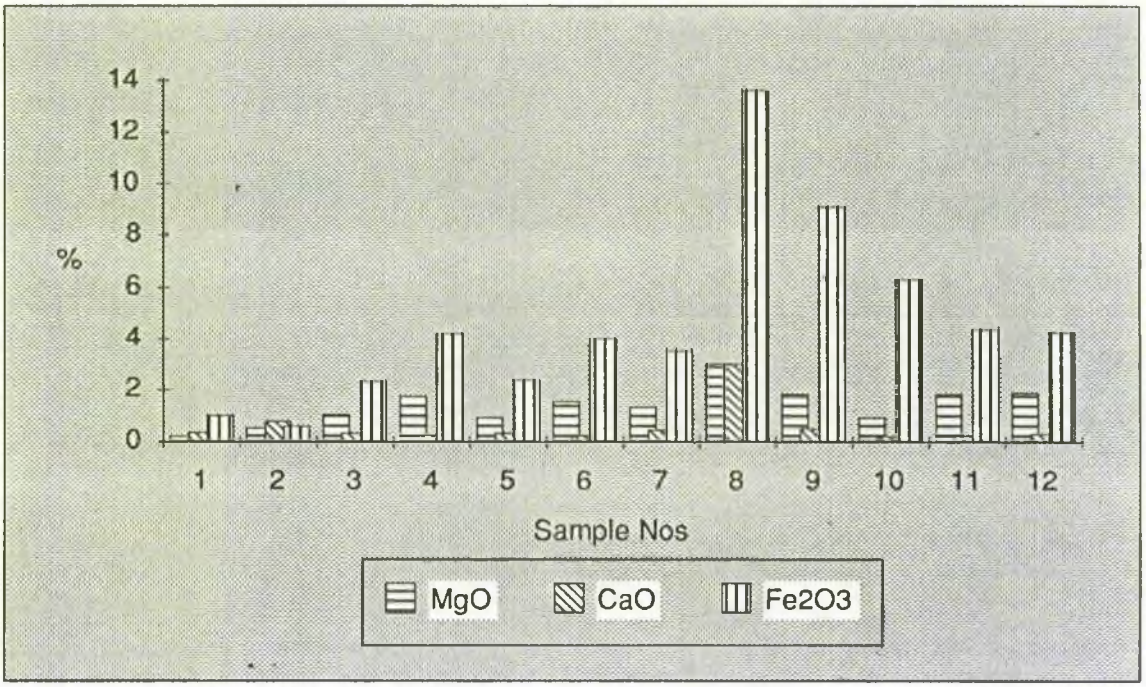

Fig. 4.22 MgO, CaO and Fe_2O_3 distributionin samples from Reith Bank-1 well.

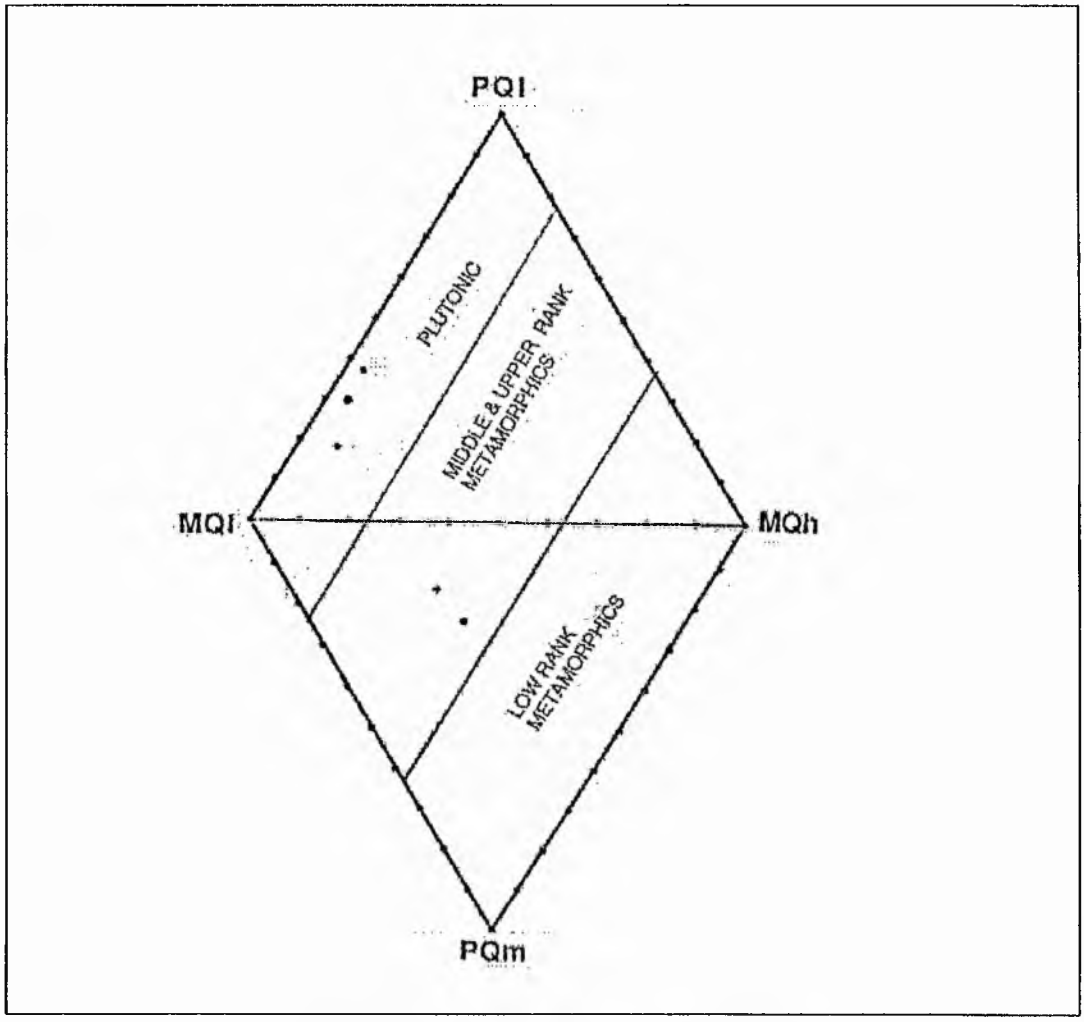

Fig. 4.23 Four variable plot of nature of quartz population in Karoo sandstones from Reith Bank-1 well. The plot is adapted from Basu (1975, 1985). The double triangle is used for determination of sources of detrital quartz grains using modal data from thin section in the grain-size range of 0.25-0.50 mm. PQ-polycrystalline quartz; MQ_l-monocrystalline quartz of low undulosity; MQ_h-monocrystalline quartz of high undulosity. If more than 25% of all polycrystalline quartz grains contain four or more units, the lower triangle is used for plotting the modal data; otherwise the upper traingle is used. The dashed lines indicate boundaries between detrital quartz populations derived from low grade metamorphic rocks, medium to high grade metamorphic rocks, and from granites and

crystallisation under hypabyssal or plutonic conditions, Matter & Ramsay, 1985), a plutonic source is envisaged.

The quartz grains when plotted on Basu's plot (Basu *et al*, 1975; Basu, 1985) fall in the plutonic and middle to upper rank metamorphic group (Fig. 4.23).

The compositional maturity of the sediments means that the low proportion of volcanic lithoclasts is probably not a true reflection of their amount in the parent rocks (Khanna & Walton ,1990).

A pre-fragmented Gondwana places Seychelles off the north-east coast of

Madagascar and India close-by to the east (Norton & Sclater, 1979; Nopec a.s., 1985; Molnar *et al,* 1988; Scotese *et al,* 1988). Walton & Khanna (1990) in their paleogeographic reconstruction of Karoo times suggest that the Seychelles Karoo basin is separated from the Majunga and Morondova basins of western Madagascar by a northerly projecting peninsula. This Madagascar source-land of metamorphic and volcanic rocks shed debris to form the Karoo sediments.

4.5. DIAGENESIS:

4.5.1. Diagenetic History:

The following diagenetic events are recognised on the basis of textural features and their chronological position illustrated in Fig. 4.24 (Khanna & Walton, 1990):-

a) Slight compaction and little pressure solution.
b) Dissolution of feldspars and lithoclasts.
c) Kaolinite growth.
d) Quartz precipitation.
e) Dissolution of feldspars.
f) Illite-smectite formation.
g) Dissolution of quartz. ?
h) Stage I carbonate precipitation. ? Chlorite
i) Quartz dissolution. ? Formation.
j) Stage II carbonate precipitation. ?

The timing of chlorite formation is not clear and varies between dissolution of quartz (g) and carbonate precipitation (h).

An early phase of compaction produced occasional bent micas, fractured feldspar and minor pressure solution of quartz (Plates 4.31, 4.32). This was followed by dissolution of primary clasts probably feldspars and lithoclasts and the development, in enlarged pores, of aggregates of kaolinite in Seagull Shoals-1 rocks (Plate 4.4-4.6, 4.15). Kaolinite is also found in some, but not all, skeletal feldspars. No distinctive authigenic kaolinite occurs in the Reith Bank-1 samples; if it were formed it has now been altered presumably to illite.

Giles & de Boer (1990) have suggested, "...Dissolution often affects the plagioclase feldspars most severely, with dissolution begining in the most calcic portions of the feldspar, which in normally zoned plagioclases is the centre. Typically, authigenic kaolinite or another clay mineral may be found in nearby primary (intergranular) or more rarely, secondary pores."

The most significant diagenetic episode was that of quartz precipitation, mostly as syntaxial overgrowths. Mineralogy Inc. (1981) petrographers concluded that this phase preceded kaolinite growth. I believe the balance of evidence, specifically, the nature of the

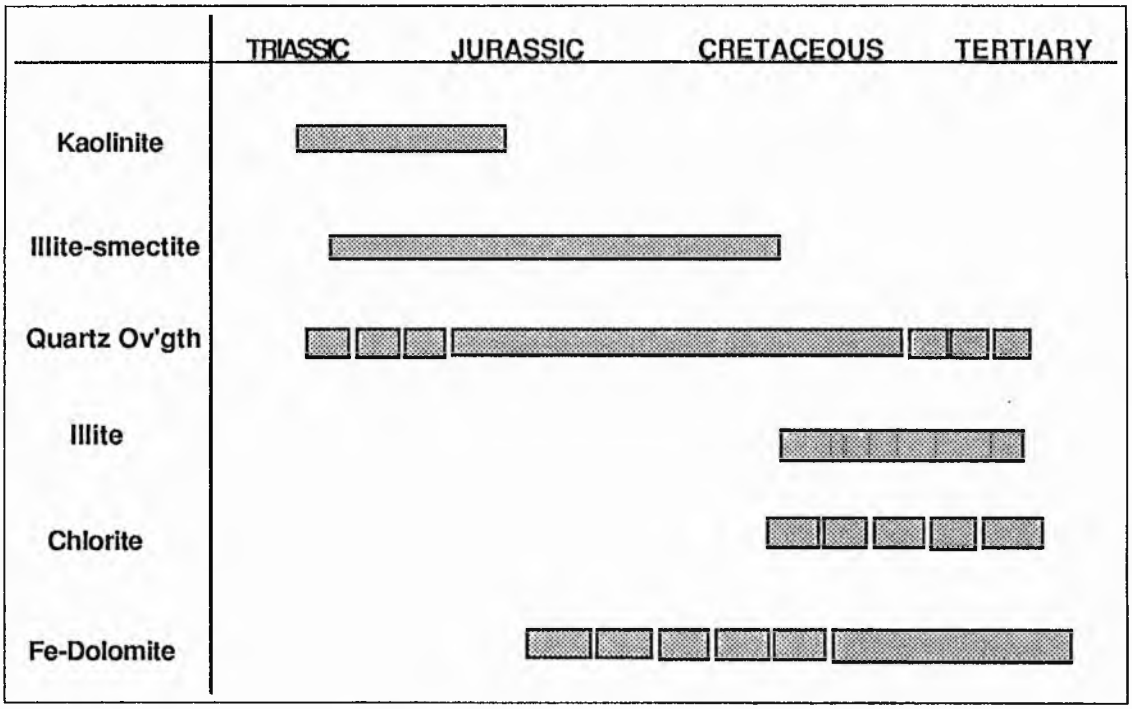

Fig. 4.24 Diagenetic episodes located in time.

margins of quartz against kaolinite favours kaolinite formation first. Burley *et al*, (1985) in their schematic diagenetic pathway (Fig. 4.25) have shown that in warm, wet non-marine diagenesis in oxygenated conditions kaolinite precedes quartz overgrowths. The absence of

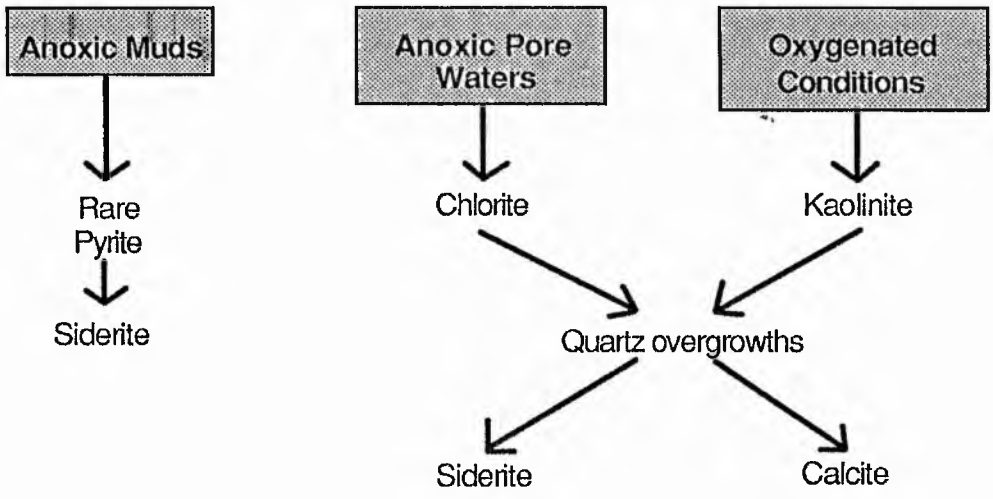

Fig. 4.25 Schematic diagenetic pathways in warm, wet non-marine sediments (from Burley *et al*, 1985).

kaolinite would have allowed the formation of complete faces of quartz overgrowths rather than the observed serrated margins (Plates 4.6, 4.33). The inhibiting effect of early clays, mostly detrital, can be seen in fine grained samples where well formed faces are scarce. Formation of overgrowths on detrital grains was due to favourable growth sites such as kinks, dislocations and other imperfections, while development of authigenic clays sometimes at sites away from dissolution locations is due to nucleation locii available around detrital fragments of clay (Giles & de Boer, 1990).

Given the abundance of quartz cements, it is probable that no single mechanism was responsible for its precipitation. Early ferromagnesian grain dissolution, mudstone dewatering, smectite to illite transformations, feldspar dissolution and pressure dissolution have been postulated to be possible sources of quartz (Burley *et al*, 1985). Cowan & Shaw (1991) have suggested that these processes operated in the Namurian sandstones of Trumfleet field, South Yorkshire and have proposed quartz cementation to be essentially continuous throughout diagenesis. A similar view is taken of the quartz cements in the Karoo sandstones.

Subsequent to the formation of quartz was the second stage of feldspar degeneration (Plate 4.34) and alteration of kaolinite, to form mixed layer illite-smectite. Due to the dissolution secondary porosity was created. This could have been generated by carboxylic acids and acids produced by thermal decarboxylation at temperatures in excess of 80°C, as suggested by Cowan & Shaw (1991) for their Namurian sandstones.

Some pores escaped total occlusion by quartz cement and this allowed the subsequent growth of carbonate with triangular or polygonal outlines. The size of most of the carbonate areas suggests a second phase of dissolution of feldspars, lithoclasts and quartz (Plates 4.3, 4.5, 4.17, 4.18). Some pores were enlarged, sometimes up to 2mm across and these were then filled with coarse-grained sometimes poikilotopic ferroan dolomite. Fluid inclusion studies reveal a temperature of 150°C at the time of origin of the carbonates.

As well as the large, sometimes poikilotopic patches of carbonate (Plates 4.4, 4.5), there are occasional euhedral crystals of dolomite. Two, perhaps three phases of precipitation have been recognised and one phase of dissolution. No particular mechanism is being proposed for the dissolution episode, however thermal decarboxylation of organic matter (Schmidt & MacDonald, 1979) and organic

acid production (Surdam *et al*, 1984, 1989) may be the possible mechanisms.

4.5.2. Diagenetic Reactions:

Pore waters in sedimentary basins have two principal origins (Fig. 4.19) (Bjorlykke, 1984): (1) meteoric water flowing into the basin, driven by the head of an elevated ground-water table, and (2) pore water (connate) buried with the sediment and forced upwards by the compaction of the sediments. For a sandstone from the time of deposition to burial to about 3 km, the total average upwards flux is of the order of 10^4-10^5 cm^3/cm^2 of pore water.

Early diagenesis (eogenesis) in Karoo sandstones has been influenced by fresh meteoric water, while the deeper later diagenesis was caused by marine waters. According to Bjorlykke (1984) a third possibility is that diagenesis can be caused by convection currents driven by density differences due to temperature (Fig. 4.26). This might have been reduced in the Karoo sequence because of the presence of low permeability barriers created by extensive cementation.

Eogenesis, as defined by Choquette & Pray (1970), is a response of the sediment under the influence of depositional pore fluids. As the

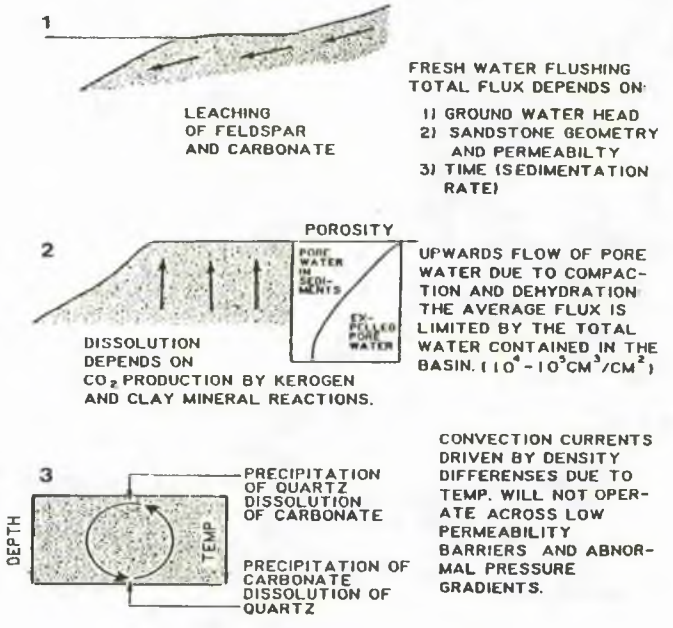

Fig. 4.26 Different types of pore-water flow in sedimentary basins: (1) meteoric (fresh) water, (2) compactional pore water, and (3) convection currents. Average porosity assumed (after Bjorlykke, 1984).

Karoo sediments were laid down by fluvial activity in a humid tropical environment, the initial (syndepositional) pore fluids would have been oxidizing and weakly acidic. The meteoric water in pores were possibly undersaturated with respect to most mineral phases. Such fluids have been proposed as causing the dissolution of feldspar and ferromagnesian grains, sourcing quartz and kaolinite cements (Huggett, 1982; Hurst & Irwin, 1983). Circulation of meteoric waters in the subsurface increased its concentration of solids.

Feldspar in general, after quartz, is the most important component in most sandstones except in the lithic sandstones. Since, the solubility of feldspars is low, for potash feldspar $3x10^{-7}$ mole/litre and for sodium feldspar $6x10^{-7}$ mole/litre (Berner, 1978), saturation is reached with a small amount of dissociation of the silicate minerals. To continue the dissociation of feldspar pore water needs to be constantly renewed by fluid flow.

It is envisaged that leaching of feldspar in Karoo sediments through continuous flushing created openings and resulted in replacement by kaolinite. Because of the low solubility of aluminium, the reaction;

$$2KAlSi_3O_8 + 2H^+ + H_2O \rightarrow Al_2Si_2O_5(OH)_4 + 4SiO_2 + 2K^+ \quad \text{....1}$$
K feldspar — kaolinite — quartz

$$2NaAlSi_3O_8 + 2H^+ + H_2O \rightarrow Al_2Si_2O_5(OH)_4 + 4SiO_2 + 2Na^+ \quad \text{....2}$$
Na feldspar — kaolinite — quartz

$$NaAlSi_3O_8 + 4H^+ \rightarrow Na^+_{(aq)} + Al^{3+}_{(aq)} + 3SiO_{2(aq)} + 2H_2O \quad \text{....3}$$
Na feldspar + fluid <===> fluid

may not have created any net increase in porosity for the sandstone as a whole, except in areas which suffered large pore water flow with efficient removal mechanism (Bjorlykke, 1984). If the reactant components are not removed from the sandstone, leached feldspar will form 60% kaolinite and 40% quartz. The abundance of kaolinite and quartz in upper Karoo sandstones is suggestive that reactant components were not removed in any great amount from the sandstone.

Disequilibrium between water and quartz or clay mineral will inhibit the formation of product minerals and might be expected to result in a net increase in porosity (reaction 1-3) (Giles & de Boer, 1990). The lack of abundant secondary porosity suggests an equillibrium between water and formation products resulting in the precipitation of the latter.

Since very little detrital muscovite can be seen, the formation of authigenic kaolinite may also have resulted from the degradation of muscovite according to the reaction;

$$2KAl_3Si_3O_{10}(OH)_2 + 3H_2O + 2H^+ \leftrightarrow 3Al_2Si_2O_5(OH)_4 + 2K^+ \quad \text{....4}$$
muscovite — Kaolinite

Leaching of K-feldspar and precipitation of kaolinite increased the K^+ concentration in the pore water so that its composition would no

longer lie in kaolinite field (Fig. 4.27) unless K^+ was effectively removed (i.e. by meteoric water) or there was an effective sink for potassium resulting in the formation of authigenic feldspar, as in reaction;

$$KAl_3Si_3O_{10}(OH)_2 + 6SiO_{2(aq)} + 2K^+ <==> 3KAlSi_3O_8 + 2H^+$$
illite silica feldspar 5

Since, no authigenic k-feldspar has been seen, it can be concluded that the K^+ rich pore waters were either constantly removed or were involved in formation of illite. The latter is more likely since with burial smectite and mixed layer minerals become unstable at 60-100°C, and are transformed to illite (Hower *et al.*, 1976; Boles & Franks, 1979) with release of Si^{+4}. Interstratified illite/smectite clays in sedimentary rocks commonly show an increase in their illite content with increasing depth of burial (Perry & Hower, 1970; Dunoyer de Segonzac, 1970, Hutcheon, 1981) (Fig. 4.28). Hower *et al,* (1976) have proposed a layer-to-layer transformation hypothesis. The transformation reaction is as follows;

smectite + K^+ + Al^{3+} -----> illite + quartz + H^+ ...6

or,

smectite + K feldspar ---> illite + chlorite + quartz 7

Various other models of transformation have been proposed by Nadeau *et al,* (1984a,

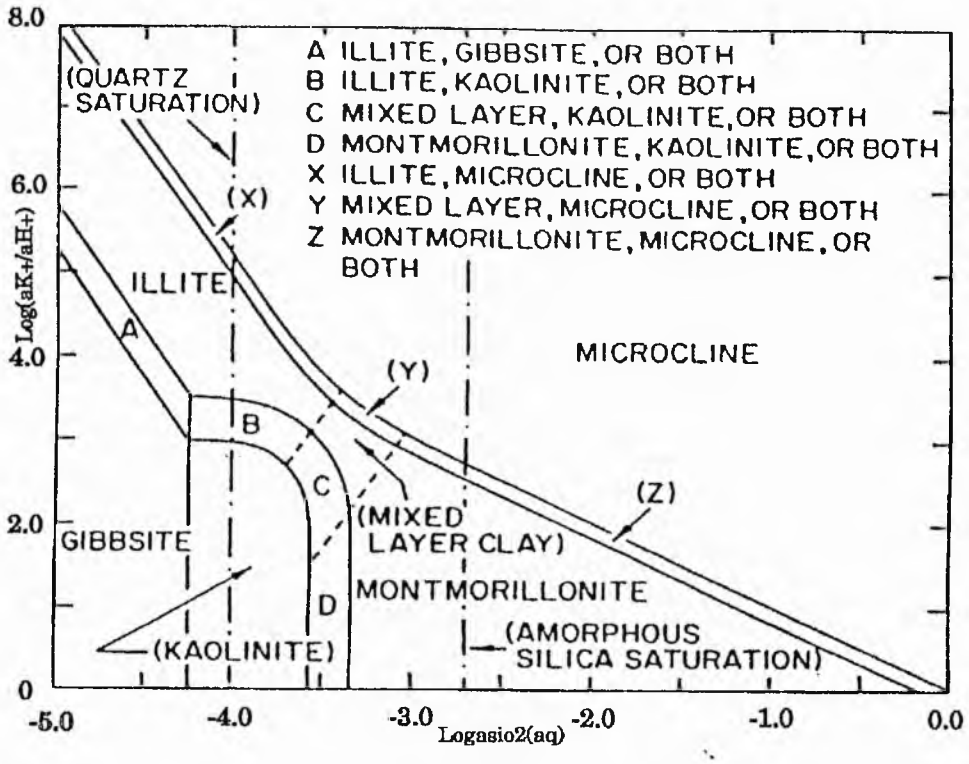

Fig. 4.27 Stability diagrams for minerals in aqueous solution at 25°C (after Aagaard, 1979).

1984b, 1985), Nadeau & Bain (1986) and Srodon *et al*, (1986).

Kaolinite too becomes unstable between 120 and 150°C and forms illite (Hower *et al.*, 1976; Hoffman & Hower, 1979);

$3Al_2Si_2O_5(OH)_4 + 2K^+ \dashrightarrow 2KAl_3Si_3O_{10}(OH)_2 + 2H^+ + 3H_2O$
Kaolinite illite 8

Reactions 5 and 6 capture cations, and expel protons which must be neutralised after reactions. This leads to a second stage of feldspar degeneration, as;

$3KAlSi_3O_8 + 2H^+ \dashrightarrow 3KAl_3Si_3O_{10}(OH)_2 + 6SiO_2 + 2K^+$
feldspar illite quartz ...9

From equations 8 and 9,

$Al_2Si_2O_5(OH)_4 + KAlSi_3O_8 \Longleftrightarrow KAl_3Si_3O_{10}(OH)_2 + 6SiO_2 + H_2O$
kaolinite K-feldspar illite quartz 10

Sass *et al*, (1987) have indicated that the stability field of kaolinite shrinks as the temperature increases resulting in the equillibrium between kaolinite and illite to move to lower values of the activity ratio K^+/H^+. The pore fluids having fixed composition initially in equilibrium with kaolinite drift into the illite field with increasing temperature resulting in the following reactions;

$5KAlSi_3O_8 + 4H^+ \Longleftrightarrow KAl_4Si_7AlO_{20}(OH)_4 + 8SiO_2 + 4K+$
K feldspar illite quartz 11

$KAlSi_3O_8 + 2Al_2Si_2O_5(OH)_4 \Longleftrightarrow KAl_4Si_7AlO_{20}(OH)_4 + 2H_2O$
K feldspar kaolinite illite 12

$5NaAlSi_3O_8 + 4H^+ + 4K^+ \Longleftrightarrow KAl_4Si_7AlO_{20}(OH)_4 + 8SiO_2 + 5Na+$
Na feldspar illite quartz 13

Thus illite may have formed in the Karoo sandstones in place of kaolinite with the production of secondary porosity within feldspars and the continued formation of quartz overgrowths.

By this time deep sub-surface diagenesis may have begun and marine pore waters precipitated carbonate cement. This is possible as Mg^{++} and Fe^{++} cations, which at

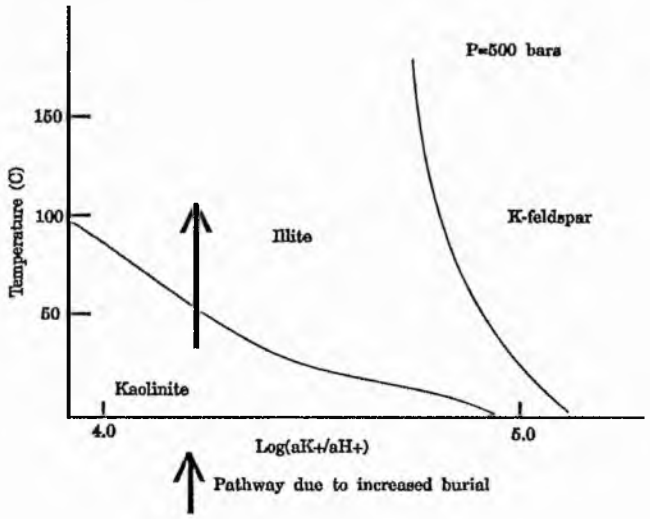

Fig. 4.28 Stability of illite as function of temperature and K^+/H^+ activity. (after Hutcheon, 1981).

shallow depths are strongly hydrated, are unable to enter the carbonate mineral lattice at low temperatures. With increasing temperatures (60-100°C at 2-3 km) these ions become less hydrated and precipitate as carbonates with low Mg^{++}/Ca^{++} ratios (0.1) in the pore water (Usdowski, 1968). The precipitation of low iron dolomite led to the increase of the iron content in the pore waters resulting in the precipitation of high iron dolomite. The ferroan dolomite at this depth was probably formed at the expense of low iron dolomite/calcite and the concentration of iron and magnesium was limited by the availability of Fe^{++} and Mg^{++} both of which are thought to have been derived from silicates such as biotite and chlorite.

The timing of chlorite formation is uncertain (Khanna & Walton, 1990). One possibility regarding the formation of chlorite coats was by mechanical infiltration of colloidal clay-rich waters through the vadose zone and/or alteration of feldspars (Burns & Ethridge, 1979; Galloway, 1974). On the other hand it seems much more likely that it formed much later by the alteration of kaolinite and quartz. Altering biotite, smectite and/or iron rich shales may have provided the source of Fe^{++} and Mg^{++}.

Shamugam (1985) has written, "...The reaction of clay minerals with carbonates during deep burial diagenesis provides a powerful mechanism for generating large quantities of CO_2 by inorganic origin (Hutcheon *et al*, 1980). The disappearance of kaolinite and the intimate association of chlorite with corroded dolomite indicates:

$$\underset{\text{dolomite}}{5CaMg(CO_3)_2} + \underset{\text{kaolinite}}{Al_2Si_2O_5(OH)_4} + \underset{\text{quartz}}{SiO_2} + 2H_2O \longrightarrow \underset{\text{chlorite}}{Mg_5Al_2Si_3O_{10}(OH)_8} + \underset{\text{calcite}}{5CaCO_3} + 5CO_2 \quad \text{....13"}$$

Since, very little calcite is seen in the Karoo sandstones as cements, it is thought that it may have been corroded as;

$$CaCO_3 + CO_2 + H_2O \Longleftrightarrow Ca^{2+} + 2HCO^{3-} \quad \text{....14}$$

enriching the fluids in ions for the continued deposition of dolomite.

Table 4.1 Representative modal analysis data of Karoo sandstones. Studies up to depth of 10,303 ft for Reith Bank-1 well are based on non-impregnated/unstained thinsections provided by Robertson Research International. Reith Bank Members- 5: 6140-7680 ft; 4:7680-8812 ft; 3:8812-9837 ft; 2: 9837-11,190 ft; 1: 11,190-12,500 ft. Flow test were carried out between 6152-6182 ft, 8060-8090 ft, 8545-8575 ft and 9235-9255 ft for Reith Bank-1 were carried out. (A-abundant; S-scarce; R-rare; Ill-illite; Chl-chlorite; Kl-kaolinite; I/S-illite-smectite; Smec-smectite; Hem-hematite; P-poor; M-moderate; G-good; VG-very good; SA-subangular; SR-subrounded; BP-interparticle porosity; WP-intraparticle porosity)

Depth (ft)	Grainsize (mm)	Sorting	Roundness	Packing	Porosity (%) BP	WP	Primary: Quartz (%)	Feldspar (%)	Lithoclasts (%)	Mica (%)	Opaques (%)	Secondary: Carbonate (%)	Clay (%)
Reith Bank-1													
6152	0.25-1.0	M	SR-SA	Interlocking	0		61	5	1	3		15	15 Kl(C),Ill(C)
6164	0.5-2.0	M	SA	Loose	0		71	2	1	0.5	0.5		25 Kl(C),Ill(C),Chl(R)
6168	0.25-1.0	M	SA	Loose	0		71	1.5		0.5			27 Ill(C),Kl(S)
6171	0.25-1.0	M	SA	Loose	0		63	1		1		11	24 Ill(C),Kl(S),Chl(R)
6179	0.5-2.0	P	SA	Loose	1 Fracture		53	1	4	0.5	0.5	12	28 Ill(C),Kl(S),Chl(R)
6266	0.25-2.0	P	SA-SR	Interlocking	0		77	1	2			10	10 Kl(C),Ill(S),Chl(R)
6285	0.25-2.0	P	SA-SR	Loose	0		63	1	5		1		30 Kl(C),Ill(R)
6500	0.25-4.0	P	SA	Loose	0		50	0.5	42.5			0.5	14.5 Ill(C),Kl(S)
6635	0.5-2.0	P	SR	Loose	0		68	9	13			5	5 Ill
6644	0.25-2.0	P	SA-SR	Loose	0		68	10	5	2			15 Kl(C),Ill(C)
6717	0.5-2.0	P	SA-SR	Interlocking	0		80	7	2	1		0.5	9.5 Ill
6835	0.25-2.0	P	SR	Loose	0		64	4	17			0.5	14.5 Ill(C),Kl(C)

Depth (ft)	Grainsize (mm)	Sorting	Roundness	Packing	Porosity (%) BP	Porosity (%) WP	Primary: Quartz (%)	Feldspar (%)	Lithoclasts (%)	Mica (%)	Opaques (%)	Secondary: Carbonate (%)	Clay (%)
7010	0.25-1.0	P	SA	Loose	0		71	2	4	0.5	0.5		22 Ill(C),Kl(C)
7280	1.0-2.0	P	SR-SA	Interlocking	0		81	5	4			1.5	8.5 Kl(C),Ill(C)
7283	0.5-2.0	M	SA	Interlocking	2		84	1	3			2.5	7.5 Ill(C),Kl(C)
7414	0.25-1.0	M	SA	Loose	0		87	2	1				10 Ill
7415	0.5-2.0	M	SA	Interlocking	5		77	4	4				10 Ill(C),Hem(S),Kl(S)
7455	0.5-2.0	P	SA-SR	Loose	5		63	4	2.5	0.5			25 Ill(C),Kl(R)
7465	0.5->2.0	P	SA	Interlocking	2	Fracture	76	0.5	1.5			5	15 Ill
7318-7475	0.25-0.5	G	SA	Loose	7		54	6	1	2		6	24 Ill(C),Hem(R)
7495	0.25-0.5	G	SA	Interlocking	0		70	4		1			25 Ill(C),Kl(R),Hem(R)
7533	0.5-1.0	M	SA	Interlocking	0		76	1.5	1.5		1	2	18 Ill(C),Hem(R)
7600	0.25-1.0	P	SR	Loose	0		72	2.5		0.5		7.5	17.5 Ill(C),Kl(S)
7629	0.25-1.0	G	SA-SR	Loose	8		44	1	0.5	0.5		46	
7765	1.0-2.0	G	SA	Interlocking	0		72	9	4			3	12 Ill(C),Chl(S),Kl(R)
7825	0.5-1.0	G	SR	Interlocking	5	Fracture	72	5.5	2	0.5		1.5	13.5 Ill(C),Kl(R)
7875	0.5-1.0	M	SA	Interlocking	20	Fracture	65	4	0.5	0.5			10 Ill(C),Kl(R)

Depth (ft)	Grainsize (mm)	Sorting	Roundness	Packing	Porosity (%) BP	Porosity (%) WP	Primary: Quartz (%)	Feldspar (%)	Lithoclasts (%)	Mica (%)	Opaques (%)	Secondary: Carbonate (%)	Clay (%)
7935	0.5-1.0	M	SA	Loose	0		78	2				2	18 Ill(C),Hem(R)
8058	0.5-2.0	M	SA	Loose	5		72	6	6	1			10 Ill(C),Kl(S)
8095	1.0-2.0	G	SA	Interlocking	0		85	3	1.5	0.5		0.5	9.5 Ill(C),Hem(R)
8102	1.0-2.0	G	SA	Interlocking	0		85	3	1.5	0.5		0.5	9.5 Ill(C),Hem(R)
8111	0.5-1.0	G	SA	Loose	0		73	5	1.5	0.5			20 Ill
8125	0.25-1.0	P	SA	Loose	1		82	3.5	2.5	1			10 Ill
8140	1.0-2.0	G	SA	Loose	2		82	3.5	2	0.5		0.5	9.5 Ill
8215	0.25-2.0	P	SA	Loose	0		81	3.5	5.5			0.5	9.5 Ill
8235	0.25-2.0	M	SA	Loose	12		74	2	2			0.5	9.5 Ill
8247	0.5-2.0	M	SA	Loose	5		64	6	5			1	19 Ill(C),Kl(R)
8255	0.25-4.0	P	SA	Loose	5		64	7	14			0.5	9.5 Kl(C),Ill(R),Hem(R)
8417	0.25-4.0	P	SA	Loose	Fracture 0		76	3	1			0.5	19.5 Ill
8445	0.5-2.0	M	SA	Loose	0		83	1	4			5	7 Ill
8465	0.25-1.0	M	SA	Loose	0		82	3				3	12 Ill(C),Kl(S)
8483	0.25-2.0	P	SA	Loose	0		82	3				3	12 Ill(C),Kl(S)

Depth (ft)	Grainsize (mm)	Sorting	Roundness	Packing	Porosity (%) BP	Porosity (%) WP	Primary: Quartz (%)	Feldspar (%)	Lithoclasts (%)	Mica (%)	Opaques (%)	Secondary: Carbonate (%)	Clay (%)
8525	0.5-1.0	G	SR	Loose	0		88	2				2	8 Ill(C),Kl(S)
8628	0.25-0.5	G	SA	Loose	5 Fracture		51	3			1		40 Ill
8655	0.25-2.0	P	SA	Loose	8		79	1	1.5		0.5		10 Ill
8704	0.25-2.0	P	SA	Loose	0		86	4				0.5	9.5 Ill
8771	1.0-2.0	G	SA	Loose	0		37	2	1			60	
9035	0.25-2.0	P	SA	Loose	12		70	3				6	9 Ill(C),Hem(R)
9646	0.5-1.0	G	SA	Interlocking	0		90	5				0.5	4.5 Ill(C),Kl(R)
9842	0.5-1.0	G	SA	Interlocking	0		90	3	2			3	2 Ill
9985	>4.0	P	SA	Loose	10 Fracture		42	18				9	21 Ill
10012	1.0-2.0	P	SA	Loose	0		81	2	2			7.5	7.5 Ill(C),Hem(R)
10140	0.5-1.0	G	SA	Interlocking	0		90	1	4			1.5	3.5 Hem(C),Ill(R)
10303	0.25-0.5	G	SA	Loose	0		66	3.5	0.5			7.5	22.5 Hem(C),Ill(R)
10,445	0.5-1.0 2.0-4.0	P	SA-SR	Interlocking	8	35 65	46	3	21			2	20 Ill(A),Hem(R)
10,447	0.625-0.25	P	SA-SR	Loose	0		47	2		1			50 Ill
10,449	1.0-4.0	M	SA-SR	Loose	10	40 60	62	7	6			5	10 Ill

Depth (ft)	Grainsize (mm)	Sorting	Roundness	Packing	Porosity (%) BP	Porosity (%) WP	<----------Primary----------> Quartz (%)	Feldspar (%)	Lithoclasts (%)	Mica (%)	Opaques (%)	<----------Secondary----------> Carbonate (%)	Clay (%)
10,451	>4.0	G	SA-SR	Interlocking	12	60 40	64	7	6	1		2	8 Ill(A),Hem(R),I/S(R)
12,726	0.25-0.50	G	SR	Interlocking	1	10 90	75	18		1		4	1 Ill
12,728	0.25-0.50	G	SA	Interlocking	1	10 90	63	25	1	0.5	0.5	1	8 Chl(A),Ill(A)
12,730	0.25-0.50	VG	SR	Interlocking	1	10 90	52	13	9	0.5		3.5	21 Chl(A),Ill(S),Hem(R)
12,732	0.25-0.50	G	SR	Interlocking	0		65	14	1		0.5	17.5	2 Ill
12,734	0.125-0.25	M	SA	Loose	0		64	1		0.5			34.5 Ill(A),Chl(A)
12,736	0.125-0.25	M	SA	Loose	0		68	7		1			24 Ill
12,738	0.125-0.25	G	SA	Loose	0		63	6.5		0.5			30 Ill
12,740	0.125-0.50	M	SA	Interlocking	1	10 90	65	13		1	1	7	12 Ill
12,742	0.0625-0.250	M	SA	Loose	0		68	9		1.5	1		20.5 Ill(A),Chl(R)
12,746	0.125-0.25	G	SA	Loose	0		60	2		4	5		29 Ill
12,750	0.125-0.25	G	SA	Interlocking	0		56	16		8		13	7 Ill
12,752	0.125-0.25	G	SR	Interlocking	0		70	6		3	1	1	19 Ill(A),Chl(R)
12,754	0.125-0.50	M	SA	Loose	0		55	8		1	1		35 Ill(A),Chl(R)
12,755	0.125-0.25	G	SA	Interlocking	0		59	6		4	1		30 Ill

Depth (ft)	Grainsize (mm)	Sorting	Roundness	Packing	Porosity (%) BP	Porosity (%) WP	Primary: Quartz (%)	Primary: Feldspar (%)	Primary: Lithoclasts (%)	Primary: Mica (%)	Primary: Opaques (%)	Secondary: Carbonate (%)	Secondary: Clay (%)
Seagull Shoals-1													
8973	0.50-1.0	Bi-modal	SA-SR	Interlocking	5		70	8		4	2	1	10
	1.0-2.0				10	90							Kl(A),Ill(O),I/S(R)
8975	0.50-1.0	Bi-modal	SA-SR	Interlocking	5		68	5		1.5	0.5	6	14
	2.0-4.0				25	75							Kl(A),Ill(O),I/S(R)
8977	0.50-2.0	M	SA-SR	Loose	10		58	4		4	4	4	16
					25	75							Kl(A),Ill(O),I/S(R)
8979	0.50-2.0	M	SA-SR	Interlocking	10		72	6		2		4	6
					40	60							Kl(A),Ill(O),I/S(R)

Table 4.2 Mineralogy of Karoo sandstones from XRD analysis.

Sample	Quartz	Feldspar	Illite	Smectite	Illite-Smectite	Chlorite	Kaolinite	Calcite	Dolomite
Seagull Shoals-1									
Sandstones									
8973 ft	X	X					X		
8979 ft	X	X	X				X		
8982 ft	X				X				
8985 ft	X		X	X			X		
Mudstones									
8977 ft	X						X		X
8987 ft	X	X	X						
8989 ft	X	X	X				X	X	
8993 ft	X		X		X				
8995 ft	X		X						
Reith Bank-1									
Sandstones									
10429 ft	X		X						
10445 ft	X	X	X						
10447 ft	X	X	X				X		
10449 ft	X	X							
10451 ft	X	X							
12730 ft	X	X							X
12732 ft	X	X							
12736 ft	X	X	X				X		
12746 ft	X	X	X			X	X		
12750 ft	X	X					X		
12752 ft	X	X	X			X	X		
12754 ft	X	X	X			X	X		
12755 ft	X	X				X	X		
Mudstones									
10433 ft	X	X	X						X
10435 ft	X	X	X						
10441 ft	X	X				X	X		
10443 ft	X	X					X		

Table 4.3 Whole rock geochemical data for Reith Bank-1 well samples. Wt loss: Loss on ignition. The difference in total from 100% is due to analytical conditions.

	Depth	SiO_2	TiO_2	Al_2O_3	Fe_2O_3	MnO	MgO	CaO	Na_2O	K_2O	P_2O_5	Wt. Loss	Total	K_2O/Na_2O	MgO/CaO
Sandstones															
1	10451	84.95	0.05	3.29	1	0.03	0.22	0.36	0.82	0.57	0	8.39	99.68	0.70	0.61
2	12732	81.11	0.25	7.67	0.61	0.05	0.54	0.8	3.07	0.69	0.01	3.4	98.2	0.22	0.68
3	12736	76.85	0.49	11.29	2.34	0.01	1.04	0.34	2.05	2.39	0.07	2.6	99.47	1.17	3.06
4	12746	68.94	0.62	13.81	4.22	0.01	1.74	0.28	1.65	2.95	0.06	8	102.28	1.79	6.21
5	12752	78.17	0.49	10.99	2.37	0.02	0.94	0.33	2.46	1.83	0.07	0	97.67	0.74	2.85
6	12754	68.62	0.68	14.39	4.01	0.02	1.54	0.25	2.1	2.84	0.07	1	95.52	1.35	6.16
7	12755	72.35	0.46	12.19	3.55	0.03	1.33	0.45	2.49	1.99	0.06	4.19	99.09	0.80	2.96
Mudstones															
8	10433	49.24	0.73	14.64	13.63	0.56	3.02	2.99	0.74	3.93	0.08	9.19	98.75	5.31	1.01
9	10435	55.98	0.95	18.91	9.11	0.06	1.84	0.51	0.75	5	0.09	6.6	99.8	6.67	3.61
10	10441	60.06	0.94	19.31	6.3	0.01	0.93	0.23	0.87	3.59	0.02	6.4	98.66	4.13	4.04
11	12744	66.46	0.68	14.69	4.37	0.02	1.84	0.25	1.46	3.34	0.07	5.4	98.58	2.29	7.36
12	12748	63.29	0.76	15.75	4.25	0.02	1.87	0.32	1.6	3.64	0.06	4	95.56	2.28	5.84

Table 4.4 Whole rock geochemical data for Seagull Shoals-1 well samples. Wt loss: Loss on ignition. The difference in total from 100% is due to analytical conditions.

	Depth	SiO_2	TiO_2	Al_2O_3	Fe_2O_3	MnO	MgO	CaO	Na_2O	K_2O	P_2O_5	Wt Loss	Total	K_2O/Na_2O	MgO/CaO
Sandstones															
1	8973	87.26	0.15	5.27	0.41	0.04	0.43	0.7	0.72	0.64	0	3.6	99.22	0.89	0.61
2	8985	64.31	0.85	13.79	6.64	0.01	1.2	0.34	0.32	4.22	0.06	7.4	99.14	13.19	3.53
Mudstones															
3	8977	80.45	0.18	7.31	0.97	0.04	0.83	1.65	0.7	1.08	0	6.19	99.4	1.54	0.50
4	8987	61.91	0.85	14.38	6.83	0.01	1.39	0.25	0.4	4.32	0.03	7	97.37	10.80	5.56
5	8989	58.98	0.73	11.89	5.94	0.06	1.7	6.03	1.21	1.8	0.06	9.39	97.79	1.49	0.28
6	8993	61.4	0.92	16.09	6.37	0.01	1.18	0.21	0.34	4.55	0.04	6.8	97.91	13.38	5.62
7	8995	57.23	0.88	17.02	8.17	0	1.03	0.32	0.42	5.02	0.13	10.8	101.02	11.95	3.22

Plate 4.1 General view of sandstone texture, quartz mosaics (bottom right, top left), feldspar coarse-grained and carbonate cement; with a few quartzose lithoclasts. (x40) (Reith Bank-1; 12,726 ft).

Plate 4.2 General view of texture of feldspathic sand. Feldspars twinned and untwined with straight and stepped margins against quartz. Quartz margins often straight except against clay rich (stippled) aggregates. (x40) (Reith Bank-1; 12,750 ft).

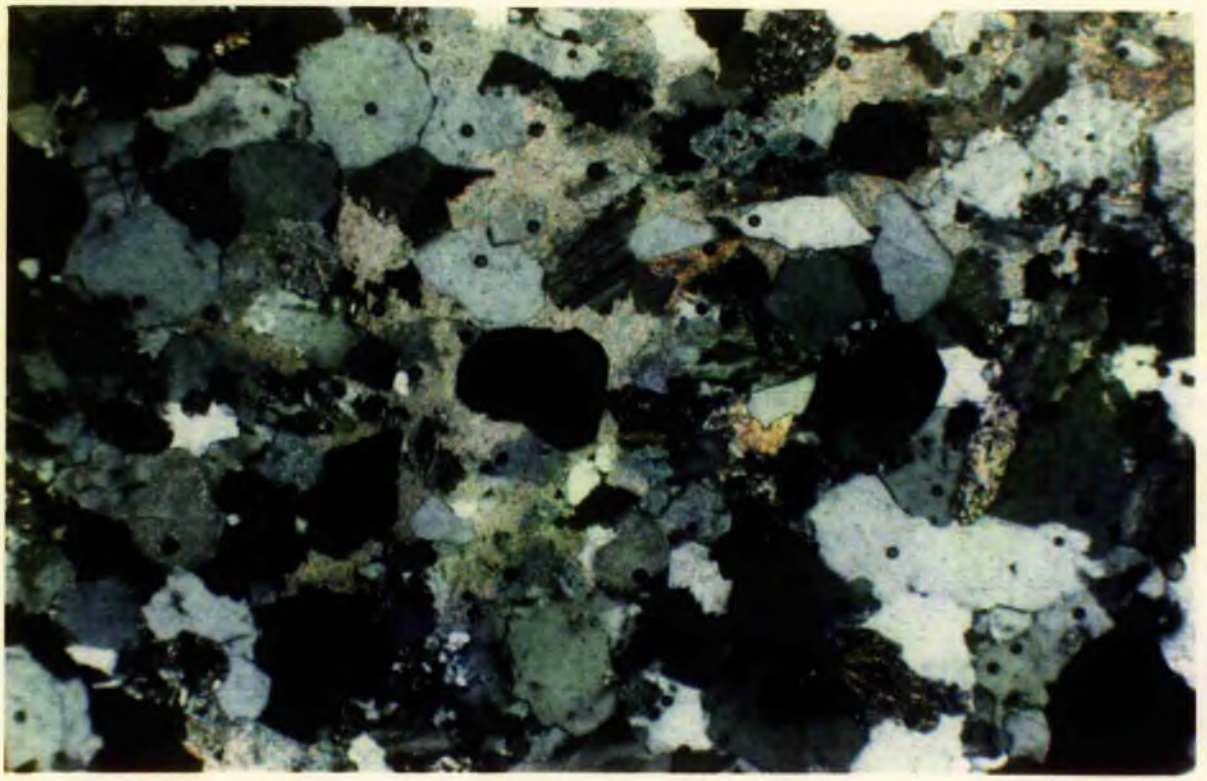

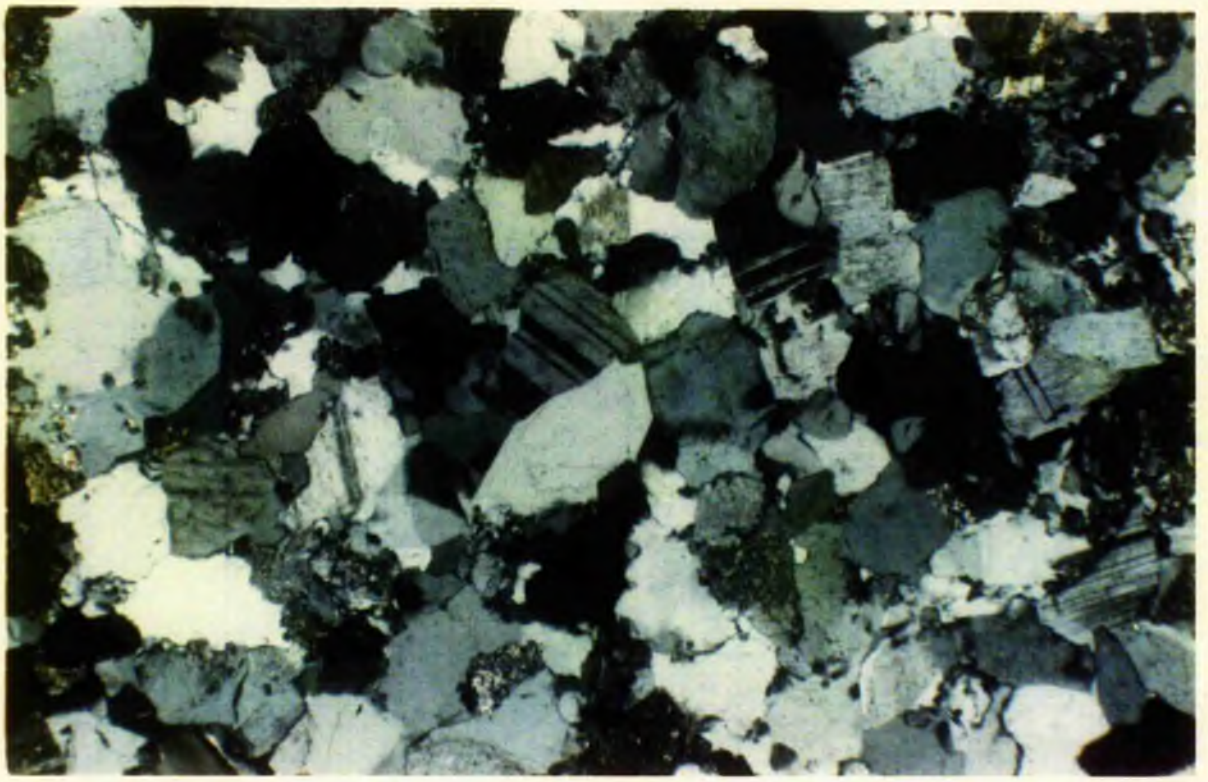

Plate 4.3 Quartz mosaic with straight, stepped margins due to overgrowth. Quartz has serrated boundary against feldspar (lower left) as does the carbonate. Carbonate against quartz is straight or serrated (centre left) and carbonate (bottom right in extinction) has straight triangle margins. (x40) . (Seagull Shoals-1; 8979 ft).

Plate 4.4 Kaolinite filling pore with carbonate. Serrated margin of feldspar and carbonate against clay. Straight and stepped margins between quartz/feldspar and feldspar/carbonate. Top right scalloped quartz against clay. (x100) (Seagull Shoals-1; 8975 ft).

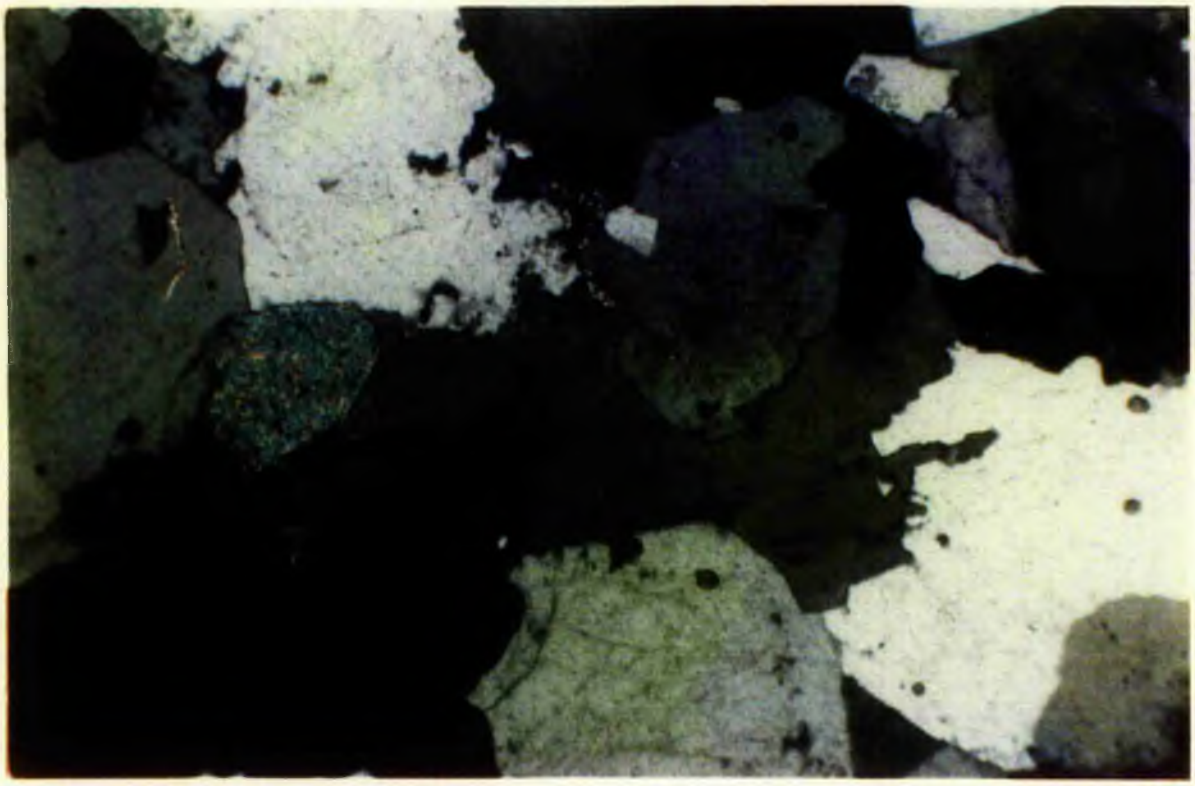

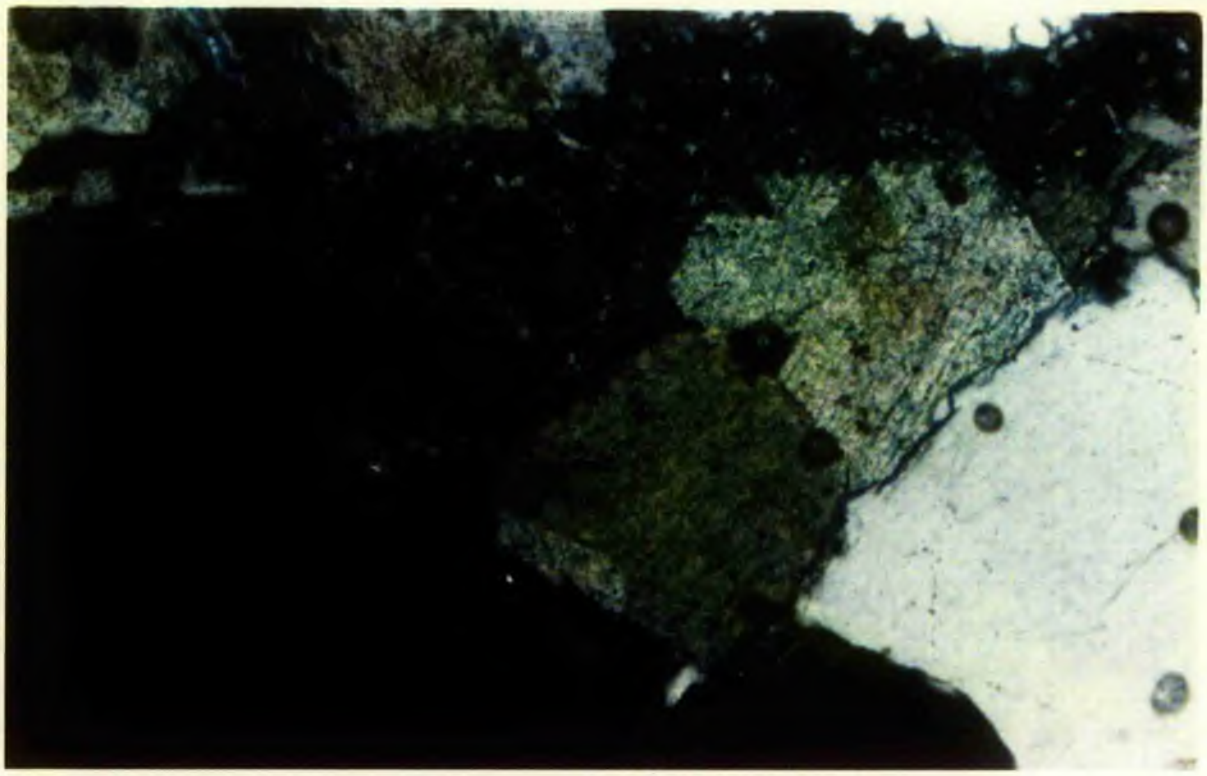

Plate 4.5 Greatly reduced macroporosity with triangular primary pore in the centre. Well developed ferroan-dolomite has reduced the primary porosity considerably. However, secondary microporosity can be seen amongst the authigenic clays and skeletal feldspar. Carbonate growing against the clay is reducing the micro-porosity and compacting the clay. (x40) (Seagull Shoals, 8975 ft).

Plate 4.6 Enlarged pore filled with well-formed 'books' of kaolinite. Quartz has serrated or lobate margins with clay. White mica 'trapped' by quartz overgrowth. (x200) (Seagull Shoals-1; 8977 ft).

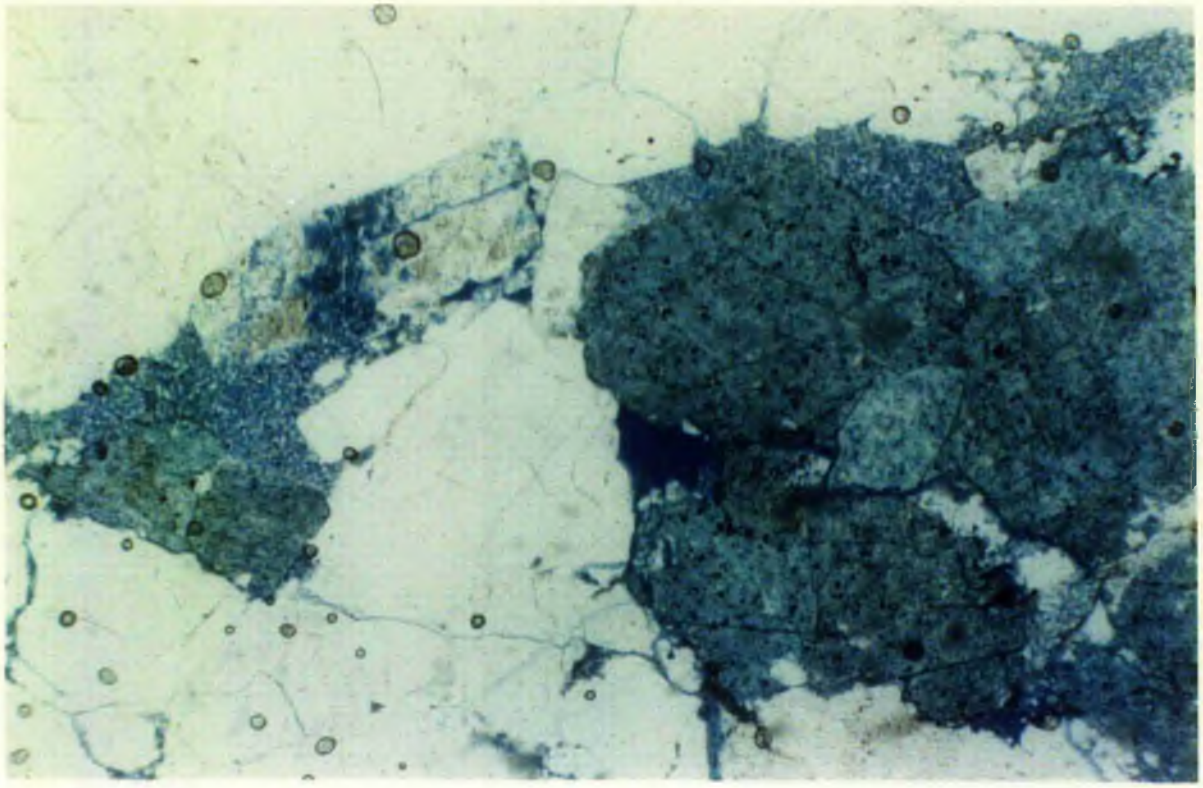

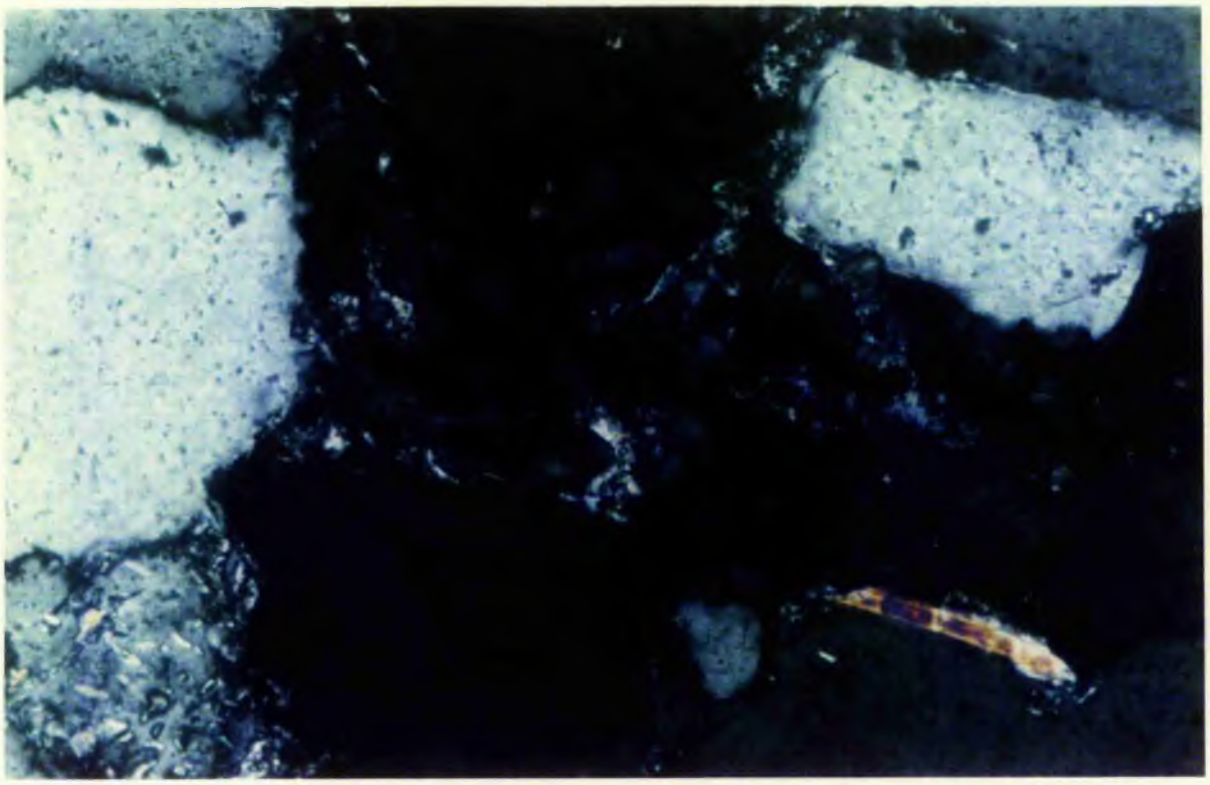

Plate 4.7 Photograph showing quartz luminescing in violet, corroded feldspar in deep blue and clay in golden yellow. Clay can be seen to grow into the feldspar grain. (Reith Bank, 10,449 ft).

Plate 4.8 Violet quartz grain of igneous origin with clay filling in the pores in the lower part of the picture. (Seagull Shoals, 8879 ft).

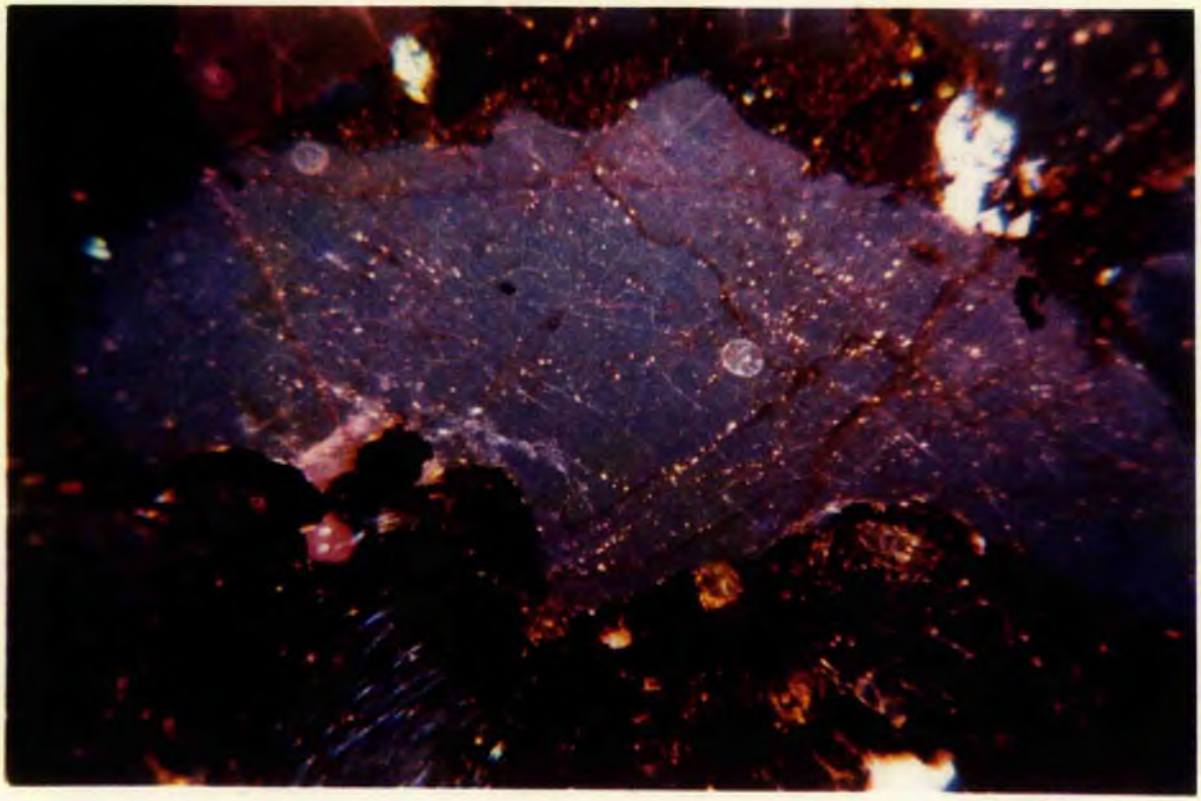

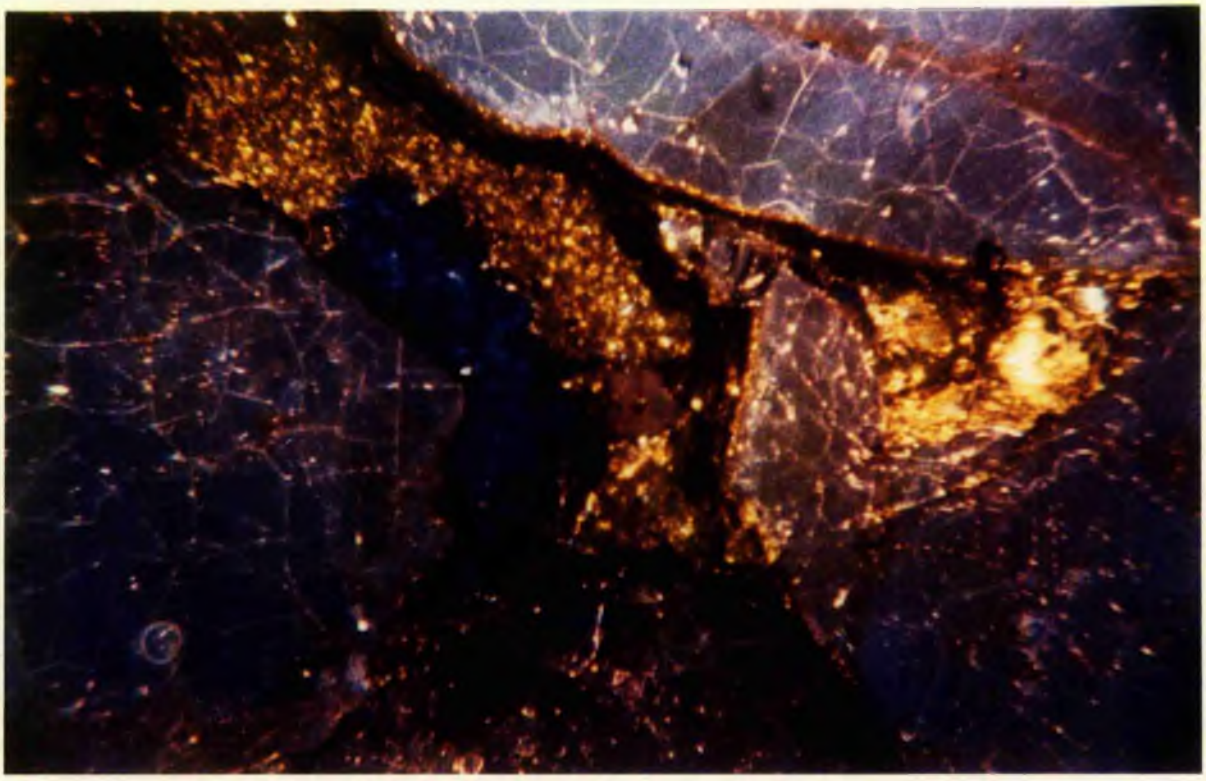

Plate 4.9 Quartzite grain with abundant pore filling kaolinite. Quartz scalloped and serrated against clay, non-undulose except for grain (upper right). Straight, overgrowth boundaries between grains (upper left and top middle). Mosaic boundary in vein quartz clast (lower left). (x40) (Seagull Shoals-1; 8977 ft).

Plate 4.10 Carbonate-grain relations. Quartzose lithoclast (top right) scalloped, feldspar (top middle) irregularly embayed. Quartz (lower right) with overgrowth partly preserved and partly corroded (left side of grain). Fine-grained siliceous lithoclast also preserved (bottom middle). (x150) (Reith Bank-1; 12,750 ft).

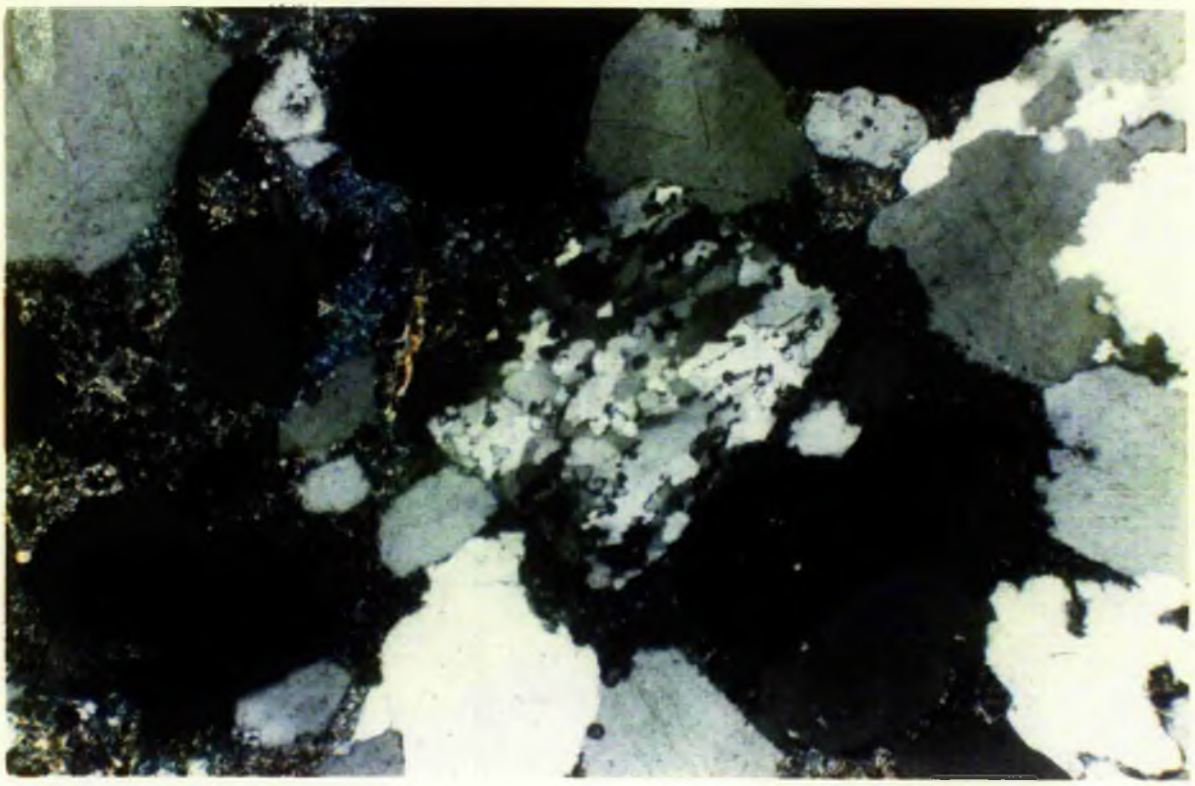

Plate 4.11 Mixed layer illite-smectite. (Seagull Shoals-1; 8979 ft).

Plate 4.12 Authigenic Na-feldspar (15u) (right centre) surrounded by illitic clays. Quartz with well formed faces embedded in the clay. (Seagull Shoals-1; 8979 ft).

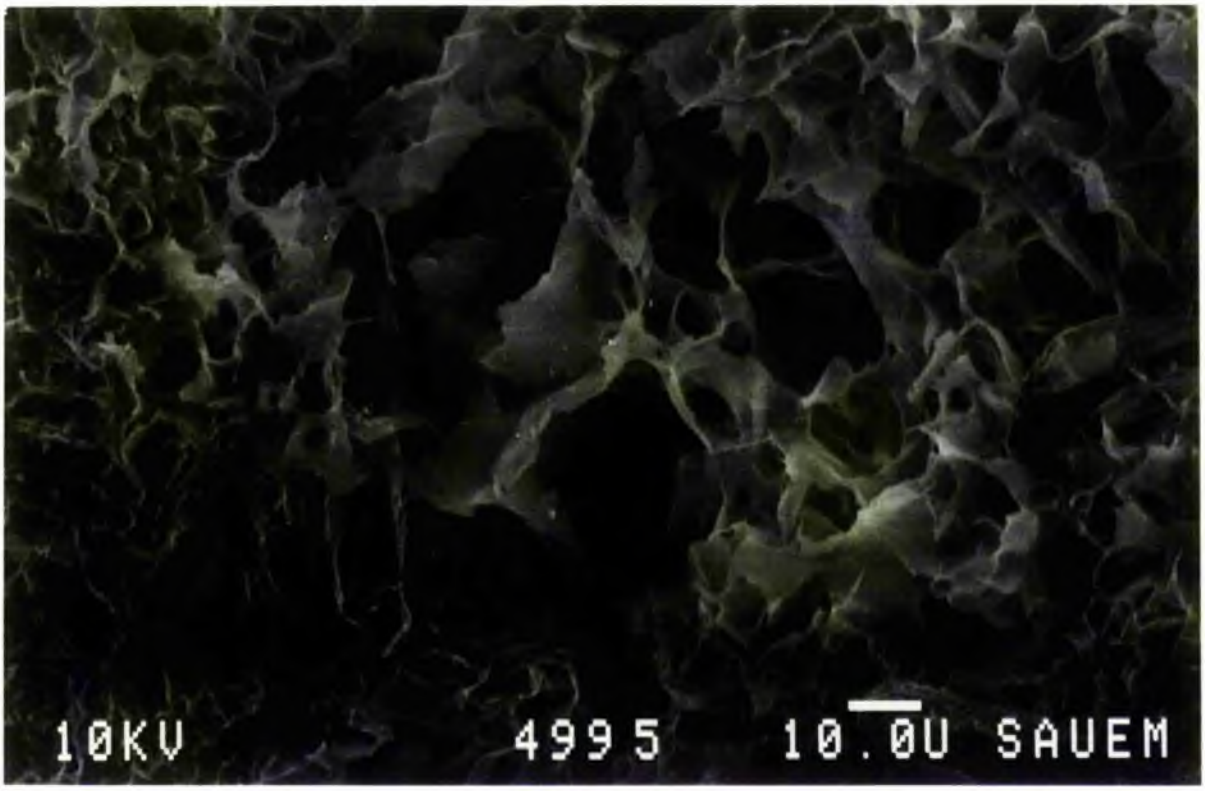
10KV
4995
10.0U SAUEM

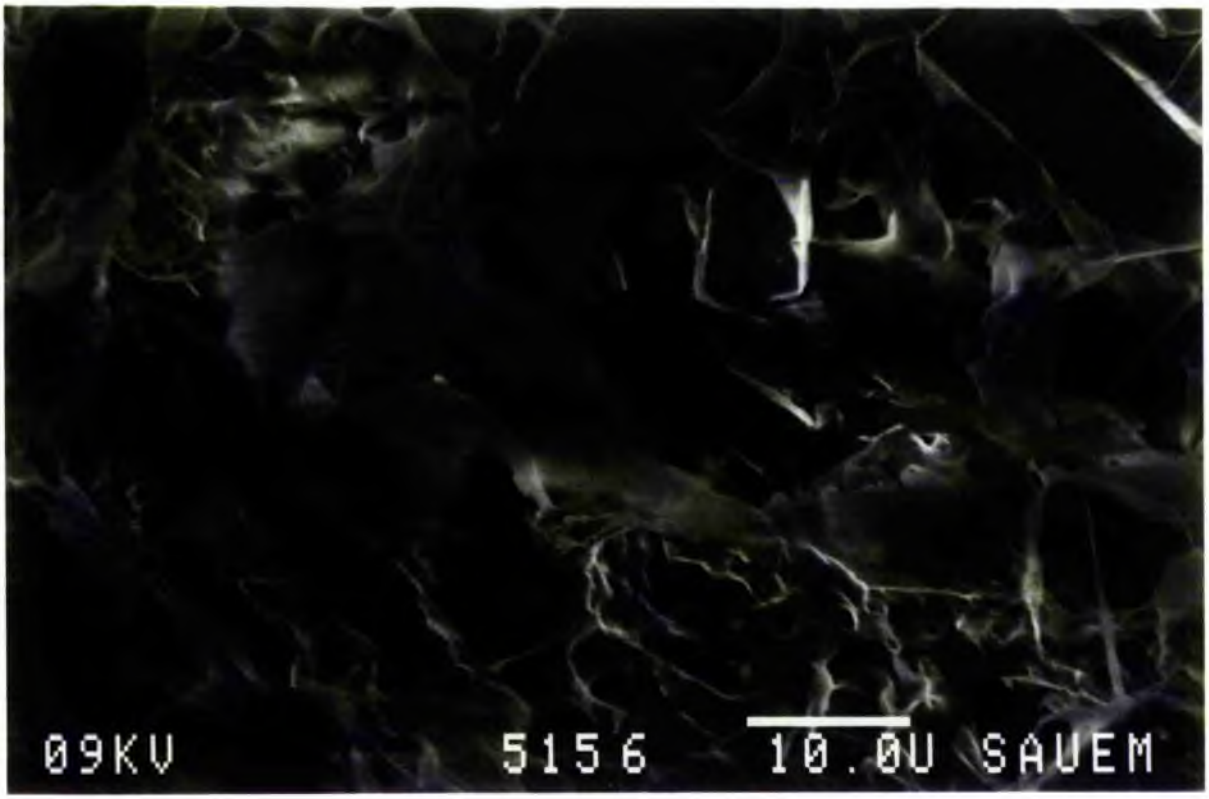
09KV
5156
10.0U SAUEM

Plate 4.13 Illite seams between grains and quartz mosaics. (x40) (Seagull Shoals-1; 8977 ft). 

Plate 4.14 Expanded biotite (blue pores) partly kaolinite filled. Partially corroded feldspar (right) with WP secondary pores. Volcanic fragment (left). (x200) (Seagull Shoals-1; 8975 ft). 

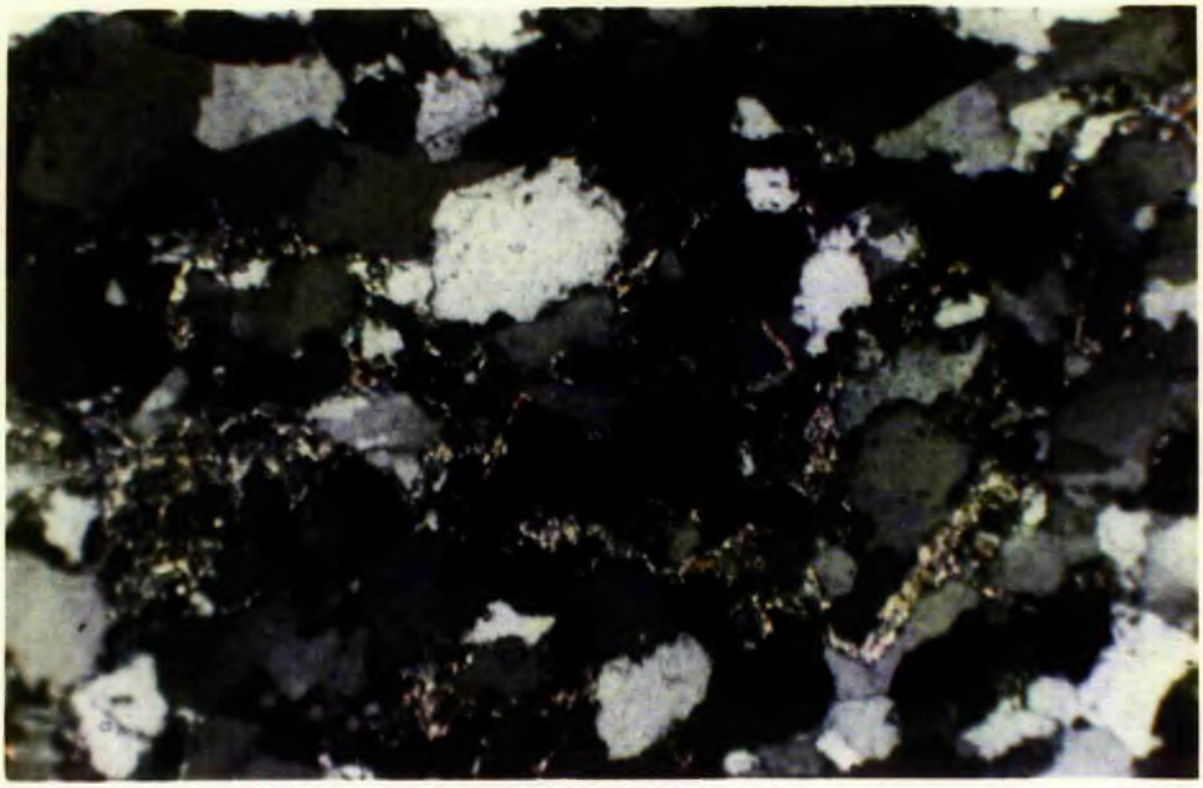

Plate 4.15 Pore filling kaolinite in form of books. (Seagull Shoals-1; 8975 ft).

Plate 4.16 Illite-smectite mixed layer over authigenic quartz. (Reith Bank-1; 12,451 ft).


10KV 4991 10.0U SAUEM

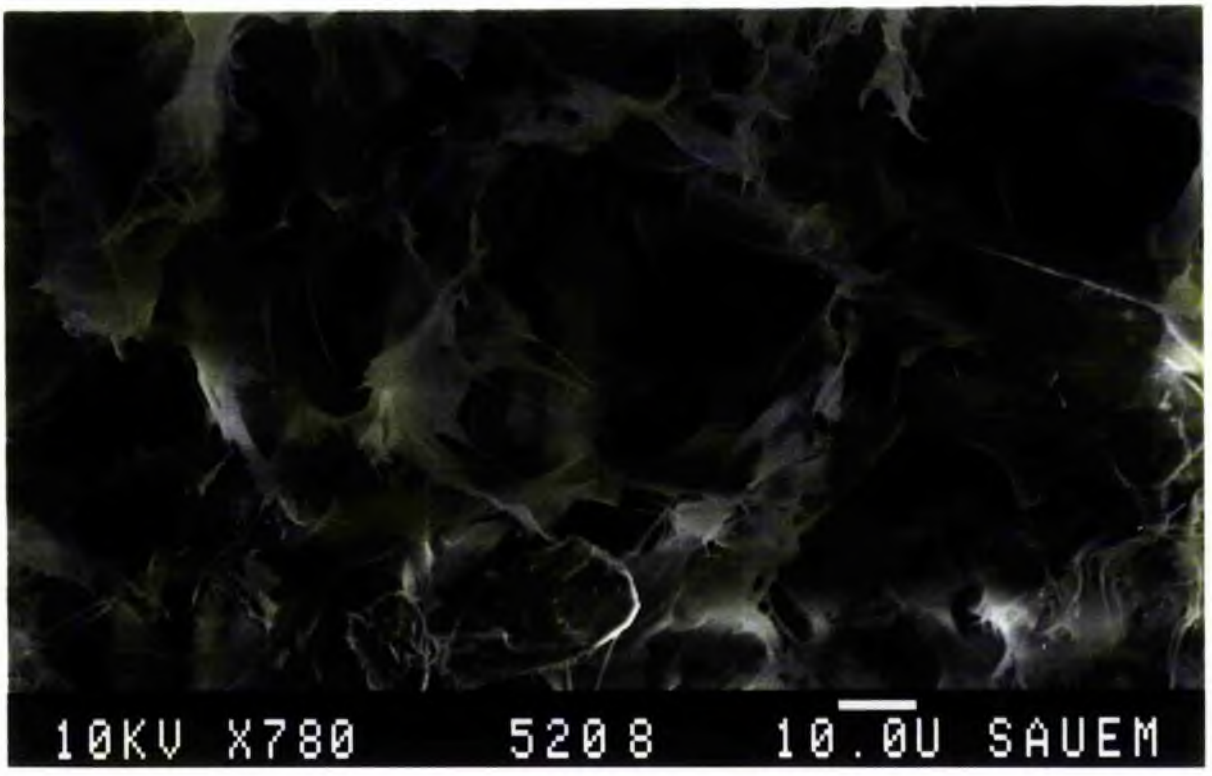
10KV X780 5208 10.0U SAUEM

Plate 4.17. Close up of part of Plate 4.1, showing grain-carbonate relations. Feldspar irregularly embayed and serrated against carbonate (middle bottom and top left). Quartz grain (in extinction top right) shows euhedral overgrowth outline in part and lobate and serrated margin with a remnant 'ghost' of original boundary before corrosion. Quartz grain (lower left) has overgrowth (left margin of grain irregular and corroded; corrosion more obvious on top and right margin of the grain). (x200) (Reith Bank-1; 12,726 ft).

Plate 4.18 Embayed and scalloped quartz grains against coarse grained carbonate filling enlarged pore space. (x40) (Reith Bank-1; 12,750 ft).

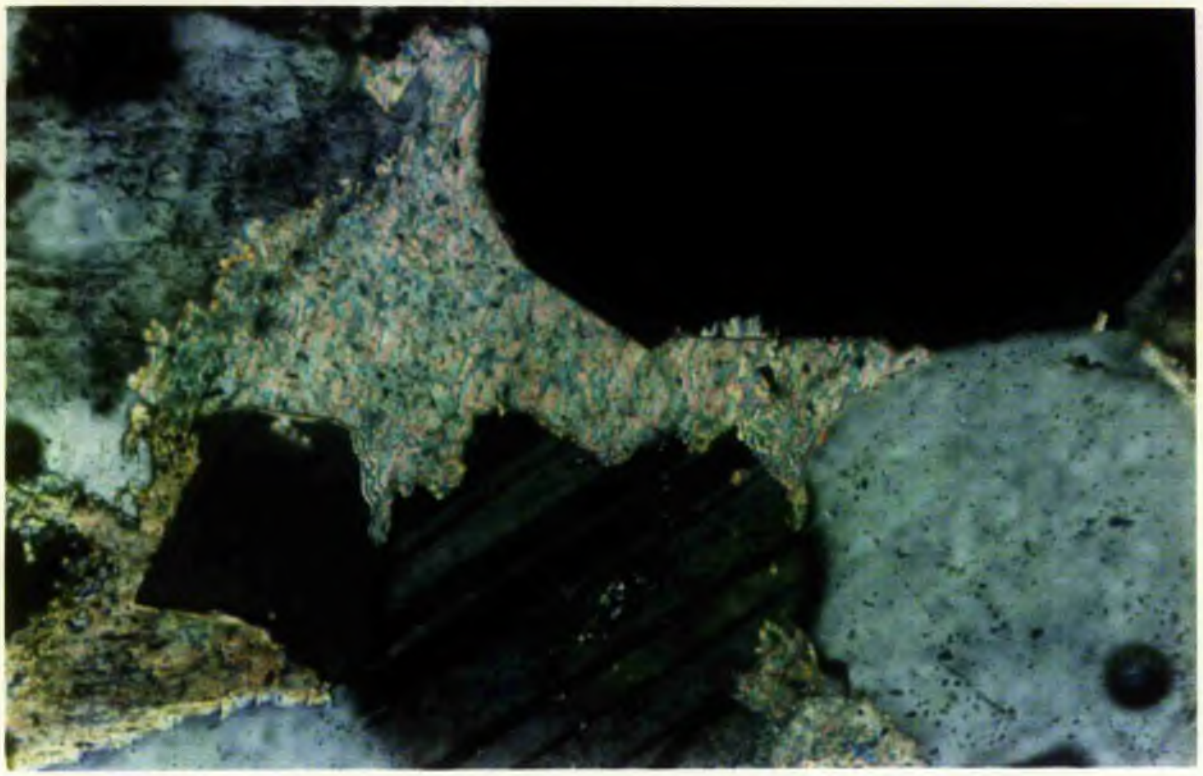

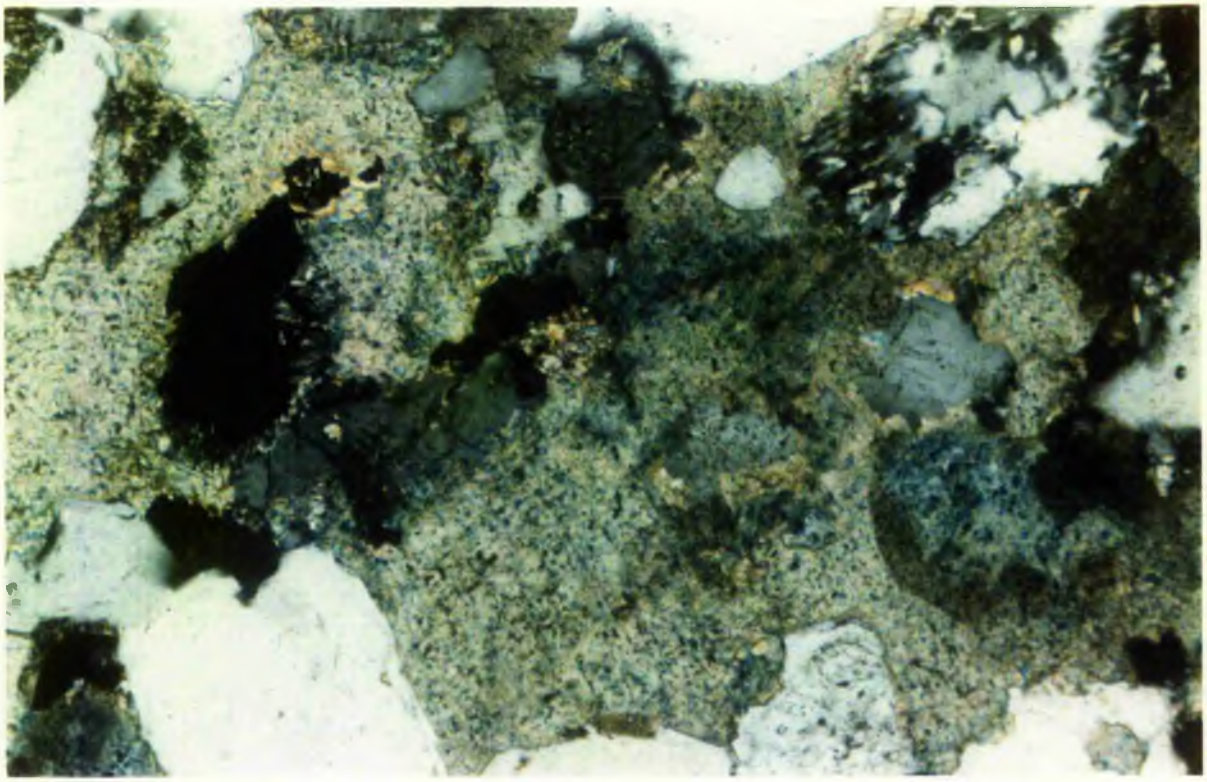

Plate 4.19 Carbonate cementation filling the between particle spaces. The carbonate is ferroan-dolomite in composition (turquoise staining), corroding the quartz, feldspar and lithoclast fragments. (x100) (Reith Bank-1, 12,732 ft).

Plate 4.20 Reduced primary porosity due to carbonate cement. The carbonate is calcite (brownish pink) and ferroan-dolomite (turquoise) in composition. Ferroan dolomite appears to have been formed by replacement of calcite margins. The carbonate has penetrated and slightly expanded the quartz grain. Skeletal feldspar is present, top middle. Porosity has also been reduced by opaques. (x40) (Reith Bank-1, 10,449 ft).

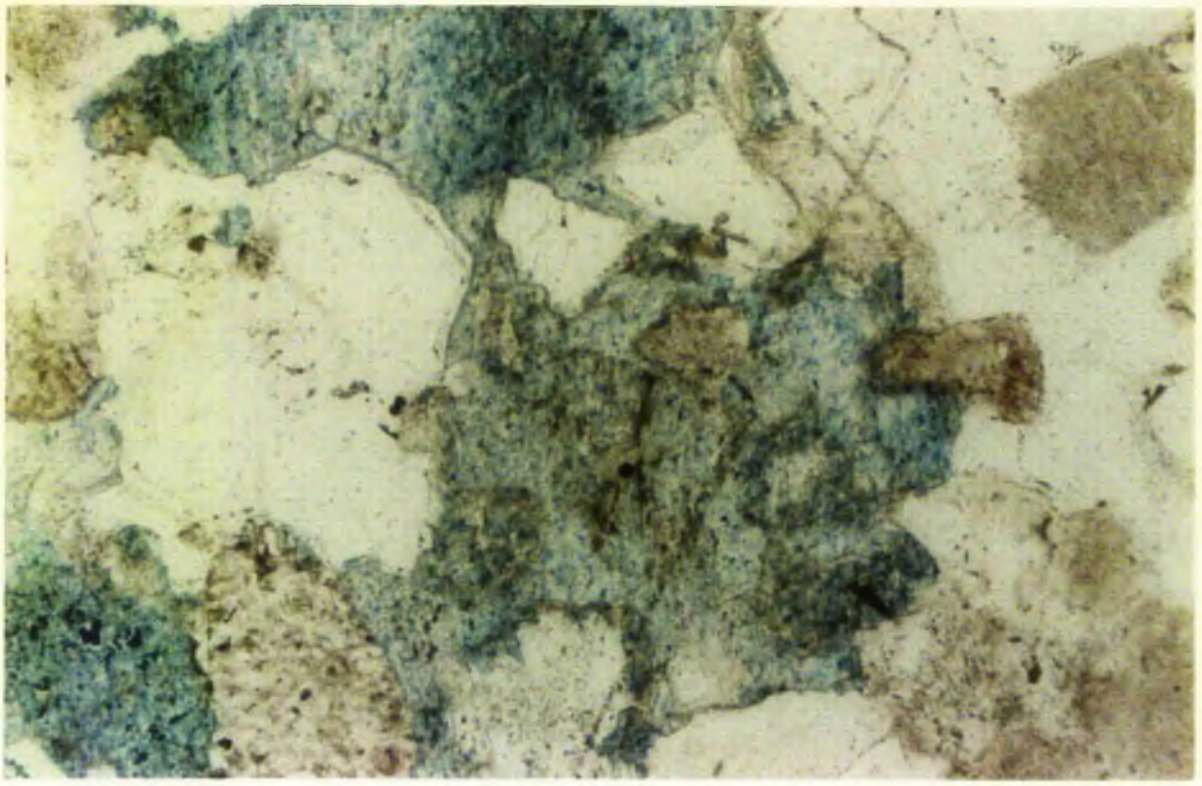

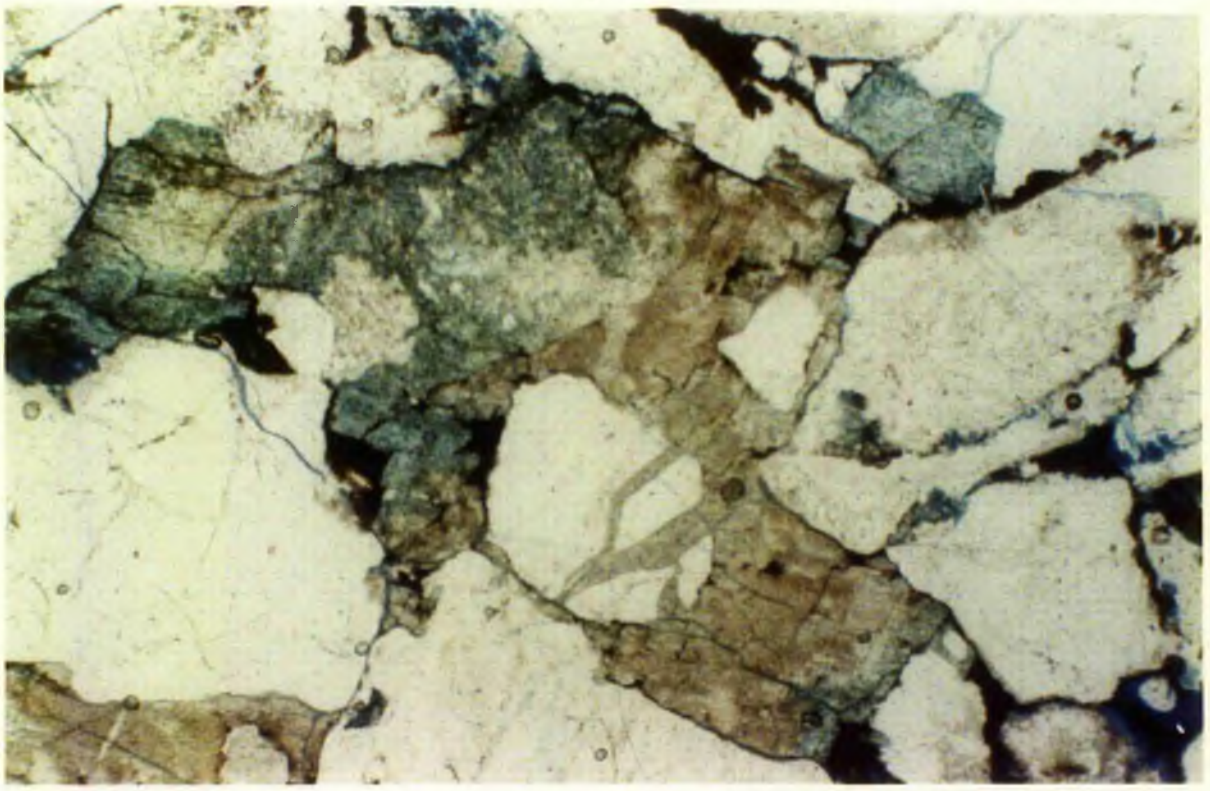

Plate 4.21 Quartz-calcite-Na-feldspar relation. Both quartz and feldspar have been corroded along their margins with calcite. The latter scalloping into the former two. (Reith Bank-1; 12,726 ft).

Plate 4.22 Clay-dolomite rhomb-quartz relation. Well formed dolomite crystals growing amongst clays. Quartz margins are corroded. (Reith Bank-1; 12,726 ft).

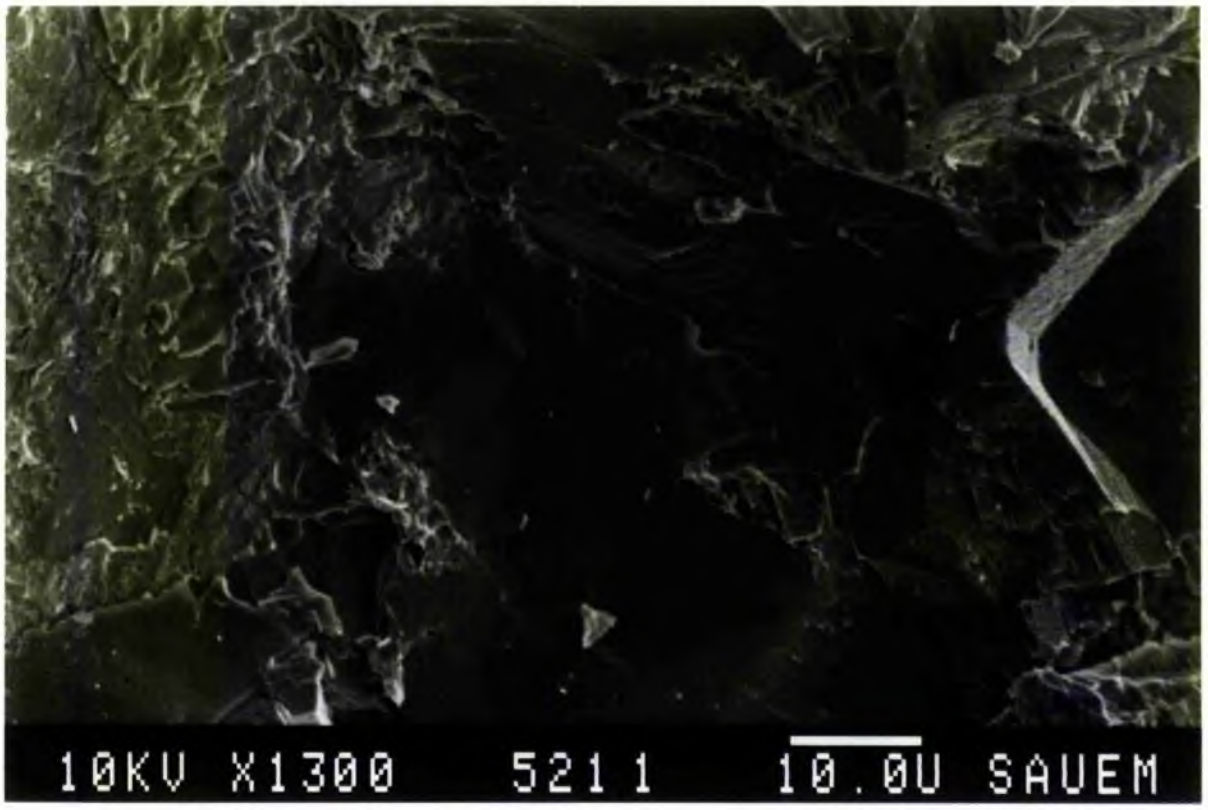
10KV X1300 5211 10.0U SAUEM

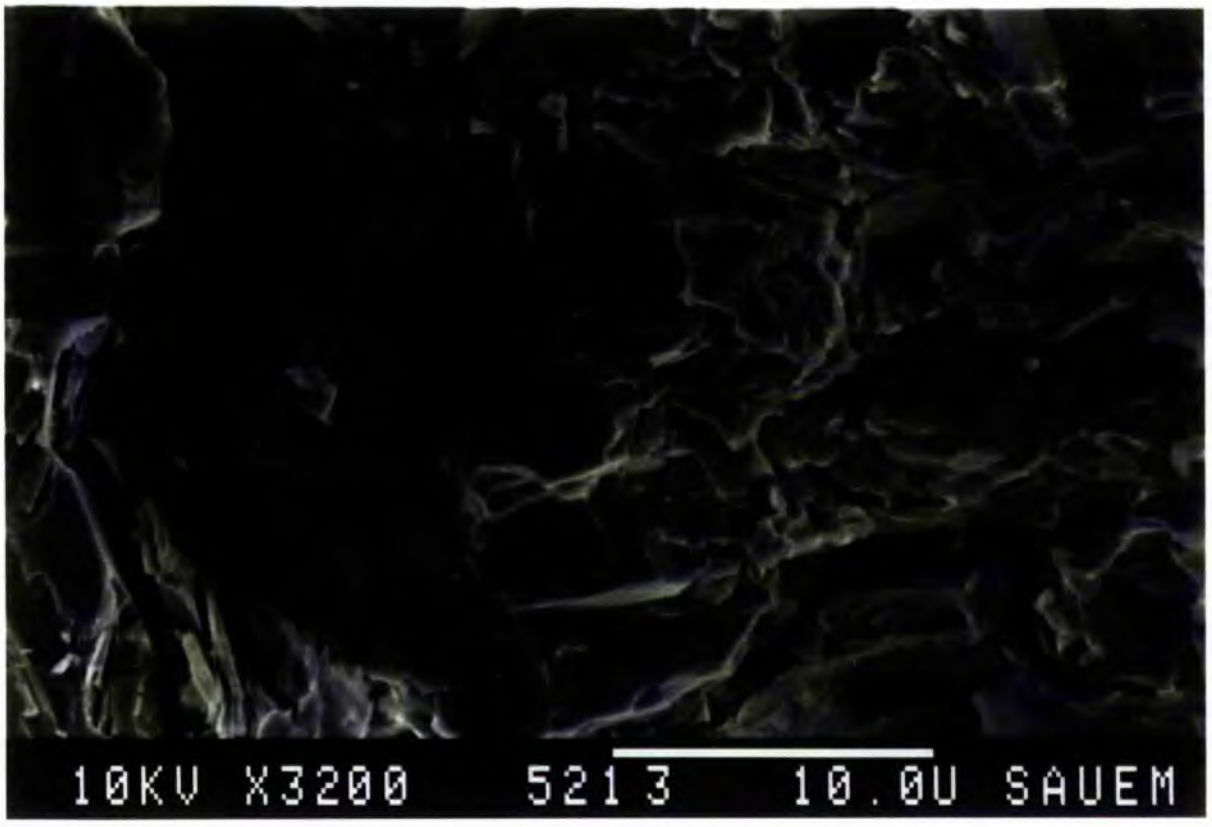
10KV X3200 5213 10.0U SAUEM

Plate 4.23 Manganese rich dolomite, showing zoning in growth with well developed rhomboidal core (yellowish-orange in colour) to massive carbonate (orange in colour) growing into the surrounding quartz. (Reith Bank, 10,451 ft).

Plate 4.24 Massive pore filling carbonate with little zoning (top centre), with quartz all round. (Reith Bank, 10,449 ft).

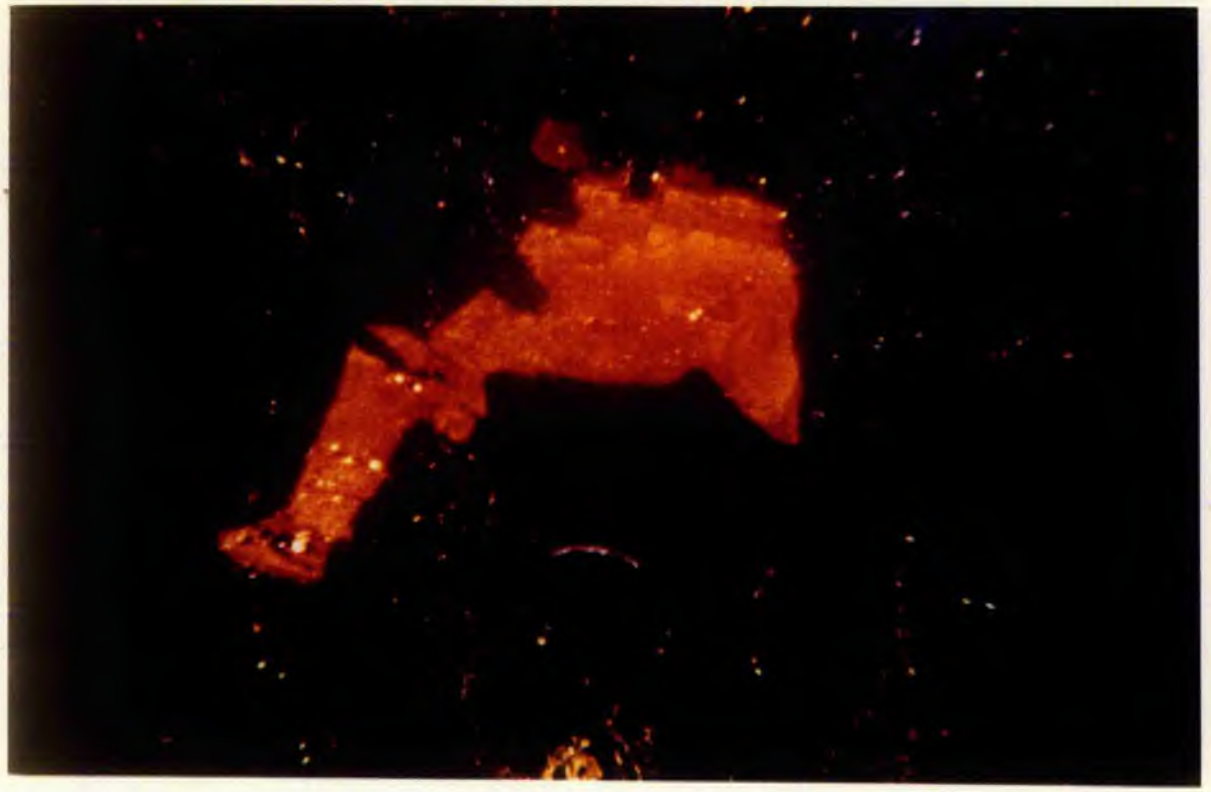

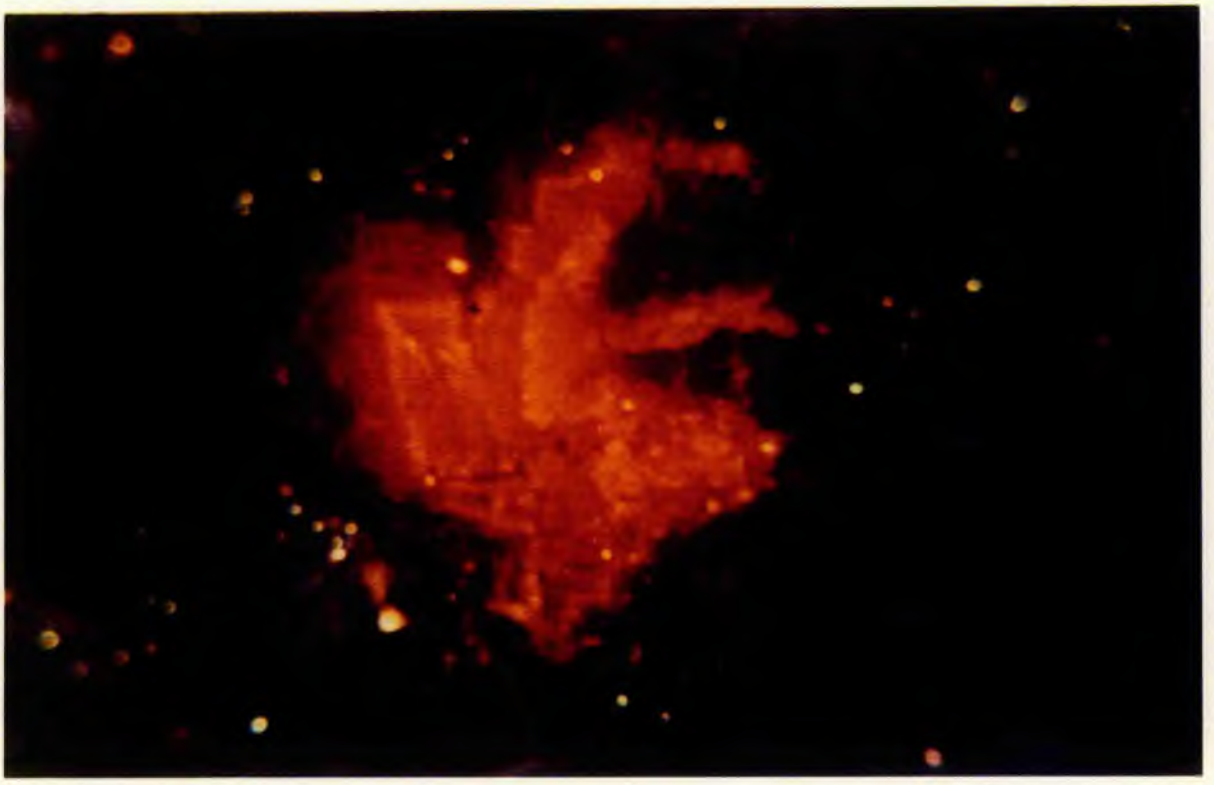

Plate 4.25 Zoned carbonate cement (white) amongst quartz grains (grey). The carbonate is poikilotopic towards the left and has engulfed a satellite grain of quartz (lower part). Towards the upper part the carbonate margins are well developed against clay as the former made room for its growth by compressing the latter. (Back Scatter photograph) (Seagull Shoals-1, 8875 ft).

Plate 4.26 Enlarged part of Plate 4.25 showing distinct zonation in carbonate cement with zones marked by differing chemical compositions. The darker zone is stage I (peripheral), followed by a lighter central stage II carbonate which was precipitated after the dissolution of the first stage. Towards the periphery (at points 1 & 4) lighter iron rich dolomite has been precipitated. This later carbonate has straight well formed rhomboidal margins. (The spot numbers point to the locations at which analysis was carried out; c.f. Fig 4.13). (Back Scatter photograph) (Seagull Shoals-1, 8875 ft).

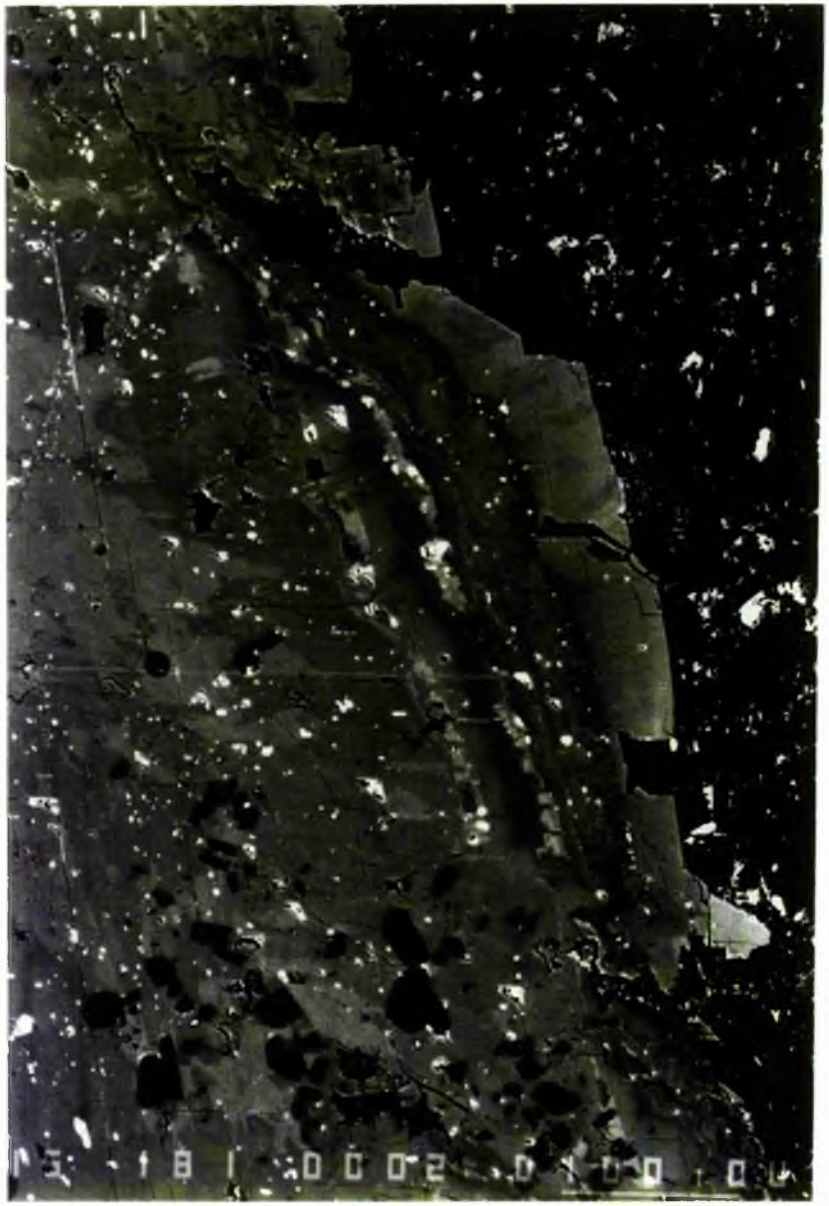

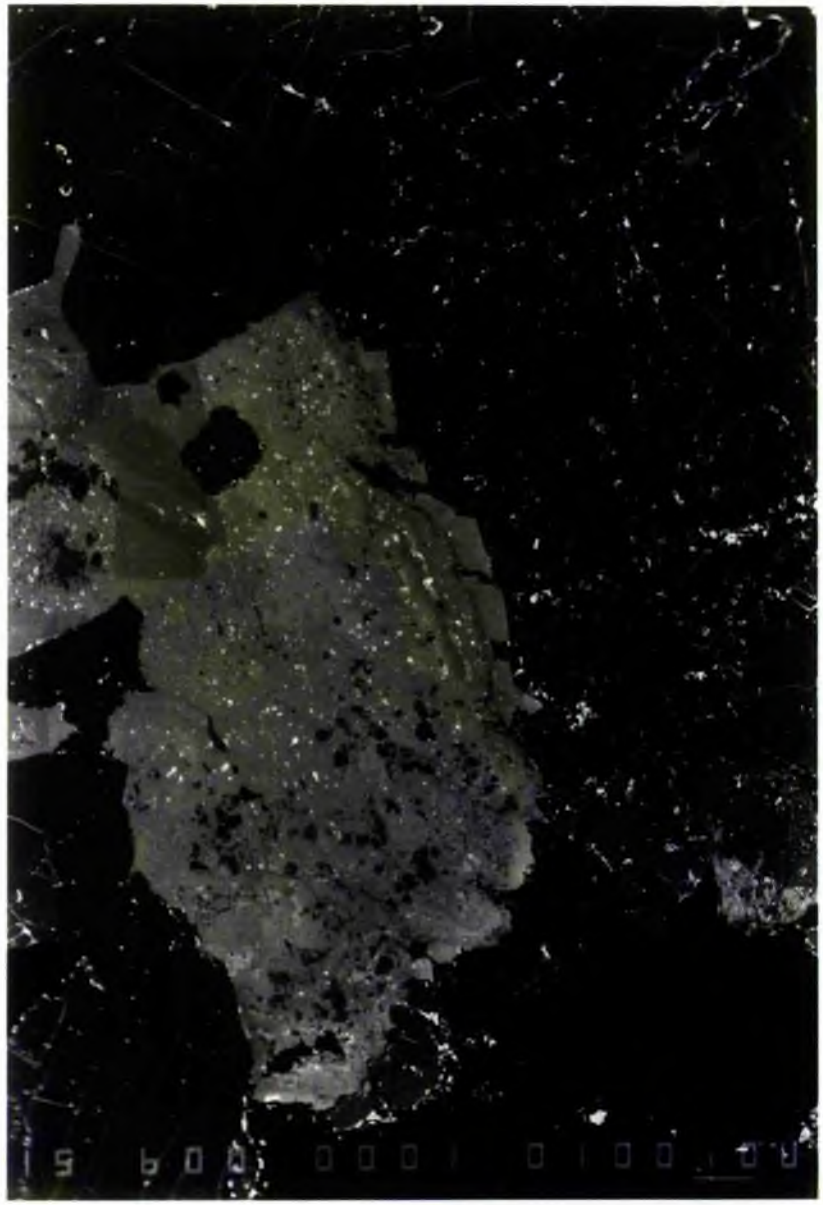

Plate 4.27 Enlarged part of Plate 4.25 showing two generation of cementation. The darker coloured carbonate is the first stage, while lighter colour carbonate is second stage. In the middle the carbonate has probably replaced a feldspar grain. (The spot numbers point to the locations at which analysis was carried out; c.f. Fig. 4.14) (Back Scatter photograph) (Seagull Shoals-1, 8875 ft).

Plate 4.28 Well formed euhedral crystals of dolomite. (Back Scatter photograph) (Seagull Shoals-1, 8875 ft).

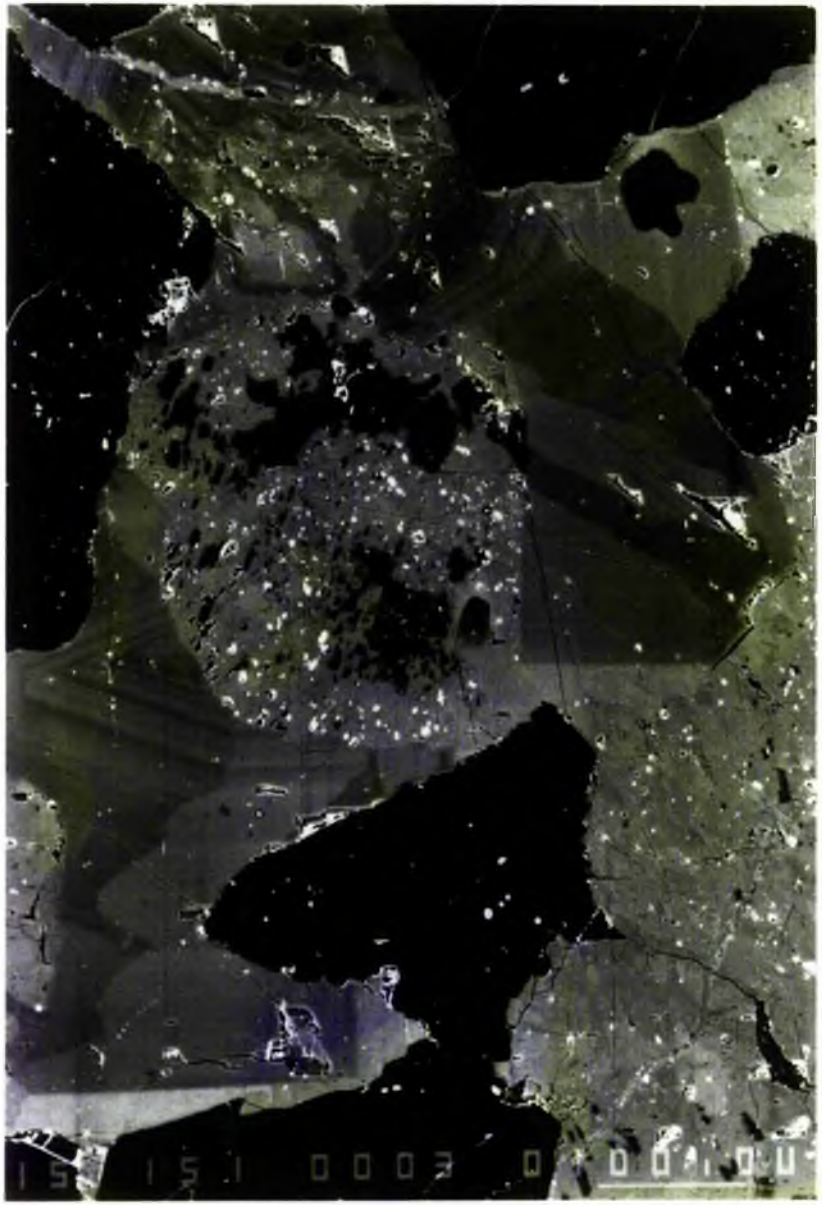

Plate 4.29 & 4.30 Carbonate is growing in conformity with the pore spaces. Where there is clay the faces of carbonate are well developed while, in places of quartz (appears as black) the faces take the shape of the quartz margin sandwiching the clay in between. (Back Scatter photograph) (Reith Bank-1, 10,449 ft).

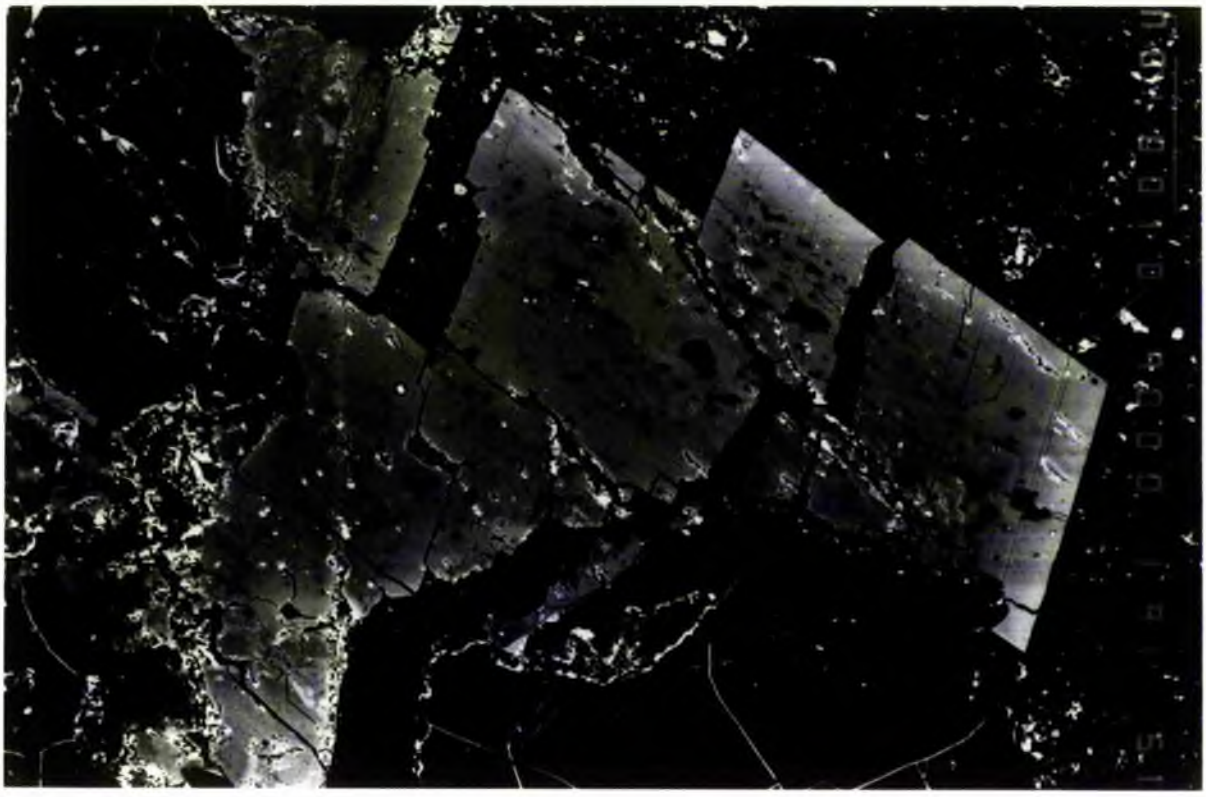

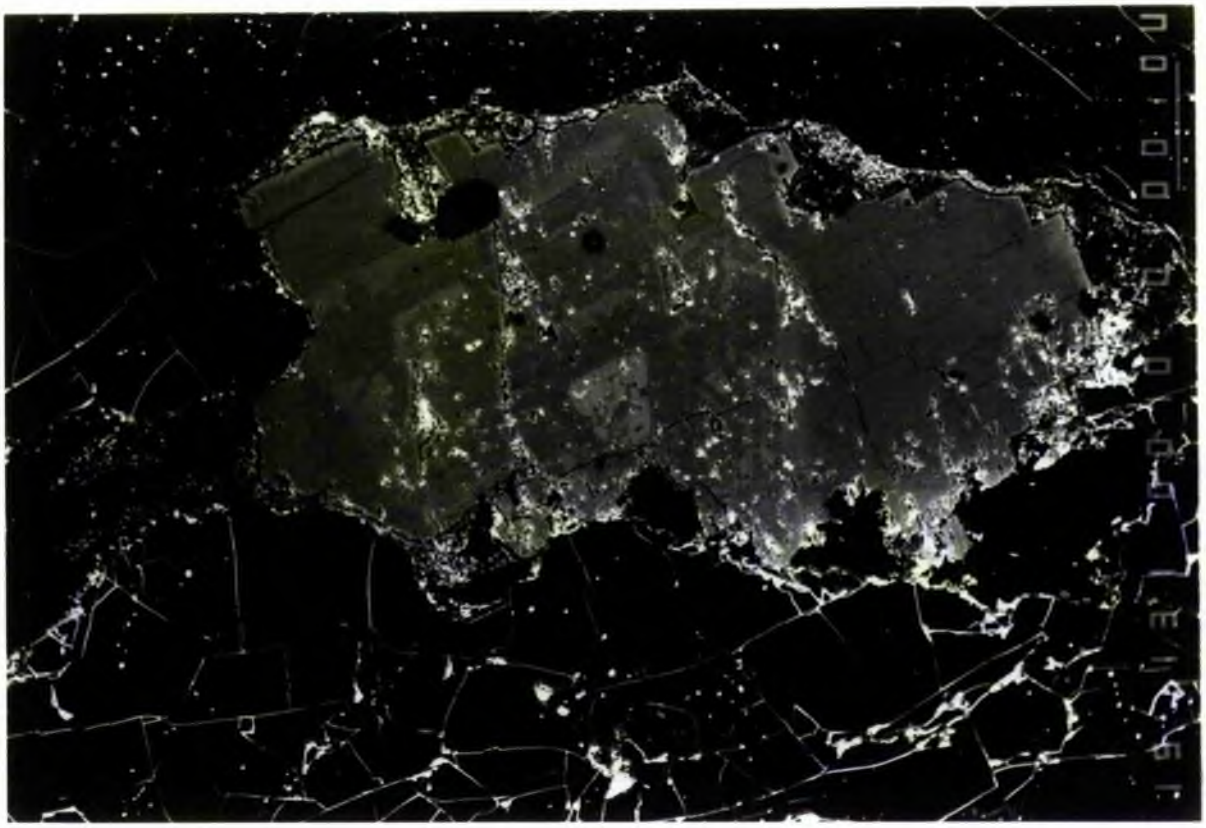

Plate 4.31 Deformed mica (lower right); straight mica (middle) confined by quartz with overgrowth. Overgrowth also fills one side of the scalloped and embayed plagioclase and carbonate on the opposite margin. Illite seams and aggregates (upper left and right). (x150) (Seagull Shoals-1; 8973 ft).

Plate 4.32 Quartz mosaic; plagioclase grains fractured, with straight margins parallel to twin planes and scalloped margins normal to lamellar twinning. Kaolinite fills pores and forms seams between feldspar and quartz grains. Carbonate (upper left) scalloped against feldspar and serrated and scalloped against clay. (x100) (Seagull Shoals-1; 8977 ft).

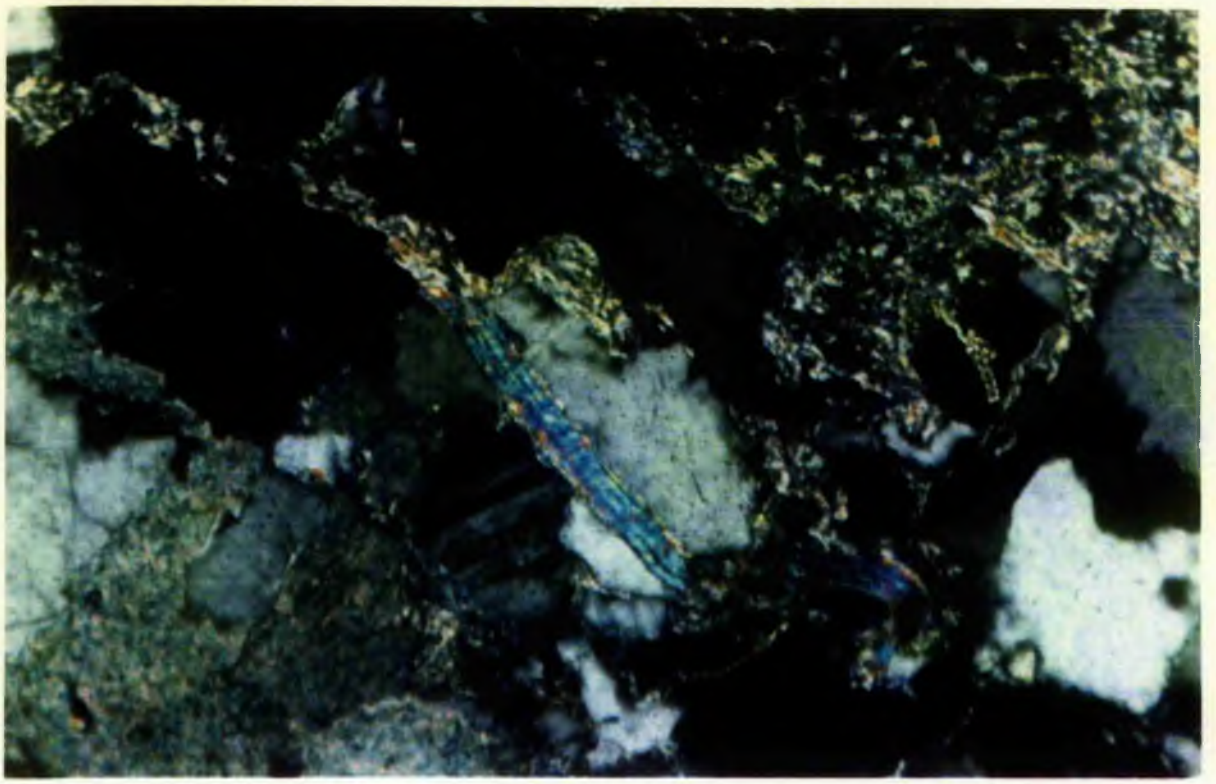

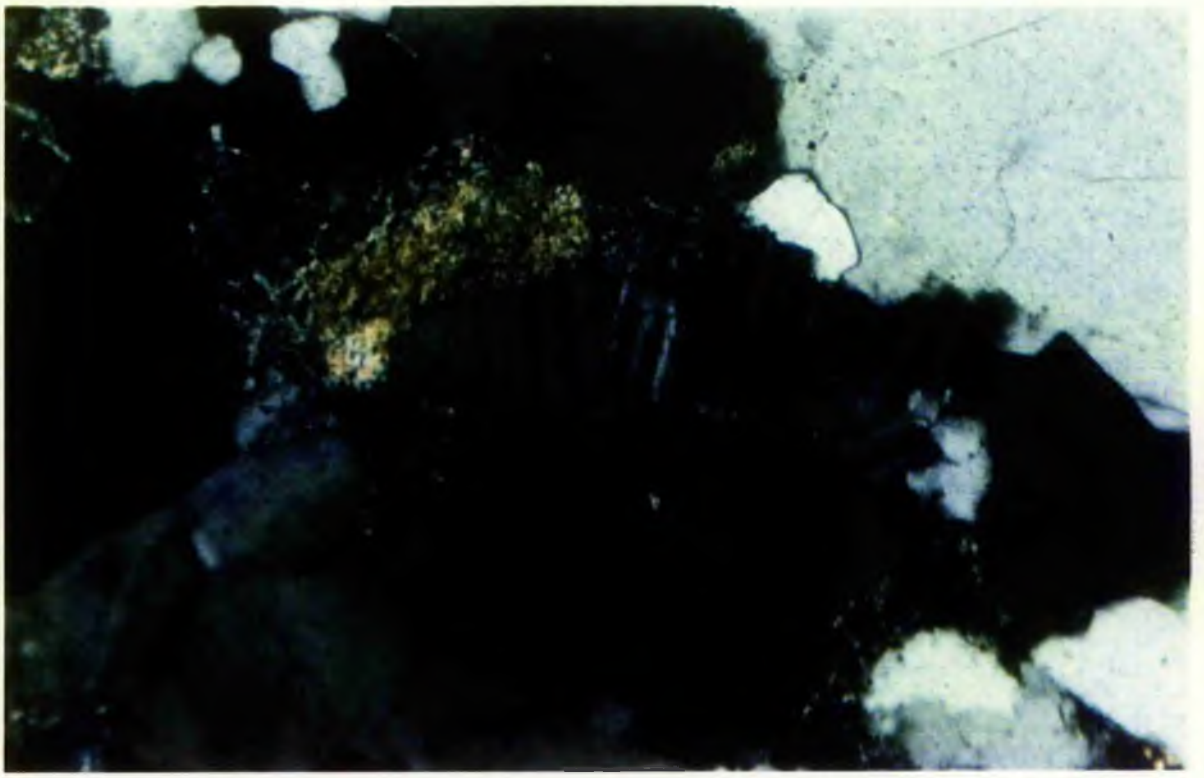

Plate 4.33 Quartz overgrowth trapping some clay fragments (middle and left top), with K-feldspar on the right and bottom left. Detrital rutile grain is also present in the left middle of the fig. (Reith Bank-1; 12,750 ft).

Plate 4.34 Corroded detrital K-feldspar. The corrosion occurring along the cleavage planes. Illitic clays are eating into the feldspar (extreme left and right). (Reith Bank-1, 12,748 ft).

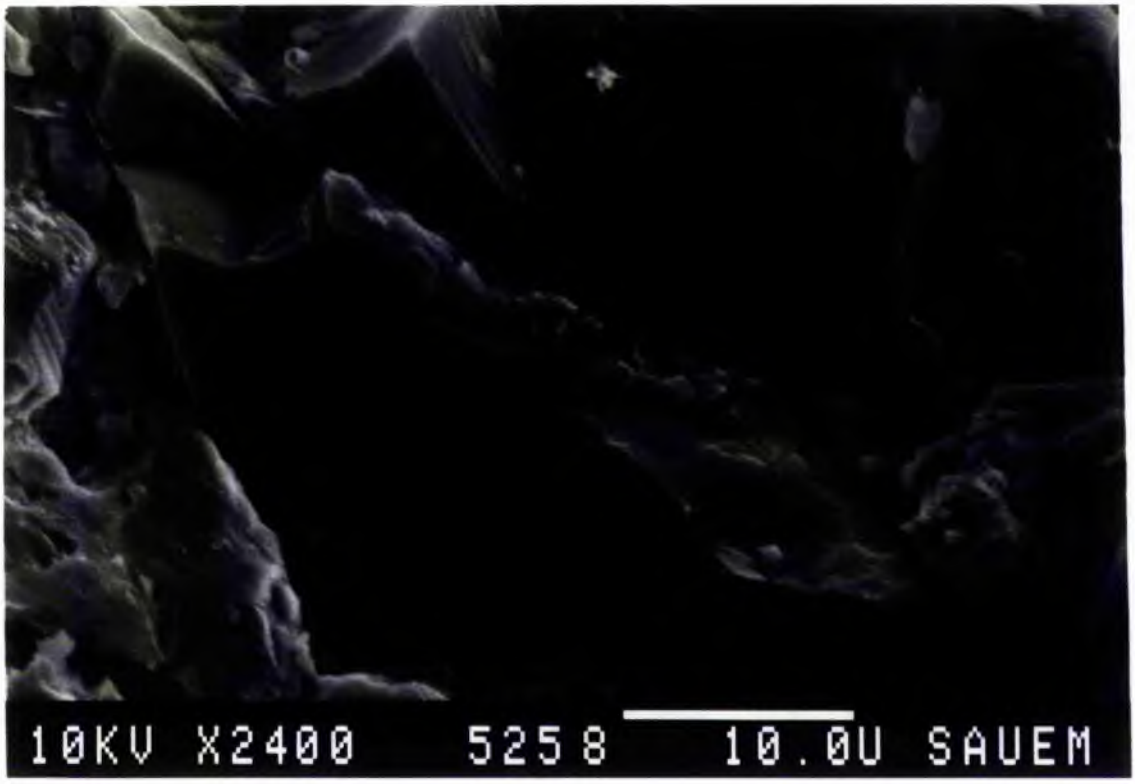
10KV X2400 5258 10.0U SAUEM

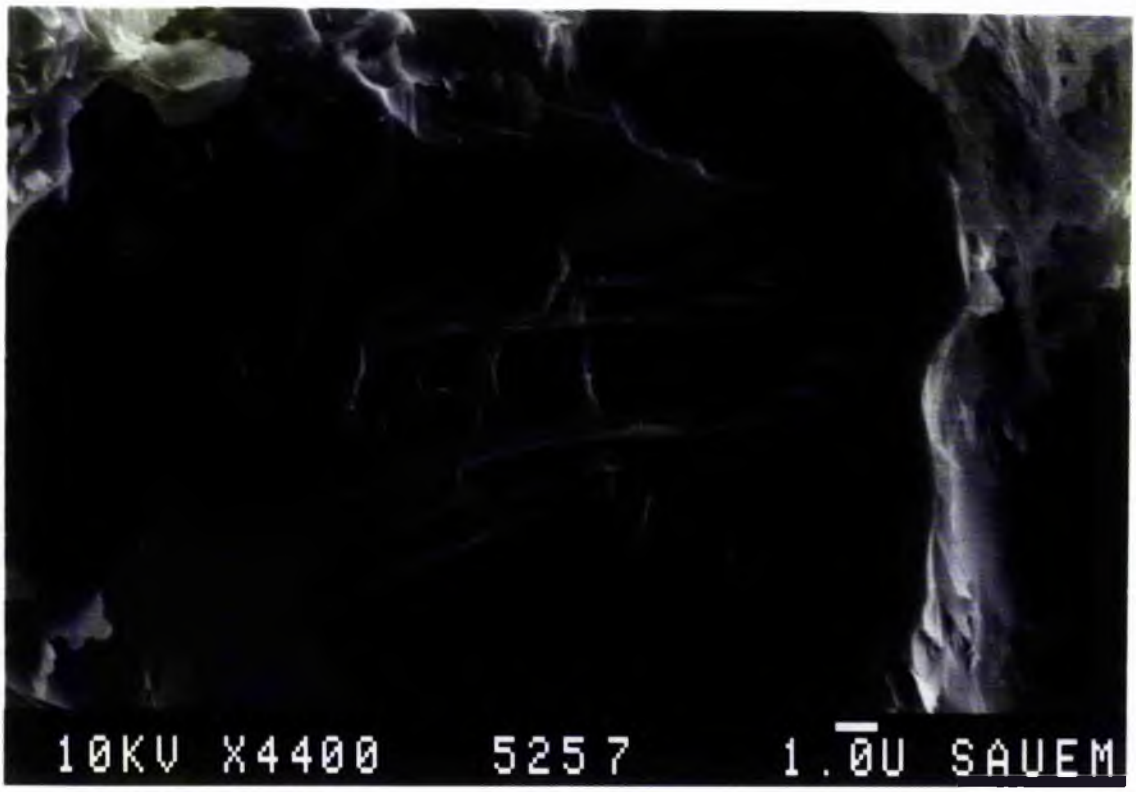
10KV X4400 5257 1.0U SAUEM

Plate 4.35 Corroded quartz surrounded by clay. Quartz has etched pits (left top and right middle). Clay entrapped between the quartz grains (top middle). (Reith Bank-1; 12,740 ft).


5221
10.0U SAUEM

CHAPTER 5: PALEOGEOGRAPHY & BURIAL HISTORY

(with 3 figures)

5.1. PALEOGEOGRAPHY:

Although there is still some debate regarding the drift history of the Seychelles and the development of associated basins, recent work suggests that pre-fragmentation Gondwana has the Seychelles off the north-east coast of Madagascar and India close-by to the east (Fig. 5.1, Norton & Sclater, 1979; Nopec a.s., 1985; Molnar *et al*, 1988; Scotese *et al*, 1988). In this position the 'Seychelles' Karoo basin is separated from the Majunga and Morondova basins of western Madagascar by a northerly projecting peninsula. This 'Madagascar' source land shed debris (see section 4.2) eastwards to the Seychelles area as well as westwards to the Majunga and Morondova basins. Marine connections to the north allowed occasional trangressions far south to form the marine horizons of the Morondova basin.

Though the evidence from the three wells is sparse, it may be used to develop a tentative model of the paleogeography during the accumulation of the Karoo sediments (Fig. 5.2) (Walton & Khanna. 1990).

In this model, the eastern margin of the source-land was a major fault, a line similar to the present coast-line. In the immediate vicinity of the fault line, alluvial fans spread out towards a braid plain and beyond, to a meander belt of a major river draining northwards to Tethys and skirting the inner part of the Seychelles. The Karoo sediments did not spread on to the Seychelles region (Khanna & Pillay, 1988) which persisted as a positive, but not a major source area. The evidence for a westerly source rather than a 'Seychelles' source lies in the paleocurrent observations. The present SW and SSW directions resolve into NW and WNW on rotation of the Seychelles back to their 'Gondwana' position.

The megacycles comprising upward fining sequences find an explanation as the result of major rejuvenation events of the source area which took place at lengthy intervals along the boundary fault zone. This is recorded twice in the coarse Members 2 and 4 in Reith Bank-1. In time scarp retreat, topographic lowering and spread or swing of the meander belt zone westwards to the Reith Bank-1 and Seagull Shoals-1 would have brought in the sandstones and mudstones of Member 5.

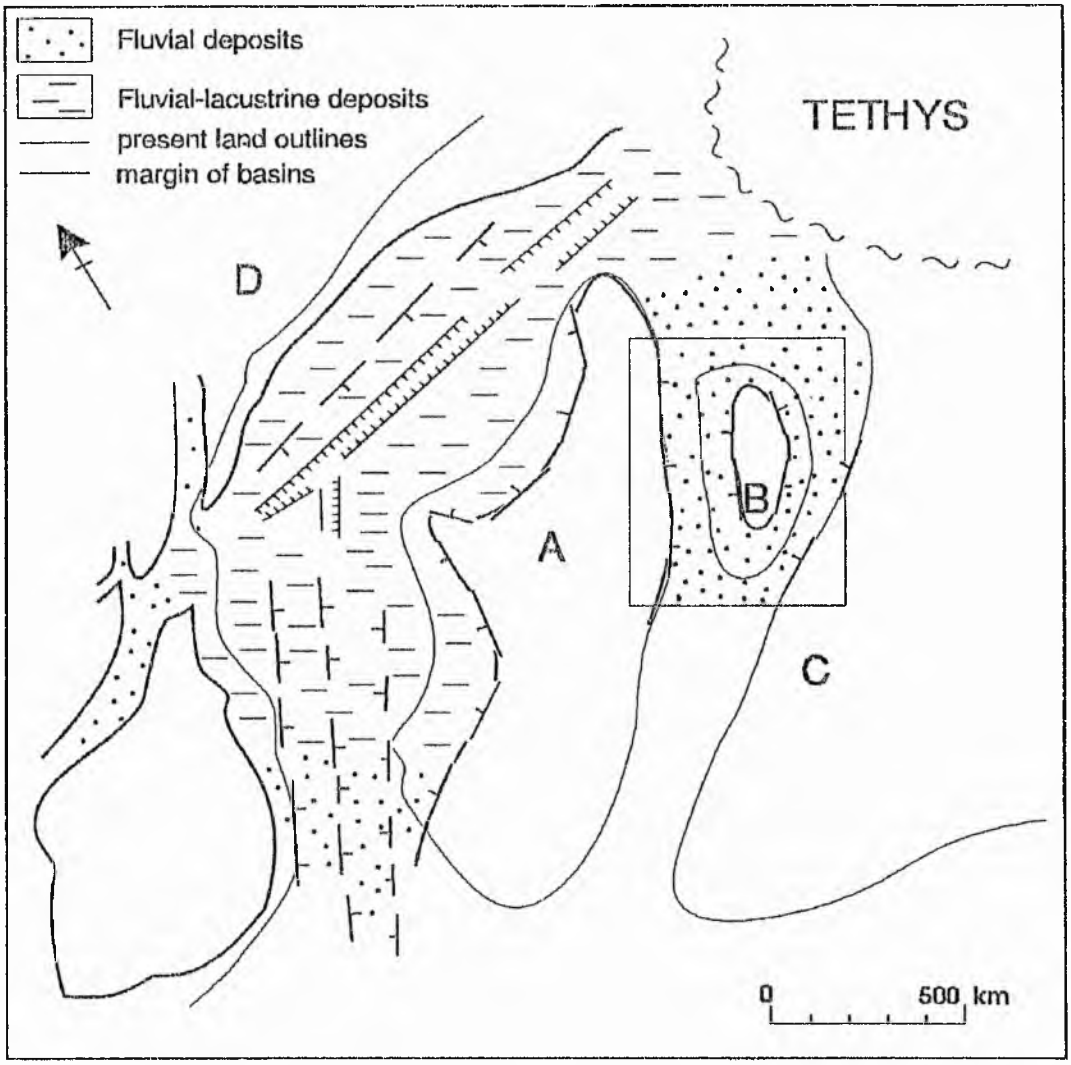

Fig. 5.1 Triassic Gondwana reconstruction. (western part based on Narayanan & Vollset, 1987). A-Madagascar, B-Seychelles, C-India, D-Africa. Dotted ornament-fluvial deposits. Dashed ornament-fluvial-lacustrine passing north-eastwards into fluvio-marine. Major rift developing between Madagascar and Africa.

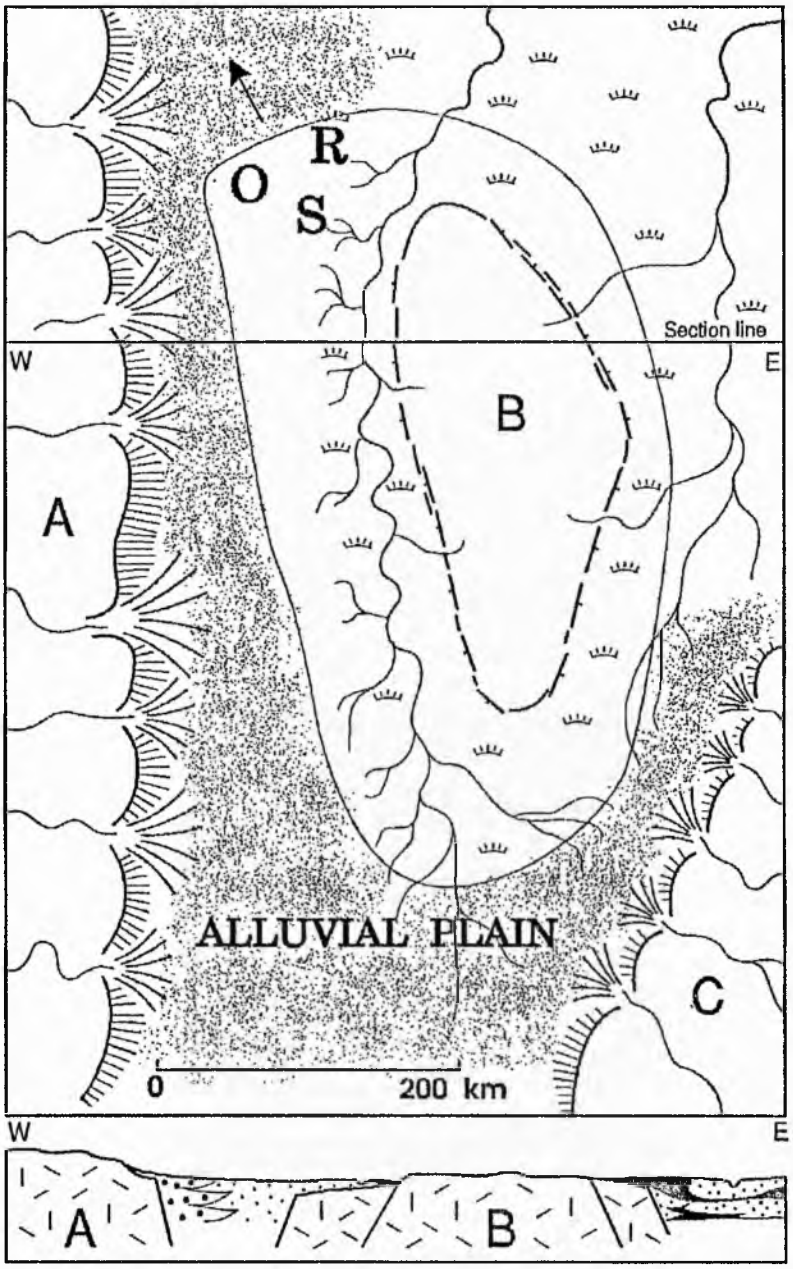

Fig. 5.2 Enlarged portion of 5.1 showing Karoo paleogeography of Seychelles area. R-Location of Reith Bank area; S-Location of Seagull Shoals area; O-Location of Owen Bank area. A-Madagascar with faulted escarpment, alluvial fans (divergent lines) leading to braid plain (stippled). B-Seychelles; margin dashed line; central positive, non-depositional area surrounded by meander belts and flood plains (pecked lines). C-India with faulted escarpment, alluvial fans and alluvial plain giving way to meander belt and flood plain. W-E - schematic cross section across area.

5.2. BURIAL HISTORY:

The thickness of sediments and the positions of unconformities together with maturation indices of organic content give an indication of the burial history of Karoo and subsequent sequences (Fig. 5.3). This allows diagenetic episodes to be related to depth-time curves. The story is complicated by active faulting especially through Mesozoic times which has meant differential movements between all three areas represented by the wells.

5.2.1. Reith Bank-1:

Karoo sediments of Reith Bank Which were dominantly terrestrial were laid down at a height at or above sea-leve) from Middle to Late Triassic times (Fig. 5.3a). By Jurassic times, terrestrial conditions gave way to marine. Member 5 would have accumulated near sea-level by which stage the lowest beds penetrated the borehole were more than 6000 ft deep (uncorrected for compaction). These lower members by this time had suffered i) leaching by meteoric waters, ii) kaolinite formation, iii) some smectite-illite mixed layer transformations, and iv) possibly early quartz overgrowths. Both the transgression, and the thinness of the Jurassic marine sediments were a consequence of crustal thinning and block faulting (Fig. 5.3a). Around middle or late Jurassic times the movements were associated with the passive margin of Madagascar-Seychelles moving southwards from East Africa.

Interpretation of the burial history during Jurassic and Cretaceous times depends on the stratigraphic positions (determined by Robertson Research International (1980, 1981a, 1981b) of sequences above the Middle Jurassic beds which follow the Karoo. The first, are conformable beds above the Middle Jurassic very tentatively given a Late Jurassic age. If these are in fact Middle Jurassic, the unconformity above could have begun as early as about 160 Ma.

The succeeding horizon (5796-5940 ft) is, again tentatively, identified as Cenomanian-Albian. If this is its correct age then uplift must have occurred before this time (an interpretation represented by thin dashed curve Fig. 5.3a). On the other hand, a Santonian age is not ruled out; considerable subsidence may have occurred. A thickness comparable with the Jurassic-Cretaceous rocks of Owen Bank (Fig. 5.2) may have accumulated before uplift and erosion (Fig. 5.3a, solid curve). Some support for this interpretation lies in the jump in Spore Colour Index from 3.5 in Late Cretaceous beds to 8 in the upper part of the Karoo sequence (Khanna & Pillay, 1988). Some of the scarce

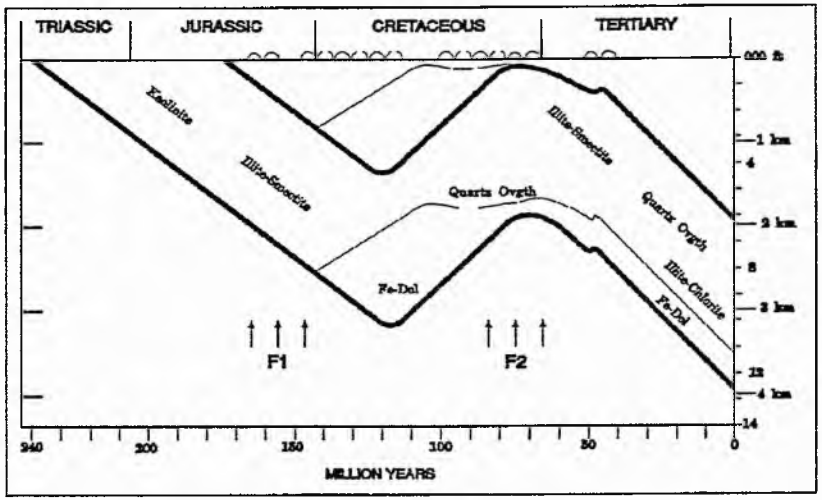

(a) Reith Bank

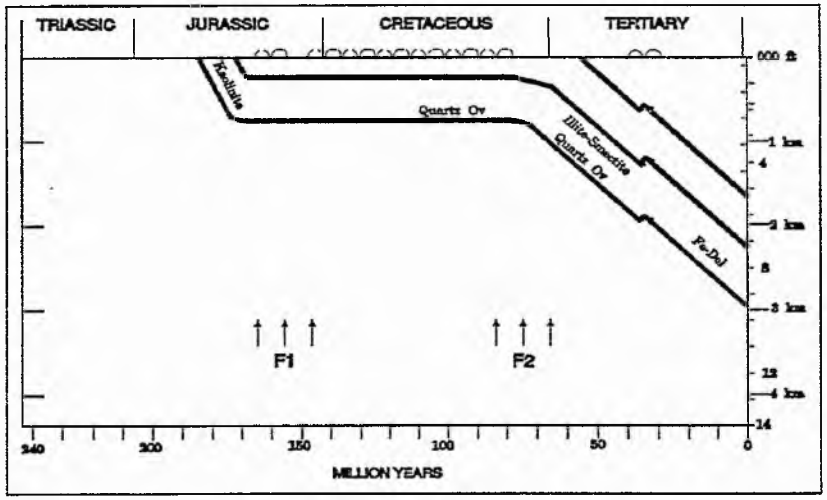

(b) Seagull Shoals

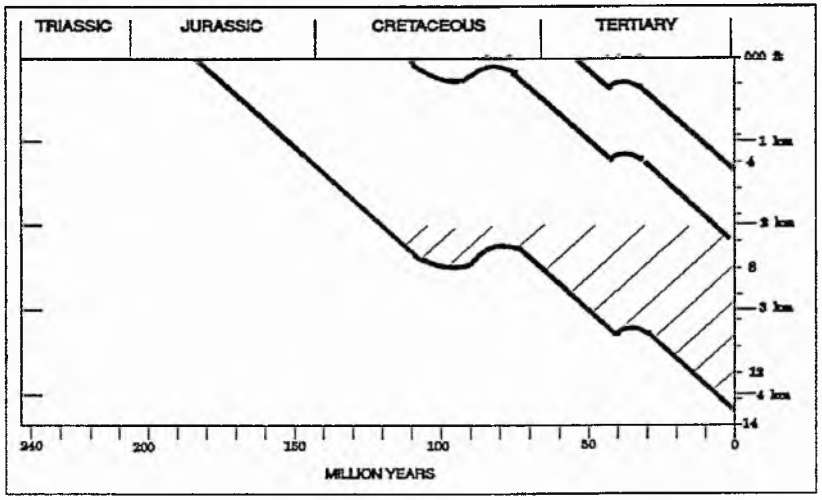

(c) Owen Bank

Fig. 5.3 Burial curves for the sediments of the Western Shelf, Seychelles, showing possible time-depth positions of diagenetic minerals. The curves are designed to be illustrative rather than precise. No allowance has been made for compaction; depths are those in wells; undulating lines indicate positions of unconformiies in time. F1 & F2- tectonism related to drift episodes. Thin dashed curve in Fig. (a) is based on main unconformity between Middle Jurassic and Cenomanian-Albian, while solid curve is on the assumption that the unconformity occured between Middle Jurassic and Santonian. Diagonal ornamentation in Fig. (c) indicates zone of potential oil generation.

calcite cement may have formed over this period, but little now remains. At deeper levels illite-smectite reactions would have continued as well as quartz cementation.

On either interpretation late Cretaceous uplift was followed by significant subsidence (over 5000ft) during the Tertiary, subsidence which was interrupted for a short while during the Eocene with an unconformity developed during the middle of that epoch. At the same time the Karoo suffered deeper burial which resulted in the elimination of kaolinite and illite-smectite and the production of the illite-chlorite assemblage. Late fluids would also have been responsible for the corrosion of quartz and feldspar and the growth of ferroan dolomite (see Burley *et al*, 1985, Fig. 17).

5.2.2. Seagull Shoals-1:

The burial history of the Karoo rocks at Seagull Shoals-1 (Fig. 5.2b) is similar to that at Reith Bank-1 with the difference that the upper boundary now lies at over 7000 ft compared with 6000 ft. The difference from Reith Bank-1 lies almost entirely in the presence of 1290 ft of Maastrichtian basalts. The boundary fault to Seagull Shoals, uplifted periodically during the Jurassic and Cretaceous became dormant and the thick basalts were able to accumulate and avoid any subsequent erosion; their thickness is similar to that of the Owen Bank-1A trough.

On the Seagull shoals block, like Reith Bank many of the diagenetic changes, apart from perhaps some early leaching and embryonic kaolinite, would have taken place during Tertiary times (Fig. 5.3b). Kaolinite is still present, as in Member 5, with quartz overgrowths, illite-smectite and a little ferroan-dolomite.

5.2.3. Owen Bank:

Although the post-Karoo sediments have not been addressed in this study it is instructive to consider Owen Bank in relation to possible hydrocarbon generation (Fig. 5.3c). The sequence here is remarkable in revealing 14,000 ft of Tertiary and Mesozoic marine sediments down to Middle to Lower Jurassic. While boundary faults to Seagull Shoals and Reith Bank were active from at least Jurassic to the beginning of Tertiary times, leaving Jurassic and Cretaceous successions very attenuated, the Owen Bank block was less affected. Subsidence was persistent and broken only by mid-Cretaceous unconformity (Fig. 5.3c). Similar rates of subsidence ensued through the Cretaceous and Tertiary with some 2000 ft of Maastrichtian basalts and a minor unconformity during middle Eocene.

With such a subsidence history and a temperature gradient of 40° C/km (indicated by organic maturation studies of Khanna and Pillay, 1987) oil generation would have been possible from marine source rocks during the Cretaceous with a main phase probable during early Tertiary times. Karoo and younger rocks would have provided potential reservoirs.

SECTION II

CHAPTER 6: GENERAL GEOLOGY

(with 7 figures and 1 table)

This section of the thesis is based on the studies carried out under the auspices of Shawa Geoconsultants Ltd. of Calgary, Canada. Identification and description of lithologies, sedimentation and environmental reconstructions were primarily carried out by Shawa Geoconsultants, while the present author has worked on refining the model of deposition using available data, and has studied the petrology and diagenesis of the sediments.

6.1. METHODOLOGY:

The interpretation of sedimentation and environment of deposition is based on data collected from stratigraphic synthesis and the geometry of sand bodies, cutting and core description and gamma ray curves which mimic the vertical distribution of grain-size.

Lithology of the sandstones has been studied from the core logs and core cuttings supplied by M/s Shawa Geoconsultants Ltd., Calgary.

Further description of sandstones is based on the lithological logs supplied by M/s Shawa Geoconsultants, however, some of the characters are from hand specimen descriptions of samples by the author.

6.2. NOMENCLATURE & PREVIOUS WORK:

The Elk Point Group forms the basal unit of the Devonian System in Western Canada and consists of a sequence of evaporite, carbonate and clastic rocks that range up to 2000 feet thick in the Plains and to over 3500 feet in the northwestern Rocky Mountains. It rests directly on eroded Lower Paleozoic or Precambrian strata and is overlain by carbonates and shales of the Upper Devonian Beaverhill Lake and Souris River Formations. The distribution of these beds illustrates the slow expansion and filling of the basin.

The term Elk Point was coined by McGhee (1949) in the Elk Point area of east-central Alberta for the variable sequence of beds between dolomites of Ordovician age and the carbonate-shale sequence of late Middle or Upper Devonian age. The type section was taken from the Anglo-Canadian wells in townships 56 and 57, ranges 5 and 6, west of the fourth meridian. Workman (1953) demonstrated the existence of the Peace River high (a positive source area) during Elk Point time and briefly described and subdivided the Elk Point Group, but did not apply formational names. Crickmay (1954) adopted the Anglo-Canadian Elk Point No. 11 well (2-21-57-5W4) as the type section and divided it into nine members (Fig. 6.1).

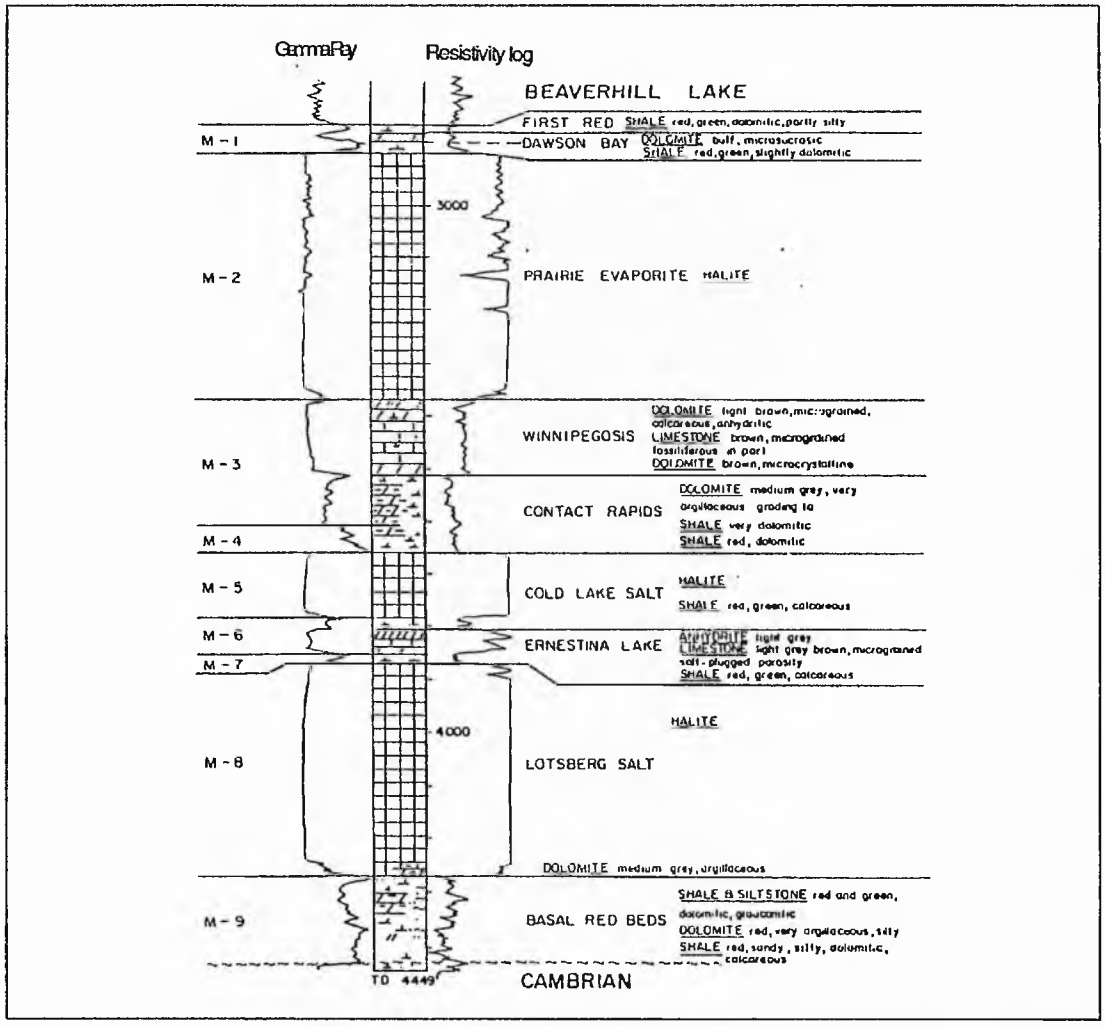

Fig. 6.1 Type section of Anglo Canadian Elk Point well (2-21-57-5W4) (after Crickmay, 1954).

The Watt Mountain Formation derives its name from the prominent hill at 58°40'N, 117°40'W and was named by Law (1955), with the type section in the California Standard Steen River well in 2-22-117-5W6 (Table 6.1). Van Hees (1956) divided the Elk Point Group at the base of the Ashern (Table 6.1) into an Upper Elk Point and a Lower Elk Point. However, regional studies by Sherwin (1962) indicate that the Ashern, as defined in the type locality, loses its identity northwest of the Meadow lake escarpment. He therefore took the base of the Keg River Formation as the division between Upper and Lower Elk Point subgroups.

The Gilwood Sandstone was referred to as a member of the Watt Mountain Formation by Guthrie (1956). The relationship of the Gilwood Sandstone Member to the older clastic detritus

Table 6.1 Distribution and correlation of the Elk Point Group.

Baillie 1953 Manitoba & Saskatchewan	Crickmay 1954 Central Alberta	Van Hees 1959	Law 1955 Northern Alberta	Grayston et al 1964 Manitoba & Saskatchewan	Grayston et al 1964 Central Alberta	Grayston et al 1964 Northern Alberta	Age
First Red Bed		U	Watt Mt	First Red Bed	First Red Bed	Watt Mt	M Givetian
Dawson Bay Second Red Bed	Member 1	P		Dawson Bay Second Red Bed	Dawson Bay Second Red Bed		I
ELK POINT Praire Evaporite	Member 2	P	Muskeg	Praire Evaporite	Praire Evaporite	Muskeg	D
		E					D
		R					E
	Member3		Keg River	Winnipegosis	Winnipegosis	Keg River	V O N I A N
Ashern				Ashern			Emsian
			Chinchaga		Contact Rapids	Chinchaga	
	Member4		Red Beds				
	Member5	L			Cold Lake	Cold Lake	L
	Member6	O			Ernestina Lake	Ernestina Lake	O
	Member7					Basal Red Beds	W
		W					E
	Member8	E			Lotsberg		R
		R					D
							E
							V
							O
	Member9				Basal Red Beds		N I A N

and to the Precambrian regolith was discussed by Pugh (1972). Petrological characters and depositional environments have been discussed by Kramers and Lerbekmo (1967), Christie (1971), Thachuk (1968), Shawa (1969), Jansa & Fischbuch (1974), Rottenfusser & Oliver (1977), Aulstead & Spencer (1985) and Trotter & Hein (1988).

6.3. LITHOLOGICAL SUCCESSION:

The Elk Point Group as so defined has been divided, for mapping purposes, into Lower Elk Point and Upper Elk Point subgroups (Fig. 6.2). The division is taken at the first widespread correlatable horizon - the base of the Winnipegosis-Keg River carbonate. This boundary essentially separates underlying beds of restricted distribution from the overlying much more widespread Upper Elk Point Group.

Sherwin (1962), has divided the section into four apparently conformable formations, the Lotsberg, Ernestina Lake, Cold Lake and Contact Rapids formations, with a basal Basal Red Beds section.

The Elk Point Group is represented in the study area by a basal Granite Wash lithology, followed by Chinchaga, Keg River and Muskeg Formations. The topmost Formation is called the Watt Mountain. The Granite Wash lies over the Precambrian basement granites and gneisses of the Peace River Arch, while the top of the Elk Point sequence is marked by an unconformity overlain by anhydrites and shales of the Fort Vermilion Formation. A transgressive sea completely blanketed the Fort Vermilion Formation with argillaceous limestones of the Slave Point Formation. Since the top of the Slave Point is depositionally flat lying, it provides an excellent stratigraphic datum for the area (Alcock & Benteau, 1976).

During the course of this work, with the exception of Muskeg evaporites, all of the formations were studied.

6.3.1. Granite Wash:

The basal lithology of the Elk Point in central and northwest Alberta is called "Granite Wash" and is of diachronous origin. "Granite Wash" is a term applied by the petroleum industry to the Paleozoic basal clastics that lie unconformably on Precambrian granites and gneisses of the Peace River Arch in northwestern Alberta.

In the study area Granite Wash beds are of doubtful age and rest on the Precambrian (Fig. 6.3). They form a sandy unit of variable thickness between 2 m and 35 m, although exceptional sequences between 54 m and 62 m

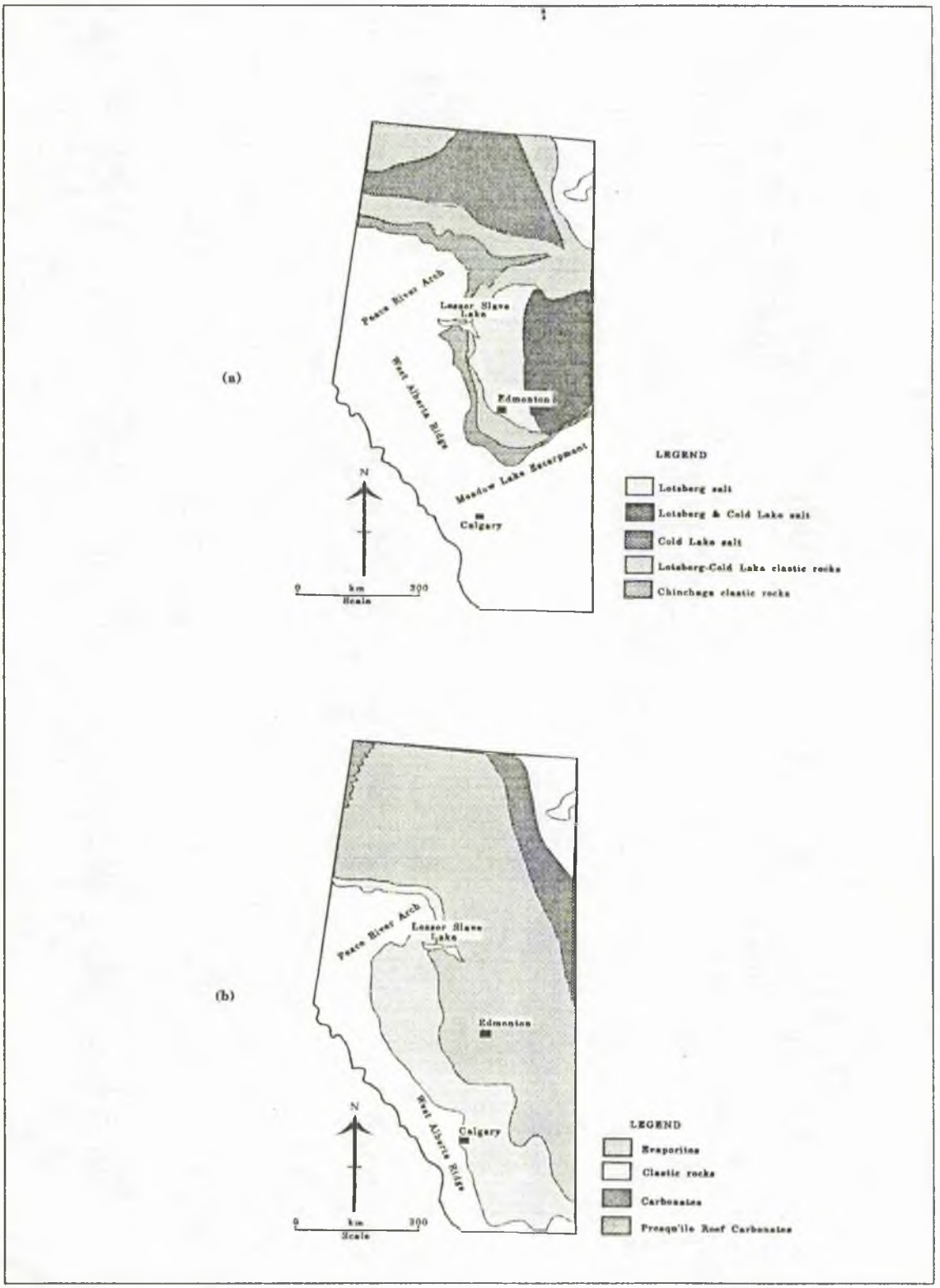

Fig. 6.2 Lithofacies distribution of (a) the Lower Elk Point, and (b) the Upper Elk Point Group (modified from Grayston *et al.*, 1964).

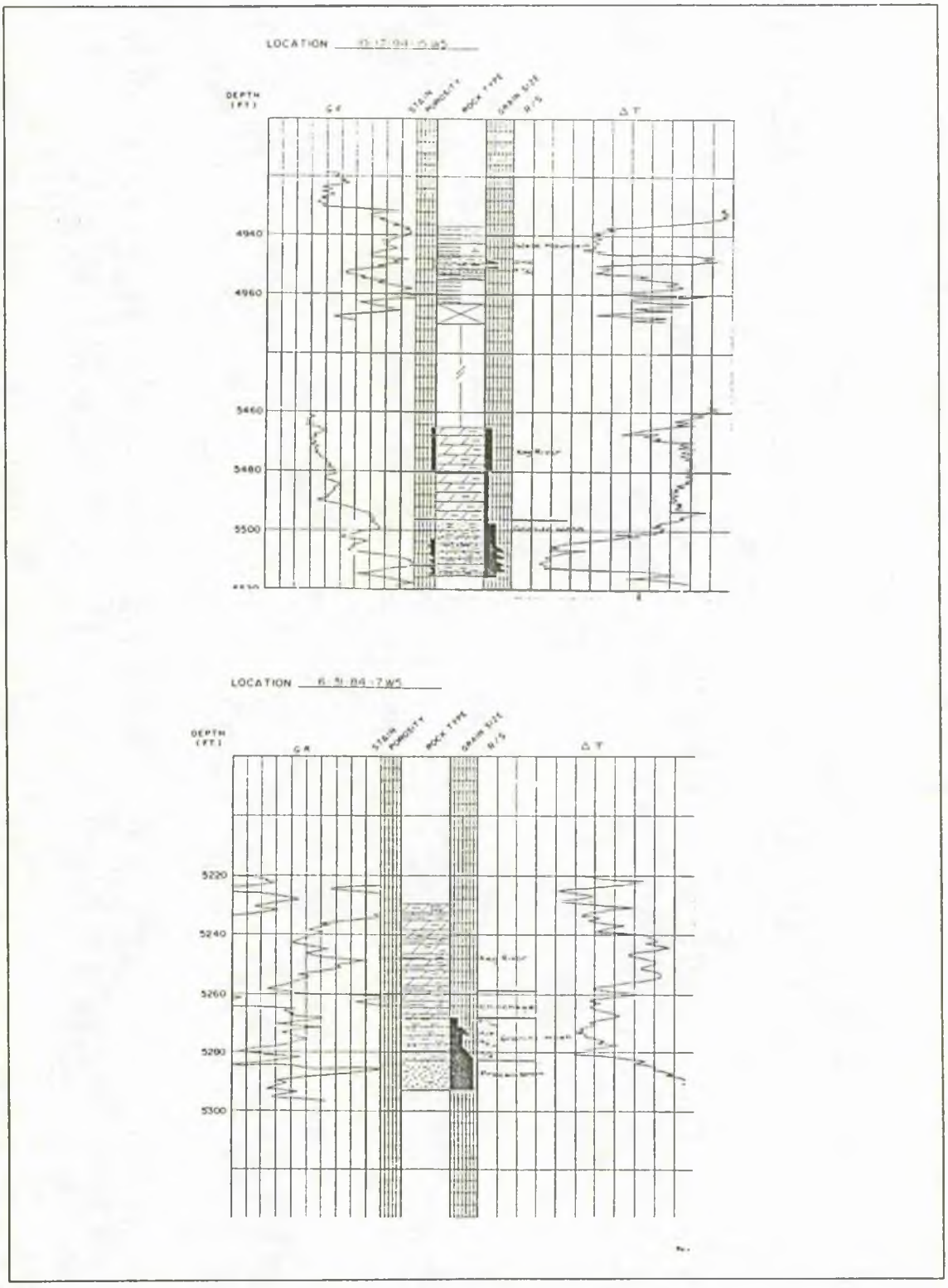

Fig. 6.3 Examples of lithological logs, gamma-ray profile and sonic response of various formations of the Elk Point Group in the study area. (Souce M/s Shawa Geoconsultants Ltd., Calgary, Canada)

and even 124m occur in the southwestern part of the area.

The various lithologies that make up the Granite Wash include sandstone and shale (Fig. 6.3). Limestone and dolomite, though not common, also occur in some wells, and in a few wells pink coloured intrusive rocks occur.

6.3.2. Chinchaga Formation:

The Chinchaga Formation extends over a much wider area than the older Elk Point beds. Northwards it crosses the eastern extension of the Peace River Arch into Northern Alberta where all but the basal red shale grade into anhydrite. This anhydrite was named the Chinchaga Formation by Law (1955). Around the eastern margin of the Peace River Arch the Chinchaga Formation includes thick feldspathic sandstones (Fig. 6.2) (Grayston *et al*, 1964).

There were sandstones deposited during the Chinchaga times, marginal to the basin and varying in thickness from 1 m to 43.6 m in the northeast (Fig. 6.3). The general thickness of the formation increases towards the northeast, while in the central part there is a thin deposit.

The close of the Lower Elk Point time was recorded by a widespread deposition of the Chinchaga anhydrite, shales and carbonates that interfinger with nearshore sandstone around the Peace River Arch.

6.3.3. Keg River Formation:

The widespread basal carbonate unit of the Upper Elk Point is named the Keg River Formation in Northern Alberta, Northwest Alberta and the southern part of the North-west Territories (Law, 1955). It lies unconformably upon the Chinchaga Formation. In Alberta the Keg River Formation is divided into a lower carbonate and an upper shale and argillaceous member. In the study area, the upper member becomes dominantly sandstone towards the Peace River Arch.

This unit is present only in the thickest sections of the Elk Point sequence (Fig. 6.3). Although the typical Keg River lithology comprises dolomite and/or limestone; sandstones also occur. The thickness of the formation varies from 9 m in the north of the area to 40 m in the centre.

6.3.4. Muskeg Formation:

The Muskeg Formation conformably overlies the Keg River Formation and underlies the Watt Mountain Formation. It consists of evaporites and is interbedded by dolomite, anhydrite, salt and a few thin beds of shale.

6.3.5. Watt Mountain Formation:

The Watt Mountain Formation is the uppermost unit of the Upper Elk Point Group (Fig. 6.3). It conformably overlies the Muskeg Formation and underlies the Fort Vermillion Member of the Slave Point Formation.

The Watt Mountain Formation consists of shale, siltstone, sandstone, limestone breccia with occasional dolomite. Bordering the Peace River Arch the unit includes coarse-grained sandstones, known as the Gilwood Sandstone south of the arch, and the Manning sandstone north of the arch.

The Watt Mountain Formation is a sandy unit of variable thickness between 1.5 m and 33.0 m. It is a clastic wedge which is thickest in the north near the Peace River Arch and thins to the east and northeast (Rottenfusser & Oliver, 1977).

The lithologies that comprise the formation consist predominantly of sandstone, siltstone and shale with lesser amounts of conglomerate, marlstone, anhydrite, limestone and dolomite. Conglomerate is found as thin beds at the base or, sometimes, in the middle of the formation. Anhydrite, marlstone, limestone and dolomite when they occur, are concentrated towards the top, rarely at the middle, of the formation.

6.4. AGE:

McGhee (1954) and Crickmay (1954) assigned Middle Devonian age to the Elk Point Group. Van Hees (1956) suggested a Lower Devonian age and Walker (1957) proposed an Ordovician age for Lower Elk Point beds in Saskatchewan. Buller (1958) has supported the idea of a Middle Devonian age for these beds. The Watt Mountain Shale has been considered Middle Devonian (Law, 1955, Grayston *et al*, 1964, Norris, 1965 and Kramers & Lerbekmo, 1967). McGill (1966) and Braun (1966) suggested a Middle Devonian boundary on top of Slave Point Formation which overlies the Watt Mountain Shale. Thachuk (1968) reported phosphatic brachiopod Lingula and *Eochara wickendeni* Choquette (Charophyta) from the Watt Mountain Formation, assigning it a Middle Devonian age.Shawa (1969) has shown conclusively that Watt Mountain Shale is of Upper Devonian age by identifying *Bothriolepis(?)* and *Asmussia canadensis* which are both Upper Devonian fossils.

6.5. SEDIMENTARY MODEL:

The sediments of Watt Mountain, Keg River and Chinchaga Formations have been treated together due to similarity in the observed sedimentary features. The two types of

environments of deposition for the Elk Point are, (i) Deltaic for Watt Mountain, Keg River and Chinchaga Formations, and (ii) Fan delta for the Granite Wash.

6.5.1. Deltaic Model for Watt Mountain, Keg River and Chinchaga Formations:

The dominant depositional element is a fluvially dominated fan-delta system that prograded eastward during the Watt Mountain time. During the Chinchaga period of deposition the delta was not well developed and there were fewer channels and so restricted deposition, while during the Keg River period it grew in size with increase in the number of channels. The Watt Mountain period saw the most extensive delta development with large number of channels.

A braided-meandering-deltaic model for the Gilwood Member, north of Peace River Arch was proposed by Rottenfusser & Oliver (1977). The presence of fish remains, shell fragments and rare occurrence of glauconite support a marine origin for the sediments in the far east and north-east of the area.

A regressive-marine or deltaic model for the Watt Mountain Formation of the Mitsue-Nipsi area was suggested by Kramers & Lerbekmo (1967). According to them deposition took place in a near-shore environment that ranged from shallow-water marine to continental nearer the Peace River high.

Three main realms of deposition for the Gilwood Member of Watt Mountain Formation of Utikuma Lake area were recognised by Shawa (1969) (Fig. 6.4). These include fluvial (gravel and

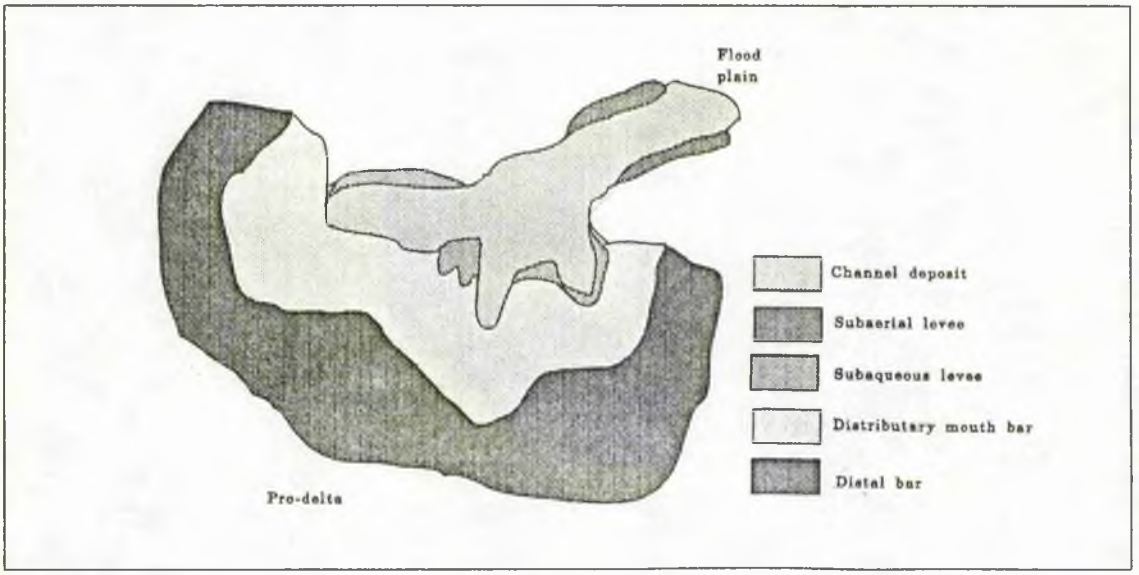

Fig. 6.4 Depositional model for the Gilwood Member (after Shawa, 1969).

very coarse sand, poorly sorted and a high silt content), transitional, and near shore marine (medium sand, moderately sorted and a low silt content). The fluvial realm is represented by the floodplain and the river channel subenvironments; the transitional includes the beach and upper delta environment, while the near shore is made up of delta fronts including distributary mouth bars and distal bars, and the prodelta area of deposition of fine silt and clay.

Within the Watt Mountain delta system of the Nipsi Field Alcock and Benteau (1976) have proposed three main facies (Fig. 6.5): (1) alluvial plain-tributary channel facies, (2) delta plain - distributary channel facies and (3) delta front - marine destructive facies.

On studying the Watt Mountain Formation in a greater detail, there is evidence that there were two stages of marine transgression represented by bioturbated shales, followed by rapidly prograding sequences (Fig. 6.6). In the southern part of the area the trangressions are more prominent. In the north and northwest evidence is in favour of a number of marine incursions, possibly due to the land being lower and more susceptible to flooding.

The depositional environments recognised from the petrophysical and lithologs by Shawa Geoconsultants (1986) and in the present study include: *delta plain*, which includes the distributary channels, crevasse and overbank deposits; *interdistributary bay*, a transitional phase between the open bay and channels; *delta front* or *distributary mouth bar* with sometimes minor channels; *prodelta*, the subaqueous distal part of the delta; and the *bayfill* deposits. *Restricted marine* influence is also seen in some of the logs (eg. 16-3-84-14W5). *Open shelf* sediments comprise the deposits present out in the sea. The transitional nature between most of these environments is reflected in the sediments by gradational contacts. Only the distributary channel has a sharp base and lateral contact with adjacent environments.

6.5.2. Fan delta model for Granite Wash lithology:

Fan sediments are well developed in the southern part of the study area and a prograding fan delta sequence has been suggested by Shawa (1987a, 1987b).

The fan model proposed by Shawa (*op. cit.*) includes a sharp gradient from a high Peace River Arch to the narrow plains fanning out into the sea in form of a delta. The fans were built outward by braided channels. Sediment supply was abundant from the Peace River Arch. The coarse grain-size of the sandstones and

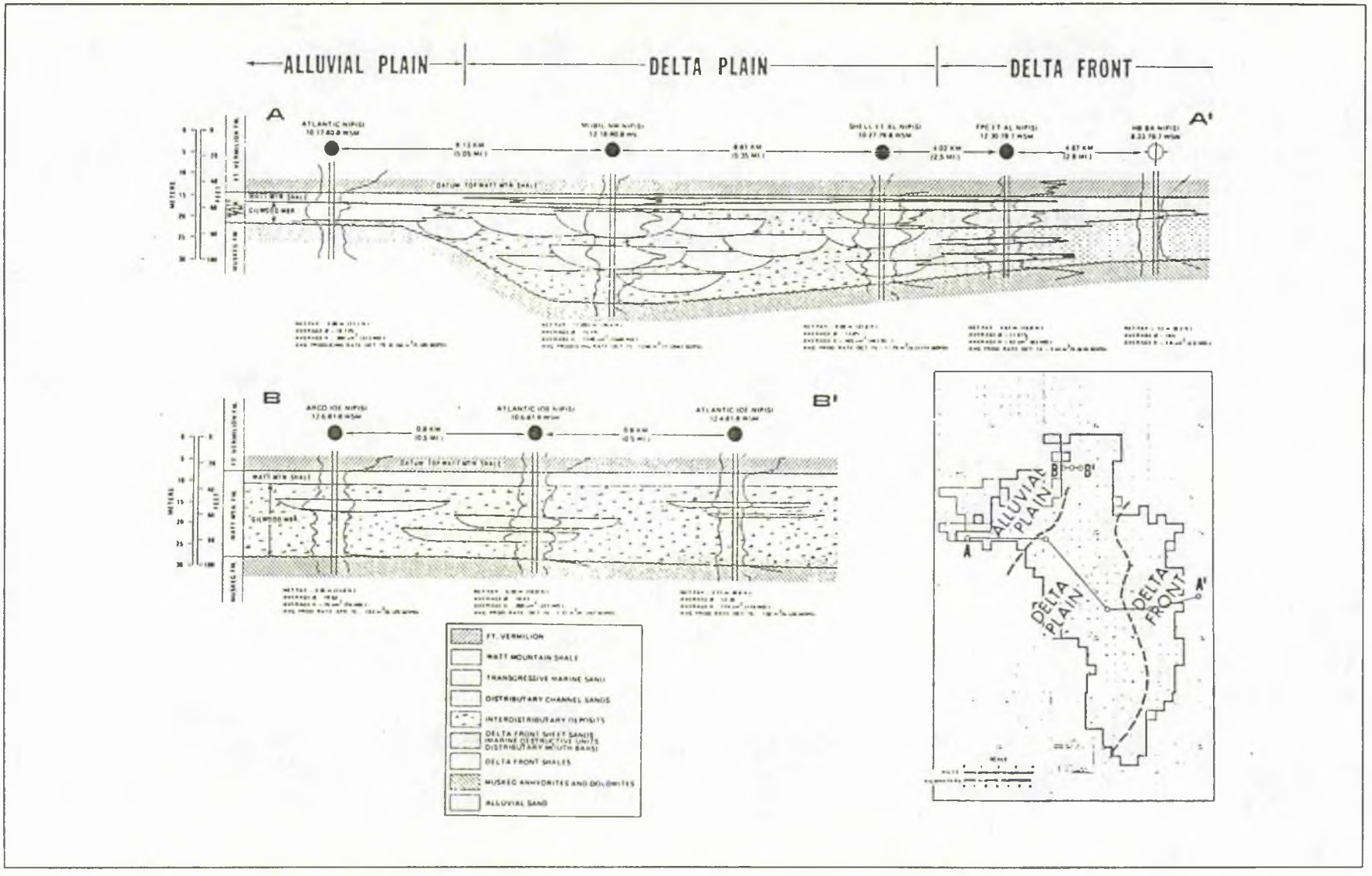

Fig. 6.5 Typical stratigraphic cross-sections showing the Watt Mountain Formation across the Nipsi field (from Alcock & Benteau, 1976).

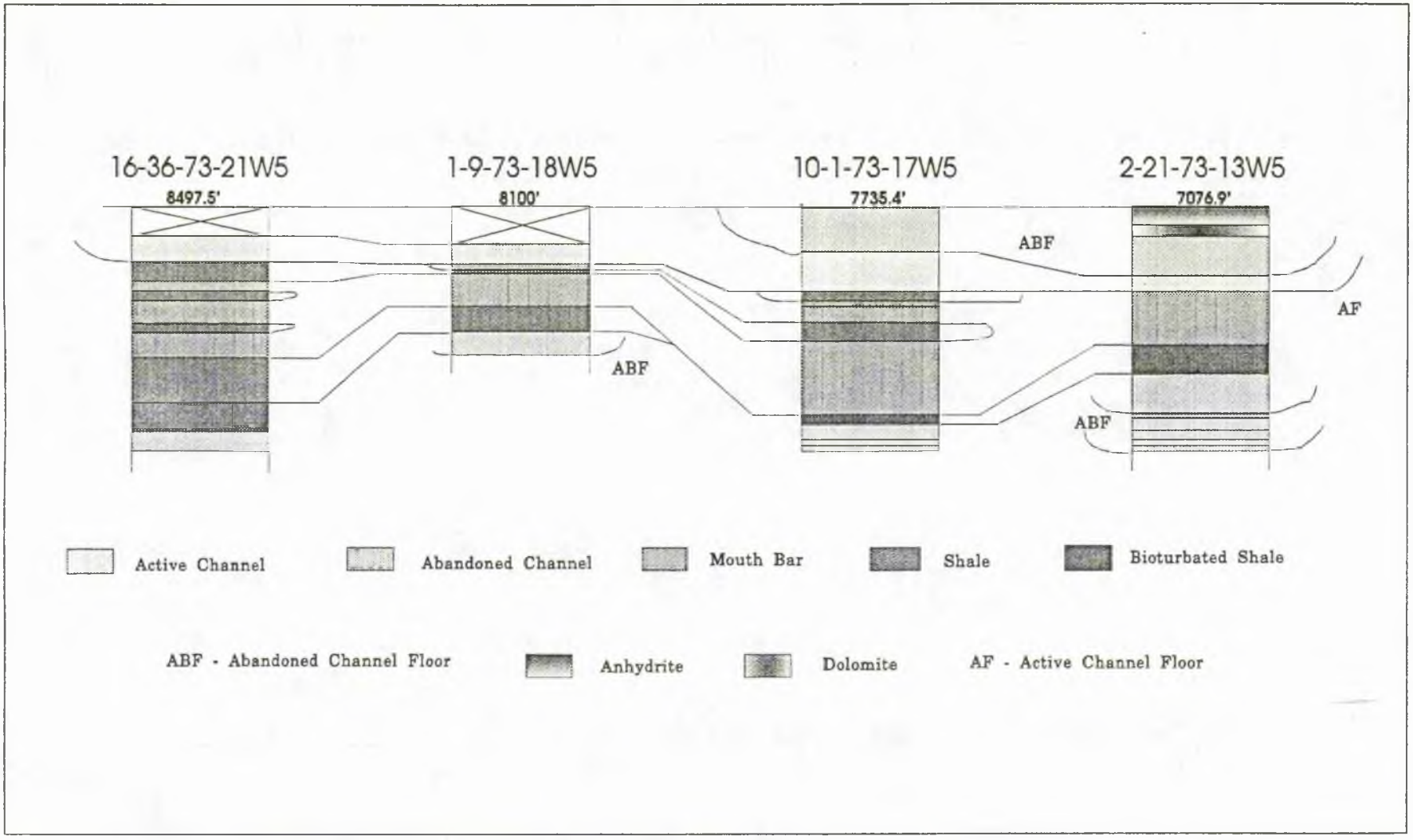

Fig. 6.6 Typical stratigraphic cross-sections showing interpretation of the Watt Mountain Formation across the study area.

theabundance of degraded feldspars support a rapid mechanical weathering of the source area and a possibly small distance of transport.

The depositional environments recognised by Shawa Geoconsultants, from the petrophysical and lithologs include: *proximal*, *middle* and *distal* fan deposits; *channel flow* and *isolated marine deposits* have also been recognised. Both *debris flow* (well no. 5-36-80-18W5, 6-15-82-16W5; Appendix 6) and *water laid* deposits have also been identified. The *debris flow* deposits are poorly sorted and show graded bedding in the upper segment of the fans especially towards the Peace River Arch, while the lower reaches of the fan are normally dominated by *sheet flood* deposits.

6.6. SEQUENCE STRATIGRAPHY MODEL OF THE ELK POINT GROUP:

Lithological and subsurface (Wireline logs) data have been modelled into a sequence stratigraphic framework in order to achieve a fuller understanding of diagenetic effects from the chronostratigraphic succession and eustatic changes.

The basic concepts of sequence stratigraphy comprise a fundamental unit, the *sequence*, which is bounded by unconformities and their correlative conformities. A *sequence* can be divided into *systems tracts*, which are defined by their position within the sequence, and by the stacking patterns of the *parasequence sets* and *parasequences* bounded by *marine flooding surfaces (Mar FS).* A *parasequence*, as defined by Van Wagoner *et al*, (1988) is a relatively conformable succession of genetically related beds or bedsets bounded by Mar FS. *Parasequence sets* consists of a succession of parasequences deposited in related environments, and bounded by Major Marine Flooding Surfaces and their correlative surfaces (Wilson, 1991).

The Elk Point Group in the study area can be classified as Elk Point '*sequence*' (Van Wagoner, 1988; Walker, 1990; and Wilson, 1991). The base of the *sequence* is characterised by an onlapping Granite Wash lithology (Fig. 6.7). The subsequent formations of the Elk Point, Chinchaga, Keg River, and Watt Mountain, and the overlying Fort Vermillion Formation are bounded by *Marine Flooding Surfaces* (Mar FS) (Fig. 6.7). The Granite Wash, Chinchaga, Keg River and Watt Mountain are referred to as individual *parasequences.* Watt Mountain Formation is a *parasequence* set as there are evidences of Mar FS, as picked out in the form of shales with bioturbation. The Muskeg Formation

is taken as the off-shore equivalent of Watt Mountain *parasequence set.*

The Elk Point *sequence* was deposited as a *Highstand Systems Tract*, when the relative rise in sea level was slowed and sediment progradation began initiating a marine regression. Thus the Granite Wash *parasequence* was laid over an initial surface of transgression or resumed transgression (IT/RT). With the continued rise in sea level sediments of Chinchaga, Keg River, Watt Mountain and Fort Vermillion *parasequences* were deposited as downlaping sequence on top of one another. The whole sequence represents a retrogradational system.

After the deposition of Fort Vermillion the sea level had risen to a maximum marking a Max FS. Over this Max FS was deposited the Slave Point Formation.

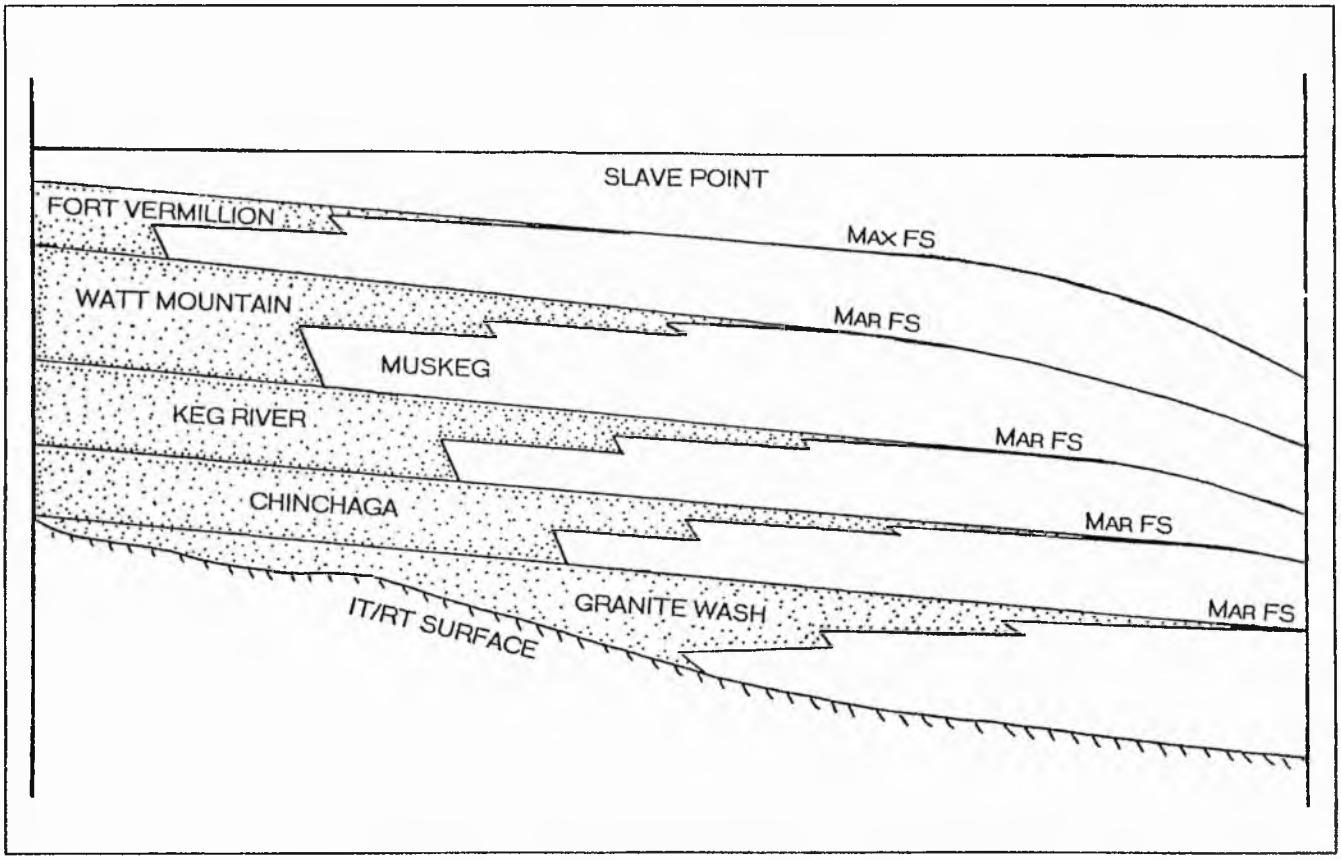

Fig. 6.7 The Highstand Systems Tract model of the Elk Point sequence. Granite Wash, Chinchaga, Keg River, Watt Mountain and Fort Vermillion are parasequences separated by marine flooding surfaces (Mar FS). Granite Wash represents an onlapping sequence over an IT/RT surface.

CHAPTER 7: PETROLOGY & DIAGENESIS

(with 13 figures, 13 tables and 42 plates)

This chapter aims to study the petrological details of Elk Point sandstones in order to determine their probable sources as well as their depositional and diagenetic history. The petrography of the four formations has been dealt with together, however, the significant differences amongst the various formations are brought out in each of the sections (Table 7.1-7.7).

7.1. METHODOLOGY:

Core cuttings were made available for this study. A total of 145 samples were studied from 90 wells. Of these 33 samples were from 29 wells with Granite Wash lithology; 9 samples were from 6 wells with Chinchaga Formation; 10 samples came from 5 wells with Keg River Formation; and 93 samples were from 53 wells with Watt Mountain Formation. These core samples were studied as thin sections under optical microscope and the scanning electron microscope (SEM). Energy dispersion elemental analysis (EDAX) was routinely used to study the composition of various grains under SEM. The sections were impregnated with blue araldite and stained for carbonates with alizarin red S and potassium ferricyanide. No potassium feldspar stain was used. Clay analysis was carried out using X-ray diffraction (XRD) on 25 samples from 19 wells with the Granite Wash lithology; 6 samples from 4 wells with the Chinchaga Formation; 8 samples from 6 wells with the Keg River Formation; and 30 samples from 18 wells with the Watt Mountain Formation, giving a total of 69 analyses. Modal analysis was carried out by point counting 300 points per section and the interval carefully chosen so that nothing was counted more than once.

Use of reflected light was made to differentiate between various iron oxides and sulphides.

Backscatter and Cathodoluminescence studies were carried out on 2 samples from Granite Wash lithology and the Chinchaga Formation each and 3 from the Keg River Formation and the Watt Mountain Formation respectively. Fluid inclusion analyses on cements were carried out on 5 samples from the Granite Wash lithology, 1 from the Chinchaga Formation and 2 from the Watt Mountain Formation.

Whole rock geochemical analysis was carried out on forty eight samples by X-ray fluoroscence (XRF) techniques for major oxides and trace element analysis. Of the 48 samples, 22 were from Granite Wash lithology, 3 from the Chinchaga Formation, 5 from the Keg River Formation and 19 from the Watt Mountain Formation. Geochemical analysis has been

carried out on samples from Granite Wash lithology and Watt Mountain Formation only.

Stable isotope analysis was carried out on 4 samples from the Chinchaga Formation and 2 from the Watt Mountain Formation for sulphur from anhydrite cement. Four samples from Granite Wash lithology, 2 from the Keg River Formation, 1 from the Chinchaga Formation and 4 from Watt Mountain Formation were also used for stable isotopes of carbon and oxygen from carbonate cements. The selection of samples was based on the amount of cement and amount of material available for study.

Regional contour maps have been drawn to study lateral variation of textural parameters and compositional estimates using various programmable routines of SURFER® software package (Golden Software Inc., Golden, Colorado) on an IBM-pc computer by the methods described by Briggs (1974). However, due to scarcity of sample locations and the uneven distribution of sample sites, typical 'bulls-eye' effects were observed (Fig. 7.1) which were leading to spurious results even after manipulation (as suggested by Walker & Eyles, 1991) and were therefore discarded. On plotting

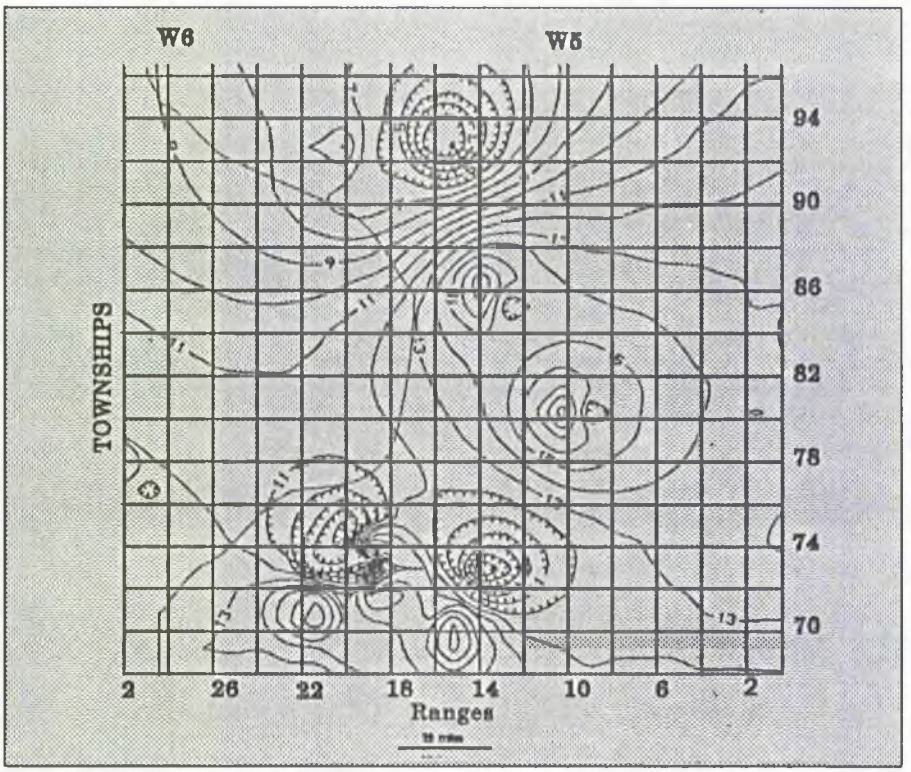

Fig. 7.1 Areal variation of porosity (expressed as percentage of whole rock) in the Watt Mountain Formation. Probable limit of Peace River Arch shown by a thin line. Contour interval 1%.

trend surfaces up to cubic level no regional trend was seen.

A summary of laboratory techniques applied to various samples is given in Appendix 3.

7.2. PETROGRAPHY:

7.2.1. Texture:

The sandstones show a grain-size range from fine to very coarse sand with conglomeratic horizons having granules and pebbles. The bulk of the samples are coarse grained with the finer material being incorporated in the interstices of the coarser grains (Plates 7.1-7.3). No individual sample is completely fine grained. Regionally the variation in the grain-size amongst the Watt Mountain samples show that there are two areas of coarser sediments, one in the north and the other in the south while the sediments of the Granite Wash formation tend to be coarser in the northeastern and southwestern parts of the area.

The sorting of the sediments is poor to good (Plates 7.1-7.4). Sediments of the Watt Mountain Formation are poorly sorted while those of the Keg River, Chinchaga and Granite Wash vary in sorting from poor to good with generally moderate sorting. In so far as even those classified as poorly sorted are generally lacking detrital silt and clay particles, virtually all the sandstones had experienced some sorting. The poor or moderately-poorly sorted samples are often those whose distribution show bimodality, where coarse or very coarse grains are scattered in a framework of medium or even fine grains. Variable high energy conditions evidently affected a sediment-supply of mixed grain-size, reworking and removing many of the fines by physical processes but not the admixture of very coarse sand and pebbles.

The grains have a variable shape, with the finer ones being largely angular to subangular, and the coarser ones being subangular to subrounded (Plates 7.2-7.6). Sometimes the original shape of the grains is difficult to identify as the quartz has syntaxial overgrowths, while the feldspars are often corroded, or they too may have overgrowths around the rim of the grains.

Overgrowths and secondary cements make it difficult to assess the original packing of the grains, however, it appears that the grains were deposited as loosely packed fragments with a little interstitial material amongst coarse ones, while those which have a wider spread of grain-size would have had finer material filling in the interstices (Plates 7.1-7.3). The grains appear to have formed an open framework with tangential contacts in the majority although well developed overgrowths now often form long

contacts. Only rarely are concavo-convex contacts present and complex suturing resulting from compaction and pressure solution does not occur. However, simple sutures may suggest some pressure solution.

Porosity as seen in the thin sections under the microscope varies between negligible and 30% by volume of the whole rock as measured by point counting (Plates 7.1-7.10). There is no distinct relationship between porosity and grain-size. The porosity decreases with increasing amounts of cement (Fig. 7.2). Major porosity controlling factors are cementation and dissolution producing redistributional secondary (RDS) porosity (Giles & de Boer, 1990). In pore-type the majority are intergranular (between particle; BP). Most of these have suffered some reduction by quartz overgrowths, carbonates, clay and anhydrite fillings (Plates 7.4, 7.7, 7.9). Reduction of pores by anhydrite and carbonate has often caused complete occlusion (Plate 7.7). Where quartz overgrowths are present pores are straight-edged triangular, polyhedral and lamellar in form, largely lined by clays (Plates 7.4, 7.10). Some pores are vuggy in nature formed by the removal of labile grains or cement and some have been enlarged up to a millimetre across. Some vugs are interconnected to form pseudo-channels (Plates 7.5, 7.6, 7.8). Most intergranular pores are of the order of 200-400 µm across depending on the amount of reduction by overgrowths. The pores show reduced to

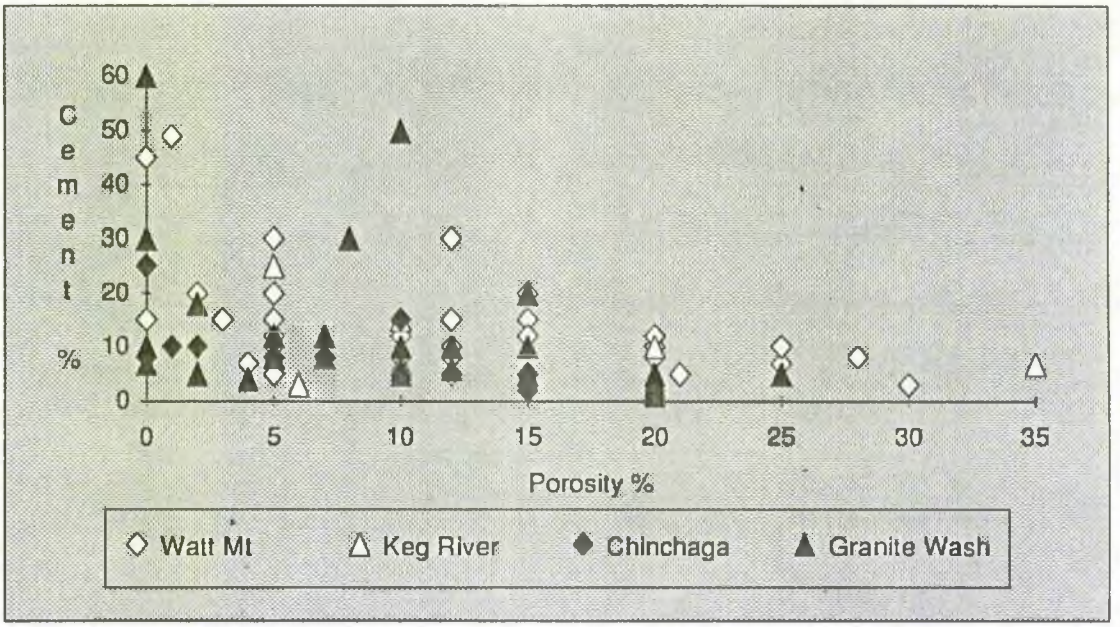

Fig. 7.2 Porosity to cement plot. Porosity varies inversely with the cement with a general trend showing a negative correlation.

enlarged intergranular and occasionally oversized pore textures as classified by Schmidt & McDonald (1979). Intragranular (within particle; WP) porosity has been formed largely due to the dissolution of feldspars, seldom due to expanded mica and occasionally due to lithoclast disintegration (Plate 7.11). The intragranular pores have been in some instances filled by clay in the feldspars, while in micas the pores are empty. The clay seems to have some between crystal microporosity.

Variation in porosity occurs on all scales. In the area of a thin section, cementation may produce patches without porosity alongside areas with 20% or more.

Vertical variation in porosity amongst Granite Wash sandstones show no distinct pattern with depth (Fig. 7.3, Table 7.1). Vertical porosity variation in Watt Mountain samples can be studied in well 10-8-73-5W5, which is represented by 9 samples (Fig. 7.4, Table 7.5) and gives an indication of variation from horizon to horizon. Porosities are around 20% for

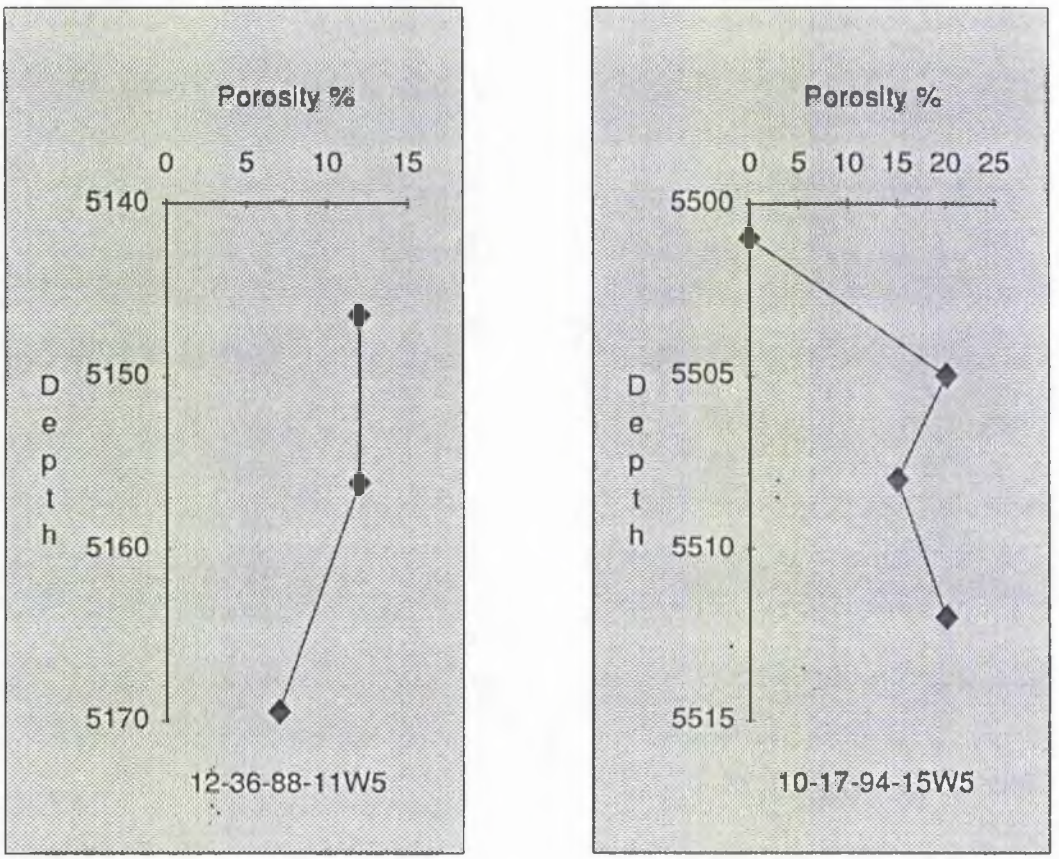

Fig. 7.3 Porosity versus depth plot for Granite Wash lithology. There is no distinct change in porosity with depth.

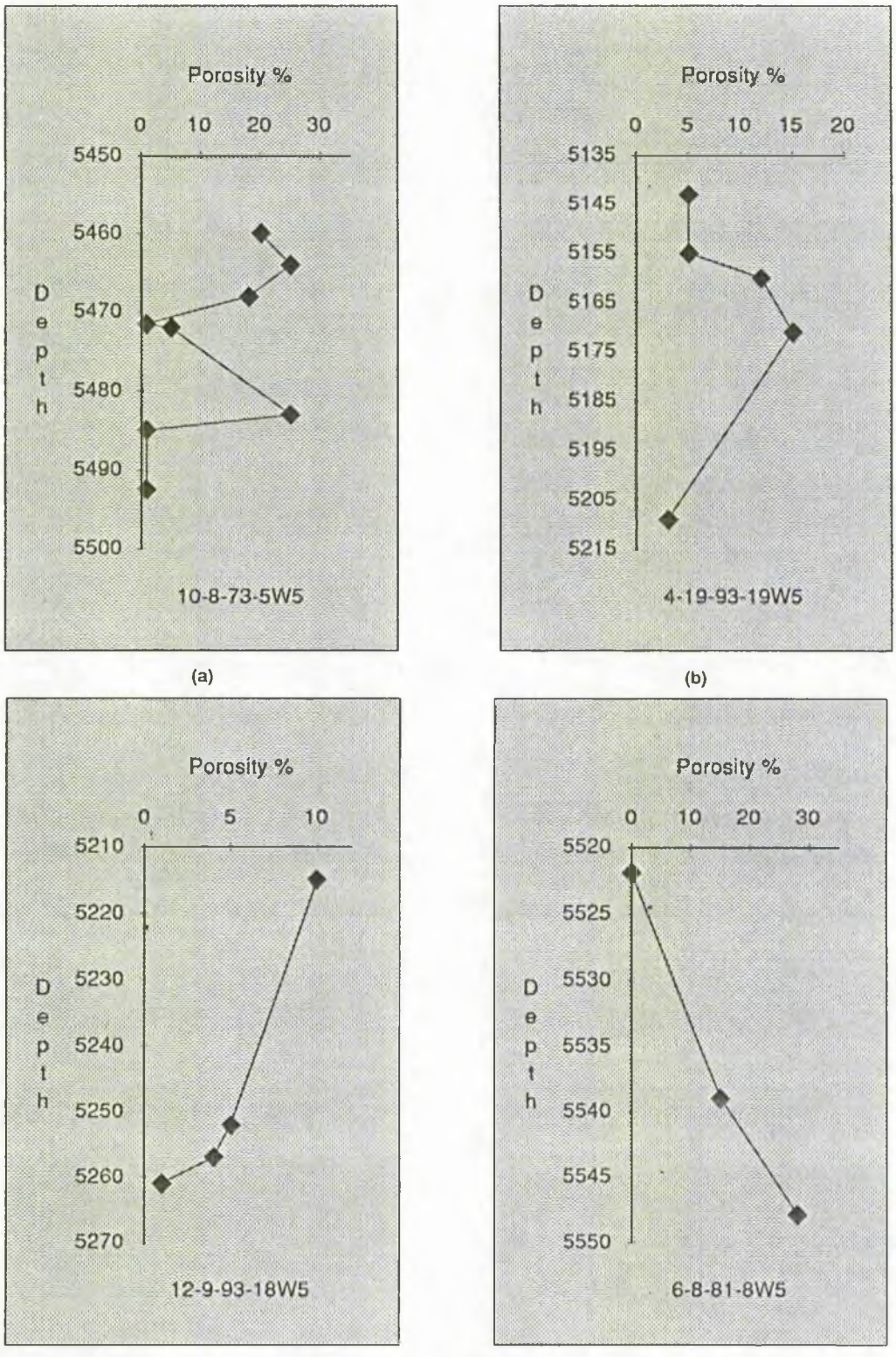

Fig. 7.4 Porosity versus depth plots for Watt Mountain Formation. No trend follows in all wells. It varies within a well as in (a) and (b). In (c) the porosity seems to decrease with depth, while in (d) the porosity is increasing.

samples between 5459.5 ft and 5468 ft, drop to very low values at 5471.5 ft, rise to 25% at 5483 ft, dropping back to negligible amounts at 5485 and 5492.5 ft. Evidently porosity differences of more than 20% may occur within a thickness of a few feet depending on cements or clay matrix associated with shale bands. On the other hand a zone of some 12 ft is present with significantly high porosities.

Samples from neighbouring wells may show considerable differences in porosity. Given the within-sample and within-well variance these differences may be a reflection of restricted sampling rather than significant differences.

Areally porosities show no simple trends. Except in the southeast where the facies tends to pass into mudstone, high porosities occur throughout the area for Watt Mountain Formation while Granite Wash sediments show higher porosity values in the south and eastern corner of the area.

7.2.2. Mineralogical Composition:

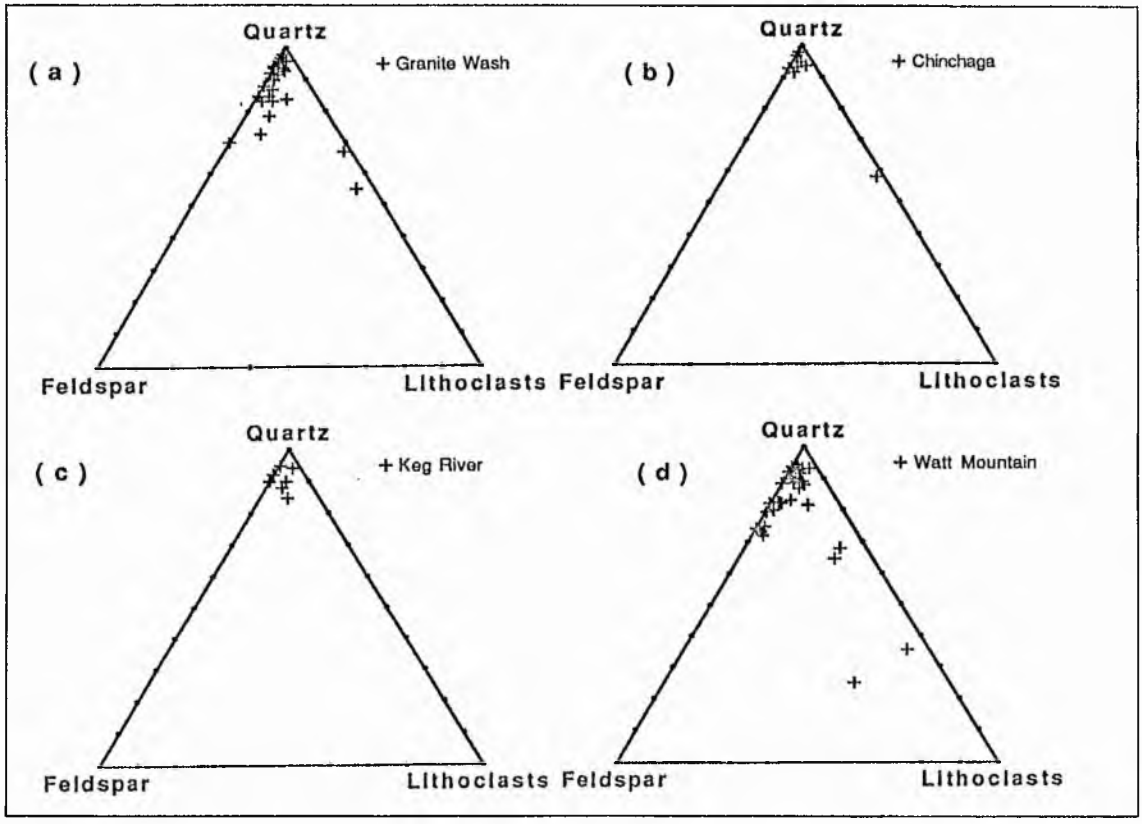

Fig. 7.5 Q-F-L plot of Elk Point samples. Most of the samples plot as quartz arenite and subarkose, however, some also plot as litharenite. (a) Granite Wash lithology, (b) Chinchaga Formation, (C) Keg River Formation, (d) Watt Mountain Formation. Each corner represents 100%.

The sandstones are predominantly quartzose with varying percentages of feldspar, lithoclasts, mica and pyrite as primary components, although the last two never constitute more than 7% of the grain content of the rock. Authigenic components are silica as overgrowths and massive pore fillings, carbonate, anhydrite, clay and rarely pyrite (Plates 7.1-7.4, 7.8, 7.7).

After Folk (1964) the Granite Wash sandstones classify as quartzarenite and subarkose while three samples are litharenite; Chinchaga and Keg River sandstones are quartz arenite and subarkose (Fig. 7.5).

Watt Mountain sandstones plot as quartz arenites, subarkoses and exceptionally as sublitharenite, feldspathic litharenite and litharenite. In contrast to the arkoses in the northwest, the quartz arenites tend to occur in the south and east.

7.2.2.1. Quartz:

Quartz grains are generally monocrystalline with non-undulose extinction, although a few grains with undulose extinction are also present (Plate 7.2). Polycrystalline clasts are usually coarse grained with individual grains made up of many units (Plate 7.3); occasionally they are quartzitic with numerous small sutured, elongate crystals showing undulose extinction. The clasts are sometimes fractured, and have subrounded outlines. Detrital quartz has well developed overgrowths, making it difficult to estimate the exact percentage of detrital quartz. 'Dust lines' along the original margins are seldom well preserved (Plates 7.4, 7.6, 7.8). The contacts between adjacent detrital grains may be scalloped, but are largely straight to stepped. Quartz mosaics with straight contacts and triple junctions are also present.

Composite grains with sutured and crenulated margins were derived from pressure metaquartzites; monocrystalline quartz with straight extinction probably had an acid plutonic source, while quartz with moderately undulose extinction may have had a vein type origin (Jansa & Fischbuch, 1974).

Under cathodoluminescence the quartz luminesced in purple. No distinct overgrowth patterns could be identified by cathodoluminescence (Plates 7.12-7.14).

The percentage of quartz (with overgrowths) in the grain-content of the rock amongst the Granite Wash sandstones varies between 47 and 97%, with the majority of the samples showing a percentage between 88% and 97%. In general, the percentage of quartz is lower in conglomeratic horizons.

Quartz forms the dominant portion of the grain content of the sandstones from the Chinchaga and Keg River Formations. Primary quartz and secondary overgrowths account for 58% to 97% of the grains (Table 7.2 & 7.3).

In the Watt Mountain Formation sandstones, with the overgrowths and secondary silica, quartz percentage varies between 30% and 92% of the whole rock. The higher figures are associated with medium and fine-grained samples, and, are antipathetic to feldspar and lithoclasts.

7.2.2.2. Feldspar:

In Granite Wash samples orthoclase, microcline and plagioclase are present in decreasing order of abundance. Samples of Granite Wash can be categorised into two major groups, one between 2% and 10% and the other between 12% and 15% feldspar. Generally, most of the samples have an average percentage of feldspar around 5% of the grains, with a maximum as high as 30% (Table 7.1 & 7.6). The percentage of feldspars varies inversely with quartz and lithoclasts, and tends to be higher amongst coarser samples. Areally no distinct trend in feldspar distribution can be traced. Vertically, the variation can be studied only in one well, where the amount decreases with increasing depth.

The feldspar content amongst the grains of sandstones from the Chinchaga Formation varies between 2% and 7% (Table 7.2). The feldspars are largely K-feldspar with some plagioclases and microcline, decreasing in that order of abundance.

The feldspar content of the grains in Keg River Formation samples varies between 2% and 10% (Table 7.3). The feldspars are largely plagioclase and orthoclase with microcline being rare. Sometimes perthite can also be seen.

Feldspars amongst Watt Mountain Formation sandstones comprise microcline, plagioclase and orthoclase, in decreasing order of abundance. The plagioclase is largely calcic, however, some oligoclase-andesine grains are also present. Feldspar content varies between 2% and 25%. However, in most samples the content lies in the range of 5% to 8% .

The feldspars are corroded with the degree of corrosion varying from slight dustiness to some sericitised grains, while others are skeletal (Plates 7.5, 7.6, 7.11). Clay is present in some of the skeletal feldspars. Some grains have been completely transformed into clay. K-feldspars in the Granite Wash and plagioclase in Watt Mountain Formation may have

overgrowth rims, but microcline rarely shows overgrowths (Plates 7.12, 7.13, 7.15, 7.16). Rarely tiny (10um) crystals of authigenic K-feldspar may also be found (Plate 7.17). Sandstones from the Chinchaga Formation and the Keg River Formation show no authigenic or feldspar overgrowth development. The feldspar luminesced in blue under cathodoluminescence and distinct overgrowth rims can be differentiated (Plates 7.12-7.14). Overgrowth patterns can also be seen under back-scatter image (Plate 7.16). Electron micro-probe analysis (15 analyses from 5 samples) has shown that detrital K-feldspar has 0.6% Na_2O, while overgrowths have none at all.

7.2.2.3. Lithoclasts:

Lithoclasts are mostly polycrystalline quartz, mainly vein quartz, exceptionally metaquartzite, coarser fragments of quartz-microcline and quartz-microcline-biotite and finer grained volcanic material (Plate 7.3).

The amount of lithoclasts present varies from negligible amounts in some samples from the Chinchaga and Keg River Formations to 50% in the conglomeratic horizons of the Granite Wash and Watt Mountain Formation (Table 7.1-7.6).

7.2.2.4. Mica:

Mica varies from trace amounts to a maximum of 4% of the grains in the rock with many samples lacking any mica at all. Most of the mica is biotite and detrital chlorite, with some muscovite. Mica is mostly trapped, bent and sandwiched between the grains (Plates 7.1, 7.2, 7.11).

7.2.2.5. Opaques:

Pyrite is the only opaque present in only two of the samples from the Chinchaga Formation (Table 7.2). It occurs as 4% of the grain content of the rock while in the Watt Mountain Formation these are usually less than one percent. Pyrite consists of cubes and aggregates of pyrite along with white-reflecting ?leucoxene.

7.2.2.6. Non-opaques:

Heavy minerals, seen as one or two grains per thin section comprise zircon, tourmaline, garnet, ?anatase and ?staurolite and represent a stable mineral association. Such an association has also been reported by Jansa & Fischbuch (1974) as less than 0.5% of the total rock volume of the Watt Mountain Formation. Silt to fine-grained sand sized glauconite grains have been rarely seen in the samples from this

Formation. They mostly occur towards the western part of the area.

7.2.2.7. Cements and clays:

The main cements are quartz, anhydrite and carbonate (Plates 7.1, 7.3, 7.4, 7.7). Overgrowths also occur on some K-feldspar grains and rarely on microcline (Plates 7.13, 7.16).

Some of the samples from the Watt Mountain Formation also show pyrite. The identities of the authigenic clays, illite, chlorite, kaolinite, corrensite (mixed layer illite-chlorite) and smectite, have been confirmed by XRD (Table 7.7). In samples from the Keg River Formation and Chinchaga Formation, with increasing cement percentage in the rock, the amount of carbonate decreases while the content of anhydrite and clay increases. Granite Wash samples show a linear increasing relationship of carbonate, anhydrite and clay individually with the the percentage of cement. In samples from the Watt Mountain Formation with increasing amounts of cement, the carbonate percentage increases while clay and anhydrite decrease.

Silica, as syntaxial overgrowths, sometimes as massive cementing medium (chert/opal), and exceptionally as small authigenic crystals is the most abundant authigenic mineral although it is impossible to measure its actual amount by optical microscopy (Plates 7.4, 7.18, 7.18-7.20). Occasional 'dust lines' around original grains reveal overgrowth rims (Plate 7.8). Overgrowth has penetrated and filled interstices amongst quartz and feldspar grains as well as forming scalloped boundaries with corroded feldspars. Where clay is present overgrowths seem to have grown compressing the clay. Sometimes nonporous quartz mosaics can also be seen severely reducing the porosity of the rock. Under SEM many euhedral faces can be seen (Plates 7.18, 7.20) although growth of completed faces has sometimes been inhibited by the presence of fringing chlorite (Plates 8.21, 7.22). Overgrowth may also take the form of numerous small crystals 'budded' on to the surface of detrital grains.

Anhydrite is present in six samples from the Granite Wash and almost every sample of the Chinchaga, Keg River and Watt Mountain Formations. The rare exceptions amongst the three formations are those in which carbonate is the all-pervasive cement (Table 7.1-7.7).

Anhydrite occurs as blocky crystals, poikilotopic with respect to quartz and feldspar, sometimes enclosing as many as ten grains (Plates 7.23-7.28). Crystals reach a maximum of 10 mm in length, although most are between 1

and 3 mm. The vast majority are tabular in habit; a smaller proportion are highly elongate prismatic crystals forming sheaves sometimes filling enlarged pores (Plate 7.25) and up to 2 mm long. Under SEM anhydrite laths are seen to be coated with clay. Most of the poikilotopic crystals fill large pores amongst loosely packed quartz and feldspar grains, but in those sands where quartz overgrowth has been abundant the anhydrite although poikilotopic is made up of 'skeletal' portions occupying small triangular and lamellar pores between the clastic grains.

The anhydrite also occurs as fillings along enlarged cleavages in feldspar (Plate 7.27) and one example of the sulphate in the Watt Mountain Formation was noted in pores of a fish-scale. Anhydrite may surround biotite but it may also penetrate along cleavages as though the biotite was forcibly displaced into partly or wholly separate flakes. In other cases (Plate 7.27) anhydrite has penetrated and disrupted polycrystalline quartz grains. Anhydrite along with quartz may completely occlude all pores but in many cases cement is restricted and the margins of the anhydrite may take on a distinctive outline. This consists of a series of narrow elongate remnants of the crystal projecting into the pore rather like a series of piers built out into the sea (Plates 7.25, 7.28). the crystals have evidently suffered corrosion controlled by their two sets of cleavage. Under cathodoluminescence anhydrite glowed in orange (Plate 7.14).

Carbonate is less widespread than anhydrite. It is usually in smaller amounts in the Watt Mountain and Chinchaga Formations than in the Keg River Formation and Granite Wash lithology where it is present in almost all the samples with exceptions of those in which anhydrite is the all pervasive cement. Many samples have traces or low percentages of carbonate, while in others it may form 100% of the cement (Table 7.1-7.7).

When in large amounts, the carbonate is calcite with some ferroan component affecting the margins of the pores; where only a few pores are occupied by the carbonate, it is often completely ferroan (Plates 7.29-7.32). Dolomite and ferroan-dolomite are also present as pore fillings in a number of samples (Plates 7.32-7.37). Under SEM tiny rhombs of dolomite show well developed faces and edges and show an intergrowth pattern amongst themselves (Plates 7.31, 7.32). Like the anhydrite the calcite and dolomite may be poikilotopic although the crystals are usually much smaller in size (Plates 7.29, 7.35). Millimetre-sized poikilotopic crystals are common (Plate 7.30); even where finer the calcite forms sparry crystals seldom less than 200 μm.

In some calcite rich samples the coarser spar shows a wavy extinction. The poikilotopic habit means that a euhedral shape is rarely seen. Exceptionally rhombs (about 100 µm) are developed in clay (Plate 7.31). Some calcite also occurs in the secondary pores of skeletal feldspars. Carbonate seems to occupy some unusually large pores, suggesting that it is partly replacive or has occupied previously enlarged pores. Calcite and dolomite have irregular boundaries against quartz and feldspar (Plates 7.33, 7.35, 7.36). By contrast corrosion of the carbonate has left it with irregular margins to voids. The carbonate lies against corroded quartz overgrowths, suggesting later formation; the former position of quartz overgrowths is marked by indistinct lines through the carbonate (Plate 7.35).

Luminescence colours of orange and red were observed for carbonate under cathodoluminescence (Plates 7.12-7.14). No distinct zonation was distinguished except for a few light and dark patches. Back-scatter images also revealed no zonation amongst the carbonate cement (Plates 7.37).

Clays occur as chlorite, illite and kaolinite with minor amounts of corrensite. The clay is widespread geographically. It is more abundant in sandy bands at or near the boundary with shales. The clay, mostly detrital, fills many pores and is usually a greenish chlorite together with illite. The pore filling clay also covers all the grains making analysis difficult under SEM (Plates 7.17, 7.22). For most of the samples the small amounts of clay appear as fringes to grains and occasionally fill pores. Chlorite is the most common and widespread; illite is fairly common in samples over the whole area; kaolinite was recognised in thin-sections from four wells (Table 7.1-7.6) but evidently is more widespread according to XRD analysis (Table 7.7).

Authigenic chlorite is seen under the SEM as blades 10-20 µm sometimes arranged in small sheaves or characteristic 'rosettes' (Plate 7.22. EDX shows it to be iron-rich with some magnesium. The crystals grow normal to grain faces of both quartz and feldspar. However, the clay seems to be sandwiched between the overgrowths and subsequent carbonate and anhydrite fillings. Chlorite-smectite mixed layer clays also occur (Plate 7.39).

Illite, like chlorite is both detrital and authigenic. The latter, often 'hairy' in habit tends to be associated with K-feldspar grains (Plates 7.15, 7.40). Some of the illite is mixed illite-smectite (Plates 7.41, 7.42). Jansa & Fischbuch (1974) have reported mainly illitic clays with small amounts of kaolinite and traces of

chlorite from the Gilwood sandstone of Sturgeon-Mitsue area, Alberta.

Kaolinite is scarce (Table 7.1-7.6) and was only found in abundance in stubby crystals and 'books' (about 10 µm across) in well 8-12-72-5W5 (Table 7.5) where chlorite also occurs but not so abundantly.

Illite and chlorite are the only two clay members present, in Chinchaga Formation samples, with the former being more abundant than the latter. Illite does not occur as well developed fibres, but instead as anastomosing masses engulfing the primary quartz and feldspar grains. Illite is also present in some of the skeletal feldspars. Some illite-smectite is also present in some of the pores. Chlorite occurs as rims around the grains.

Tiny crystals of pyrite are widely dispersed throughout in Watt Mountain Formation samples, although concentrated near the chlorite patches.

7.3 GEOCHEMISTRY:

7.3.1 Whole rock analysis:

As pointed earlier most of the sandstones have high silica content. SiO_2 values for Watt Mountain samples are above 75%, while those for the Granite Wash range between 52% and 87% (Table 7.10). The dominating quartz can be seen in most of the scatter diagrams. On plotting the analysis on SiO_2-Al_2O_3-(K_2O+Na_2O) diagram (Fig. 7.6) it can be seen that most of the samples plot near the SiO_2-Al_2O_3 axis, with the samples from Watt Mountain plotting closer

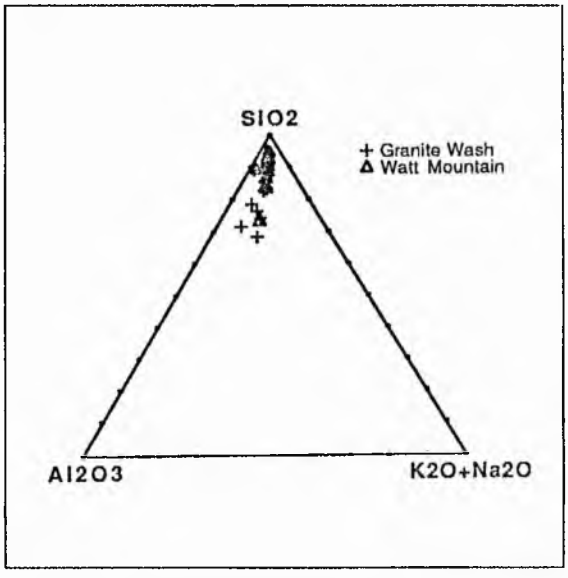

Fig. 7.6 SiO_2-Al_2O_3-(K_2O+Na_2O) scatter plot showing a greater concentration near SiO_2 corner. Each corner represents 100%.

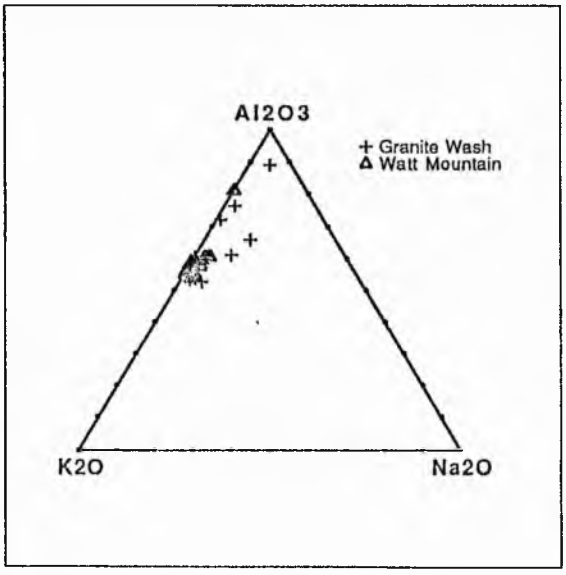

Fig. 7.7 Al_2O_3-K_2O-Na_2O scatter plot showing a greater concentration along Al_2O_3-K_2O axis. Each corner represents 100%.

towards the SiO_2 corner. This reflects the petrography, that feldspar concentration is higher in Granite Wash lithology than in the Watt Mountain Formation.

The Al_2O_3 concentration in Granite Wash samples varies between 2.5 and 14%, while for the Watt Mountain Formation the values lie between 2 and 12%. In the plot Al_2O_3-K_2O-Na_2O most of the points for Granite Wash lithology lie closer to K_2O-Na_2O axis than those from the Watt Mountain Formation (Fig. 7.7). In the Watt Mountain Formation the points lie closer to the Al_2O_3 corner. The former may be a reflection of feldspar while the latter might indicate a greater percentage of clay. Al_2O_3, K_2O and Na_2O concentration is determined not only by the feldspars but also by the clays and petrographically it is seen that the Granite Wash lithology has more feldspar and less clay than the Watt Mountain Formation.

In general feldspars are more potassic than sodic in both sets of samples. K_2O values lie between 1.8 and 7% for Granite Wash lithology, while the Watt Mountain samples vary between 2 and 7% in K_2O. The Na_2O values for the samples are much lower than the corresponding values of K_2O (Table 7.8).

On plotting Log $(CaO+Na_2O)/K_2O$ against Log SiO_2/Al_2O_3 a wide scatter is produced (Fig. 7.8). Brownlow (1979) has suggested that normally the variation of SiO_2/Al_2O_3 is more than $(CaO+Na_2O)/K_2O$ in sandstones due to difference in amount of quartz and clay minerals. However, the wider spread of both the parameters

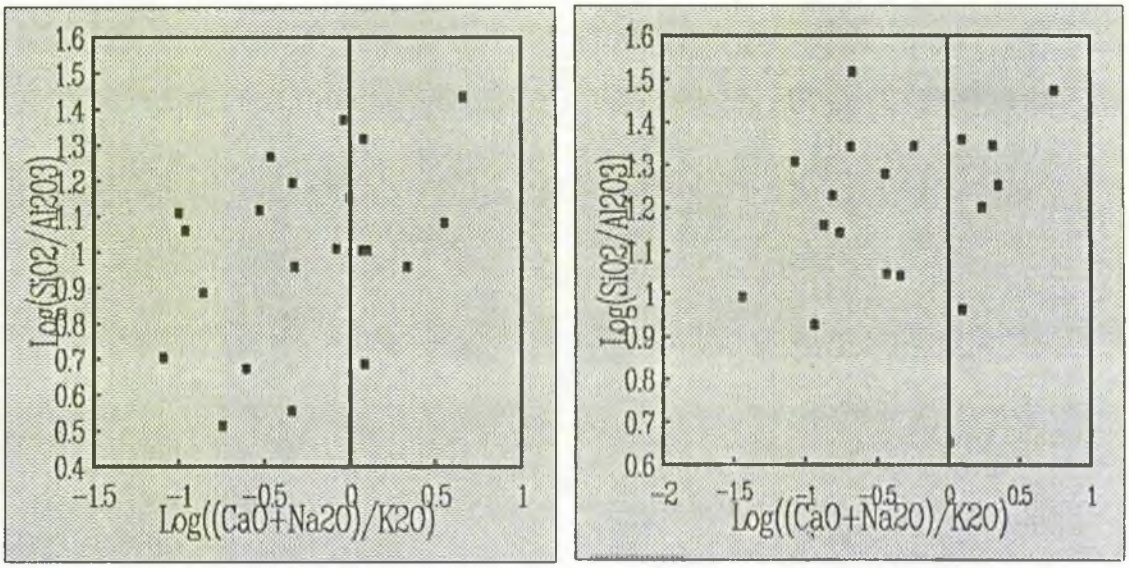

(a) Granite Wash (a) Watt Mountain

Fig. 7.8 Log $(CaO+Na_2O)/K_2O$ versus Log SiO_2/Al_2O_3 plot.
Granite Wash: Log SiO_2/Al_2O_3 = 0.5-1.4 (i.e. 0.9), Log $CaO+Na_2O)/K_2O$ = -1.2-0.7 (i.e. 1.9)
Watt Mountain: Log SiO_2/Al_2O_3 = 0.63-1.53 (i.e. 0.9), Log $CaO+Na_2O)/K_2O$ = -1.5-0.7 (i.e. 2.2)

(SiO_2/Al_2O_3 and $(CaO+Na_2O)/K_2O$) in Elk Point sandstones suggests that there was not a great difference in the amounts of quartz, clay minerals and carbonate cements. This is consistent with the petrographic analysis.

The values of CaO vary between 0.2 and 11.5% and those of MgO between 0 and 8% (Table 7.8). The MgO/CaO ratio is generally around 1, however sometimes the values are much lower. In Watt Mountain samples, the values of CaO lie between 0.1 and 11% and MgO between 0 and 5%. The low values of the MgO/CaO ratio are probably due to the presence of large amounts of anhydrite.

As seen earlier, carbonate is less abundant in the Watt Mountain Formation than in Granite Wash; anhydrite is present in both formations. The values of CaO will be governed by carbonate, calcic plagioclase and anhydrite, while MgO will be controlled by carbonate (dolomite), chlorite and rarely by Mg-garnets. Since Granite Wash has relatively little calcium plagioclase, the higher values of CaO are due to carbonate and/or anhydrite.

The carbonates in the Watt Mountain are less ferroan than in the Granite Wash, while hematite and opaques tend to be in greater amounts in the Granite Wash. The Fe_2O_3 values for the Watt Mountain Formation lie between 0.1 and 2%, while some Granite Wash values are higher in the range between 0.2 and 13% (Table 7.8). Such high values of Fe_2O_3 are probably due to oxides of iron present in greater amounts in Granite Wash lithology.

7.3.2 Isotope Analysis:

The main purpose of this section is to report and explain the stable isotope composition of anhydrite and carbonate cements from the sandstones of Granite Wash lithology, the Chinchaga Formation, Keg River Formation and Watt Mountain Formation. Oxygen-isotope compositions of successive authigenic cements can reveal much about the pore fluids and thermal history during diagenesis. In addition, the carbon-isotope ratios of carbonate cements and sulphur isotope composition of sulphate cements can help to characterise the carbon and sulphur reservoir(s) involved in their formation.

Anhydrite, calcite and dolomite were studied because they represent the major episodes of diagenesis, and certainly the last ones, in the sandstones. With some difficulty they can be obtained in sufficient abundance for sulphur, oxygen and carbon isotopic analysis.

The isotope data are presented in the usual *d* notation with respect to Standard Mean Ocean Water (SMOW) for oxygen (Craig, 1961)

and the *Belemnitella americana* for the Peedee Formation (PDB) for carbon (Craig, 1957). For sulphur the data are also presented in the usual *d* notation relative to Canyon Diablo Troilite (CDT). All values are in parts per mil $^{0}/_{00}$. Reproducibility of results was +/-0.2$^{0}/_{00}$ for $d^{34}S$, based on repeat analyses of internal and international standards at the time in the lab. For $d^{13}C$ and $d^{18}O$, reproducibility of results was +/-0.1 and +/-0.2 $^{0}/_{00}$ respectively, based on my analyses of in-house standards.

7.3.2.1 Results and Discussion:

The mineralogy of the samples used for isotope geochemistry has been examined earlier (Table 7.1-7.7), however, a summary of some petrographic features of the samples analysed is given in Tables 7.9 and 7.10.

Table 7.9 Samples selected for Sulphur isotopes from Anhydrite.

Sample No	Depth	Formation	Grains	Cement	Pores	Anhydrite % in Cement	Rock	Sulphate extracted
5-17-85-8W5	5163.84ft	Chinchaga	85	8	7	45	5.625	0.363g
1-22-86-8W5	4969ft	Chinchaga	75	15	10	60	4.0	0.319g
10-7-87-7W5	4952ft	Chinchaga	89	10	1	75	7.5	0.374g
4-34-91-7W5	4524ft	Chinchaga	88	10	2	55	5.5	0.222g
6-8-81-8W5	1678ft	Watt Mt	65	20	15	35	7.0	0.622g
8-2-87-13W5	5225.22ft	Watt Mt	65	10	25	66	6.6	0.133g

Table 7.10 Samples selected for Carbon & Oxygen isotopes from Carbonate. (FD-ferroan-dolomite; D-dolomite; FC-ferroan-calcite).

Sample No	Depth	Formation	Grains	Cement	Pores	Carbonate % in Cement	Rock	Type
11-29-86-3W5	5231ft	Chinchaga	82	3	15	80	2.5	FD
6-27-86-9W5	4816ft	Keg River	70	25	5	25	6.25	FD
9-11-87-9W5	4733ft	Keg River	75	10	15	85	8.5	FC
6-9-68-23W5	10574ft	Watt Mt	78	10	12	65	6.5	FD
6-8-81-8W5	5521.8ft	Watt Mt	82	10	8	80	8.0	FC
4-19-93-19W5	5143ft	Watt Mt	80	15	5	30	4.5	FC
10-17-94-15W5	4949ft	Watt Mt	55	45	0	90	45.0	D
10-14-72-23W5	9803ft	Granite Wash	70	30	0	100	30.0	FD
8-16-79-21W5	7704ft	Granite Wash	82	6	12	90	11.0	FC
10-17-94-15W5	5501ft	Granite Wash	40	60	0	100	60.0	FC
10-17-94-15W5	5508ft	Granite Wash	65	20	15	100	20.0	FC

Table 7.11 $\delta^{34}S$ values for samples from Elk Point Formation.

S No	Sample No	Depth	Formation	$\delta^{34}S$
1	5-17-85-8W5	5163.8ft	Chinchaga	20.2
2	1-22-86-8W5	4969ft	Chinchaga	20.7
3	10-7-87-7W5	4952ft	Chinchaga	19.3
4	4-34-91-7W5	4524ft	Chinchaga	18.6
5	6-8-81-8W5	1678ft	Watt Mt	19.3
6	8-2-87-13W5	5225.2ft	Watt Mt	20.7

Samples with higher concentration of anhydrite in the cement were selected for $\delta^{34}S$. Four samples were taken from the Chinchaga Formation and two from the Watt Mountain Formation. The isotopic compositions of $\delta^{34}S$ vary between 18.6 and 20.7‰ (mean 19.7‰, n=4) for the Chinchaga Formation, while for the Watt Mountain they are close to 20 ‰ (Table 7.11). On plotting $\delta^{34}S$ values on sulphur isotope age curves constructed by Claypool *et al.*(1980) it can be seen that the points lie either in the Devonian or Late Cretaceous-Early Tertiary periods (Fig. 7.9). However, the Elk Point Group is of Middle Devonian age (c.f. Chapter 6) (the Chinchaga Formation is Emsian in age, while the Watt Mountain Formation is Givetian). This suggests that if $\delta^{34}S$ isotope ages are Devonian then the sulphate is of the same age as the enclosing formations derived from contemporaneous seawater sulphate with little modification. This is however, not consistent with the petrographical analysis which suggests that the anhydrite is a late arrival in the rock. Likewise the spread of 18-21‰ for the Elk Point Group (Table 7.11) is tight in contrast with the range from 17 to over 30‰, reported by Buschendorf *et al* (1963) for Devonian evaporites. Hence, a much later Late Cretaceous - Early Tertiary age is a possibility for the anhydrite. However, due to the absence of any Cretaceous evaporites in the area, it is thought that remobilisation of Devonian evaporitic anhydrite was caused by Cretaceous seawaters. This led to the deposition of anhydrite as cements, with modified Devonian isotopic signatures mimicing those of Cretaceous seawaters. Richardson & Hansen (1991) have shown that $\delta^{34}S$ values remain undisturbed by chemical interaction with migrating fluids during postdepositional changes.

The $\delta^{34}S$ isotope ages of the Watt Mountain Formation, compare closely with the $\delta^{34}S$ values for recent marine environments (Pierre & Rouchy, 1986). Partial bacterial sulphate reduction in organic-rich sediments, followed by re-oxidation of reduced sulphur compounds in waters for which $\delta^{18}O$ values vary as a function of the evaporation/dilution mass balance (Fontes & Pierre, 1978; Pierre, 1982, 1985 & Pierre & Fontes, 1982) have resulted such values in recent marine environments (Pierre & Rouchy, 1986). Organic rich

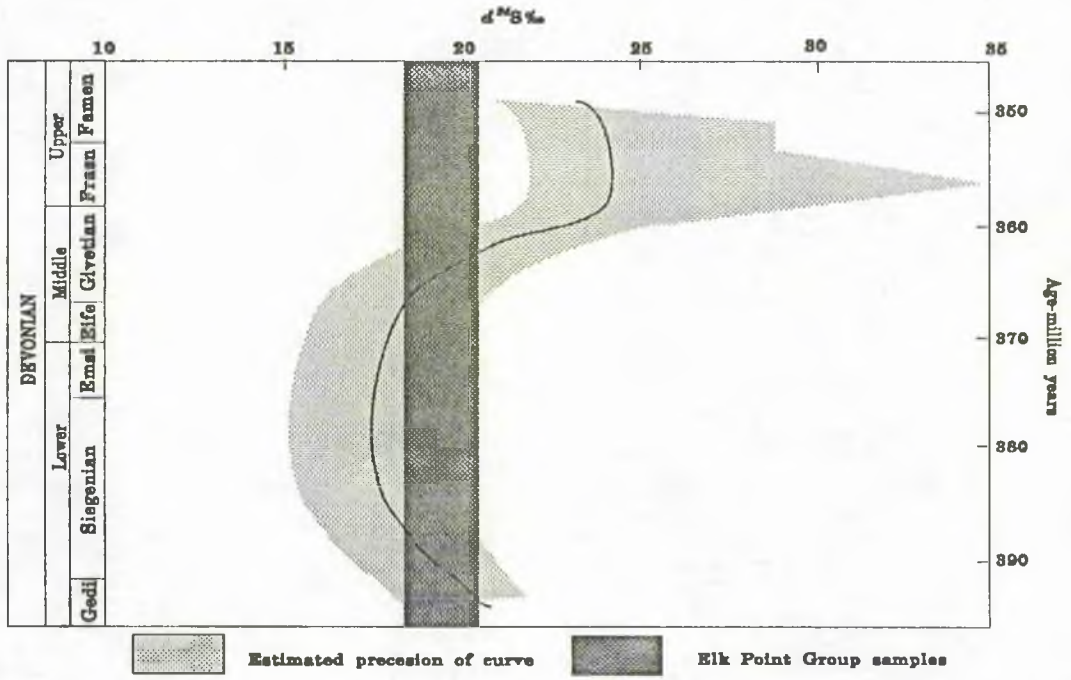

(a)

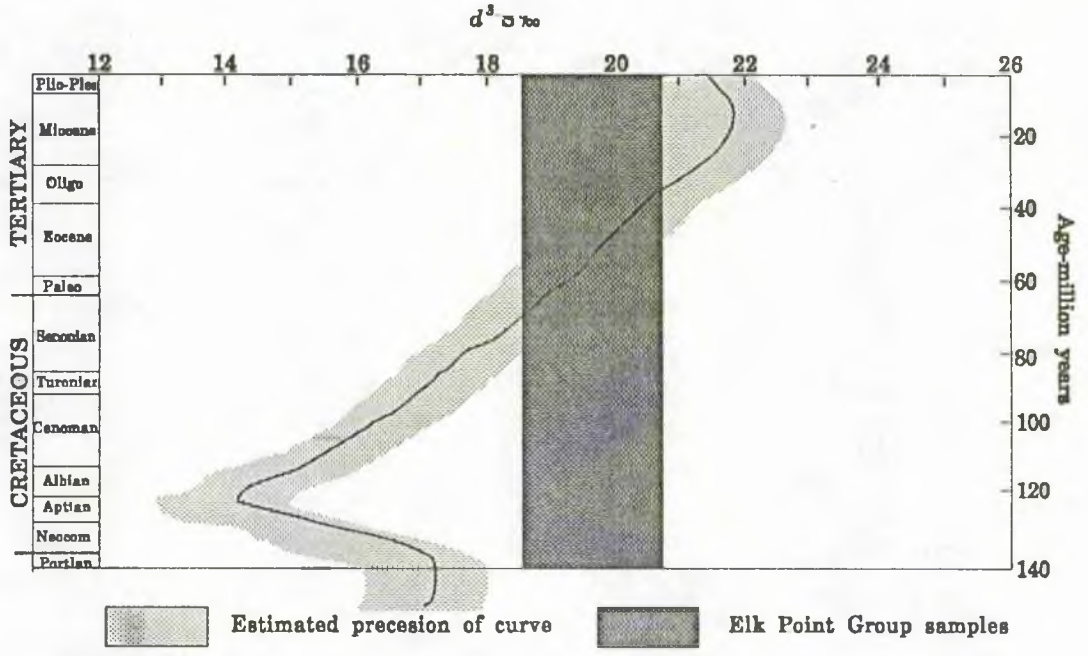

(b)

Fig. 7.9 Sulphur isotope age curve for marine sulphate during (a) Devonian and (b) Recent to Cretaceous period. Light shaded area is estimated precision of the curve. Dark shaded area represents Elk Point samples from this study (modified from Claypool *et al.*, 1980).

intercalations can also cause such effects (*op. cit.*). This hypothesis can also be applied to the Elk Point Formation as there are marine shale intercalations which may have acted as the source for bacterial sulphate reduction.

The $\delta^{18}O$ values for the carbonates of the Elk Point samples range from 17.3 to 24 SMOW with an anomalously high value of 28.3 from the Chinchaga Formation (Table 7.12, Fig. 7.10). Such values of $\delta^{18}O$ (normally >+10) typify clastic sedimentary rocks because the cementing minerals are formed at lower temperatures during weathering, sedimentation, and diagenesis than the primary components which are formed at higher temperatures (Longstaffe, 1986). The oxygen isotope fractionation between water and minerals like carbonates and most clays and water is large at low temperatures (Savin & Epstein, 1970a, 1970b; Lawrence & Taylor, 1971, 1972; O'Neil *et al*, 1969).

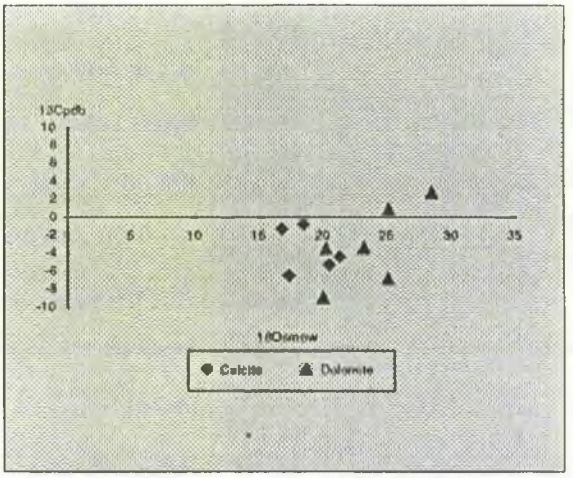

Fig. 7.10 $\delta^{18}O_{SMOW}$ vs $\delta^{13}C$ pdb plot for Elk Point samples. Calcites form a tight cluster, while the dolomites fall within a linear trend.

The $\delta^{13}C$ values range between -8.9 and 2.8, (Table 7.12, Fig. 7.10).

Table 7.12 $\delta^{13}C$, $\delta^{18}O$ and $\delta^{18}Osmow$ values for samples from Elk Point Formation.

S No	Sample No	Depth	Formation	Type	$\delta^{13}Cpdb$	$\delta^{18}Osmow$
1	8-16-79-21W5	7704ft	Granite Wash	FC	-1.28	16.77
2	10-17-94-15W5	5508ft	Granite Wash	FC	-0.8	18.45
3	9-11-87-9W5	4733ft	Keg River	FC	-6.47	17.33
4	6-8-81-8W5	5521.8ft	Watt Mt	FC	-4.44	21.24
5	4-19-93-19W5	5143ft	Watt Mt	FC	-5.25	20.42
6	11-29-86-3W5	6231ft	Chinchaga	FD	2.78	28.44
7	6-27-86-9W5	4816ft	Keg River	FD	-6.83	25.05
8	6-9-68-23W5	10574ft	Watt Mt	FD	-3.46	20.19
9	10-17-94-15W5	4949ft	Watt Mt	D	-3.37	23.13
10	10-14-72-23W5	9803ft	Granite Wash	FD	-8.89	19.95
11	10-17-94-15W5	6501ft	Granite Wash	FD	0.9	25.08

On plotting $d^{18}O$ against $d^{13}C$, calcites form a tight cluster, while the dolomites fall within a linear trend (Fig. 7.10). The $d^{18}O$ values for the dolomites have a spread between 19.9 and 28.4, while those for the calcite range between 17.3 and 21.2 (Table 7.12, Fig. 7.10). The $d^{13}C$ values for dolomites lie between -8.9 and 2.8 (Table 7.12, Fig. 7.10). The $d^{13}C$ values for the calcites are -6.5 and -0.8 (Table 7.12, Fig. 7.10). The wide range in the values indicates some variation in the conditions of the formation of the carbonate, an observation which is consistent with the petrographic data. The tight cluster of calcite (Fig. 7.10) suggest a narrow range of temperature of formation for calcite. Wider linear distribution of dolomite values (Fig. 7.10) suggest a greater range of the temperature of formation for dolomite.

The depletion of $d^{13}C$ in the carbonate values probably result from the mixing of carbon derived from marine carbonate, including shell debris ($d^{13}C$=0 +/- 4; e.g., Gross, 1964), and ^{13}C-depleted organic carbon from the maturation of organic matter (e.g. oxidation, decarboxylation, CO_2 from methane generation; Hudson, 1977; Carothers & Kharaka, 1980; Kharaka *et al*, 1983). Without knowing the specific nature of the reactions involving organic carbon, the relative contributions of organic and inorganic carbons cannot be resolved accurately. The low values of $d^{18}O$ and $d^{13}C$ are consistent with temperature and burial conditions in organic-maturation zone IV (of Curtis, 1977; Irwin *et al*, 1977) where abiotic reactions tend to produce the light isotope.

7.3.2.2 Constraints on Diagenesis:

The oxygen-isotope ratios of carbonates can be used to deduce temperature and fluid conditions during their formation, provided that the isotopic compositions of the minerals have remained unchanged since crystallisation (Longstaffe, 1986). Isotopic exchange between carbonates and fluid is not significant at temperatures typical of sedimentary environments except during solution and reprecipitation (Anderson, 1969; Land, 1980). Oxygen-isotope exchange resulting from recrystallisation becomes more important as temperatures rise, calcite being much more susceptible than dolomite. Since no detrital carbonate has been seen in the sandstones, all data were derived from diagenetic carbonates. Due to the lack of the detrital carbonates it is not possible to attempt any isotopic re-equilibration between detrital and diagenetic carbonate.

The relationships among the $d^{18}O$ of diagenetic calcite and dolomite (including ferroan-calcite, ferroan-dolomite), temperature

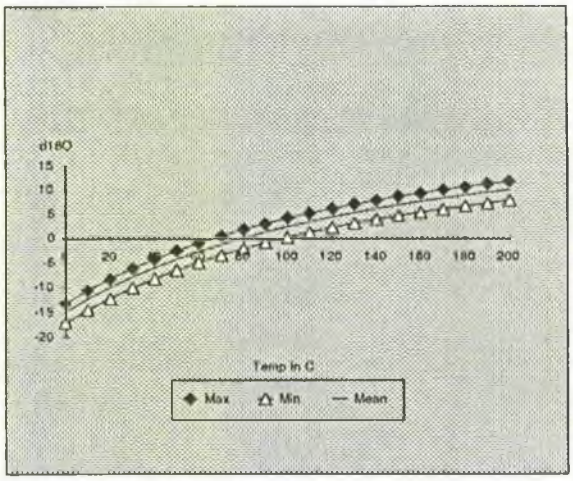

Fig. 7.11 $d^{18}O$ of formation water vs temperature for authigenic calcite for Elk Point Basin. The curves for calcite (ferroan-calcite) have been determined using minimum, mean and maximum values of $d^{18}O$ for calcite in the following equation:
$10^3 \ln x_{calcite\ H2O} = 2.78(10^6)T^{-2} - 2.89$ (Friedman & O'Neil, 1977).

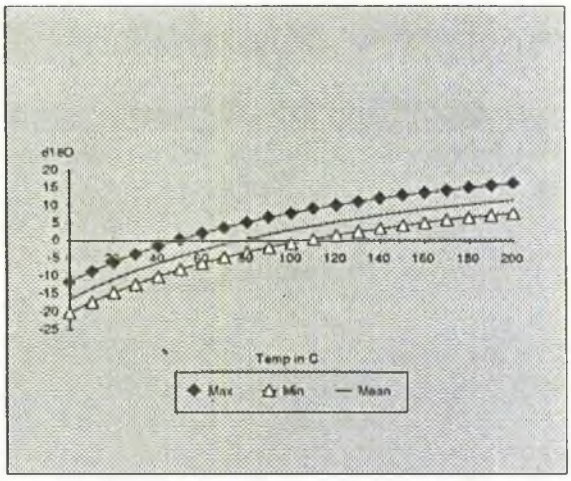

Fig. 7.12 $d^{18}O$ of formation water vs temperature for authigenic dolomite for Elk Point Basin. The curves for dolomite (ferroan-dolomite) have been determined using minimum, mean and maximum values of $d^{18}O$ for calcite in the following equation:
$10^3 \ln x_{dolomite\ H2O} = 3.14(10^6)T^{-2} - 2.0$ (Land, 1983).

and water $d^{18}O$ are shown in Fig. 7.11 and 7.12. These curves have been calculated using functions reported by Friedman and O'Neil (1977) for calcite and Land (1983) for dolomite. The same partition coefficients are used for ferroan carbonates.

To calculate an isotopic temperature for crystallization of a diagenetic mineral requires that the $d^{18}O$ of both solid and liquid be known (Longstaffe, 1986). A critical but reasonable assumption is that diagenetic calcite/dolomite formed in equilibrium with water no lower in $d^{18}O$ than that of the reservoir. Most formation waters in the western Canada sedimentary basin are believed to have formed by mixing of 1) pore fluids trapped during sedimentation (e.g., seawater, $d^{18}O$ = 0) and enriched in $d^{18}O$ by exchange with the host sedimentary rocks during diagenesis, and 2) low-$d^{18}O$ groundwater (Hitchon & Friedman, 1969).

Taking the $d^{18}O$ of water to be at least 0 (due to seawater mixing and saline brines) suggests temperatures within ranges of 65°C and 100°C for calcite (Fig. 7.11) and 50°C and 110°C for dolomite (Fig. 7.12), although a greater admixture of brines ($d^{18}O$ of 5) would increase these figures by about 50%.

7.4. PROVENANCE:

The composition of the sediment is controlled mainly by the lithology, climate and relief of the source area. The virtual absence of sedimentary rock fragments, and the abundance of feldspar in the sediments indicates that it was

derived primarily from an igneous-metamorphic terrain. The only such terrain in the immediate vicinity was the Peace River High. According to Burwash (1957) and Burwash *et al,* (1964) the Peace River high is composed mainly of Precambrian pelitic and quartzo-feldspathic metamorphic rocks and acid to intermediate igneous rocks, with only minor amounts of sedimentary, meta-sedimentary, volcanic, meta-volcanic and basic igneous rocks. There is no problem in deriving these sandstones from a source area made up of these rocks types. Some quartz grains which are well rounded appear to be at least second-cycle quartz. These are minor and may be explained by the possible existence of some pre-Middle Devonian, perhaps continental, sedimentary rocks on the Peace River high.

The presence of relatively fresh angular potash feldspar in the Watt Mountain Formation indicates that there was little time for weathering either at the source or at the site of deposition. This suggests that the relief on the Peace River high was fairly strong and that the erosion and deposition was fairly rapid as suggested by Kramers & Lerbekmo (1967). Although K-feldspar appears to be present in all the four formations, plagioclases increased in amount in the younger Watt Mountain Formation.

There appears to have been hydrothermal aplitic and pegmatitic veins in the source area which produced vein quartz and some microcline associated with the acidic plutonic rocks (Jansa & Fischbuch, 1974).

That the Peace River high is the source area is also indicated by the regional distribution of the Watt Mountain, Keg River, Chinchaga and the Granite Wash, which occurs as a fringe around the high (Grayston *et al.,* 1964; Suska, 1963).

7.5. DIAGENESIS:

7.5.1. Diagenetic History:

The following diagenetic episodes are suggested on the basis of textural features (Fig. 7.13):-

(a) Slight compaction.

(b) Dissolution of feldspars and lithoclasts.

(c) Kaolinite formation.

(d) Feldspar overgrowths.

(e) Chlorite and smectite formation.

(f) Quartz overgrowths and alteration of chlorite to pyrite.

(g) Smectite-to-illite conversion.

(h) Quartz overgrowths and silica precipitation.

(i) Dissolution of quartz overgrowths and feldspars.

(j) Ferroan calcite precipitation.

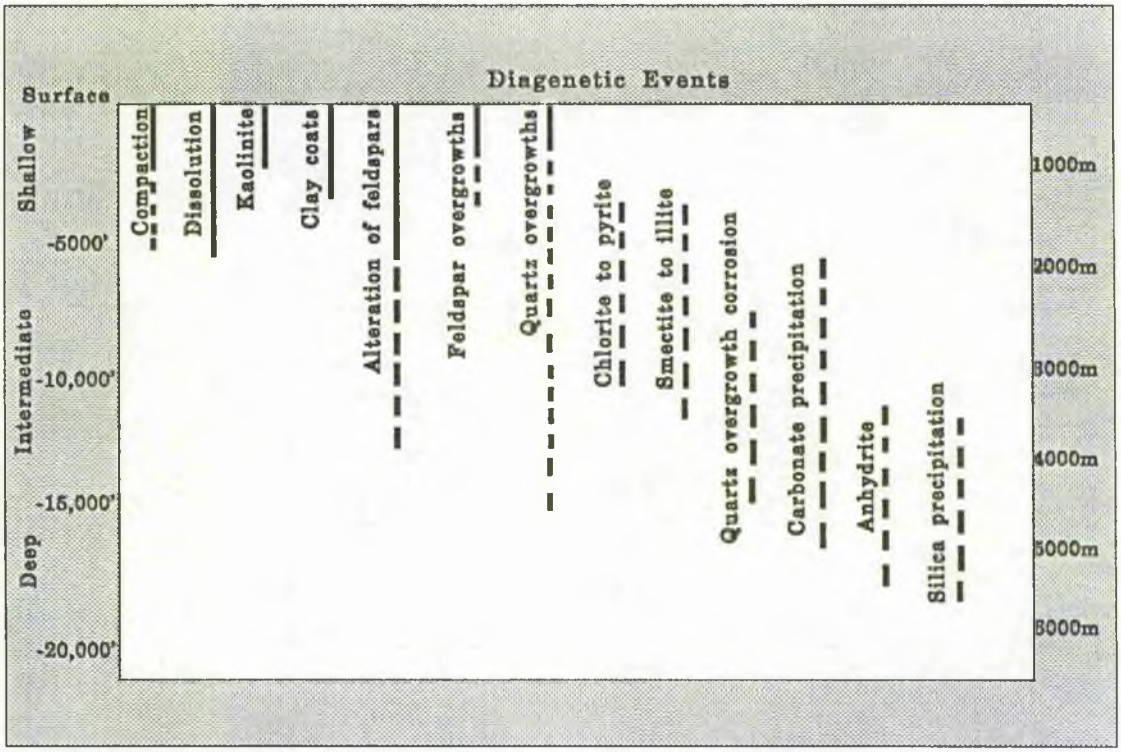

Fig. 7.13 Schematic representation of various diagenetic episodes occuring in the Elk Point sediments. Stages of compaction through to carbonate precipitation were cyclic in each of the four formations. Anhydrite formation was probably the last episode and took place as one major event in all the formations.

(k) Ferroan dolomite and dolomite precipitation.

(l) Anhydrite formation.

(m) Dissolution of carbonate and anhydrite.

(n) Late stage quartz precipitation and illite growth.

Such a complex diagenetic assemblage is developed in all the four formations even though there are marine flooding surfaces separating the formations (c.f. section 6.6). The sequence of mineral cements until carbonate precipitation (episode j & k) occurs with the same cyclicity in the four formations, except for minor variations viz: absence of authigenic feldspar overgrowths in the Keg River Formation and the Chinchaga Formation; lesser amounts of carbonate occur in Watt Mountain Formation and Chinchaga Formation than in the Granite Wash and Keg River Formation. Widespread anhydrite precipitation took place later in all four formations.

Such cyclicity suggests multiple injection of similar pore fluids due to repeated marine transgressions. Repeated movement of fluids along fault conduits might have also helped the cyclicity (Burley *et al,* 1989). A possible mixing of at least two distinct sub-surface fluids of very different chemistry and origin and some

cross formational transfer of ions from either adjacent or distant lithologies might have also occured (*op. cit.*).

Surface to shallow subsurface diagenesis began with an early phase of compaction producing bent micas and fractured feldspar followed by dissolution of primary clasts probably feldspars and lithoclasts and the development of clays (Plates 7.10, 7.11). Minor amounts of authigenic kaolinite were precipitated in the shallow diagenetic environment (Giles & de Boer, 1990). Although clay coats occupy only a small volume of pore space, they can be detrimental to permeability by reducing pore-throat diameter and causing resistance to fluid flow (Galloway, 1977). Such a resistance to fluids aided in providing a greater time for dissolution of primary grains by the moving fluids.

Alteration of feldspars began in the source area and continued at the depositional surface and in the subsurface. Feldspars were dissolved and dissolution occurred during the shallow and intermediate subsurface stages of diagenesis (Plates 7.10, 7.11). Relatively early feldspar dissolution is indicated by the presence of chlorite along some cleavage cracks.

Feldspar overgrowth around detrital feldspars and, less commonly, around volcanic rock fragments, which took place after the major phase of dissolution was also a near-surface process. Overgrowths of both plagioclase and orthoclase were noted (Plates 7.12-7.17). These overgrowths around detrital feldspars were largely due to available nucleation sites (Giles & de Boer, 1990).

Early quartz overgrowths are absent where fringing chlorite is present suggesting early chlorite growth. But there was some overlap in time because some chlorite crystals are partly enveloped by quartz overgrowths (Plates 7.19, 7.21).

Intermediate subsurface diagenesis comprised a complex stage of cementation and minor dissolution. Secondary porosity reached a maximum value near the begining of this stage. Compaction was arrested during this stage because of abundant cementation. Minor dissolution of feldspars and rock fragments continued in the intermediate subsurface, which created secondary dissolution porosity. Large quantities of mesogenic cements suggest mass transfer of solutes within an open system as implied by Burley *et al.* (1989) for the Tartan Reservoir.

Quartz overgrowth cementation was an important stage of diagenesis, that appeared in the intermediate subsurface. Overgrowths occluded pore space resulting in reduction of

compaction due to less availability of space (Plates 7.2, 7.10, 7.17)..

The alteration of chlorite into pyrite took place during this period, as indicated by pyrite being always associated with chlorite. Alteration of smectite to illite also began during this period as under EDX both tend to occur together or illite fibres develop over a smectite base.

Quartz overgrowths which had been formed during the intermediate stage started to corrode (Plates 7.29, 7.30, 7.35). Carbonate cementation that occurred after formation of quartz overgrowths exists in two modes. Calcite started to precipitate first followed by ferroan dolomite and dolomite. This carbonate cementation was also a major porosity-reducing event. Carbonate was found to replace feldspar, quartz grains and silica cement as also suggested by Kramers & Lerbekmo (1967). Anhydrite was the last to be deposited and occurs in restricted areas (Plate 7.23) (see also Kramers & Lerbekmo, 1967). Anhydrite was sourced from the expulsion of aqueous fluids from the overlying Cretaceous marine sequences which caused the remobilisation of anhydrite from Devonian evaporite deposits. Temperatures in excess of 100°C for carbonates from stable isotope data suggest a late stage precipitation. Isotope data from anhydrite cements give an age of Late Cretaceous-Early Tertiary. Present day temperature gradients for the area are 27°C/km (AAPG & U.S. Geological Survey, 1976) with surface temperatures of 5°C, however, it has been suggested that in past surface temperatures were +16°C (Piel, 1971) and geothermal gradients were 24.5°C/km (Hacquebard, 1977; Hutcheon, 1984). These values suggest that carbonate was deposited at depths greater than 3 km somewhere between Early Triassic and Late Cretaceous.

After these last stages of quartz, carbonate and anhydrite cementation, porosity was commonly reduced to 10%. This reduction in porosity could be reversed, however, by intense dissolution near the base of the intermediate subsurface zone. Components that were dissolved were feldspars, volcanic fragments, and carbonate cements. Evidence for this stage of dissolution is the dissolution of post-quartz overgrowth carbonate-anhydrite cement and the formation of embayments in quartz overgrowths where grain-margins have been dissolved. By this time temperatures would have been in excess of 80°C, so as to form carboxylic acids and acids produced by thermal decarboxylation (Cowan & Shaw, 1991) causing the dissolution of grains and creating secondary porosity.

The last cementation phase observed is Fe-rich dolomite and ankerite, however, evidence regarding to this is not very clear. Ankerite has been identified only on the basis of analysis by electron-microprobe.

A probable evidence in favour of quartz precipitation as deep subsurface diagenesis episode are the temperatures of homogenisation of fluids in the inclusions present in the fractures in silica range between 147-161°C. If these temperatures are due to diagenesis then they are very high and probably suggest rejuvenated quartz. On the other hand such high temperatures may also be due to resetting of inclusion homogenisation temperatures as the burial proceeded (Osborne & Haszeldine, 1990).

7.5.2. Diagenetic Reactions:

We have referred earlier to the three types of pore waters in sedimentary basins (Fig. 4.26; Bjorlykke, 1984). The diagenesis in the sandstones of the Watt Mountain Formation, Keg River Formation and Chinchaga Formation, and Granite Wash lithology was controlled in the shallower stages by fresh meteoric and connate waters and in later stages by marine waters (c.f. section 4.5.2). Convection currents driven by density differences (Fig. 4.26) must have played an important role in the later stages of diagenesis in the sandstones precipitating late stage cements.

Jansa & Fischbuch (1974) have suggested precipitation of early silica for the Devonian clastic coastal plain sequence of Sturgeon-Mitsue area due to the contact of lower pH river water with the saline alkaline waters of the delta front facies. The contact between fresh and marine water probably took place in the vicinity of distributary mouth bars, where presumably the pH gradient was sufficiently high to precipitate silica from solution. Electrolytes could cause silica to be adsorbed on the surface of suspended inorganic particles, or facilitate co-precipitation of silica with such inorganic particles. The process causes a significant depletion in dissolved silica and has been observed in Mississippi River waters entering the Gulf of Mexico (Bien *et al*, 1959). However, in the present study due to limited sampling and material available no distinct near surface quartz overgrowths could be differentiated from the later one.

If K-feldspars originally constituted 10% by volume of the sand fraction of sandstones (5% of the volume of the sandstones assuming 50% initial porosity), then the most likely dissolution reaction due to CO_2 dissolved in water can be written as the equation:

Table 7.13 Material fluxes during sandstone diagenesis (modified after Land, 1984).
[1]Includes 0.46 millimoles precipitated as kaolinite (eqn.1)
[2]Assuming both calcite and quartz precipitate from the same water

Reaction	Vol %	SiO_2	H_2O	CO_2	Mineral	Vol of Water Required (L)
Quartz Cementation						
$H_4SiO_4 \rightarrow SiO_2+2H_2O$	2.5	+1.1	+2.2		+1.1 Quartz	1.3
Calcite Cementation						
$Ca^{+2}+2HCO_3 \rightarrow CaCO_3+H_2O$	10		+3.1	+3.1	+ 3.1 Calcite	3.1
Secondary Porosity						
Calcite dissolution	5.0		-1.6	-1.6	-1.6 Calcite	0.5
K-feldspar dissolution (equ. 1)	5.0	-0.92	-1.6	-0.46	-0.46 K-feldspar +0.23 Kaolinite	0.15
		+0.64[1]	+2.1	+1.04		3.7[2]

$$2KAlSi_3O_8 + 2CO_2 + 7H_2O \Longrightarrow 2K^+ + Al_2Si_2O_5(OH)_4 + 4H_4SiO_4 + 2HCO3^- \quad ...1$$

If K-feldspars constituted approximately 5% of the original volume of the sands, then 0.05 cm^3 X 1 mole $KAlSi_3O_8$/109.5 cm^3 = 0.46 millimoles of K-feldspar have been regionally destroyed in each cubic centimeter during the time of burial. An equal number of moles of CO_2 were consumed, and K^+ and $HCO3^-$ released for each cubic centimeter of sandstone reacted. Comparisons of the CO_2 and H_4SiO_4 involved in this reaction with material requirements for secondary porosity generation and quartz cementation are presented in Table 7.13. The amount of CO_2 required is about one-third that required for calcite dissolution whereas the amount of SiO_2 released (0.92 millimoles per cm^3) is only slightly less than that required for quartz cementation. The amount of kaolinite formed (0.23 millimoles X 99.5 cm^3mole^{-1} = 2% of the sandstone volume) is only slightly more than the amount of kaolinite recorded from the point count data. Because some pore-filling kaolinite may have been overlooked during point counting, it can be concluded that a significant percentage of the kaolinite cement in these sandstones results from K-feldspar dissolution.

According to the above stoichiometry, about 0.46 millimoles of K^+ are released by destruction of K-feldspar for each average cubic centimeter of the sandstones.

The degeneration of K-feldspar also produces some quartz as in the reaction:

$$2KAlSi_3O_8 + 2H^+ + H_2O \Longrightarrow Al_2Si_2O_5(OH)_4 + 4SiO_2 + 2H^+ + 2K^+ \quad ....2$$

Feldspar Kaolinite Silica

The K^+ released in equation 2 could have been used up in the reaction:

$$KAl_3Si_3O_{10}(OH)_2 + 6SiO_{2(aq)} + 2K^+ \Longrightarrow 3KAlSi_3O_8 + 2H^+ \quad ..3$$

to form feldspar as overgrowths.

In general quartz cementation precedes feldspar stabilization (Land, 1984), little quartz cementation can be accomplished as a result of feldspar stabilization reactions. Equilibrium between water and quartz/clay minerals in equation 2 & 3 would result in lack of secondary porosity (Giles & de Boer, 1990).

The formation of clay coats (smectite and/or chlorite) probably took place by mechanical infiltration of colloidal clay-rich waters through the vadose zone and/or by alteration of feldspars.

Petrologic evidence by various workers (Hower *et al,* 1976; Boles & Franks, 1979) indicates that the smectite-to-illite transformation involves release of Si^{+4} and takes place over a broad temperature range, generally between 60 and 120°C. Various workers (Pery & Hower, 1970; Dunoyer & Segonzac, 1970; Hutcheon, 1981; Hower *et al,* 1976) have proposed layer to layer transformation of smectite to illite as;

Smectite + K^+ + Al^+ ==> illite + Si^{+4} + H^+ ...4

or,

Smectite + K-feldspar ==> Illite + chlorite + quartz ...5

Similar transformation seems to have taken place in Elk Point sandstones. Some of the silica released has been precipitated as quartz overgrowths on detrital quartz grains in sandstones which provide excellent loci of nucleation (see also Giles & de Boer, 1990).

Transformation of kaolinite to illite took place between 120°-150°C (Hower *et al,* 1976) and Hoffman & Hower, 1979) as in reaction:

$Al_2Si_2O_5(OH)_4 + KAlSi_3O_8 \Longrightarrow KAl_3Si_3O_{10}(OH)_2 + 6SiO_2 + H_2O$

kaolinite Feldspar Illite 6

This reaction would have led to the formation of secondary porosity in feldspars and clays of the Elk Point sandstones.

Carbonates were deposited from ground water and migrating interstitial fluids in a slightly alkaline environment. Transformation of kaolinite to illite due to the shrinking stability field of kaolinite with increasing temperature has been reported by Sass *et al.* (1987) according to the following reactions;

$5KAlSi_3O_8 + 4H^+ \Longleftrightarrow KAl_4Si_7AlO_{20}(OH)_4 + 8SiO_2 + 4K^+$

k feldspar illite quartz ...7

$KAlSi_3O_8 + 2Al_2Si_2O_5(OH)_4 \Longleftrightarrow KAl_4Si_7AlO_{20}(OH)_4 + 2H_2O$

K feldspar kaolinite illite 8

$5NaAlSi_3O_8 + 4H^+ + 4K^+ \Longleftrightarrow KAl_4Si_7AlO_{20}(OH)_4 + 8SiO_2 + 4Na^+$

Na feldspar illite quartz ...9

Thus illite could have formed in the sandstones of the Elk Point Group with continued formation of quartz overgrowths and secondary porosity in feldspars.

The deposition of carbonate presumably took place from marine pore waters brought by marine incursions.

The reactions 1-9, followed by carbonate deposition were cyclic for all the four formations.

Sulphur isotope ages of Cretaceous suggest that anhydrite precipitation was brought about in all the formations by the remobilsation of interbedded evaporitic sediments in the Muskeg, Keg River and Chinchaga Formations by Cretaceous formation waters. Due to the position of Granite Wash Lithology at great depths the percolating waters were not able to precipitate anhydrite at that depths.

The concentration of iron and hematite pigment in mudstones, shales and the argillaceous matrix of sandstones may be explained by the initial concentration of iron from iron-rich biotite, hornblende and ore minerals, and a subsequent alteration during burial processes. Some of the iron may have been deposited as detrital hematite.

Table 7.1 Representative modal analysis data of Granite Wash sandstones. (A-abundant; S-scarce; R-rare; Ill-illite; Chl-chlorite; Kl-kaolinite; I/S-illite-smectite; Smec-smectite; Hem-hematite; P-poor; M-moderate; G-good; VG-very good; SA-subangular; SR-subrounded; BP-interparticle porosity; WP-intraparticle porosity)

Sample No (All samples west meridian 5)	Depth (ft)	Grainsize (mm)	Sorting	Roundness	Packing	Porosity (%) BP WP	Primary: Quartz (%)	Feldspar (%)	Lithoclasts (%)	Mica (%)	Pyrite (%)	Secondary: Carbonate (%)	Anhydrite (%)	Clay (%)	Other (%)
10-14-72-23	9803	0.25-2.0	M	SA-SR	Loose	0	70	3				27			
11-11-73-13	7386	0.25-1.0	G	SA-SR	Loose	15 80 20	74	5		1				5 Ill	
9-30-74-21	8513.1	0.25-2.0	M	SA	Loose	20 80 20	59	12	5	1			2	1 Ill	
16-35-74-24	9084.2	0.125-1.0	P	SA	Loose	7 80 20	73	3	2.5	2.5				12 Ill	
3-4-75-18	7822.2	0.125-1.0	G	SA-SR	Loose	10 90 10	74	5	2	3		3	1	2 Ill	
6-1-75-24	9102.9	0.5-1.0	G	SA	Loose	10 60 40	26	1	12	1				50 Ill,Chl	
4-22-71-14	6953.7	0.125-2.0	VP	SA-SR	Loose	15 80 20	62	11	2			3.5		6.5 Chl(A),Ill(S)	
10-11-72-16	7489.8	0.5-1.0	G	SA-SR	Loose	10 75 25	72	10.5	0.5					5 Ill	
12-11-78-22	7704	0.125-0.50	G	SA-SR	Loose	5 75 25	84	3				5		3 Ill	
8-16-79-21	8008.7	0.5-4.0	M	SA-SR	Loose	12 90 10	79	1.5	1.5			4.5		1.5 Chl	
2-9-80-18	7132.9	0.25-2.0	G	SA-SR	Loose	0	64	3	1.5	1.5		30			
9-13-80-21	7883.8	0.5-2.0	P	SA	Loose	20 80 20	62	6	6	1		5			
10-5-81-9	15809.2	0.25-1.0 1.0-2.0 rare	G	SA-SR	Loose	25 80 20	64	6				2		3 Ill	

Sample No	Depth (ft)	Grainsize (mm)	Sorting	Roundness	Packing	Porosity (%) BP WP	Primary: Quartz (%)	Feldspar (%)	Lithoclasts (%)	Mica (%)	Pyrite (%)	Secondary: Carbonate (%)	Anhydrite (%)	Clay (%)	Other (%)
6-31-84-7	5272	0.25-2.0	G	SA-SR	Loose	10 70 30	77	3	2.5	0.5	2	2.5	1.5		1 Silica
4-9-85-9	5100	0.125-0.50	M	SA	Loose	0	85	2		2	1	2		8 Ill	
1-22-86-8	4996	0.25-4.0	P	SA-SR	Loose	0	66	19	7		1	1		6 Ill(A),Chl(A)	
10-15-86-10	4888	0.125-2.0	P	SA-SR	VLoose	8 70 30	34	3	25					30 Ill	
4-16-87-7	5004	0.125-0.50	G	SA-SR	Interlocking	4 50 50	87	4.5			0.5	4			
12-36-88-11	5146.5	0.25-1.0	M	SA-SR	Loose	12 80 20	72	6.5	2		1.5		1	4.5 Ill	0.5 Silica
12-36-88-11	5156.2	0.5-2.0	M	SA-SR	Loose	12 70 30	69	8.5			0.5	2		8 Ill	
12-36-88-11	5169.5	0.5-2.0	G	SA-SR	Loose	7 65 35	74	5		0.5	5.5			7.5 Ill	0.5 Silica
1-5-90-10	4925	0.25-0.50 1.0-4.0	P	SA-SR	Loose	5 60 40	72	8	3					12 Ill(A),Chl(S)	
9-35-91-6	4645	0.125-1.0 rare 2.0	G	SA-SR	Loose	2 90 10	78	2					18		
9-35-91-6	4649	0.25-0.50 2.0-4.0	P	SA-SR	Loose	10 75 25	38	2	40			5		1.5 Ill	3.5 Silica
12-25-91-10	4729	0.25-0.50	VG	SA-SR	Loose	2 90 10	88	5				4.5		0.5 Ill,Chl	
10-17-94-15	5501	0.25-2.0	P	SA	VLoose	0	28	12				30			
10-17-94-15	5505	0.25-2.0	P	SA-SR	Loose	20 90 10	66	12	1			20			

Sample No	Depth (ft)	Grainsize (mm)	Sorting	Roundness	Packing	Porosity (%) BP	WP	Primary: Quartz (%)	Feldspar (%)	Lithoclasts (%)	Mica (%)	Pyrite (%)	Secondary: Carbonate (%)	Anhydrite (%)	Clay (%)	Other (%)
10-17-94-15	5508	0.25-2.0	P	SA-SR	Loose	15		54	8	3			20			
						90	10									
10-17-94-15	5512	0.25-2.0	P	SA-SR	Loose	20		66	9	3					2	
						90	10								III	

Table 7.2 Representative modal analysis data of Chinchaga sandstones. (A-abundant; S-scarce; R-rare; Ill-illite; Chl-chlorite; Kl-kaolinite; I/S-illite-smectite; Smec-smectite; Hem-hematite; P-poor; M-moderate; G-good; VG-very good; SA-subangular; SR-subrounded; BP-interparticle porosity; WP-intraparticle porosity)

Sample No (All samples west meridian 5)	Depth (ft)	Grainsize (mm)	Sorting	Roundness	Packing	Porosity (%)		<-----Primary-----> Quartz (%)	Feldspar (%)	Lithoclasts (%)	Mica (%)	Pyrite (%)	Carbonate (%)	<-----Secondary-----> Anhydrite (%)	Clay (%)	Other (%)
						BP	WP									
5-17-85-8	5160.5	0.0625-0.50	G	SA-SR	Loose	0		70	2	1.5	1.5				25 Ill(A),Chl(S)	
5-17-85-8	5163.8	0.25-1.0	G	SA-SR	Loose	7	90 10	82	3					4 Chl(R),Ill(R)	2 Ill	2 Silica
5-17-85-8	5167.8	0.25-0.50	G	SA	Loose	0		86	2		4				8 Ill(A),Chl(R)	
11-29-86-3	5231	0.25-1.0	G	SA-SR	Loose	15	90 10	76	2	2			4	0.5	0.5 Ill	
11-29-86-3	5233	0.25-1.0	P	SA-SR	Loose	5	90 10	80	2	3	2		5	2	1 Ill	
1-22-86-8	>4.0	0.25-1.0	P	SA	Interlocking	10	90 10	66	4.5	2	0.5	2		9	1.5 Ill	4.5 Silica
10-7-87-7	4952	0.25-2.0	P	SA-SR	Loose	1	60 40	52	2	45				7.5		2.5 Silica
12-25-91-10	4714	0.25-2.0	P	SA-SR	Loose	15	80 20	77	4	2				0.5	1.5 Ill	
4-34-91-7	4524	0.25-2.0	M	SA-SR	Loose	2	80 20	78	6			4		5.5	3 Ill	1.5 Silica

Table 7.3 Representative modal analysis data of Keg River sandstones. (A-abundant; S-scarce; R-rare; Ill-illite; Chl-chlorite; Kl-kaolinite; I/S-illite-smectite; Smec-smectite; Hem-hematite; P-poor; M-moderate; G-good; VG-very good; SA-subangular; SR-subrounded; BP-interparticle porosity; WP-intraparticle porosity)

Sample No (All samples west Meridian 5)	Depth (ft)	Grainsize (mm)	Sorting	Roundness	Packing	Porosity (%) BP	WP	Primary: Quartz (%)	Feldspar (%)	Lithoclasts (%)	Mica (%)	Pyrite (%)	Secondary: Carbonate (%)	Anhydrite (%)	Clay (%)	Other (%)
11-18-72-17	8339	0.125-1.0	P	SA-SR	Loose	6		81	5	4	1			1	2	
						80	20								Chl(A),Ill(S)	
1-22-86-18	4950	0.25-1.0	G	SA-SR	Loose	35		54.5	1	2	0.5			5	1	1
						90	10								Ill	Silica
6-27-86-9	4816	0.25-0.50	G	SA	Loose	5		66.5	3.5				6		19	
						Fracture									Ill	
4-3-87-8	4911	0.25-1.0	M	SA	Loose	0		88	5				4	0.5	2	0.5
		2.0-4.0	bimodal												Ill	Silica
4-3-87-8	4914	0.25-2.0	G	SA-SR	Loose	10		71	4				2	10.5		2.5
						80	20									Silica
9-11-87-9	4722	0.25-2.0	P	SA-SR	Loose	20		59.5	5.5	5			1.5	6	2.5	
						60	40								Ill	
9-11-87-9	4733	0.25-1.0	G	SA-SR	Loose	15		69	7.5		0.5		8.5		1.5	
						90	10								Ill	
9-11-87-9	4736	0.25-1.0	G	SA-SR	Loose	15		72	8					2.5	2	0.5
						80	20								Ill	Silica
9-11-87-9	4746	0.25-1.0	M	SA	Loose	10		75	8						7	
						70	30								Ill	
9-11-87-9	4760	0.25-1.0	M	SA-SR	Loose	20		61.5	5.5	3			6.5		3.5	
						95	5								Chl	

Table 7.4 Representative modal analysis data of Watt Mountain sandstones. (A-abundant; S-scarce; R-rare; Ill-illite; Chl-chlorite; Kl-kaolinite; I/S-illite-smectite; Smec-smectite; Hem-hematite; P-poor; M-moderate; G-good; VG-very good; SA-subangular; SR-subrounded; BP-interparticle porosity; WP-intraparticle porosity)

Sample No (All samples west meridian 5)	Depth (ft)	Grainsize (mm)	Sorting	Roundness	Packing	Porosity (%) BP	Porosity (%) WP	Primary: Quartz (%)	Primary: Feldspar (%)	Primary: Lithoclasts (%)	Primary: Mica (%)	Primary: Pyrite (%)	Secondary: Carbonate (%)	Secondary: Anhydrite (%)	Secondary: Clay (%)	Other (%)
16-14-68-21	9689.1	0.25-2.0	P	SA-SR	Intermediate	12	75	68.5	10	4	0.5				5 Ill,Chl	25
6-9-68-23	10574	0.25-2.0	P	SA-SR	Loose	12	90	79	4	3	2		6.5	2	1.5 Ill	10
6-14-69-20	93387.7	0.5-2.0	G	SA-SR	Loose	15	90	69	5	5	1		3.75	0.75	0.5 Ill,Chl	10
4-14-70-15	8280	0.25-1.0	G	SA-SR	Loose	20	95	72	5.5		1			2		5
11-4-71-16	8288	0.25-4.0	P	SA-SR	Loose	15	85	62	4	4				15		15
13-20-71-21	9218.2	0.25-2.0	P	SA-SR	Loose	20	90	64	5	2.5	0.5			4	4 Ill	10
8-16-72-18	8430.8	0.25-2.0	M	SA-SR	Loose	21	90	67	6	1				3	2 Ill(S),Chl(R)	10
2-21-73-13	7118	0.5-2.0	M	SA-SR	Loose	5	90	60	3	2			19.5	10.5		5
10-1-73-17	7738	0.125-1.0	M	SA	Loose	15	90	69	6	2.5	2.5			1	4 Ill(C),Chl(R)	10
8-13-73-19	8308.4	0.25-2.0	P	SA	Loose	5	70	73	4	1.5	1.5		1		4 Ill(C),Chl(R)	30
16-36-73-21	8599	0.5-2.0	M	SA-SR	Loose	5	90	70	3	2			15	1	4 Ill,Chl	10
6-8-74-14	7898	1.0-4.0	M	SA	Loose	10	80	53	5	20			2	2	65 Ill	20
16-20-74-18	7783.4	0.25-2.0	M	SA-SR	Loose	20	70	57	10.5	1.5	1				10 Ill	30
10-8-75-19	7924.3	0.5-1.0 2.0-4.0	M	SA-SR	Loose	2	60	73	3	2					20 Ill	40

Sample No (All samples west meridian 5)	Depth (ft)	Grainsize (mm)	Sorting	Roundness	Packing	Porosity (%) BP	Porosity (%) WP	Primary: Quartz (%)	Feldspar (%)	Lithoclasts (%)	Mica (%)	Pyrite (%)	Secondary: Carbonate (%)	Anhydrite (%)	Clay (%)	Other (%)
6-8-81-8	5521.9	0.25-2.0	VP	A-SA	Intermediate	0		62	21	1.5	0.5		12	1		2 Pyrite
6-8-81-8	5539	0.25-2.0	M	A-SA	Intermediate	15		47	16	2			12	7		1 Pyrite
6-8-81-8	5547.9	0.125-1.0	M	SA-SR	Loose	28		51	10	1	2		2	2	4 Ill	
10-5-81-9	5562.8	0.125-0.5	G	SA	Loose	20	60 40	60.5	5	1	1.5		0.5	5	65 Ill(C),Chl(S)	
16-31-86-12	5161.2	0.25-0.50	VG	SA-SR	Intermediate	5		82	7		1			2		3 Pyrite
16-31-86-12	5164.5	0.125-2.0	VP	SA	Loose	12	80 20	17	3	29	9		10		10 Ill,Chl	10 Pyrite
8-2-87-13	5203.4	0.25-2.0	M	SA-SR	Loose	30		60	5	2			1	1	0.5 Chl	0.5 Pyrite
8-2-87-13	5209.1	0.25-2.0 >4.0	M	SA-SR	Loose	15	96 4	54	8	20					2 Chl	1 Pyrite
8-2-87-13	5219.3	0.125-2.0	P	SA-SR	Loose	25	90 10	54	5	8	1			1.5	3.5 Chl(C),Ill(R)	2
8-2-87-13	5225.2	0.125-2.0	P	SA-SR	Loose	25	95 5	56	5	3.5	0.5			6.5	3 Chl	0.5
10-5-92-19	5485	0.25-2.0	P	A	Loose	12	90 10	18	18	37					15	
10-5-92-19	5489	0.125-1.0	M	SA	Intermediate	5	80 20	78	4	0.5	0.5				12 Ill(C),Chl(C)	
10-5-92-19	5501	0.125-2.0	P	SA-SR	Loose	0		70	1	4					25 Ill(C),Chl(C)	
12-9-93-18	5215	0.25-2.0	M	SA-SR	Intermediate	10	80 20	71	7	4				0.5	7.5 Ill(C),Chl(C)	
12-9-93-18	5252	0.125-1.0	M	SA-SR	Loose	5	60 40	68	15	1.5	0.5				10 Ill	
12-9-93-18	5257	0.125-1.0	P	SA-SR	Loose	4	80 20	73	13	2.5	0.5			1	6 Ill	

Sample No (All samples west meridian 5)	Depth (ft)	Grainsize (mm)	Sorting	Roundness	Packing	Porosity (%) BP	Porosity (%) WP	Primary: Quartz (%)	Feldspar (%)	Lithoclasts (%)	Mica (%)	Pyrite (%)	Secondary: Carbonate (%)	Anhydrite (%)	Clay (%)	Other (%)
12-9-93-18	5261	0.5-2.0	G	SA-SR	Loose	1	10	41	7.5	1	0.5		37	10	1 III	
4-19-93-19	5143	0.25-1.0	M	SA-SR	Loose	5	35	58	20		2		4.5	3	7.5 III	
4-19-93-19	5155	0.125-2.0	P	SA-SR	Loose	5	75	61.5	13		0.5		16	1	3 III	
4-19-93-19	5160	0.25-2.0	M	SA-SR	Loose	12	80	62	16		2		3.5	1.5	3 III	
4-19-93-19	5171	0.125-0.50	G	SA-SR	Loose	15	60	55	7		11		5	2	5 III	
4-19-93-19	5209	0.25-2.0	M	SA-SR	Intermediate	3	40	78	3	1			15			
10-17-94-15	4949	0.125-1.0 2.0-4.0	P	SA-SR	Loose	0	60	41	12.5	1.5			45			

Table 7.5 Representative modal analysis data of Watt Mountain sandstones. (Chl-chlorite; Ill-illite; Kao-kaolinite; A-abundant; S-scarce; R-rare; Trc-traces; P-poor; M-moderate; G-good; VG-very good; SA-subangular; SR-subrounded; BP-interparticle porosity; WP-intraparticle porosity)

Sample No (All samples west Meridian 5)	Depth (ft)	Grainsize (mm)	Sorting	Packing	Porosity (%)	Primary: Quartz (%)	Feldspar (%)	Mica (%)	Lithoclast (%)	Other (%)	Secondary: Silica (%)	Anhydrite (%)	Carbonate (%)	Clay (%) Chl	Ill	Kao
8-35 68-3	5516	0.25-2.0	M	Loose	11	48	14	Trc		Bitumen	Trc	25	2	Trc	Trc	
8-35 68-3	5525	0.25-1.0	G	Loose	12.5	70	3	Trc		Bitumen	7	7	1			
4-26-70-4	6068	0.5->4.0	M	Loose		Low	75	3		Trc			A			S
4-26-70-4	6076	0.5-1.2	M	Loose	16	70	9	Trc		Pyrite	A	4	1	Trc		
11-22-70-9	6822.5	0.125-0.5	G	Loose	25	68	2	Trc		Pyrite	A	2	Trc	Trc		
4-28-71-3	5474	0.25-4.0	P Bimodal	Loose	Negligible	80	4			Pyrite Fish-Scale	A	16	Trc	Trc	Trc	
4-8-71-4	6101.5	0.5-5.0	P Bimodal	Loose	15	73	2				A	10	Trc	Trc		
4-8-71-4	6105	0.25-4.0	M	Loose	15	70	4				Trc	10	Trc	1		
4-8-71-4	6116	0.25-2.0	P	Loose	23	70	3			Pyrite	A	3	Trc			
10-26-71-5	6021	0.125-0.50	G	Loose	25	70	Trc		Trc		A	Trc	Trc			
10-26-71-5	6029	0.125-1.0	G	Loose	18	62	7	Trc		Bitumen	A	7	6	Trc	Trc	
10-26-71-5	6042	0.50-4.0	M	Loose	Negligible	A	Trc				C	A		A		
6-11-71-8	7978.5	up to 5.0	P	Loose	15	70	6				A	7	Trc	2		
6-11-71-8	7083.5	0.25-4.0	M	Loose	Negligible	70	2			Pyrite	C	20	8			

Sample No (All samples west Meridian 5)	Depth (ft)	Grainsize (mm)	Sorting	Packing	Porosity (%)	Primary: Quartz (%)	Feldspar (%)	Mica (%)	Lithoclast (%)	Other (%)	Silica (%)	Secondary: Anhydrite (%)	Carbonate (%)	Clay Chl	(%) Ill	Kao
10-11-71-12	7568	0.0625-0.50	M	Loose	30	65	4	Trc		Opaques	C	1		Trc		
10-11-71-12	7667	0.25-4.0 bi-modal	M	Loose	15	70	5	Trc	Trc	Apatite	C	8	1	Trc	Trc	
10-11-71-12	7675	0.25-0.50	G	Tight	High	80	Trc		Trc		C	Trc				
2-4-72-3	5294	0.25-2.0	M	Loose	0	80	4			Fish Scales	C	15	1			
8-12-72-5	5712.9	0.25-4.0	M	Loose	20	70	4		Trc	Pyrite	C			6		C
10-33-72-9	6211	0.25-0.50	G	VLoose	0	69	3		Trc		C	28			C	
4-4-73-4	5314.5	0.0625-0.25	VG	Tight	10	84	5		Trc	Glauconite Apatite	A	1	Trc	Trc		
10-8-73-5	5460	0.25-2.0	M	Loose	20	70	7	Trc		Fish Scales	A	1	Trc	C	Trc	
10-8-73-5	5464	0.25-1.0	G	Loose	High	Max	Trc			Pyrite	A	Trc				
10-8-73-5	5468	0.25-2.0	M	Loose	18	72	5	Trc		Opaques	C	2	3	C	C	C
10-8-73-5	5471.5	0.5-7.0	M	Loose	Negligible	70	4			Pyrite	S	12	8	5		
10-8-73-5	5472	0.75-8.0	M	Loose	5	A	R	Quartzite			C	1	18	R	Trc	
10-8-73-5	5483	0.25-4.0	M	Loose	25	66	6			Bone Pyrite	C	21		1		C
10-8-73-5	5485	0.25-10.0	P	Tight	Negligible	Max	C	Trc		Clay Pyrite	C	Trc	Trc	Trc		
10-8-73-5	5492.5	0.125-0.50	G	Loose	Negligible	Max	Trc	Trc			A	A		A		
4-27-73-7	5768	0.25-4.0	M	Loose	15	70	6	Trc	Trc	Bone	C	9	Trc		Trc	

Sample No (All samples west Meridian 5)	Depth (ft)	Grainsize (mm)	Sorting	Packing	Porosity (%)	Primary: Quartz (%)	Feldspar (%)	Mica (%)	Lithoclast (%)	Other (%)	Secondary: Silica (%)	Anhydrite (%)	Carbonate (%)	Clay (%) Chl	Ill	Kao
4-2-74-5	5418.6	up to 1.2	M	Loose	4	87	4	Trc		Bone	S	5	Trc	Trc	R	
14-22-74-6	5905.7	up to 0.50	G	Loose	24	70	4	Trc		Opaque	C	2	Trc	Trc	Trc	
14-22-74-6	5917.6	0,25-2.0	G	Loose	Low	Max	Trc				C	A	Trc	A		
12-23-74-6	5568	0.25-0.50	G	Loose	10	78	4			Opaque	A	8	Trc	C	C	
3-14-74-10	6076	0.25-4.0	P	Loose	Low	Max	4				C	C	C			
3-14-74-10	6086	up to 2.0	G	Loose	2	64	6		Trc		C	20	10	Trc	Trc	
4-19-75-5	6019.5	0.25-2.0	P	Tight	Negligible	82	6	Trc	Opa	Fish Scales	A	12				
6-35-75-9	5865	0.25-4.0	M	Loose	3	52	18	Trc			C	17	Trc	<------10------>		
10-35-75-10	5976.5	0.10-2.0	M	Loose	18	73	5	Trc		Trc Pyrite	C	2		Trc		
10-35-75-10	5994	0.25-7.0	P	Loose	Low	70	4				C	20				
7-30-76-7	6102.1	0.25-4.0	P	Loose	5	66	4				C	20	5			
7-30-76-7	108.9	0.50-4.0	G	Loose	10	50	25	Trc		Pyrite	C	20	Trc	1	Trc	C
10-14-76-12	6602.5	up to 2.0	P	Loose	20	66	8	Trc			C	4	Trc	2	Trc	
11-23-77-8	5934	0.25-1.0	G	Loose	15	73	3	Trc			C	Trc	5			
11-23-77-8	5942	0.25-4.0	P	Loose	25	47	25	Trc		Pyrite	C	3		Trc		

Sample No (All samples west Meridian 5)	Depth (ft)	Grainsize (mm)	Sorting	Packing	Porosity (%)	Primary: Quartz (%)	Feldspar (%)	Mica (%)	Lithoclast (%)	Other (%)	Secondary: Silica (%)	Anhydrite (%)	Carbonate (%)	Clay (%) Chl	Ill	Kao
11-23-77-8	5962	0.25-2.0	P	Loose	10	60	10				C	20	Trc	A	A	Trc
6-21-77-9	6139.7	0.15-2.0	G	Loose	22	65	10	1 Biotite			C	2	1	Trc	Trc	
6-21-77-9	6146.3	0.25-2.0	P	Loose	Moderate	60	15	Trc			Trc		Trc	Trc		
4-21-77-10	6290.8	0.25-4.0	P	Loose	12	50	20	Trc		Pyrite	C	18	Trc	Trc	Trc	
12-30-78-7	5683.6	0.20-4.0	M	Loose	20	62	8	Trc Biotite		Glauconite Zircon	C	10	Trc	Trc	Trc	
12-30-78-7	5704.1	0.2-3.0	P	Tight	V Low	60	15	Trc			C	Trc	25			
4-2-79-7	5695.5	0.40-5.0	P	Loose	10	47	15					Trc	13	<-----15----->		
4-2-79-8	5703.4	0.50-4.0	M	VLoose	High	65	10				C	C			C	
2-6-80-7	5618.9	0.25-2.0	G	Loose	Negligible	55	15	Trc	Trc		C		30	Trc	Trc	
2-11-80-8	5627.2	0.5-5.0	P	Loose	18	50	23	Trc		Garnet	C	2	6			
2-11-80-8	5642.3	0.5-5.0	G	Loose	High	70	4	Trc			C	5	Trc			

Table 7.6 Representative modal analysis data of Granite Wash sandstones. (Chl-chlorite; Ill-illite; Kao-kaolinite; A-abundant; S-scarce; R-rare; Trc-traces; P-poor; M-moderate; G-good; VG-very good; SA-subangular; SR-subrounded; BP-interparticle porosity; WP-intraparticle porosity)

Sample No (All samples west Meridian 5)	Depth (ft)	Grainsize (mm)	Sorting	Packing	Porosity (%)	Primary: Quartz (%)	Feldspar (%)	Mica (%)	Lithoclast (%)	Other (%)	Secondary: Silica (%)	Anhydrite (%)	Carbonate (%)	Clay Chl	Clay Ill (%)	Clay Kao
10-27-78-11	6103	up to 2.2	M	Loose	Negligible	55	15	Trc				Trc	30	Trc	C	
14-13-79-11	5914	0.50-4.0	P	Loose	Negligible	65	5				C	20	Trc		10	
2-32-80-11	5934.7	up to 2.0	M	Loose Opa	10	42	18	Trc		1	C		30	Trc		
2-32-80-11	5939.3	0.35-8.0	P	Loose	Moderate	35	45	Trc	Trc		C	Trc	Trc	C		

Table 7.7 Mineralogy of Elk Point Group sandstones from XRD analysis.

Sample	Depth (ft)	Quartz	Feldspar	Illite	Smectite	Kaolinite	Chlorite	Anhydrite	Dolomite	Calcite
Watt Mountain Formation										
6-14-69-20W5	9338.6	X	X	X	X	X	X			
4-14-70-15W5	8280	X	X	X	X	X	X			
11-4-71-16W5	8288	X	X		X		X			
13-20-71-21W5	9218.2	X	X	X	X		X			
2-21-73-13W5	7118	X	X	X	X		X			
10-1-73-17W5	7738	X	X	X		X				
8-13-73-19W5	8308.4	X	X	X						
6-8-74-14W5	7826.9	X	X	X	X					
16-20-74-18W5	7783.4	X	X	X		X				
10-8-75-19W5	7924.3	X	X	X		X				
6-8-81-8W5	5521.9	X	X	X		X				X
6-8-81-8W5	5539.1	X	X	X		X		X	X	
6-8-81-8W5	5547.9	X	X	X		X				X
16-3-84-14W5	5847.9	X	X	X			X		X	
16-31-86-12W5	5161.2	X	X					X	X	X
16-31-86-12W5	5164.5	X	X	X						
8-2-87-13W5	5203.4	X	X							X
8-2-87-13W5	5209.1	X	X							X
10-5-92-19W5	5489	X	X	X		X				
10-5-92-19W5	5501	X	X	X		X				
12-9-93-18W5	5215	X	X	X		X	X			
12-9-93-18W5	5252	X	X	X						
12-9-93-18W5	5257	X	X	X						
12-9-93-18W5	5261	X	X	X						
4-19-93-19W5	5143	X	X	X				X	X	X
4-19-93-19W5	5155	X	X	X	X				X	X
4-19-93-19W5	5160	X	X	X						X
4-19-93-19W5	5171	X	X	X			X			

Sample	Depth (ft)	Quartz	Feldspar	Illite	Smectite	Kaolinite	Chlorite	Anhydrite	Dolomite	Calcite
4-19-93-19W5	5209	X	X							X
10-17-94-15W5	4949	X	X	X			X		X	
Keg River Formation										
11-18-72-17W5	8339	X	X	X						
1-9-73-18W5	8151	X	X	X						
1-22-86-8W5	4950	X	X					X	X	X
4-3-87-8W5	4911	X	X	X						X
4-3-87-8W5	4914	X	X	X				X	X	
9-11-87-9W5	4733	X	X	X			X	X	X	X
9-11-87-9W5	4736	X	X	X	X			X		X
5-25-90-11W5	5101.1	X	X	X	X			X		X
Chinchaga Formation										
5-17-85-8W5	5160.5	X	X	X			X	X		
5-17-85-8W5	5167.8	X	X	X		X				
11-29-86-3W5	5231	X	X			X			X	
11-29-86-3W5	5231	X	X			X			X	
1-22-86-8W5	4969	X	X					X	X	X
4-34-91-7W5	4524	X	X	X		X		X		
Granite Wash lithology										
10-14-72-23W5	9803	X	X	X		X			X	
11-11-73-13W5	7386	X	X			X				
6-1-75-24W5	9020.9	X	X							
4-22-77-14W5	6891.1	X	X		X		X			
10-11-77-16W5	7422.4	X	X	X			X			
12-11-78-22W5	7704	X	X					X		
8-16-79-21W5	7936.5	X	X	X			X			
9-13-80-21W5	7812.8	X	X	X						
6-31-84-7W5	5272	X	X	X			X	X		X
4-9-85-9W5	5100	X	X			X				X
1-22-86-8W5	4996	X	X					X	X	X

Sample	Depth (ft)	Quartz	Feldspar	Illite	Smectite	Kaolinite	Chlorite	Anhydrite	Dolomite	Calcite
10-15-86-8W5	4881	X	X	X		X				
10-15-86-8W5	4888	X	X	X		X				
4-16-87-7W5	5004	X	X	X						X
12-36-88-11W5	5100.1	X	X	X				X		
12-36-88-11W5	5109.7	X	X	X						
12-36-88-11W5	5122.9	X	X	X		X		X		
1-5-90-10W5	4925	X	X	X		X				
9-35-91-6W5	4645	X	X	X				X		
12-25-91-10W5	4729	X	X	X			X	X		X
12-23-92-16W5	5870	X	X	X		X	X			
10-17-94-15W5	5501	X	X	X			X		X	
10-17-94-15W5	5501	X	X	X						X
10-17-94-15W5	5501	X	X	X	X		X	X		X
10-17-94-15W5	5501	X	X	X	X		X	X		X

Table 7.8 Whole rock geochemical data for Granite Wash and Watt Mountain Formation samples. Wt loss: Loss on ignition. The difference in total from 100% is due to analytical conditions.

S.No	Well Number	Depth (ft)	SiO_2	TiO_2	Al_2O_3	Fe_2O_3	MnO	MgO	CaO	Na_2O	K_2O	P_2O_5	Wt Loss	Total
Granite Wash Samples														
1	10-14-72-23	9803	70.06	0.14	2.57	2.37	0.17	4.09	8.29	0.10	1.83	0.05	10	99.67
2	9-30-74-18	8513.1	84.47	0.07	7.32	1.43	0.01	0.21	0.35	0.25	5.50	0.03	1	100.64
3	3-4-75-18	7823.8	82.22	0.09	5.26	0.55	0.02	0.99	1.64	0.16	3.90	0.01	1.2	96.04
4	6-1-75-24	9102.9	66.99	0.71	13.24	5.66	0.02	2.71	0.21	0.19	4.86	0.09	5.8	100.47
5	10-11-77-16	7489.8	85.65	0.07	6.66	0.26	0.01	0.26	0.32	0.21	5.34	0.00	1	99.78
6	12-11-78-22	7704	75.65	0.11	8.29	1.38	0.04	1.62	2.52	0.46	6.32	0.04	3.4	99.82
7	8-16-79-21	8008.7	79.09	0.01	4.14	0.21	0.09	0.21	7.63	0.11	3.24	0.03	6	100.74
8	9-13-80-21	7883.8	87.26	0.02	8.51	0.47	0.04	0.34	4.99	0.33	6.41	0.06	2	110.43
9	6-31-84-7	5272	79.29	0.27	5.60	0.43	0.03	0.00	4.35	0.00	4.38	0.06	1	95.39
10	4-9-85-9W5	5100	67.05	1.00	13.78	6.11	0.09	1.88	3.09	2.56	4.65	0.31	0.31	100.84
11	1-22-86-8	4996	62.39	0.64	17.37	5.02	0.04	0.72	1.22	2.66	8.49	0.27	1.2	100.02
12	10-15-86-10	4881	59.32	0.79	18.19	6.85	0.03	1.53	0.31	0.58	4.99	0.06	7	99.66
13	4-16-87-7	5004	85.07	0.05	4.09	0.20	0.05	0.15	3.75	0.15	3.26	0.00	2.4	99.16
14	12-36-88-11	5109.7	80.25	0.18	8.80	0.37	0.00	0.27	0.66	0.55	0.56	0.00	2	93.63
15	1-5-90-10	4925	78.15	0.51	10.13	0.81	0.00	0.48	0.21	0.59	5.79	0.02	2.4	99.09
16	9-35-91-6	4649	68.15	0.23	6.72	2.04	0.07	3.95	5.10	0.00	4.36	0.21	8.19	99.02
17	12-25-91-10	4729	68.13	0.25	6.71	1.99	0.07	3.65	5.09	0.42	4.38	0.16	0.6	91.42
18	12-23-92-16	5870	56.43	0.87	11.96	13.03	0.06	5.20	1.13	0.61	7.08	0.50	4.19	101.08
19	10-17-94-15	5501	52.28	0.16	4.32	1.46	0.07	7.56	11.51	0.19	3.31	0.00	17	97.87
20	10-17-94-15	5505	83.65	0.37	6.38	0.48	0.00	0.08	1.24	0.30	5.23	0.01	1	98.74
21	10-17-94-15	5508	86.65	0.19	3.69	0.60	0.00	0.10	2.43	0.25	2.92	0.00	1.4	98.22
22	10-17-94-15	5512	86.55	0.41	4.68	0.45	0.00	0.16	0.74	0.51	3.64	0.01	1	98.12
Watt Mountain Samples														
23	16-14-68-23	9777.2	91.60	0.07	4.51	0.31	0.01	0.25	0.19	0.10	3.39	0.01	0.2	100.64
24	6-9-68-23	10574	84.80	0.14	3.70	0.97	0.06	1.19	3.38	0.00	2.71	0.03	2.4	99.38
25	4-14-70-15	9476	93.27	0.24	2.84	0.76	0.01	0.25	0.44	0.00	2.06	0.02	0.6	100.515
26	11-4-71-16	8288	73.94	0.03	4.12	0.18	0.00	0.26	7.36	0.02	3.29	0.02	0.4	89.63
27	13-20-71-21	9302	81.96	0.15	7.43	0.91	0.04	1.12	2.31	0.15	5.35	0.10	1.2	100.72

S.No	Well Number	Depth (ft)	SiO_2	TiO_2	Al_2O_3	Fe_2O_3	MnO	MgO	CaO	Na_2O	K_2O	P_2O_5	Wt Loss	Total
28	8-16-72-18	8507.5	89.32	0.04	4.69	0.46	0.01	0.22	1.17	0.14	3.61	0.03	0.6	100.27
29	2-21-73-13	7118	72.13	0.02	2.42	0.14	0.01	0.25	10.66	0.00	1.91	0.01	0.6	88.14
30	10-1-73-17	7738	88.39	0.13	5.22	0.26	0.00	0.22	0.63	0.03	4.28	0.02	1	100.19
31	8-13-73-19	8383.9	89.01	0.11	6.15	0.58	0.01	0.58	0.22	0.29	3.73	0.02	0.4	101.09
32	16-36-73-21	8599.1	75.30	0.12	3.39	1.27	0.10	2.84	5.62	0.07	2.77	0.02	8.6	100.09
33	6-8-74-14	2371.8	89.63	0.06	4.05	0.31	0.01	0.37	1.43	0.14	2.73	0.07	1.4	100.21
34	16-20-74-18	7854.1	80.53	0.09	9.50	0.47	0.01	0.47	0.26	0.49	6.45	0.03	2.6	100.88
35	10-8-75-19	7996.3	81.70	0.30	8.33	0.51	0.00	0.58	0.06	0.02	1.92	0.05	3.6	97.06
36	10-5-81-9	5562.8	79.43	0.19	7.14	0.45	0.00	0.00	1.93	0.00	5.24	0.11	1.2	95.69
37	6-8-81-8	5539.1	76.45	0.06	4.81	0.51	0.02	1.41	5.72	0.00	3.31	0.11	5.2	97.59
38	16-3-84-14	5828.1	53.39	0.39	11.88	2.18	0.04	5.23	6.25	0.80	6.92	0.05	11.6	98.73
39	8-2-87-13	5209.1	91.83	0.34	4.17	0.47	0.00	0.10	0.41	0.27	3.21	0.00	0.2	100.99
40	16-31-86-12	5161.2	82.35	0.14	5.92	3.14	0.00	0.10	0.60	0.24	4.82	0.04	2.4	99.76
41	10-17-94-15	4949	66.56	0.17	7.24	0.63	0.02	3.28	5.89	0.34	5.01	0.00	8.2	97.34

Plate 7.1: Texture of a fine grained sandstone with some very coarse grains of lithoclasts and traces of mica. On the right is a patch of pore filling massive ferroan calcite. (Granite Wash 4-9-85-9W5; 5100 ft) (CP x20).

Plate 7.2: Coarse grained sandstone with dominantly quartz and some feldspar. Lithoclasts are largely quartz-feldspar and polycrystalline quartz grains. Some pores have been reduced by carbonate (left and centre) and anhydrite (top) (Granite Wash 3-4-75-18W5; 7823.8 ft) (CP x20).

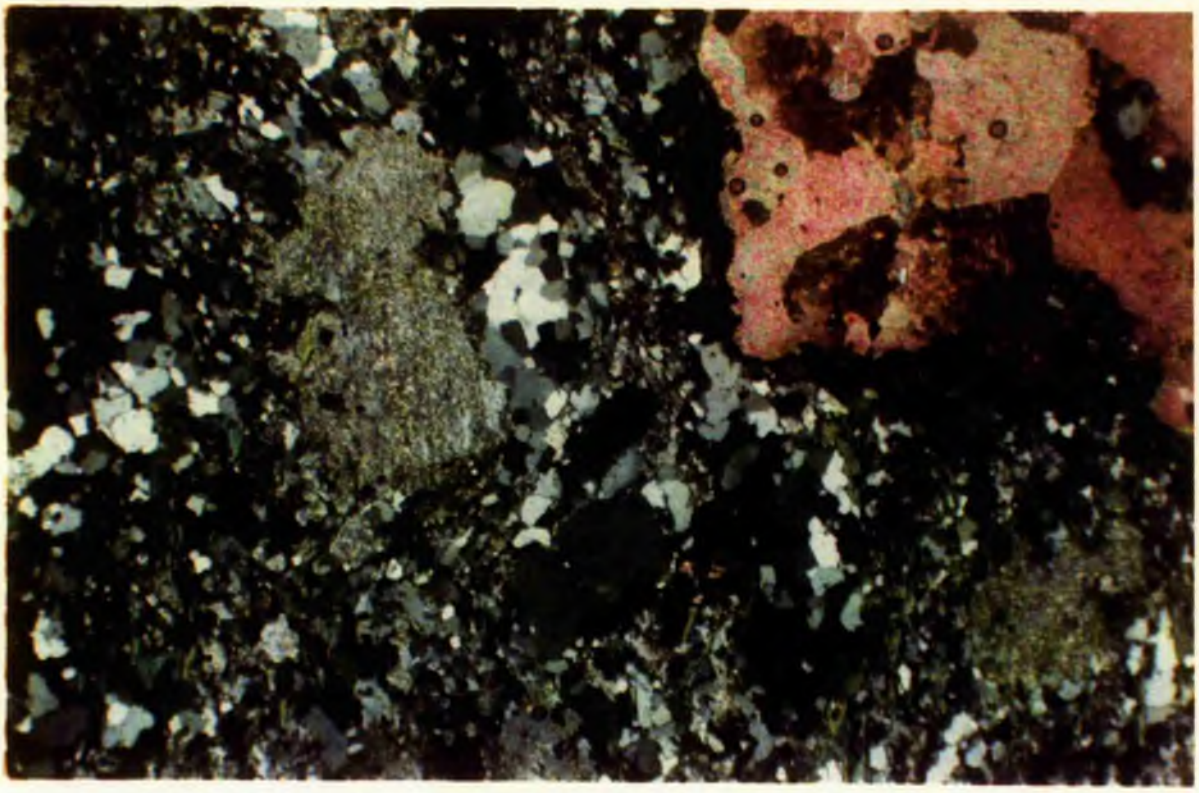

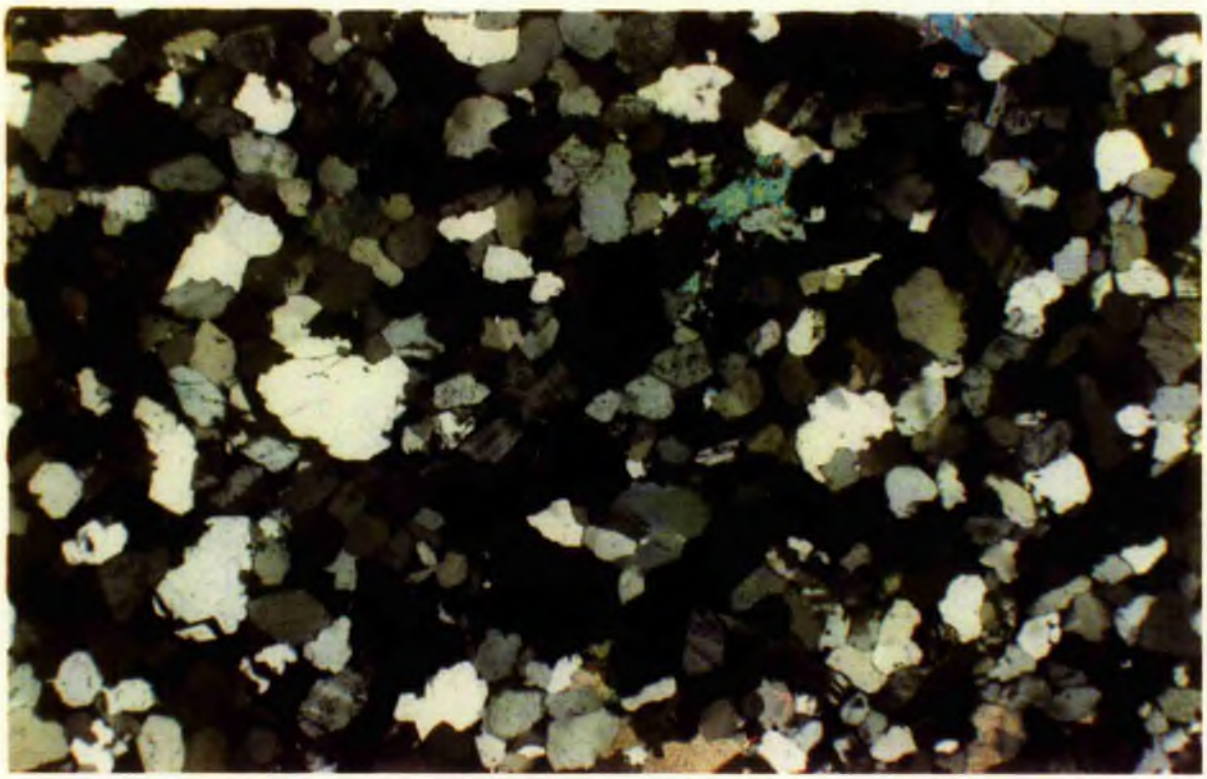

Plate 7.3: Texture of a coarse grained rock with moderatly good sorting and original shape of grains obscured by quartz overgrowths. Due to overgrowths the grains are interlocking with very low porosity. Lithoclasts are composed of quartz-feldspar. Anhydrite is also the cementing medium. (Keg River 4-3-87-8W5; 4914 ft) (CP x12).

Plate 7.4: Between particle porosity in sandstones. Right in the middle of the plate is a big pore bounded by quartz overgrowth. The margins of the overgrowths are euhedral. At bottom right corner the grain has a scalloped margin suggesting intense corrosion by secondary cements which are now dissolved away. (Watt Mt 16-14-68-21W5; 9777.2 ft) (PPL x100).

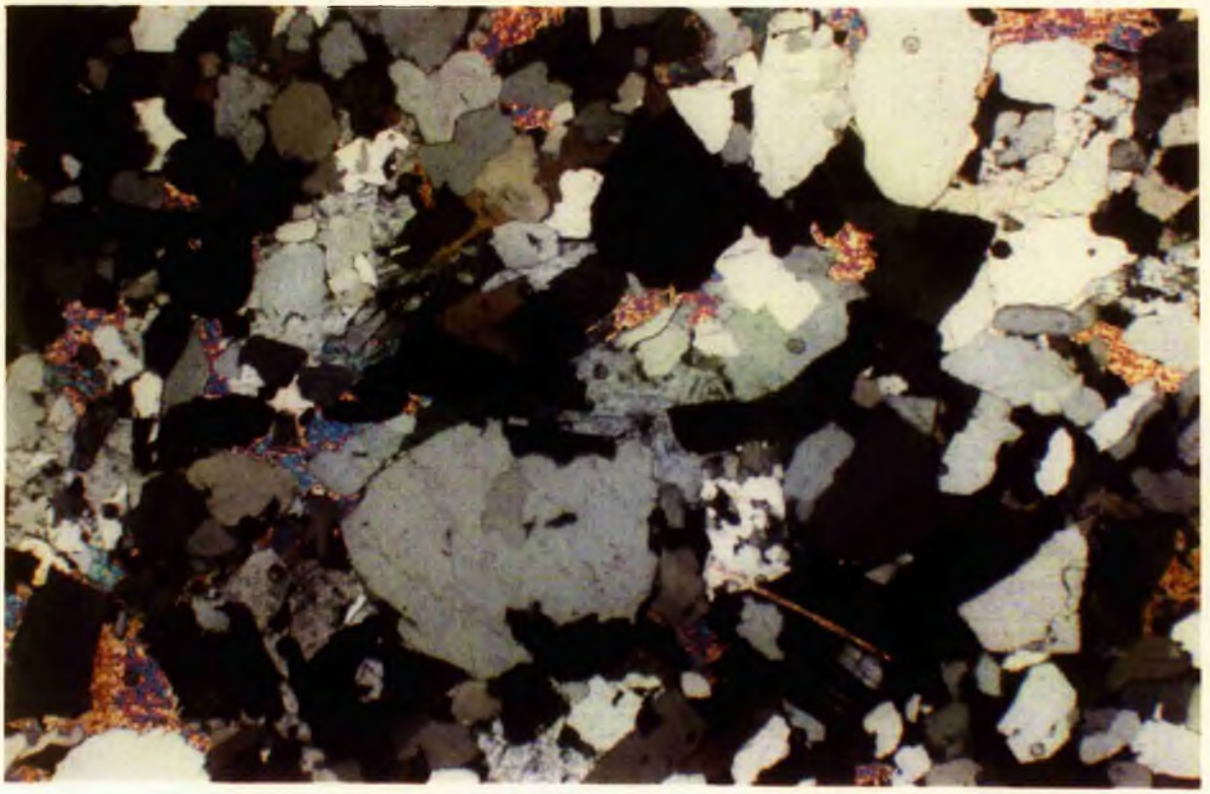

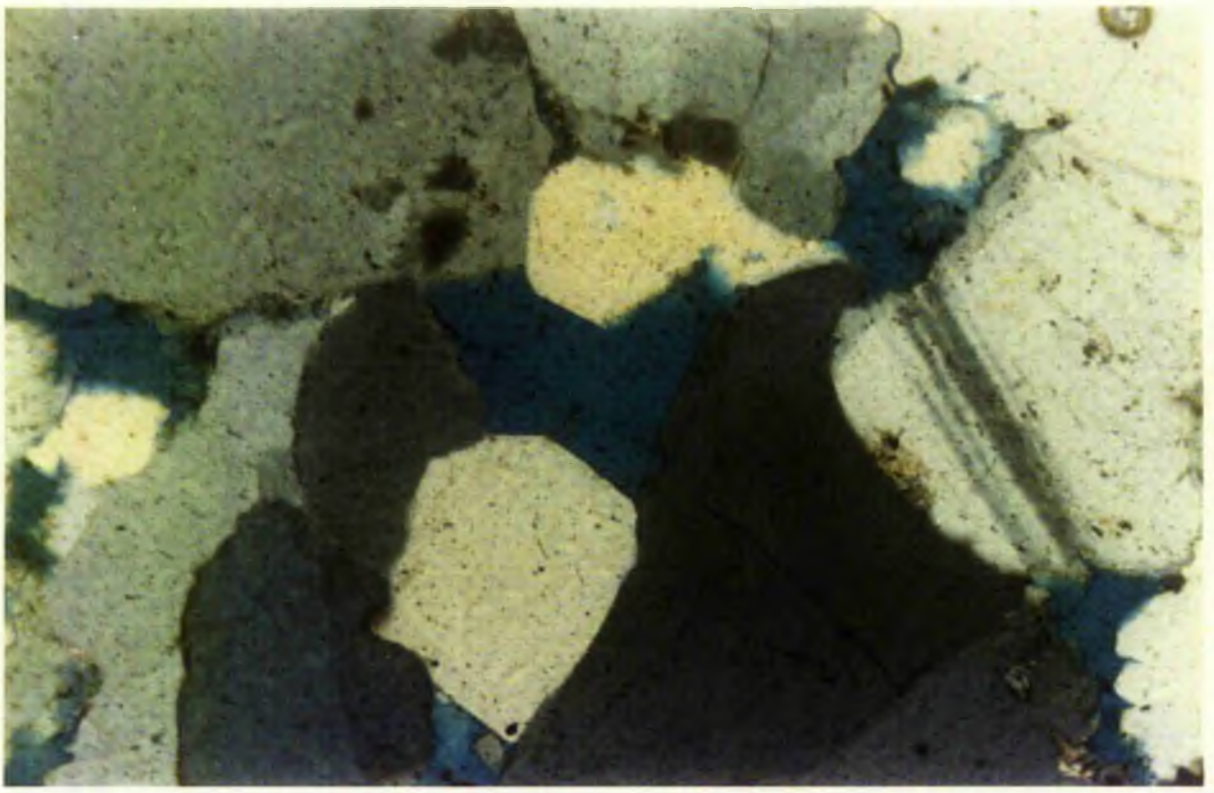

Plate 7.5: Coarse grained rock with quartz and feldspar and pore bridging chlorite. The porosity in the rock is moderate with the pores forming vugs which are interconnected to form channels. (Watt Mt 8-2-87-13W5; 5203.4 ft) (PPL x40).

Plate 7.6: Skeletal feldspars showing various stages of dissolution; middle left and lower left partly removed; right middle large pore with fragmentary feldspar grain, mostly blue of pore space. Straight-edged pores due to quartz overgrowths; 'dust' lines and overgrowths clearly marked in grains (middle left). Blocky anhydrite (lower right). (Watt Mt 6-21-77-9W5; 1860.5 m) (PPL x50).

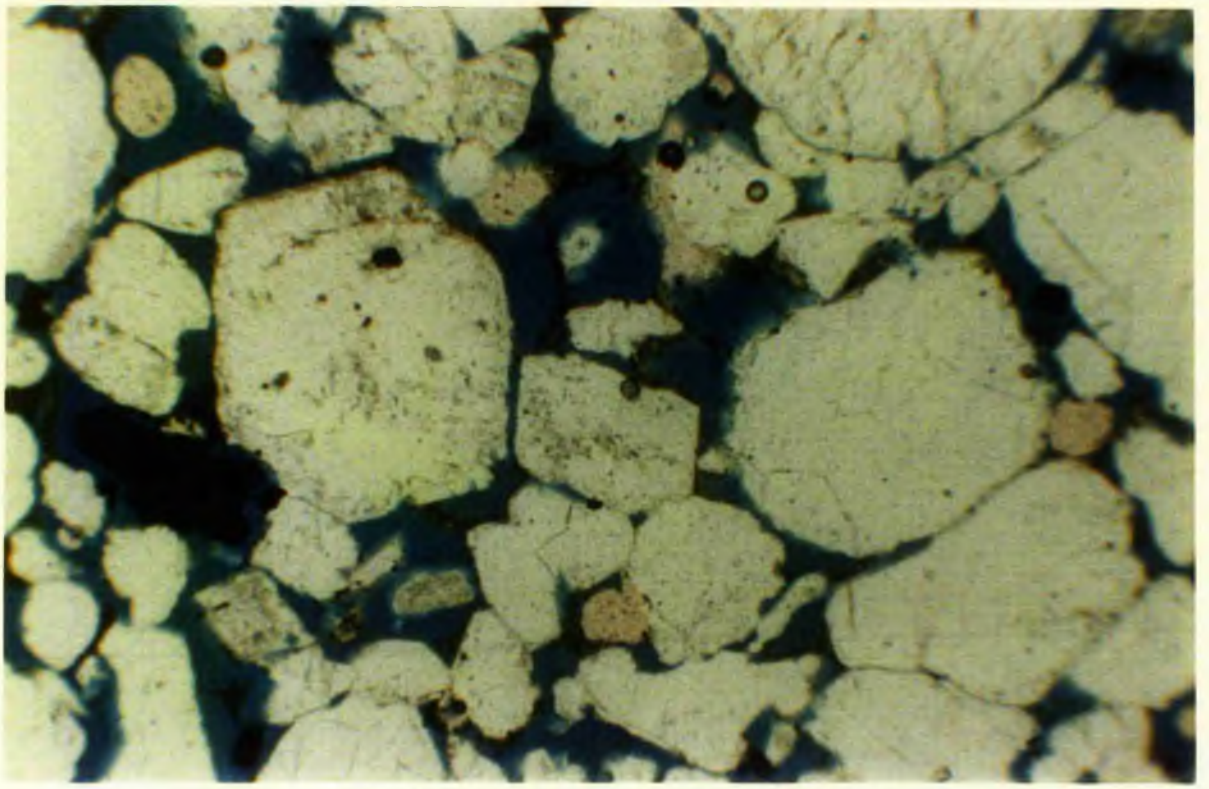

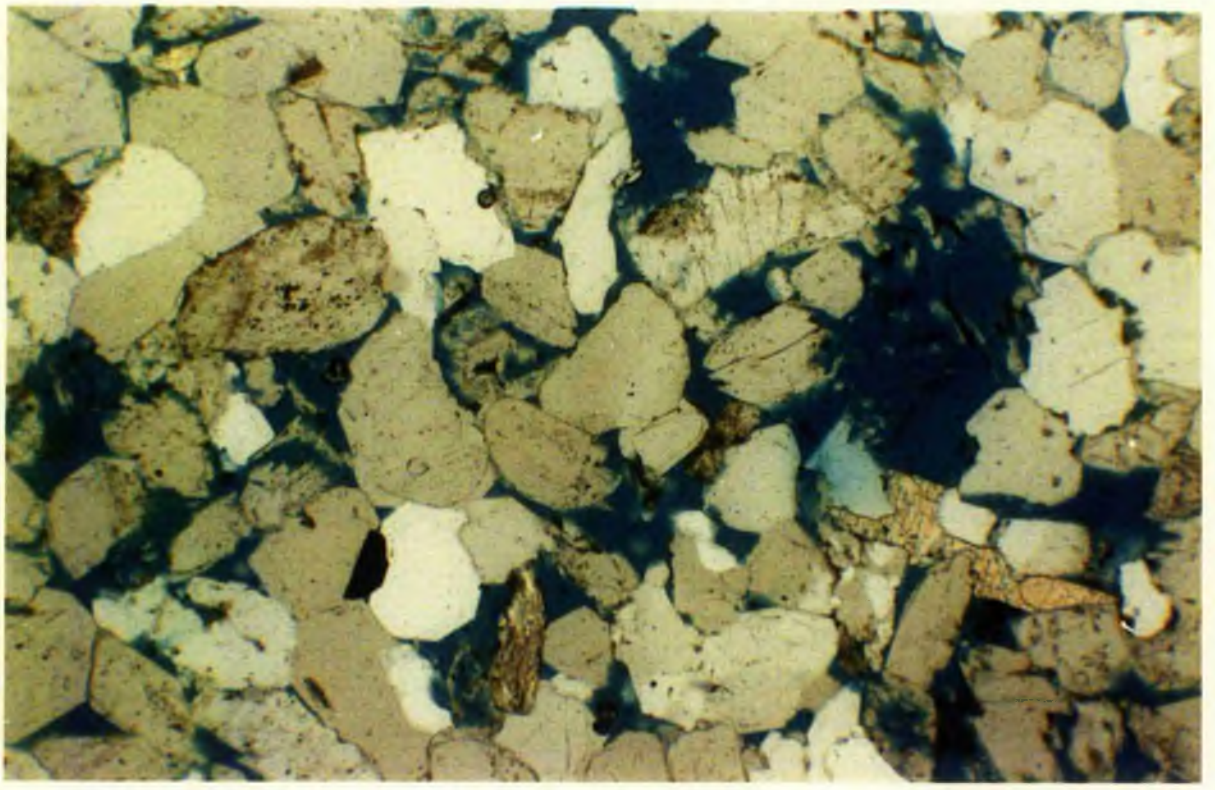

Plate 7.7: Anhydrite-carbonate relationship (the carbonate is greenish). Primary grains along with the secondary overgrowths have corroded margins with anhydrite and carbonate cements. The porosity has been completely reduced and carbonate appears to be corroded along its margin with the anhydrite. (Watt Mountain) (CP x40).

Plate 7.8: Large quartz grains with very well preserved dust lines. The grain to the left has a thick overgrowth rim. The pores between the grains are enlarged due to dissolution giving rise to vuggy porosity. (Keg River 9-11-87-9W5; 4736 ft) (PPL x100).

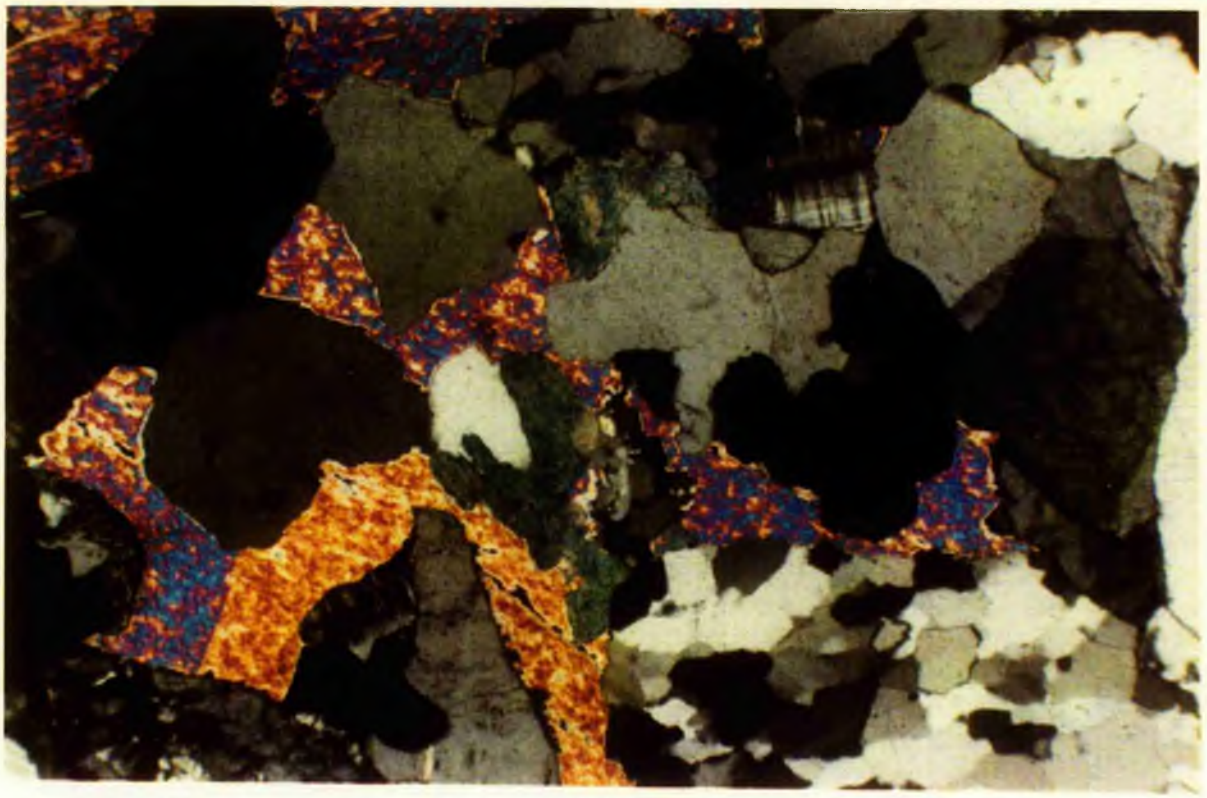

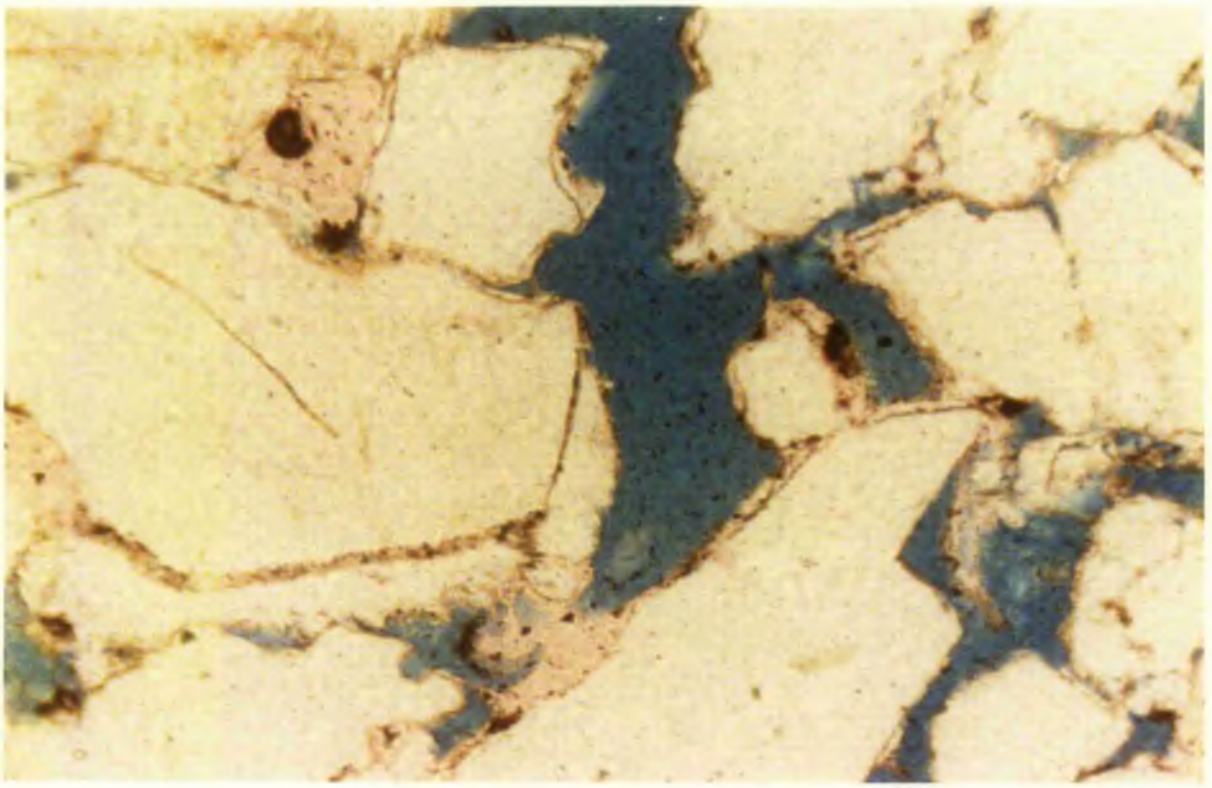

Plate 7.9: General view showing quartz and feldspar grains with between particle porosity. The pores are largely triangular to polygonal, sometimes lamellar. The grains are covered with clay. (Watt Mt 8-2-87-13W5; 5219.3 ft) (SEM scale bar 100um).

Plate 7.10: Lamellar pores between quartz grains with overgrowths and feldspar (and overgrowths) corroded along cleavage. Microporosity within feldspar in cleavage. (Watt Mt 6-21-77-9W5; 1860.5m) (SEM scale bar 10um).

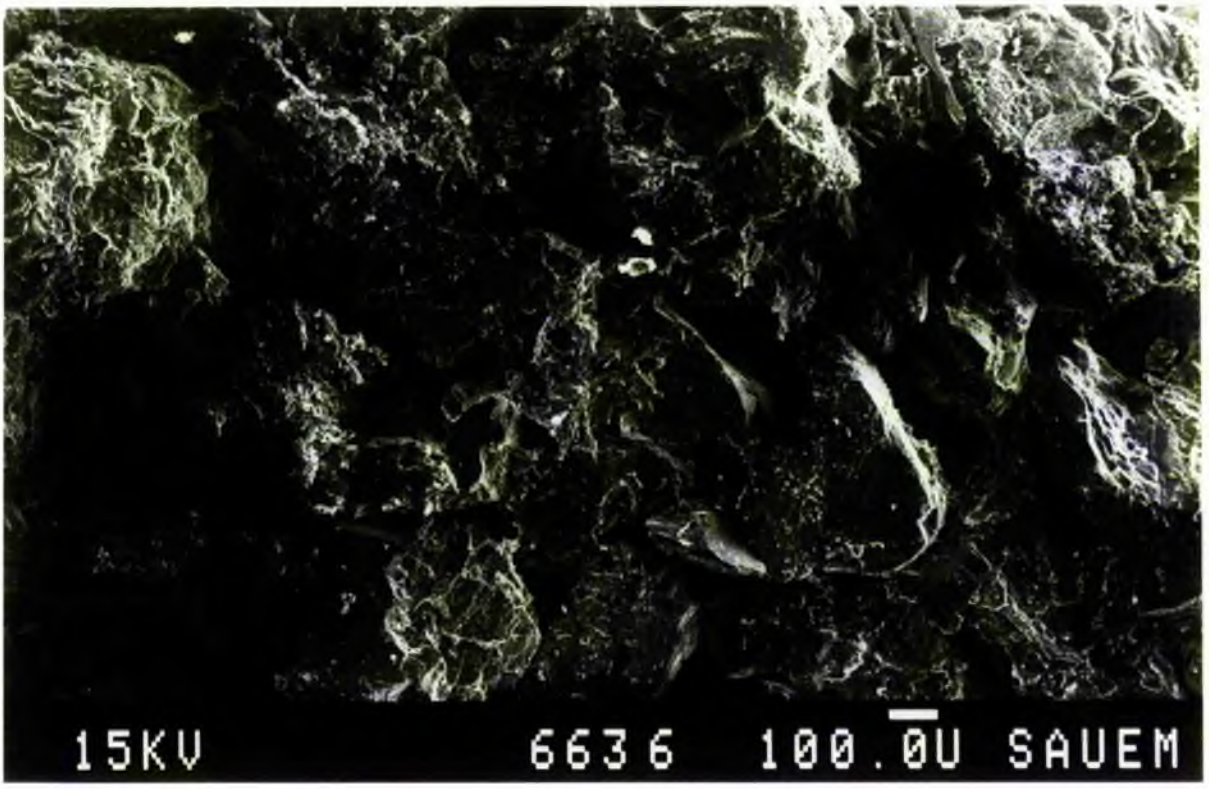
15KV 6636 100.0U SAUEM

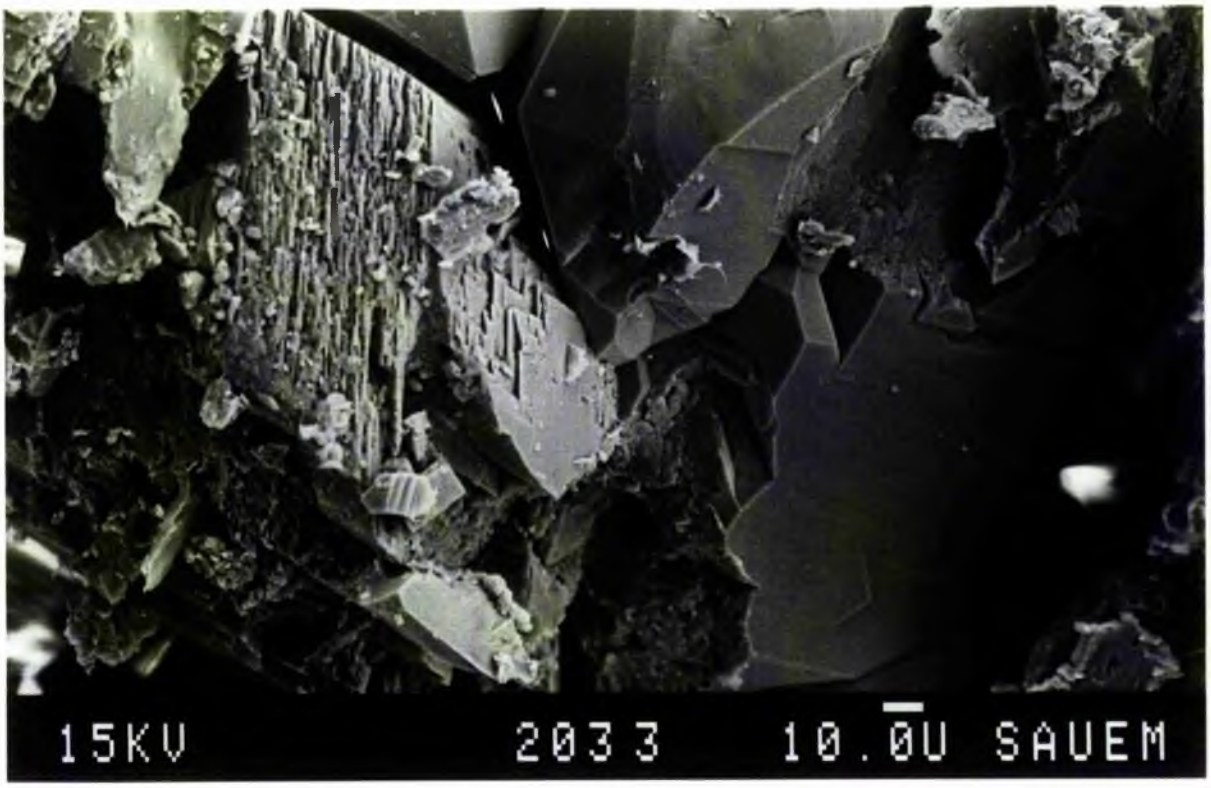
15KV 2033 10.0U SAUEM

Plate 7.11: Quartz with dust lines (lower right), corroded feldspar (left), and expanded mica. In mica the flakes have separated, broken and bent. The feldspar has clays along the cleavage planes and along the margin of the grain. (Keg River 9-11-87-9W5; 4733 ft) (PPL x100).

Plate 7.12: CL image of quartz (purple), feldspar (blue) and ferroan-calcite (bright yellow). Ferroan-calcite shows varying shades due to zonation. (Keg River 4-3-87-8W5; 4911 ft) (CL x250).

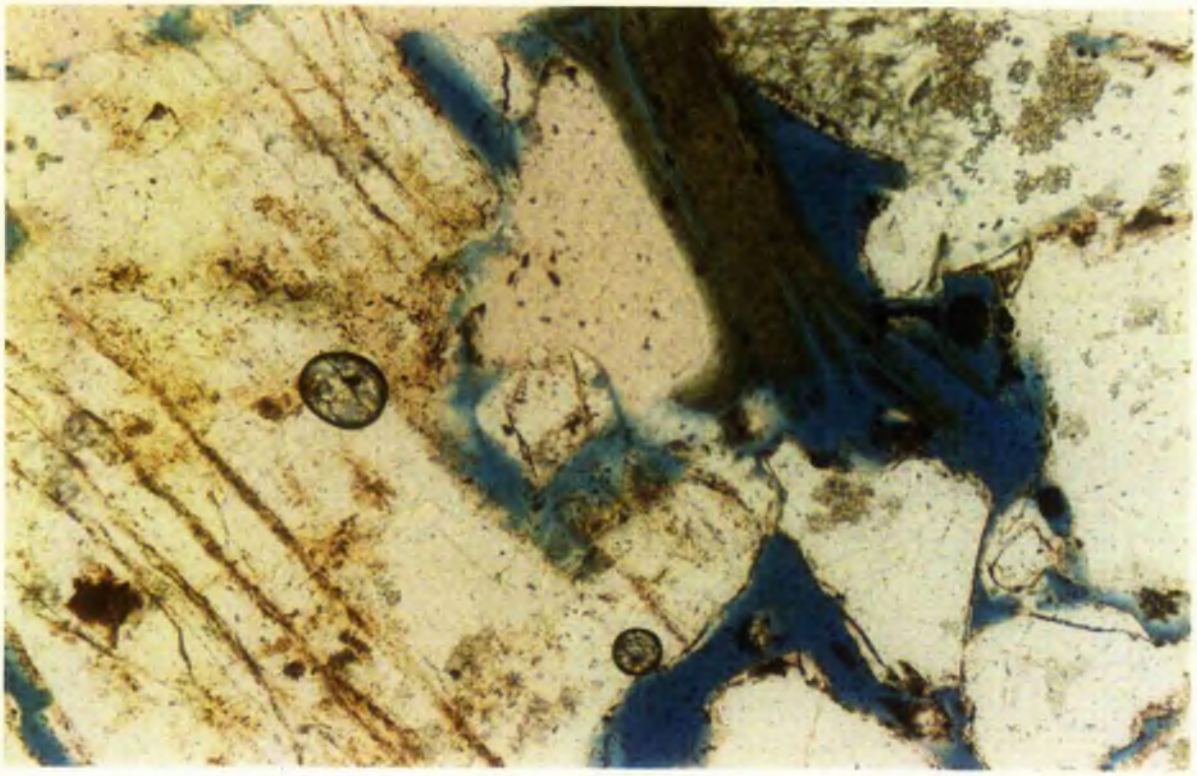

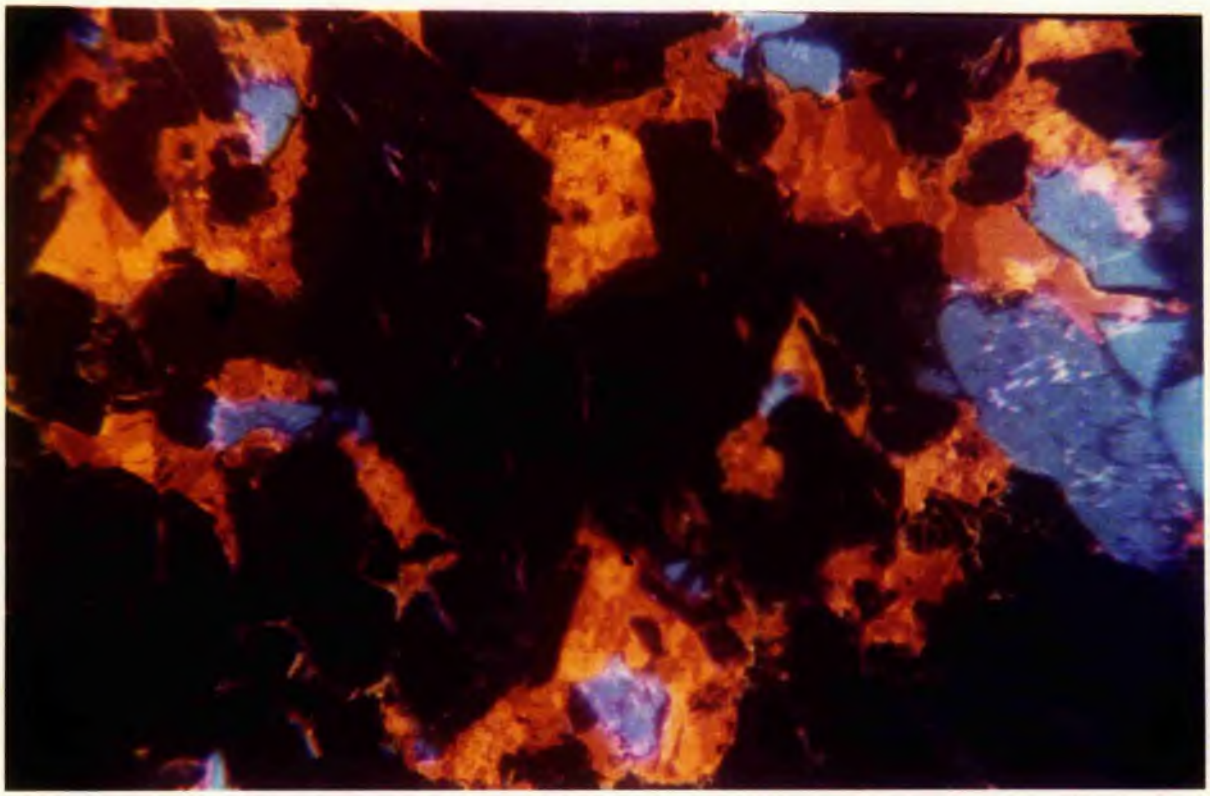

Plate 7.13: CL image of quartz (purple), feldspar (blue) and dolomite (red). The fedlspar grain on the right shows a thick overgrowth rim. No overgrowth patterns on quartz can be seen. (Watt Mountain 10-17-94-15W5; 4949 ft) (CL x250).

Plate 7.14: CL image of quartz (purple), feldspar (blue) and anhydrite (orange). (Chinchaga 10-7-87-7W5; 4952 ft).

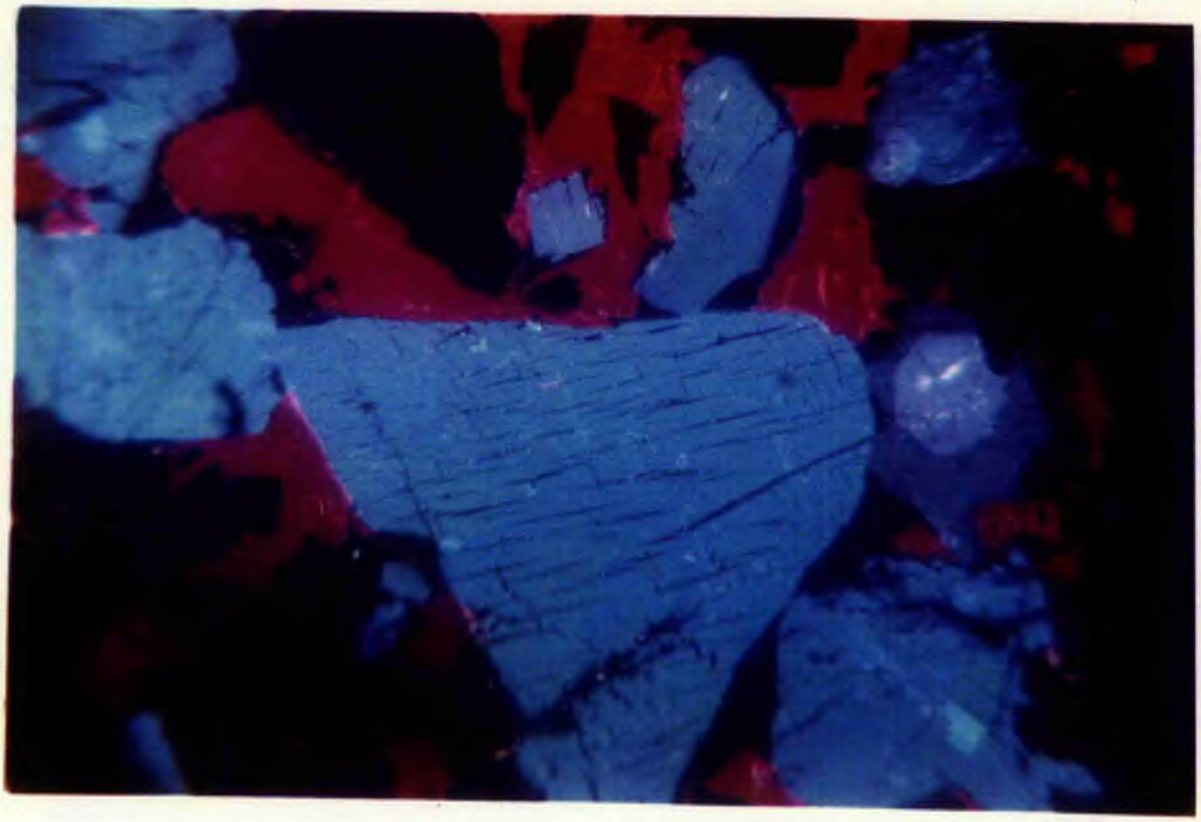

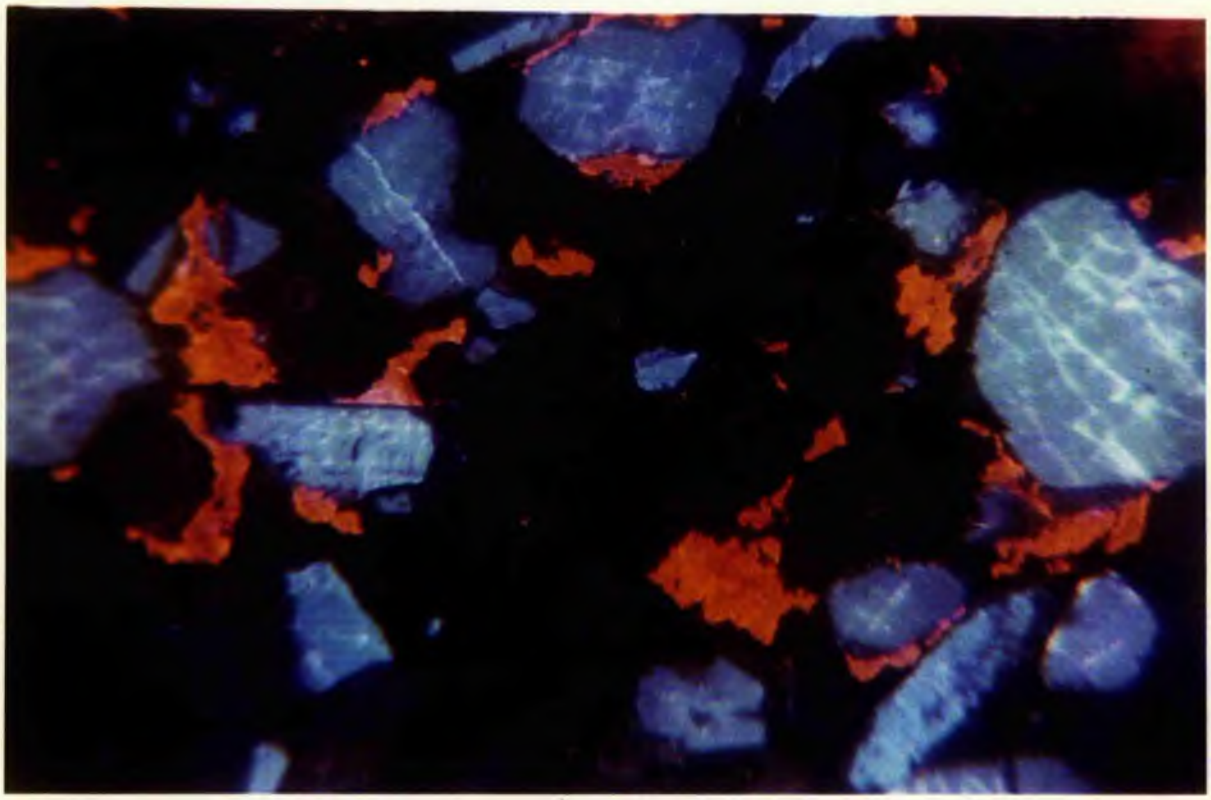

Plate 7.15: Illite on K-feldspar overgrowth. (Watt Mt 4-2-79-8W5; 1725.9 m) (SEM scale bar 10um).

Plate 7.16: Back-scatter image of K-feldspar (grey) and quartz (opaque). Feldspar shows dark grey overgrowth rims which have been corroded and lined by clays (bright white in colour). Quartz is also corroded by clays; clays are also present as linings between the quartz grains. (Watt Mountain 10-17-94-15W5; 4949 ft) (Back-scatter scale bar 100um).

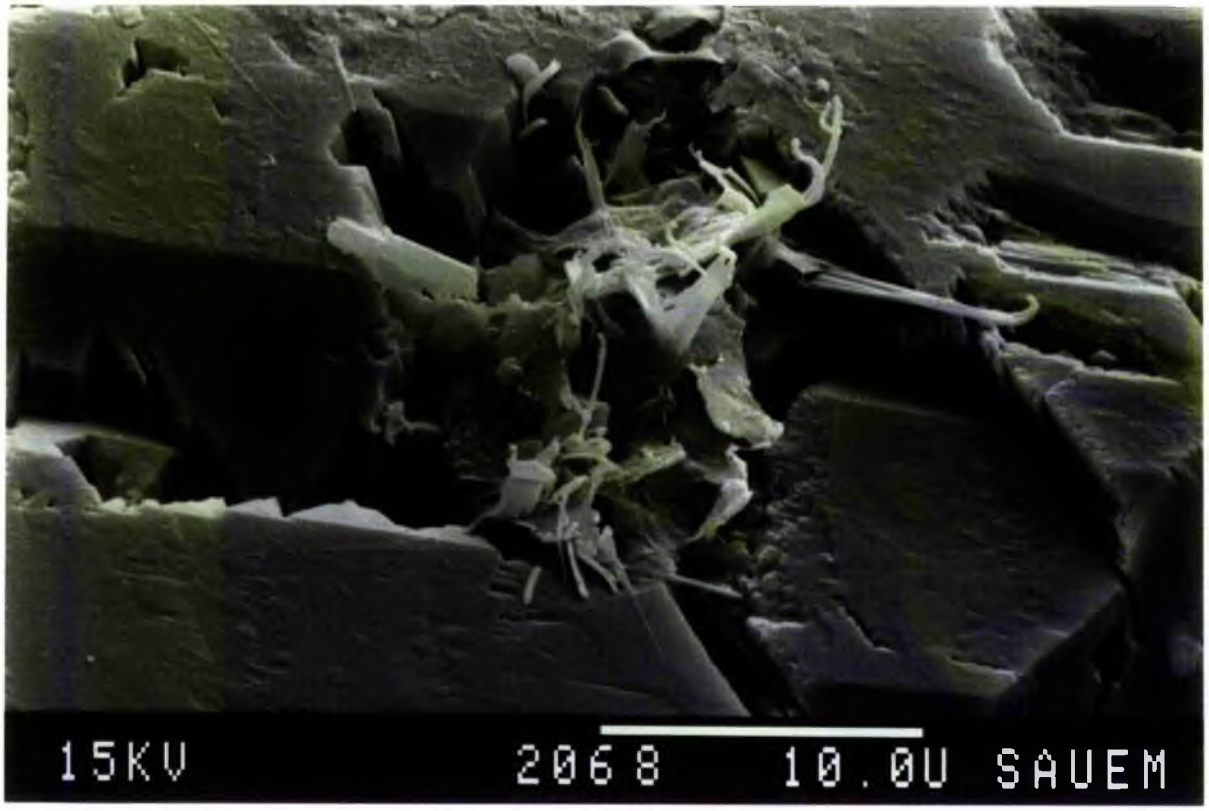
15KV
2068
10.0U SAUEM

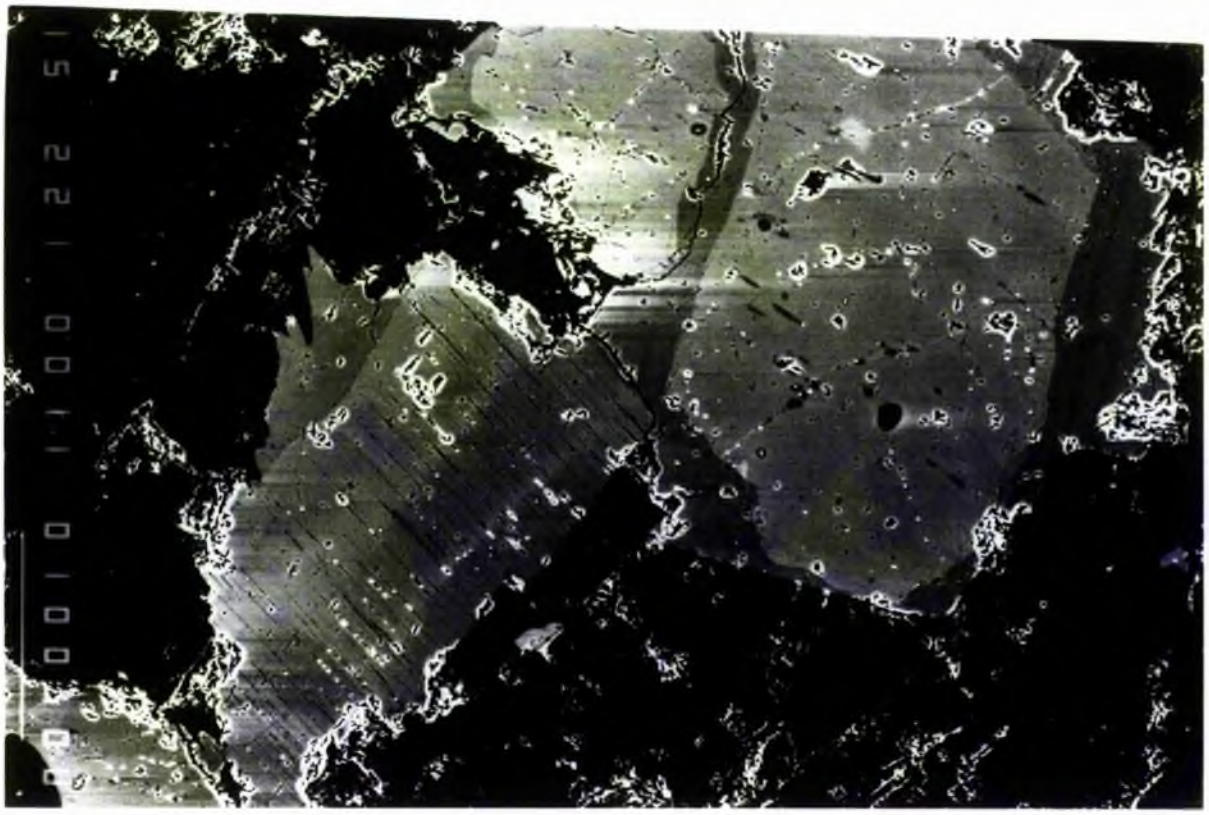
0010 1100 122 15

Plate 7.17: Authigenic K-feldspar amongst detrital corroded K-feldspar. (Watt Mt 16-31-86-12W5; 5164.5 ft) (SEM scale bar 10um).

Plate 7.18: Quartz grains with euhedral faces developed by overgrowths. Full growth of faces often absent where adhering clays are present (centre grain). Porosity reduced to lamellar pores along long contacts or small straight-edged pores. (Watt Mt 12-23-74-6W5; 5568 ft) (SEM scale bar 100um).

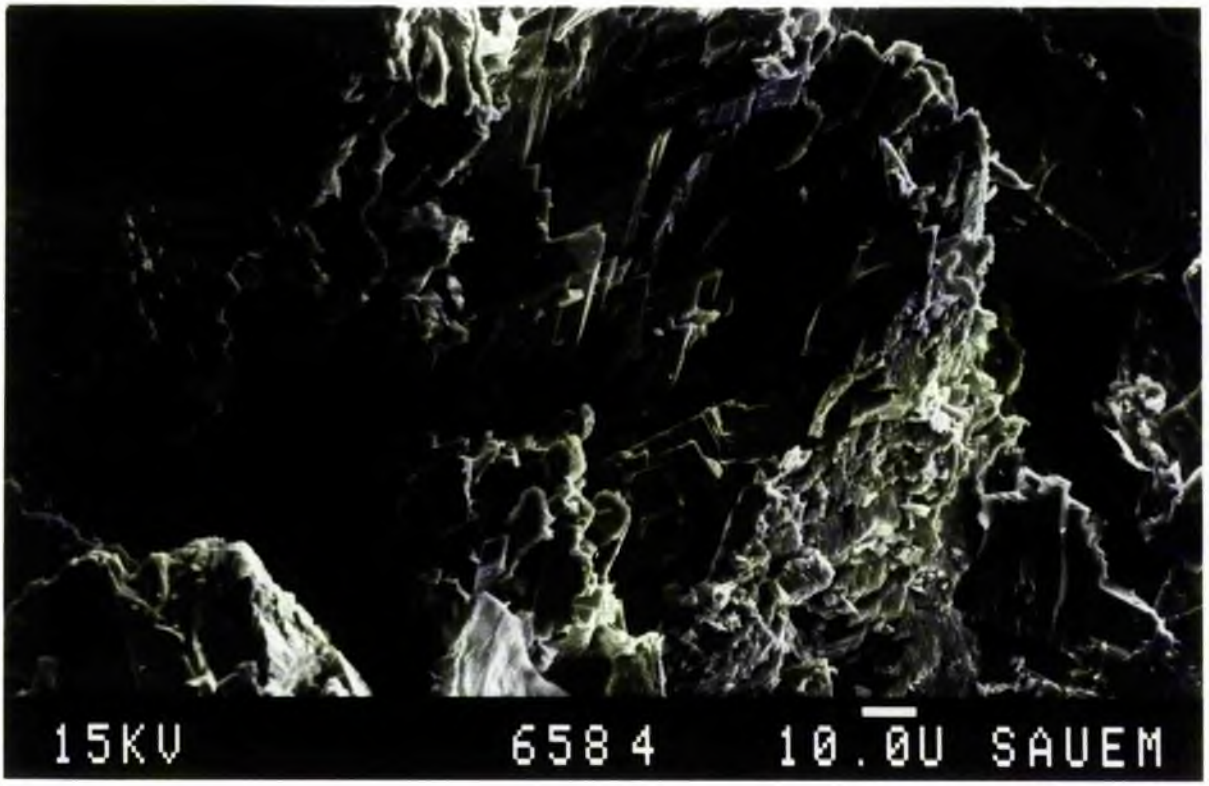
15KV 6584 10.0U SAUEM

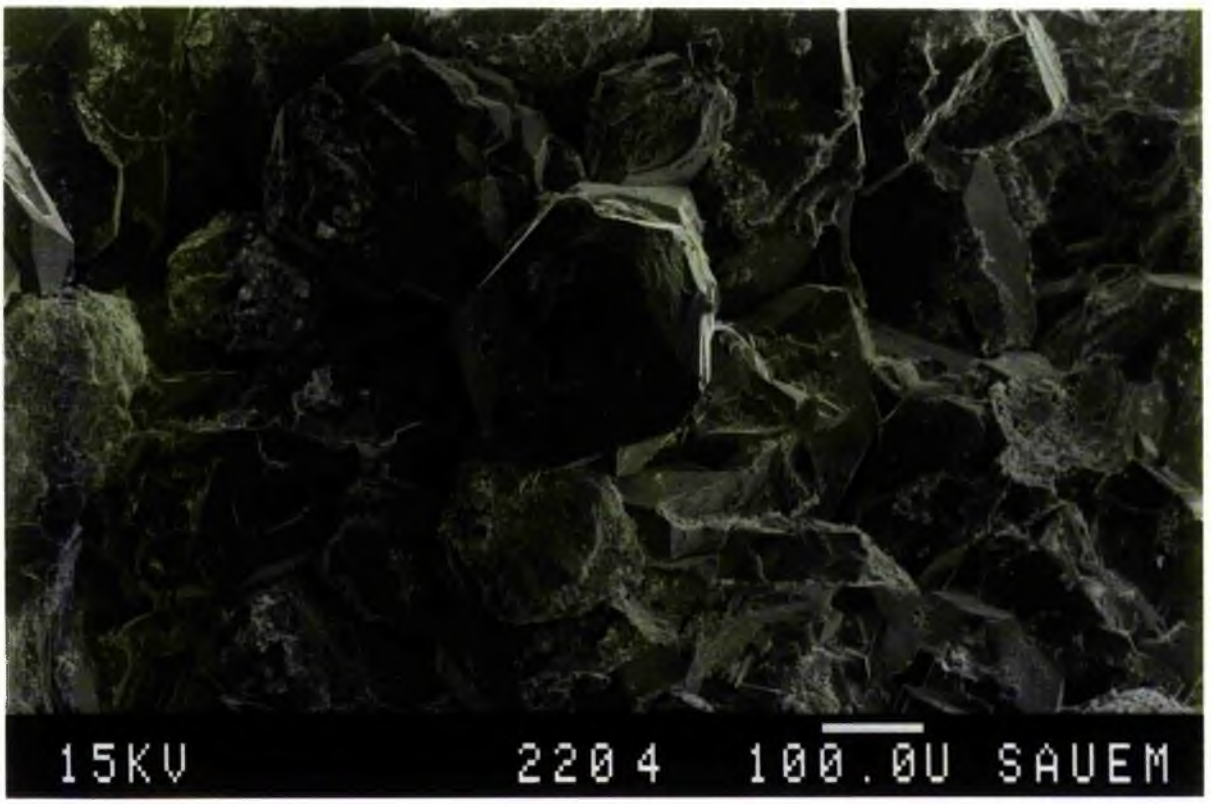
15KV 2204 100.0U SAUEM

Plate 7.19: Quartz overgrowths developed on grain but apparently inhibited (lower middle) by presence of clay. Overgrowth partly encloses some clay flakes. (Watt Mt 12-30-78-7W5; 1722.3 m) (SEM scale bar 10um).

Plate 7.20: Well formed faces of quartz overgrowth on detrital grain. Chlorite (top right) is growing over corroded overgrowths. (Granite Wash 9-35-91-6W5; 4649 ft) (SEM scale bar 10um).

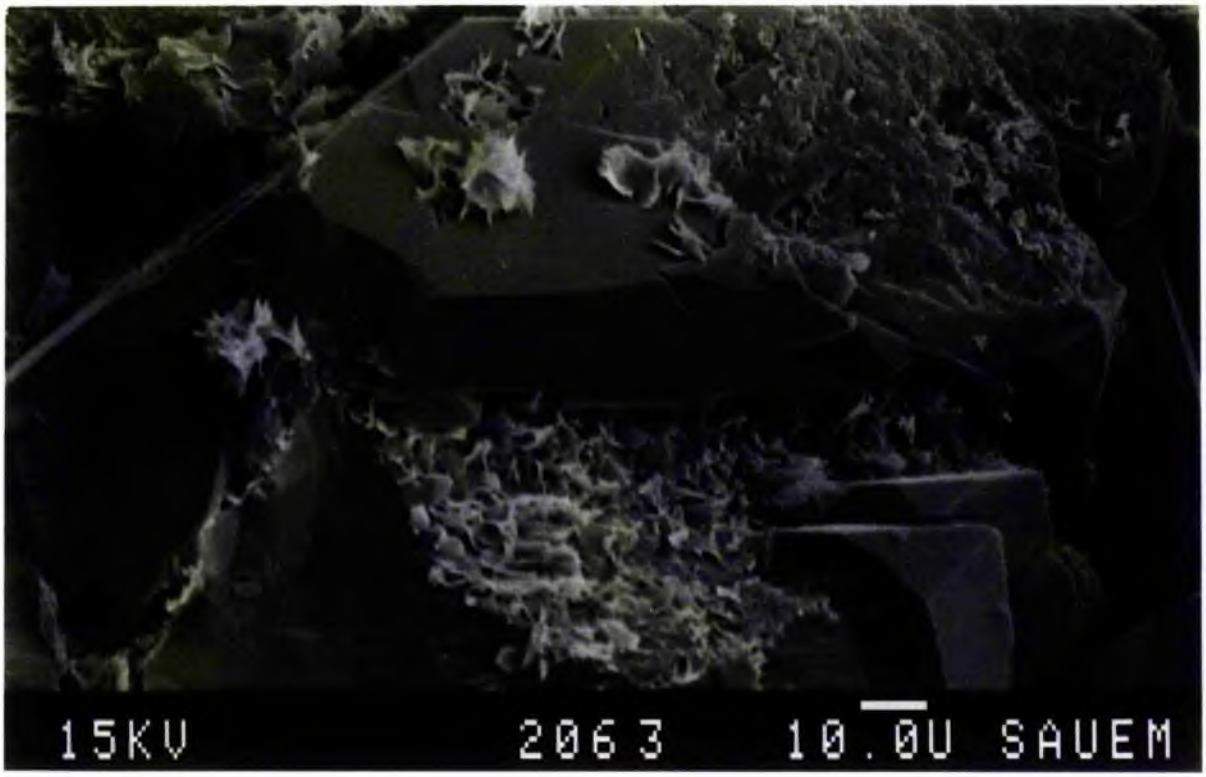
15KV 2063 10.0U SAUEM

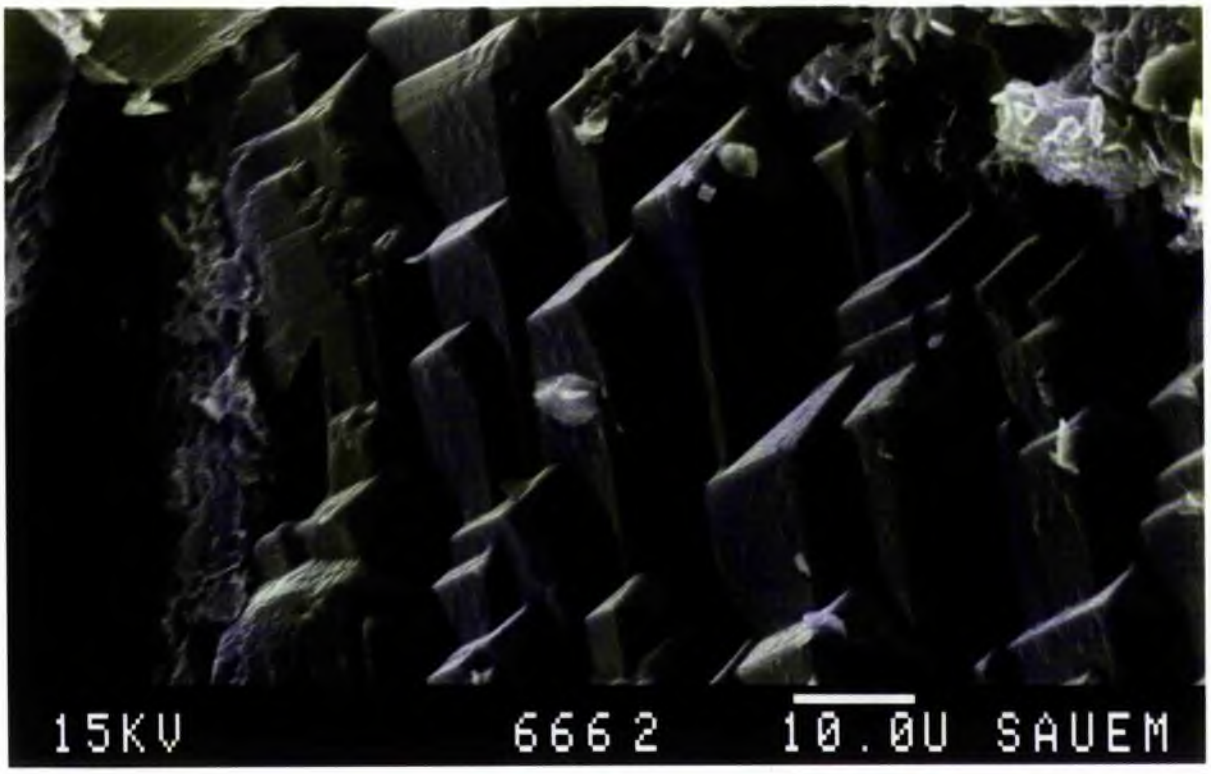
15KV 6662 10.0U SAUEM

Plate 7.21: Chlorite crystals fringing and inhibiting quartz overgrowth. (Watt Mt 12-23-74-6W5; 5568 ft) (Scale bar 10um).

Plate 7.22: Quartz and chlorite grain relationship. Quartz overgrowths are covered by chlorite flakes. Quartz overgrowth edges are being inhibited by chlorite. (Watt Mt 10-5-92-19W5; 5489 ft) (SEM scale bar 10um).

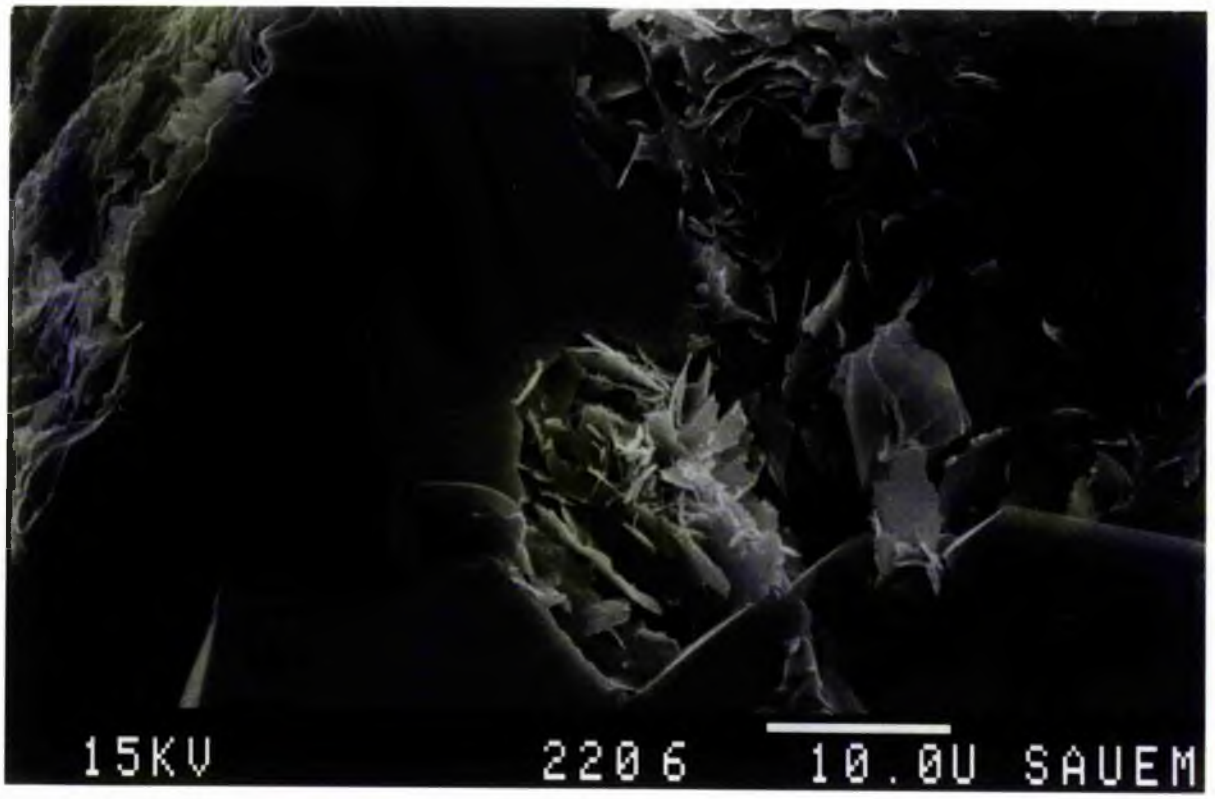
15KV
2206
10.0U SAUEM

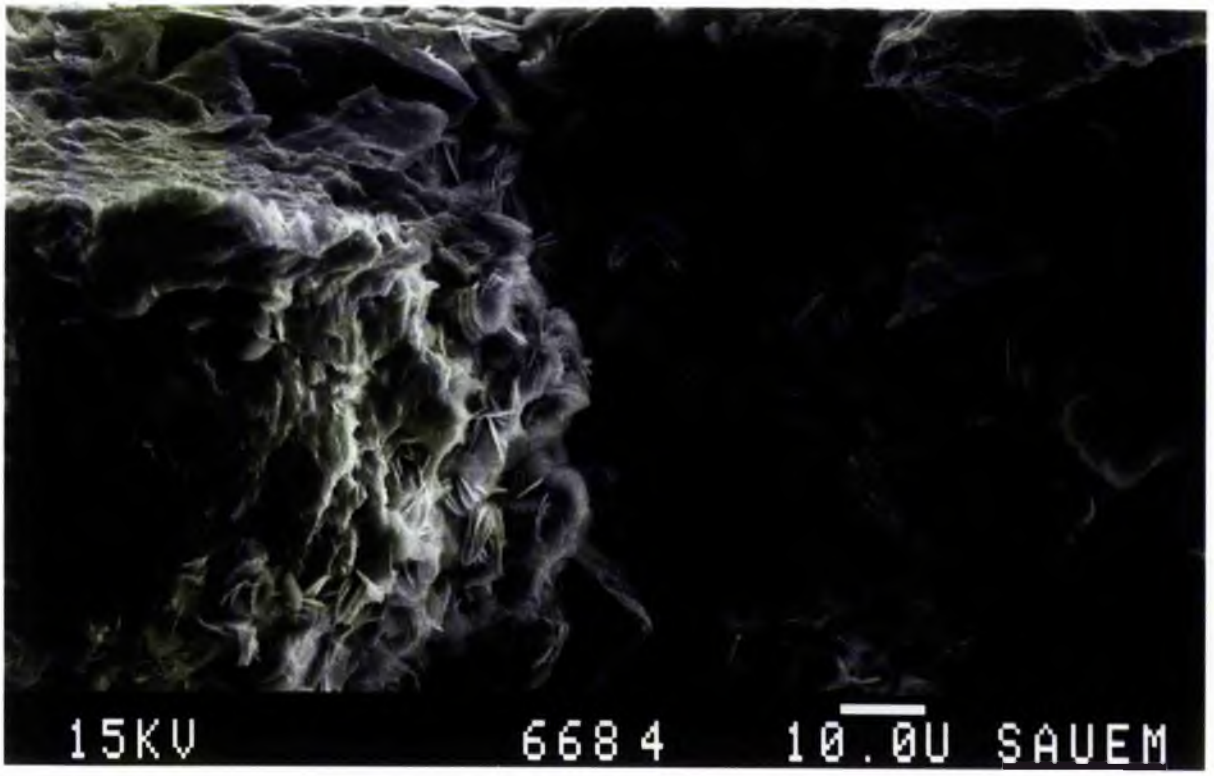
15KV
6684
10.0U SAUEM

Plate 7.23: Anhydrite-quartz, anhydrite-feldspar and anhydrite-carbonate relationship. Feldspar overgrowths and quartz have been corroded before anhydrite precipitation. Carbonate is also corrosive against quartz. The carbonate boundary towards the anhydrite is sutured (centre), while at other places it is also almost straight to stepped (right). This suggests that anhydrite is later than carbonate. (Watt Mt 2-21-73-13W5; 7118 ft) (CP x40).

Plate 7.24: Quartz with undulose extinction and K-feldspar with overgrowths. The cement is anhydrite which has formed against corroded overgrowths of feldspar. (Watt Mt 12-9-93-18W5; 5261 ft) (CP x40).

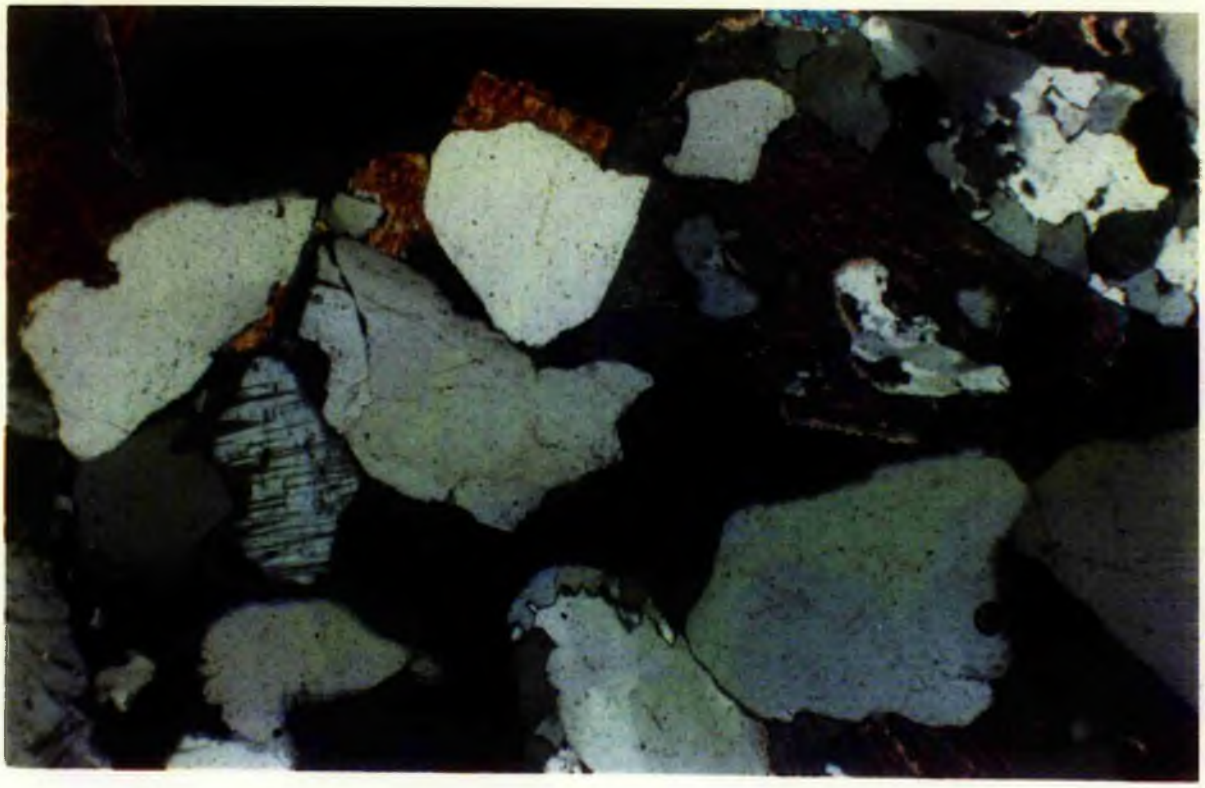

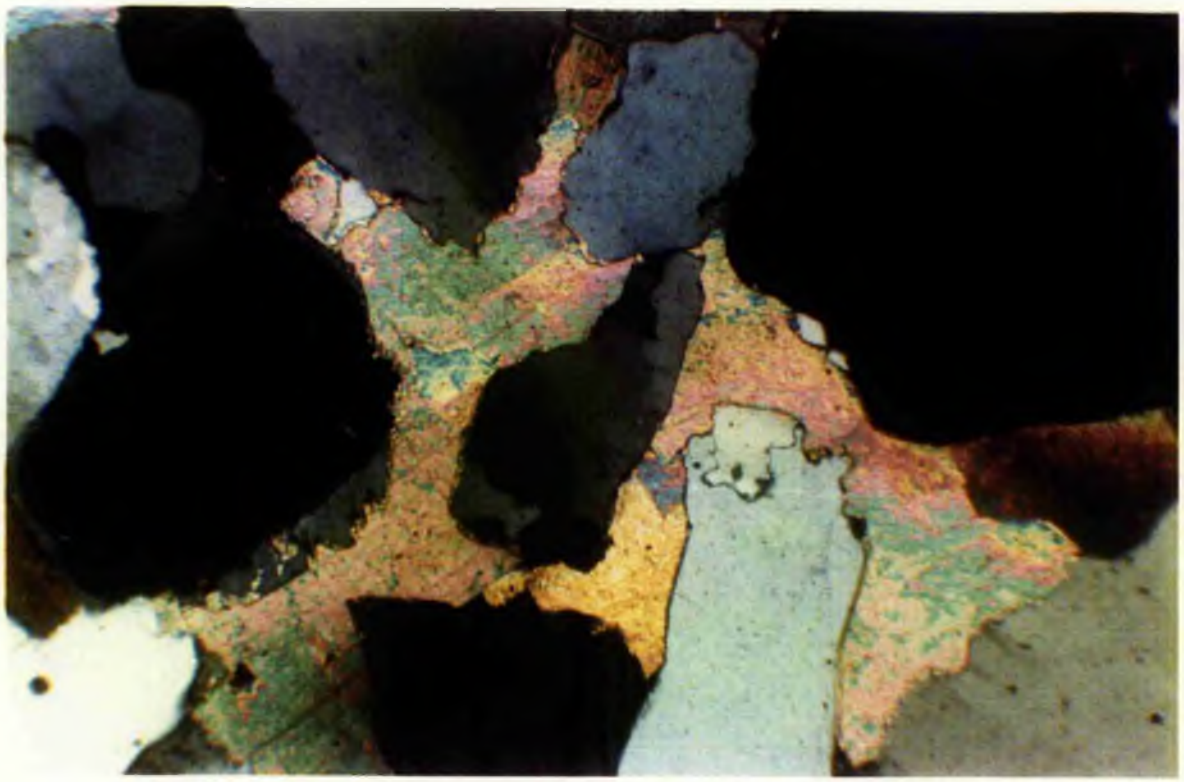

Plate 7.25: Poikilotopic anhydrite which has suffered dissolution leaving rectangular 'piers' projecting into large secondary pore (middle right) formed by dissolution of the anhydrite. Quartz grains within the anhydrite have suffered some corrosion before or associated with the precipitation of the anhydrite. (Watt Mt 10-11-71-12W5; 7658 ft) (PPL x120).

Plate 7.26: Anhydrite cement penetrating polycrystalline quartz grain. K-feldspar grains (bottom middle). (Watt Mt 8-35-68-3W5; 5516 ft) (CP x50).

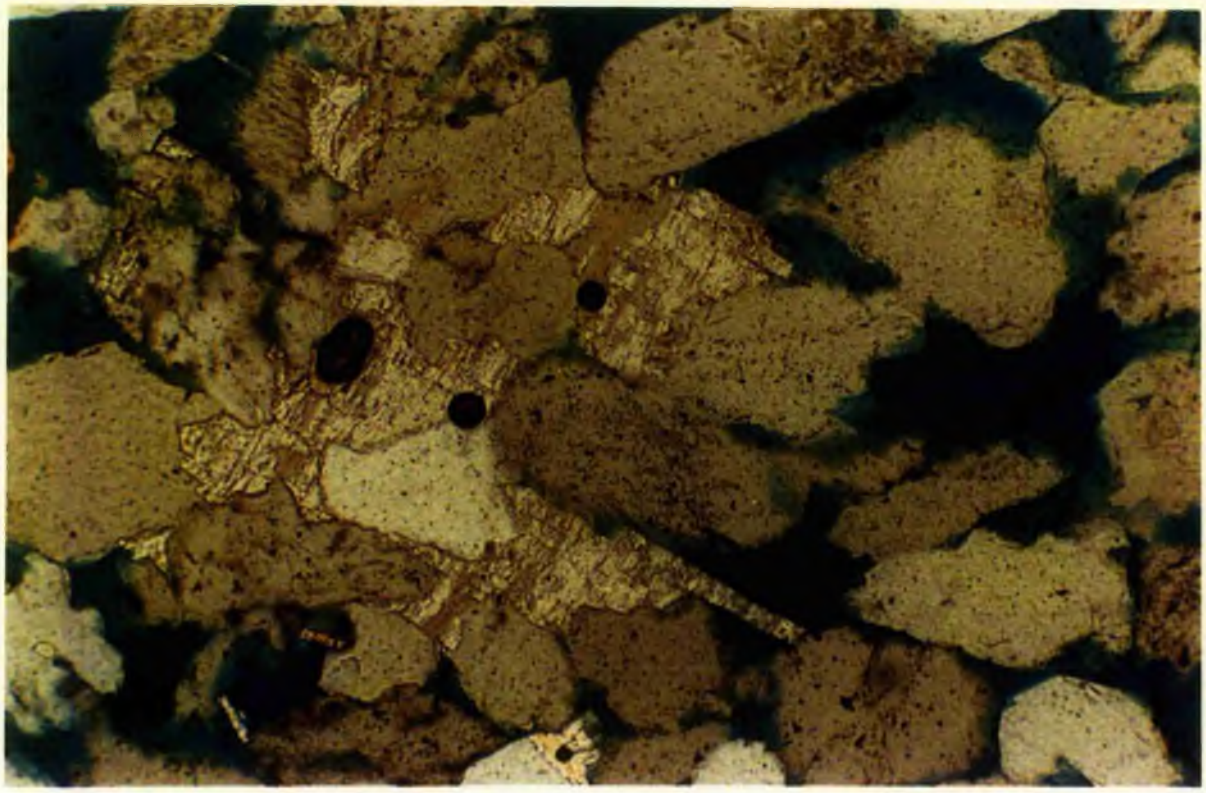

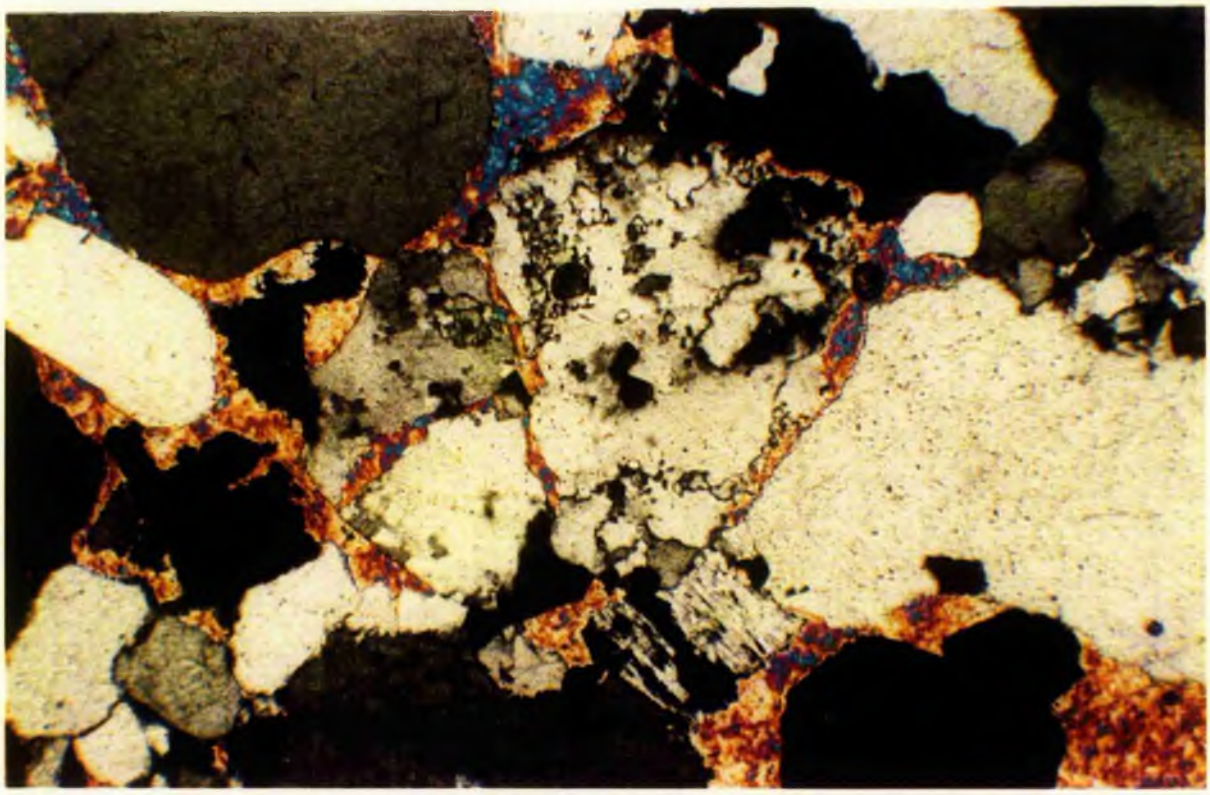

Plate 7.27: Blocky anhydrite filling pores and displacing a biotite crystal along cleavage. Polycrystalline vein quartz clast with overgrowth forms (right) the boundary of a large straight-edged polygonal pore (bottom right). (Watt Mt 7-30-76-7W5; 6108.9 ft) (PPL x120).

Plate 7.28: Blocky, pore-filling anhydrite around skeletal feldspars (middle). Anhydrite slightly corroded leaving small secondary pore (lower left) with feldspar showing corrosion along cleavage producing within-particle secondary porosity. Pore (upper right) also formed by partial dissolution of anhydrite. (Watt Mt 10-8-73-W5; 5460 ft) (PPL x120).

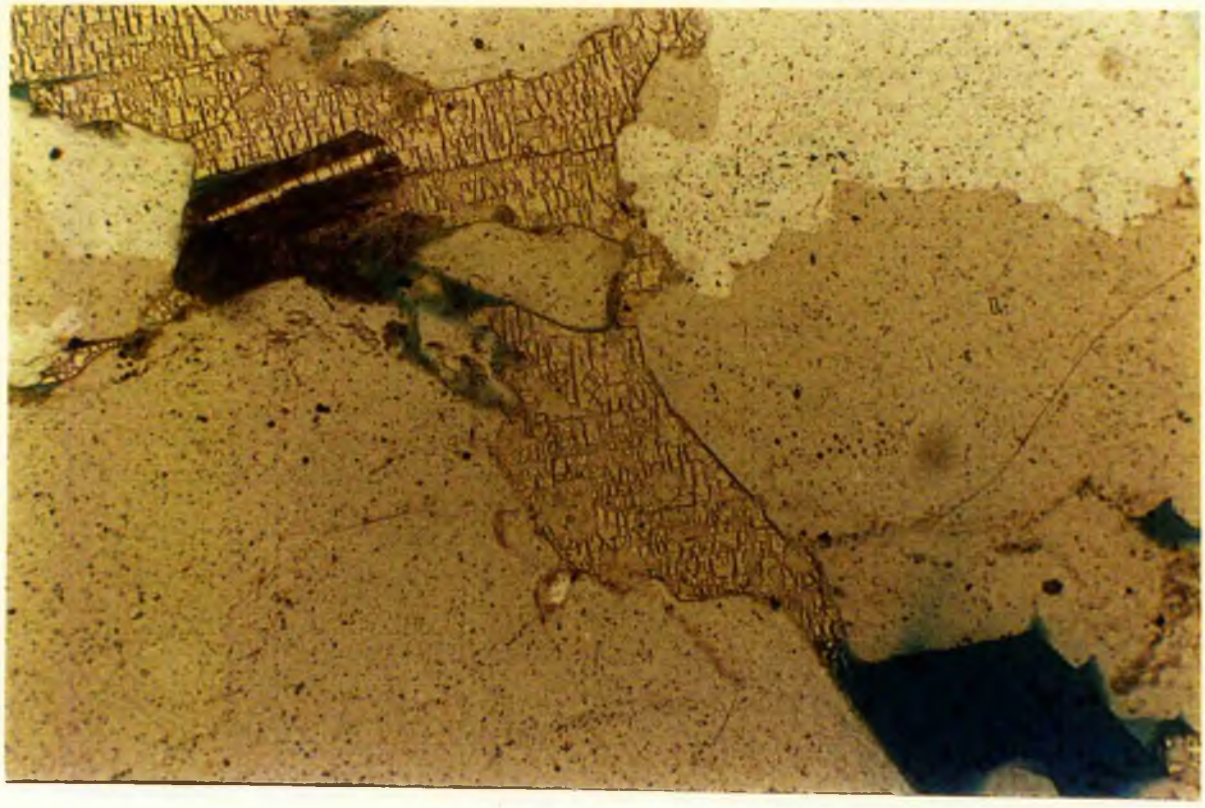

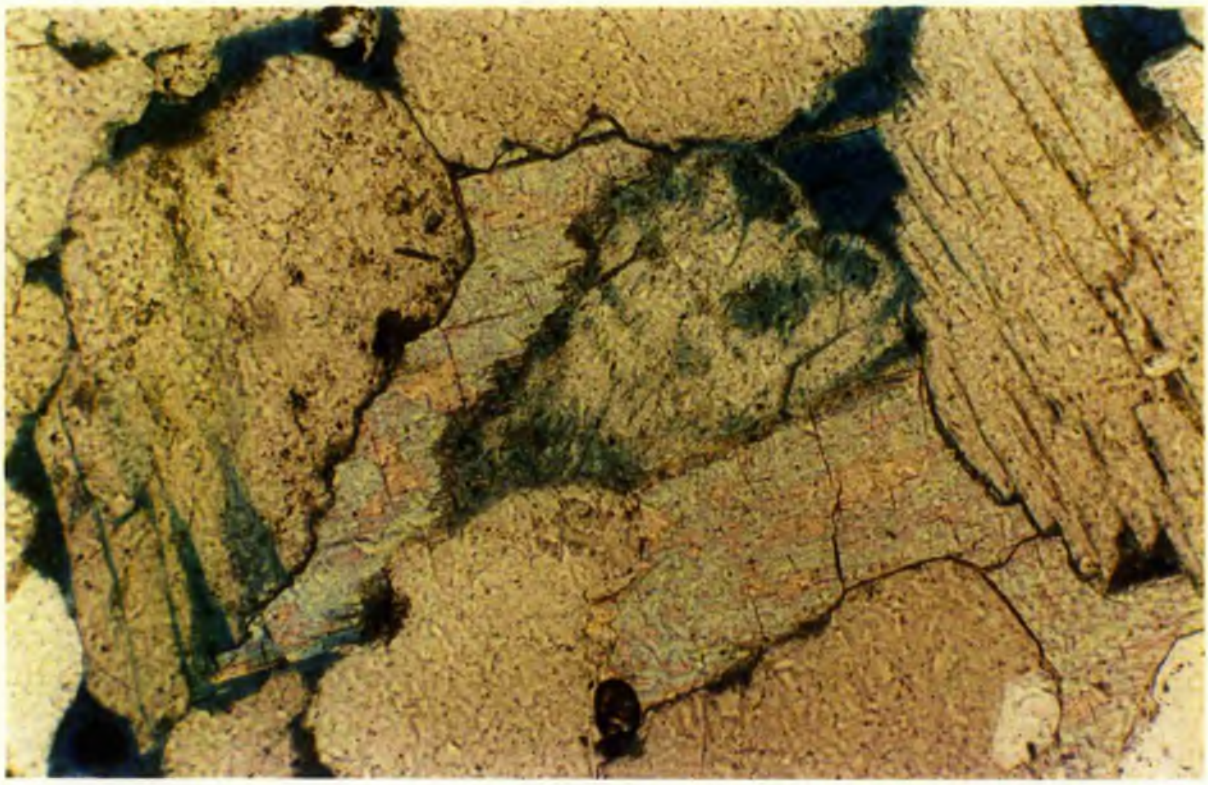

Plate 7.29: Pervasive, porosity-destroying calcite, poikilotopic and with wavy extinction. Quartz and feldspar grains have been partially replaced by calcite producing a 'floating' texture. Feldspars prominent, microcline (upper middle and bottom) perthite (bottom left). (Watt Mt 2-6-8-7W5; 5618.9 ft) (CP x50).

Plate 7.30: Ferroan calcite as coarse-grained spar filling pores with chlorite fringes between calcite and quartz grains. Straight-edged pores (lower half) formed by quartz overgrowths. (Watt Mt 4-8-71-4W5; 6105 ft) (PPL x120).

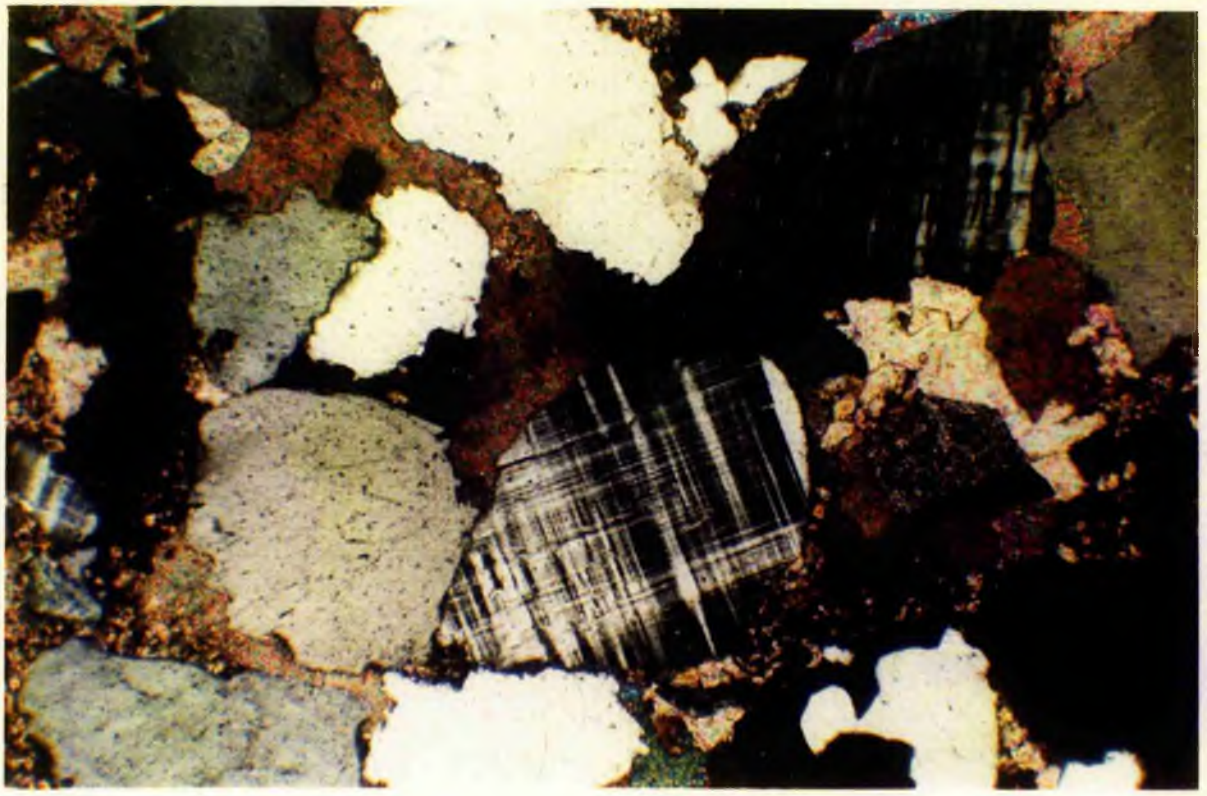

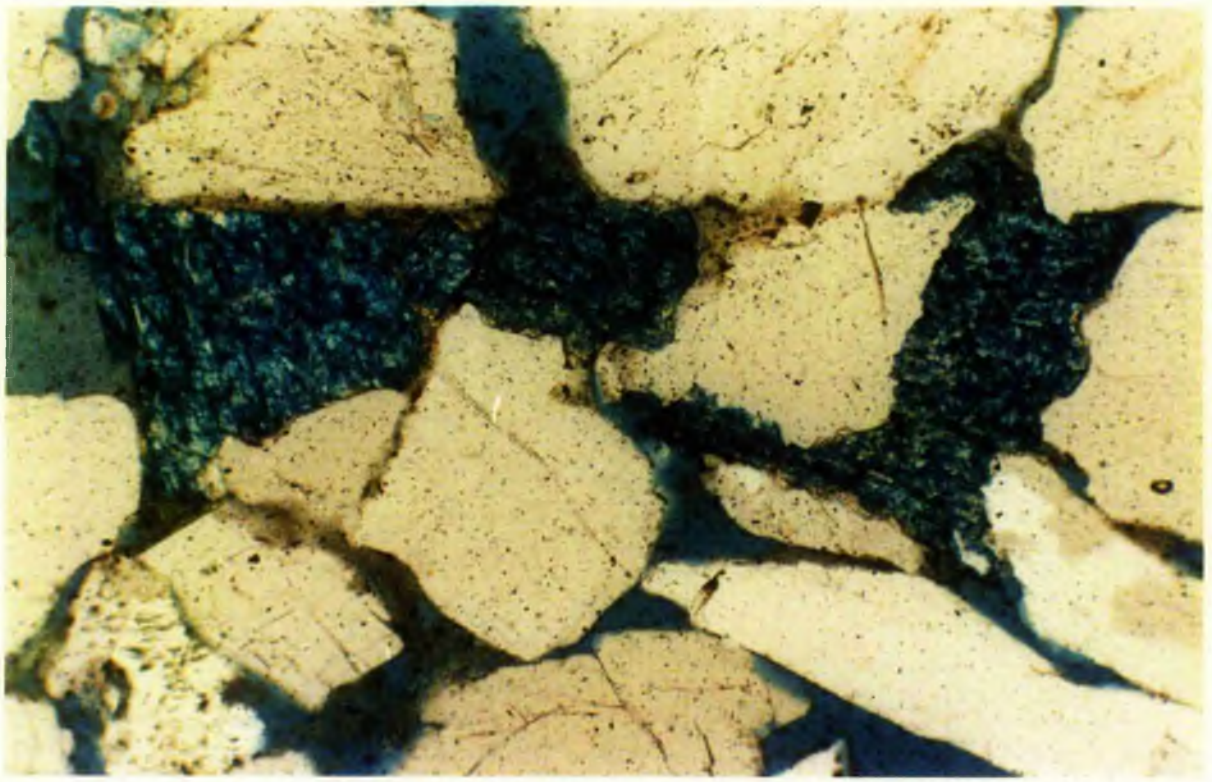

Plate 7.31: Calcite (bottom) and dolomite (top) relationship. Calcite is massive and is bigger in size than smaller rhombs of dolomite. The carbonates have chlorite flakes over them. (Granite Wash 9-35-91-6W5; 4649 ft) (SEM scale bar 10um).

Plate 7.32: Corroded calcite (bottom) and dolomite rhombs. The well formed rhombs of dolomite suggest that calcite was probably formed earlier. Some smectite is also intermixed with the calcite. (Chinchaga 11-29-86-3W5; 5231 ft) (SEM scale bar 10um).


15KV 6665 10.0U SAUEM

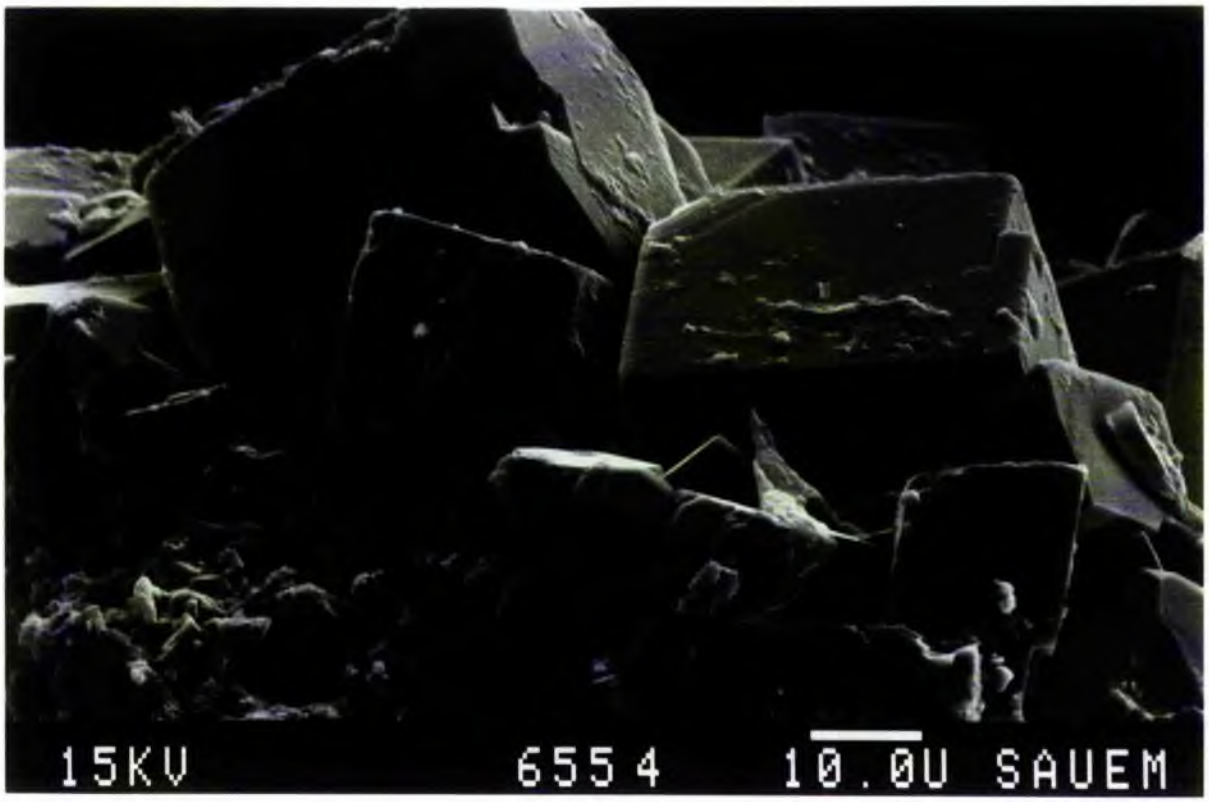
15KV 6554 10.0U SAUEM

Plate 7.33: Massive pore filling poikilotopic dolomite against grains some of which have corroded margins, while others have straight edges. (Watt Mt 4-19-93-19W5; 5160 ft) (CP x100). 

Plate 7.34: Pore filling dolomite rhombs. (Watt Mt 16-3-84-14W5; 5847.9 ft) (CP x100). 

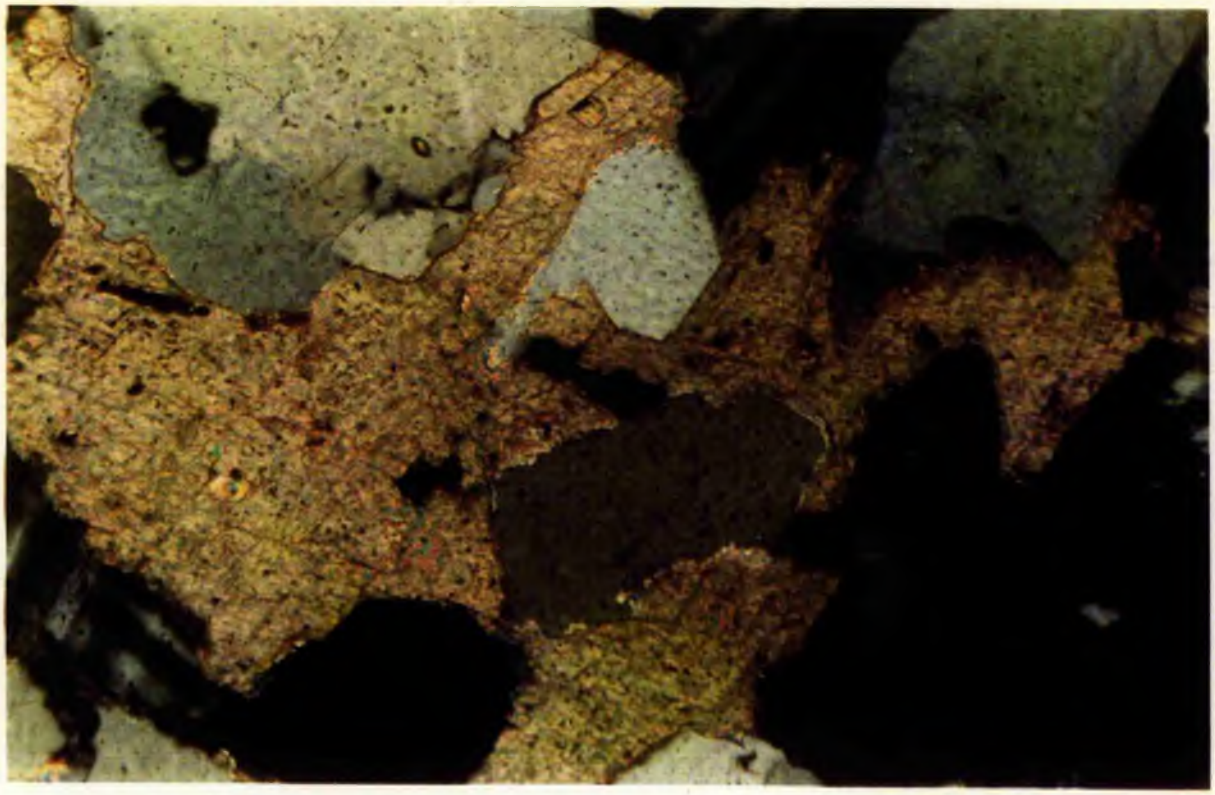

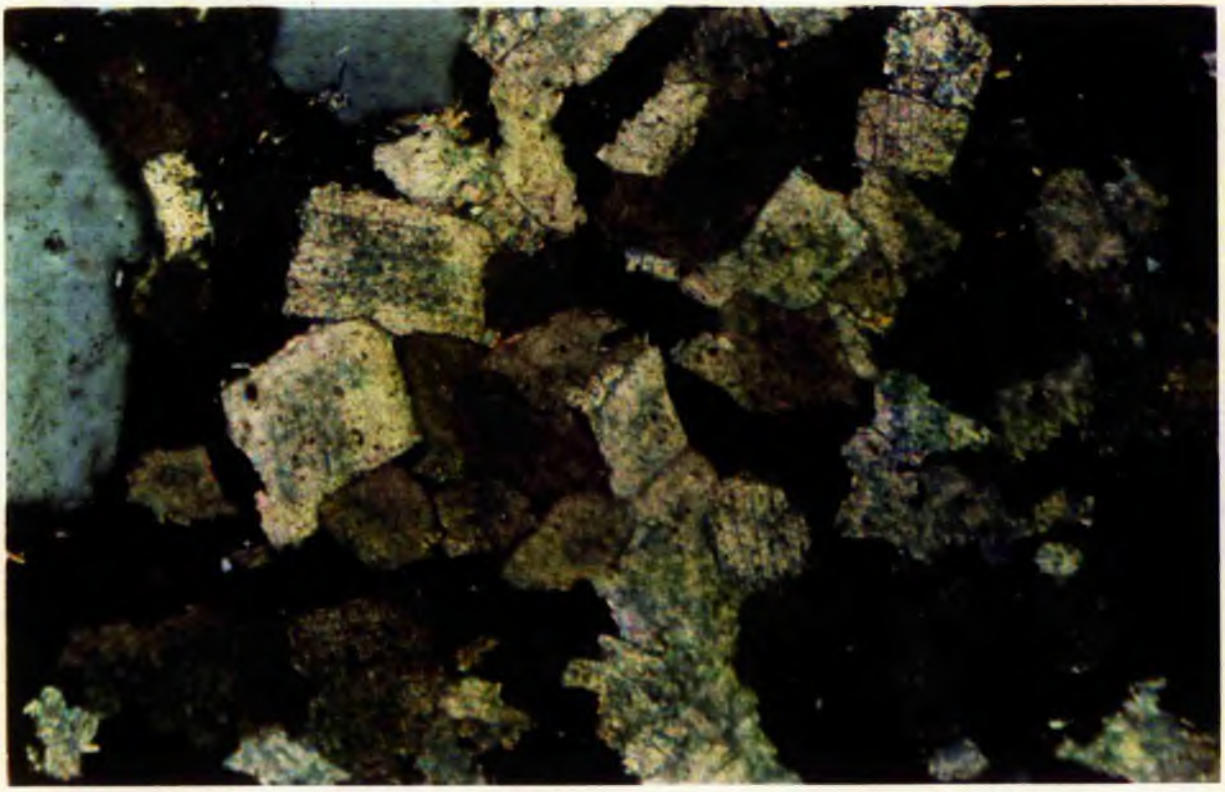

Plate 7.35: Quartz grains with dust lines. The overgrowths and feldspar have been partly corroded against dolomite. (Granite Wash 10-14-72-23W5; 9803 ft) (PPL x100).

Plate 7.36: A high magnification figure showing the carbonate-quartz and carbonate to feldspar relationship. The feldspar has been corroded and its margin with the carbonate is scalloped; carbonate penetrating the feldspar. Quartz to carbonate margin is sometimes complicated; it is sutured to scalloped at some places while at others it is straight (lower right). (Keg River 4-3-87-8W5; 4911 ft) (CP x200).

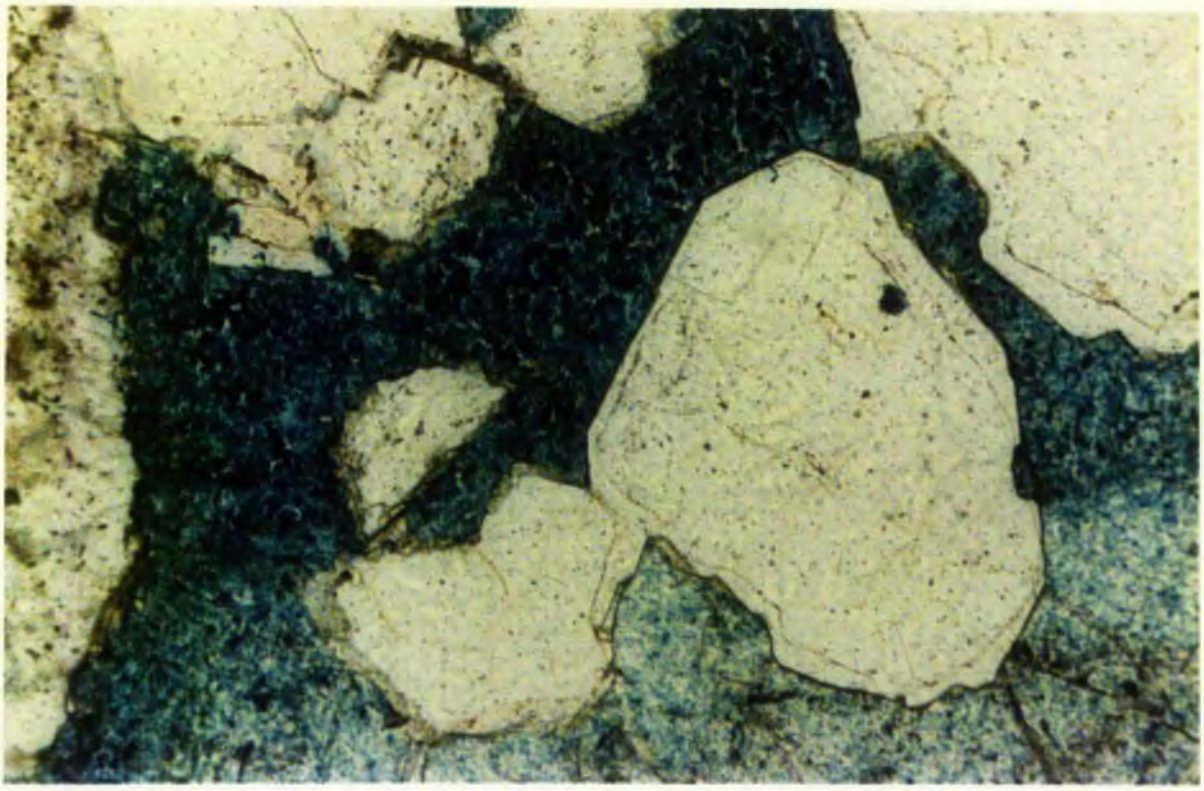

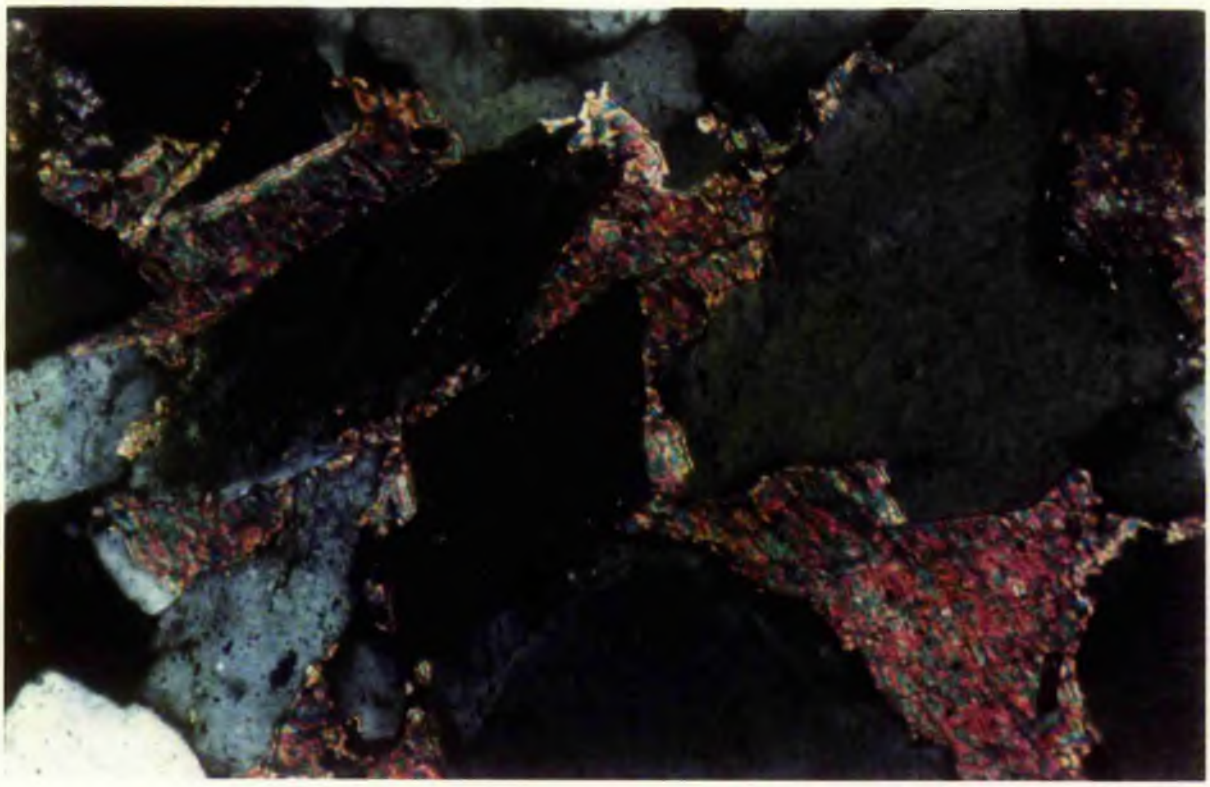

Plate 7.37: Back-scatter image of quartz (opaque), feldspar (white) and ferroan-dolomite (grey). Carbonate is a massive pervasive cement. (Watt Mountain 16-14-68-21W5; 5539.1 ft) (Back-scatter scale bar 100um).

Plate 7.38: Grain fringing clays, chlorite with illite partly occluding porosity. (Watt Mt 2-11-80-8W5; 5627.16 ft) (SEM scale bar 10um).

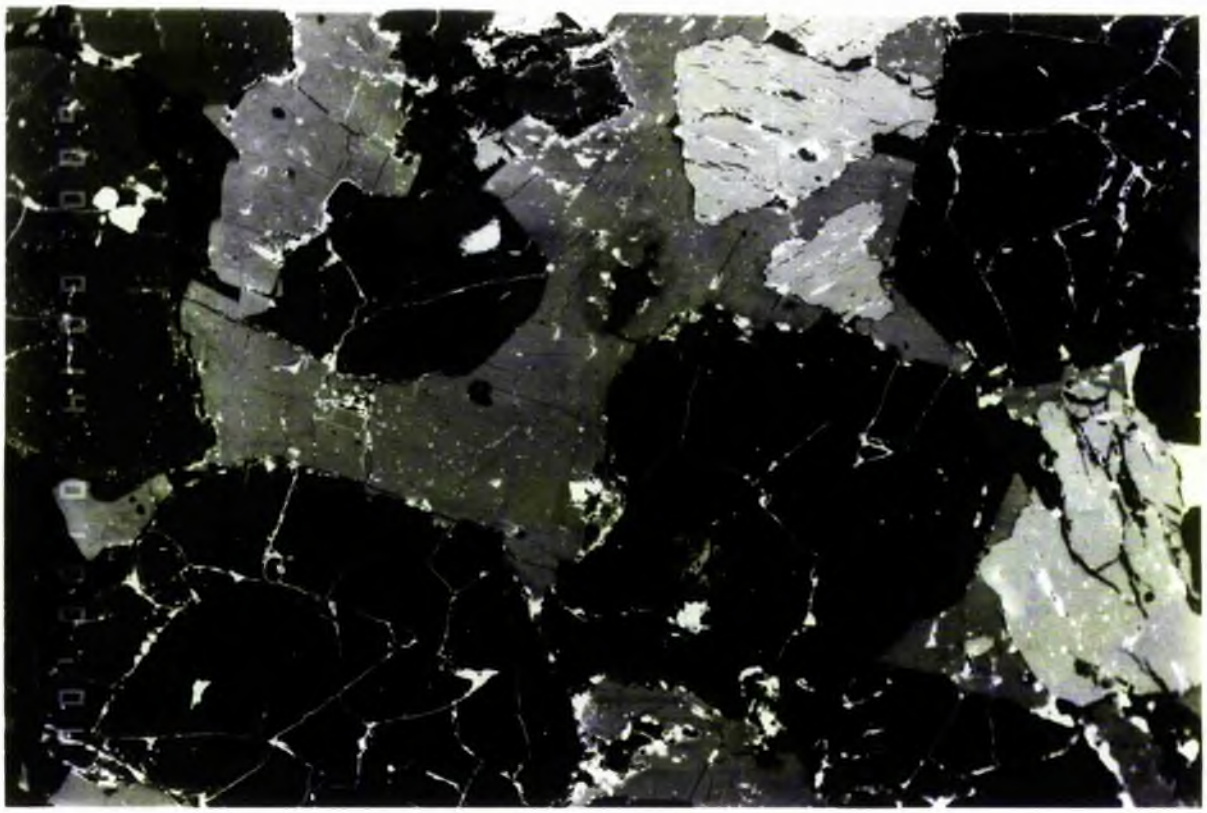

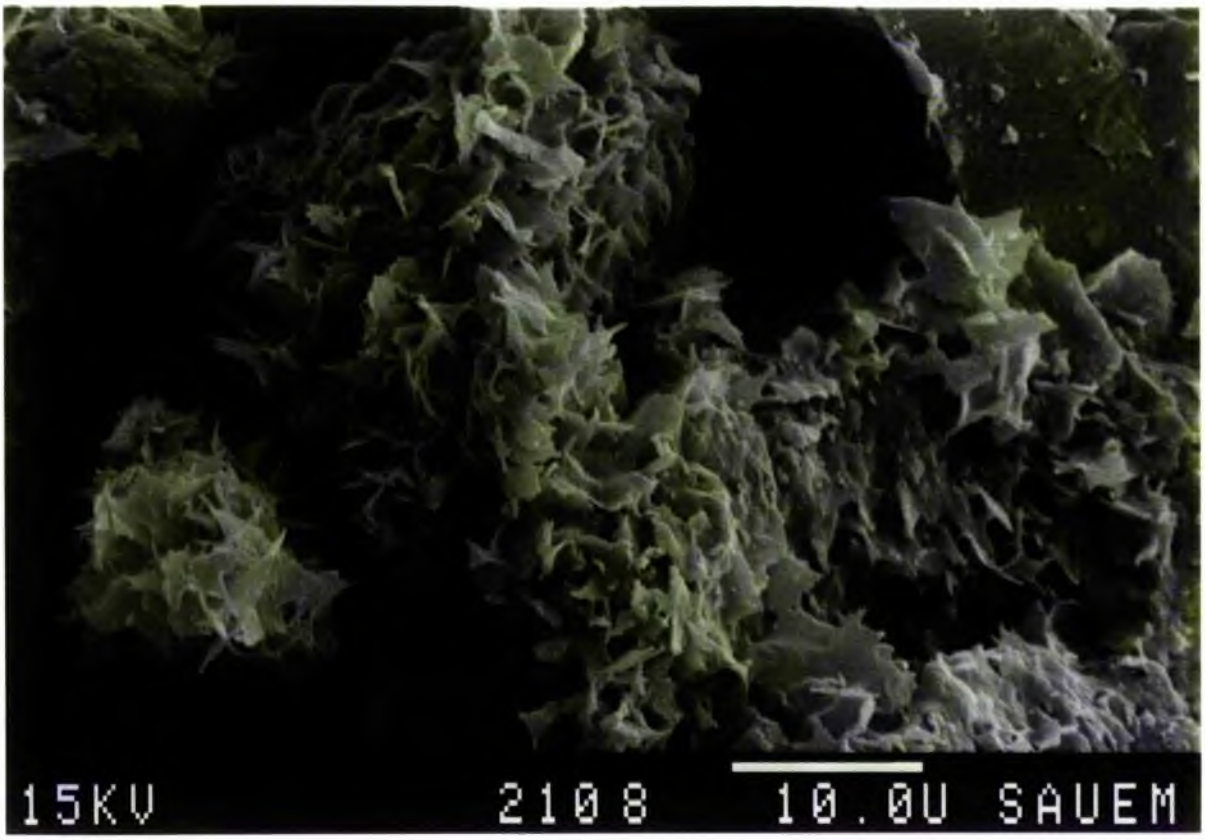
15KV
2108
10.0U SAUEM

Plate 7.39: Chlorite-smectite fringing quartz overgrowth. (Watt Mt 16-14-68-21W5; 9689.13 ft) (SEM scale bar 10um).

Plate 7.40: Hairy illite grown on K-feldspar. (Watt Mt 6-21-77-9W5; 6139.7 ft) (SEM scale bar 10um).

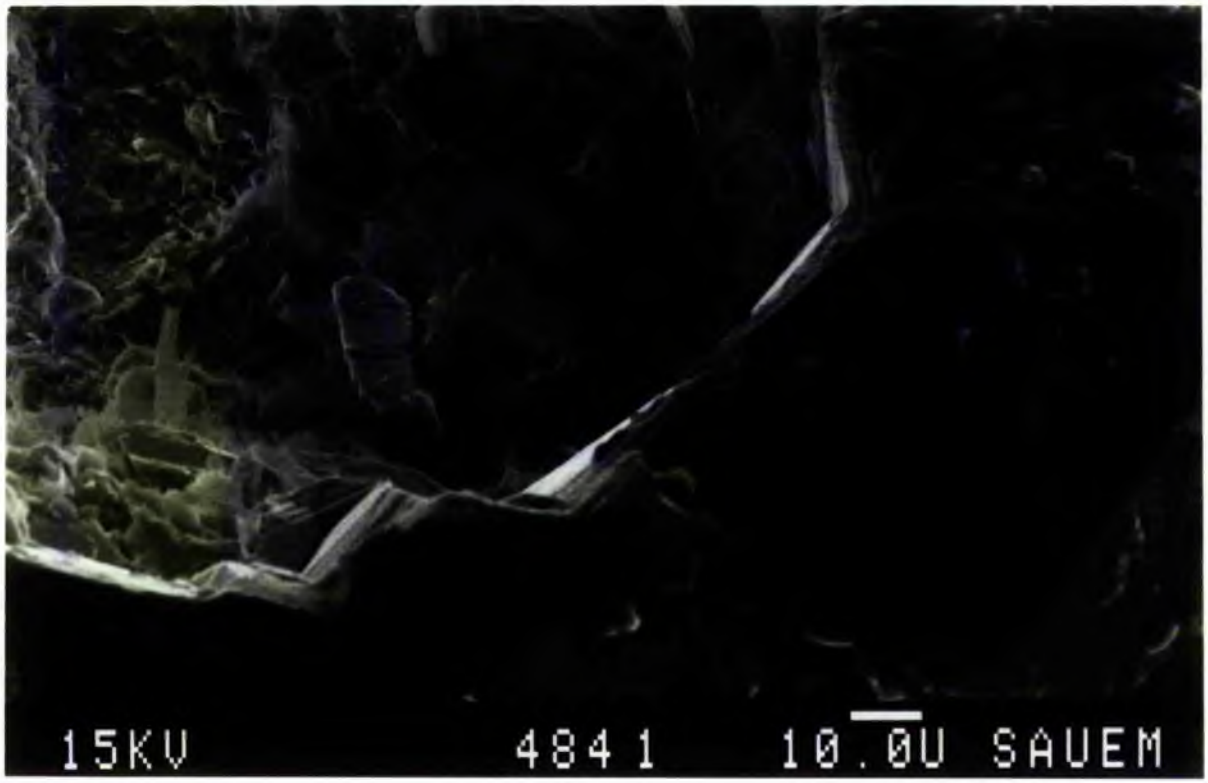
15KV 4841 10.0U SAUEM

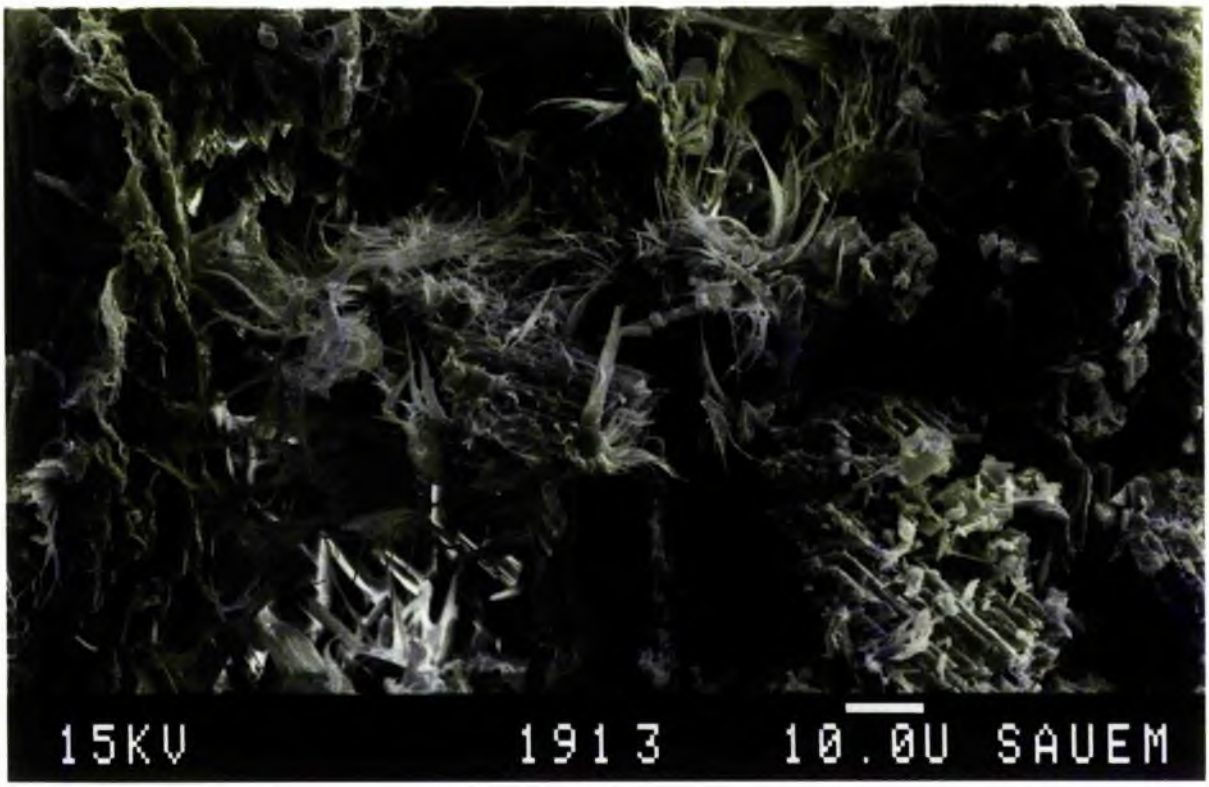
15KV 1913 10.0U SAUEM

Plate 7.41: Pore filling illite, reducing all the primary between particle porosity. Feldspar (bottom Left) has been corroded and so has the quartz grains, with clay penetrating the grains. (Keg River 9-11-87-9W5; 4746 ft) (CP x100).

Plate 7.42: Massive pore filling illite. The illite has been formed in situ due to alteration of feldspar. The quartz grains are well cemented. The boundary between quartz grains are straight to slightly scalloped, with no evidence of pressure solution. Mica flakes are also trapped between grains. (Granite Wash 4-9-85-9W5; 5100 ft) (CP x100).

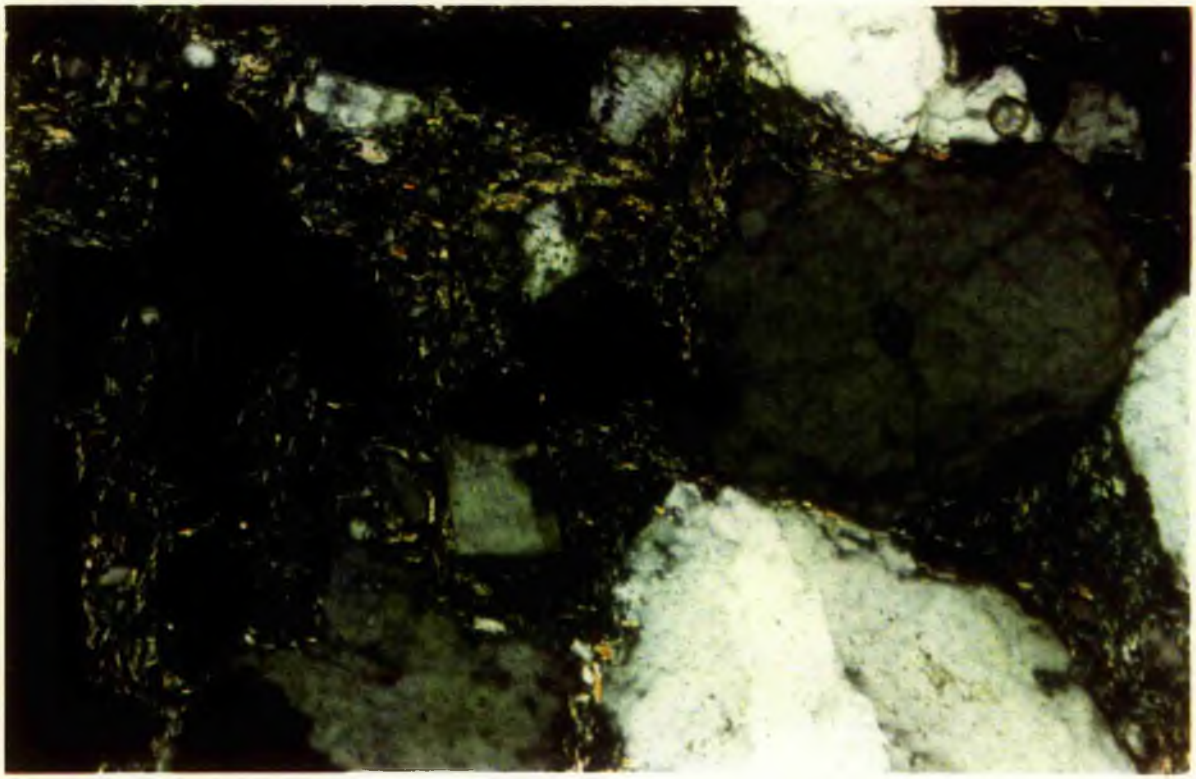

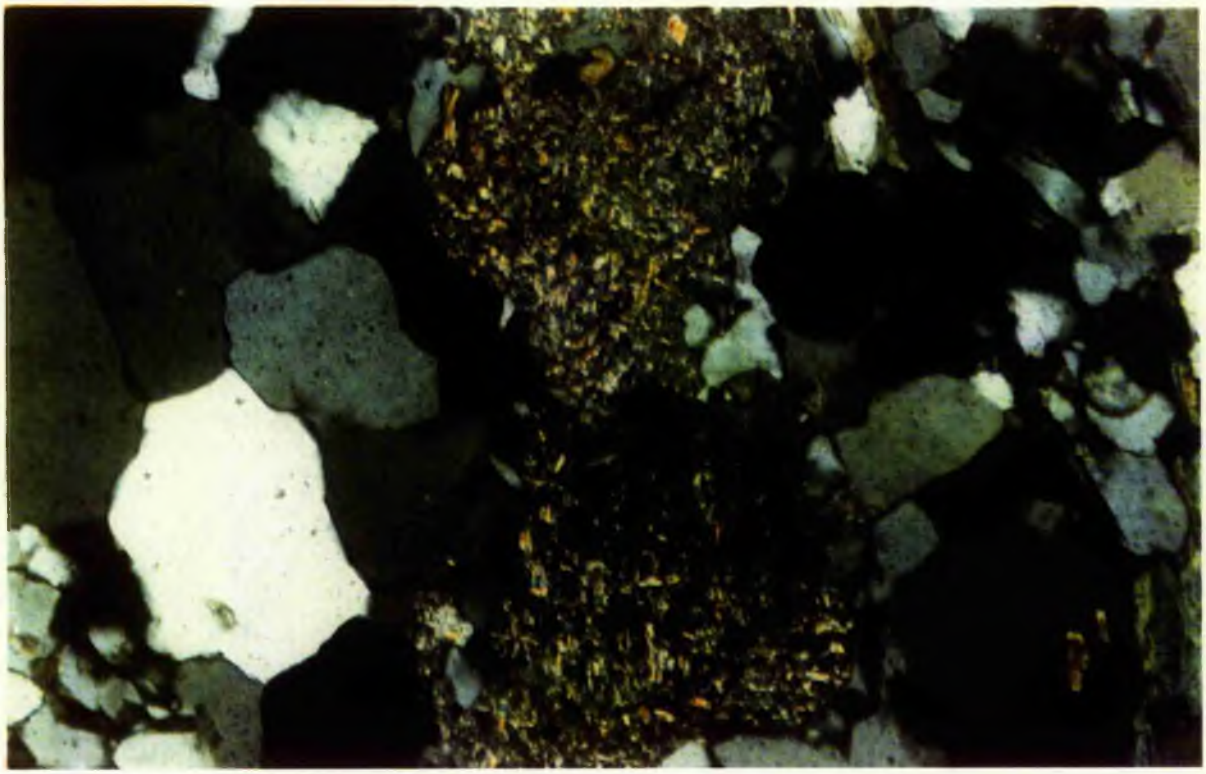

CHAPTER 8: SUMMARY & CONCLUSIONS

(with 4 figures)

8.1 SUMMARY:

8.1.1 Karoo Supergroup:

The Karoo sediments in the Western Shelf of Seychelles are continental deposits over 6,000 ft thick. Wireline logs, sidewall core cuttings and lithological logs have been utilized to study the stratigraphy of the entire succession. The succession can be divided, mainly on the basis of grain-size, into five members (Table 3.1), which record three mega-sequences. Only the upper part of the first mega-sequence occurs as fine grained sands and muds (Member 1). The other two mega-sequences (first, Members 2 and 3, and second, Members 4 and 5) show coarse-grained occasionally conglomeratic sands below (2 and 4) and finer grained sands above (3 and 5). Member 5 of the Reith Bank-1A correlates with the Karoo sequence of the Seagull Shoals-1. The first mega-sequence may have been initiated by climatic change subsequent to the Dwyka glaciation. Comparison with Madagascar and Southern Africa suggests that tillite may occur at no great distance below the bottom of the Reith Bank-1A well although the scanty micro-paleontological evidence puts the sequence much later. The two later mega-sequences could have been initiated by tectonic uplift of their source area.

In the four lower members sand/mud ratios are high (3.3-7.7), while in the fifth the ratio is only 1.5 and both sands and muds occur in very thick beds. Dipmeter profile and sand/mud ratios have been used to develop a model in which Members 1-4 were formed on an alluvial plain east of a faulted highland area; rivers were predominantly braided. Member 5, by contrast, formed in a meander belt flood plain further from the source than the previous members (Fig. 3.7). This model does not account for two important features. A possible unconformity has been recognised from dipmeter logs at 8812 ft. This occurs between Member 3 and 4 and coincides with a marked change in the character of measured dip directions. Unimodal in the lower succession, the distributions above are distinctly polymodal. This evidence suggests that sinuosity of channels may have increased during the deposition of Member 4 giving rise to meandering conditions for Member 5. The possibility of drier climatic conditions and a steady water flow can not be ruled out fot the deposition of Member 5.

Petrological and geochemical studies of sidewall and conventional core samples assign sandstones to the arenite or feldspathic arenite categories with the feldspar content in the lower beds reaching 25%. Lithoclasts are scarce; some quartzitic and volcanic fragments are present. A

granitic provenance with minor contributions from metamorphic and volcanic sources is inferred.

Paleocurrent evidence from dipmeter logs indicates dominant flow from a south-westerly quadrant as measured in the present geography. Rotating Seychelles to a Gondwana position transposes the current directions from south-west to west or northwest.

Paleogeographic reconstruction of Triassic times places the Seychelles off the north-east coast of Madagascar. Eroded detritus from a basement of granitic rocks was transported eastwards to a Karoo basin in which the Seychelles formed in part a positive area of little or no deposition (Fig 5.1, 5.2).

Diagenesis is dominated by quartz overgrowth. Preliminary results from fluid inclusion studies indicate a temperature of 100°C associated with quartz precipitation. Porosity is also reduced by clays. Authigenic kaolinite, illite-smectite and chlorite are present (Fig. 8.1). The last diagenetic mineral is ferroan dolomite which, as well as clays, occupies enlarged pores.

The apparent lack of porosity visible in thin sections contrasts with significant flow rates measured by drill stem tests. Microporosity associated with clays and corroded feldspars may contribute to the permeability while flow rates may also be enhanced by bedding surfaces (which are not recognisable in chippings) and fracturing both of sandstones and mudstones. Another possibility is that cemented and uncemented zones alternate in the sandstones and only cemented samples were obtained.

The burial history of Karoo and later sediments suggests that hydrocarbon generation in Jurassic and Cretaceous rocks, such as those in down-faulted troughs like those indicated by Owen Bank-1 well, may have taken place in early Tertiary times after quartz precipitation. Migration of these hydrocarbons would have been possible into uplifted Karoo sediments.

8.1.2 Elk Point Group:

The Elk Point Group of Alberta is a cyclic sequence of evaporites, carbonate and clastic rocks deposited in a slowly expanding and filling basin. The sediments of the Elk Point Group are found at depths greater than 4500 ft. The thickness of sediments is of the order of few hundred feet.

The dominating lithologies of the Watt Mountain, Keg River, Chinchaga and Granite Wash Formations in the study area are shale and sandstone with minor amounts of limestone, dolomite, anhydrite and marlstone.

The sediments of the Chinchaga, Keg river and Watt Mountain Formations were laid

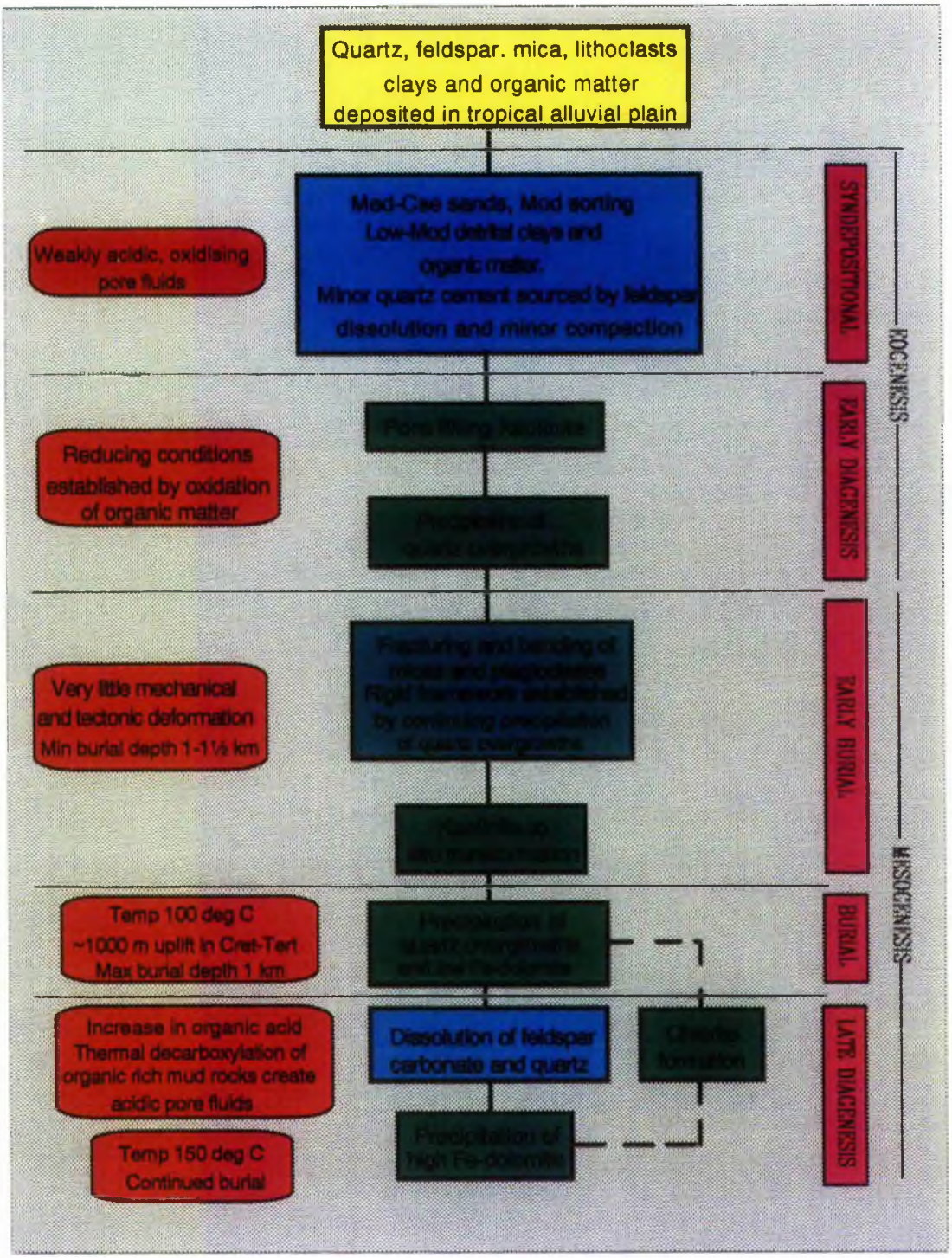

Fig. 8.1 Flow chart showing principal diagenetic reactions in the Karoo sandstones.

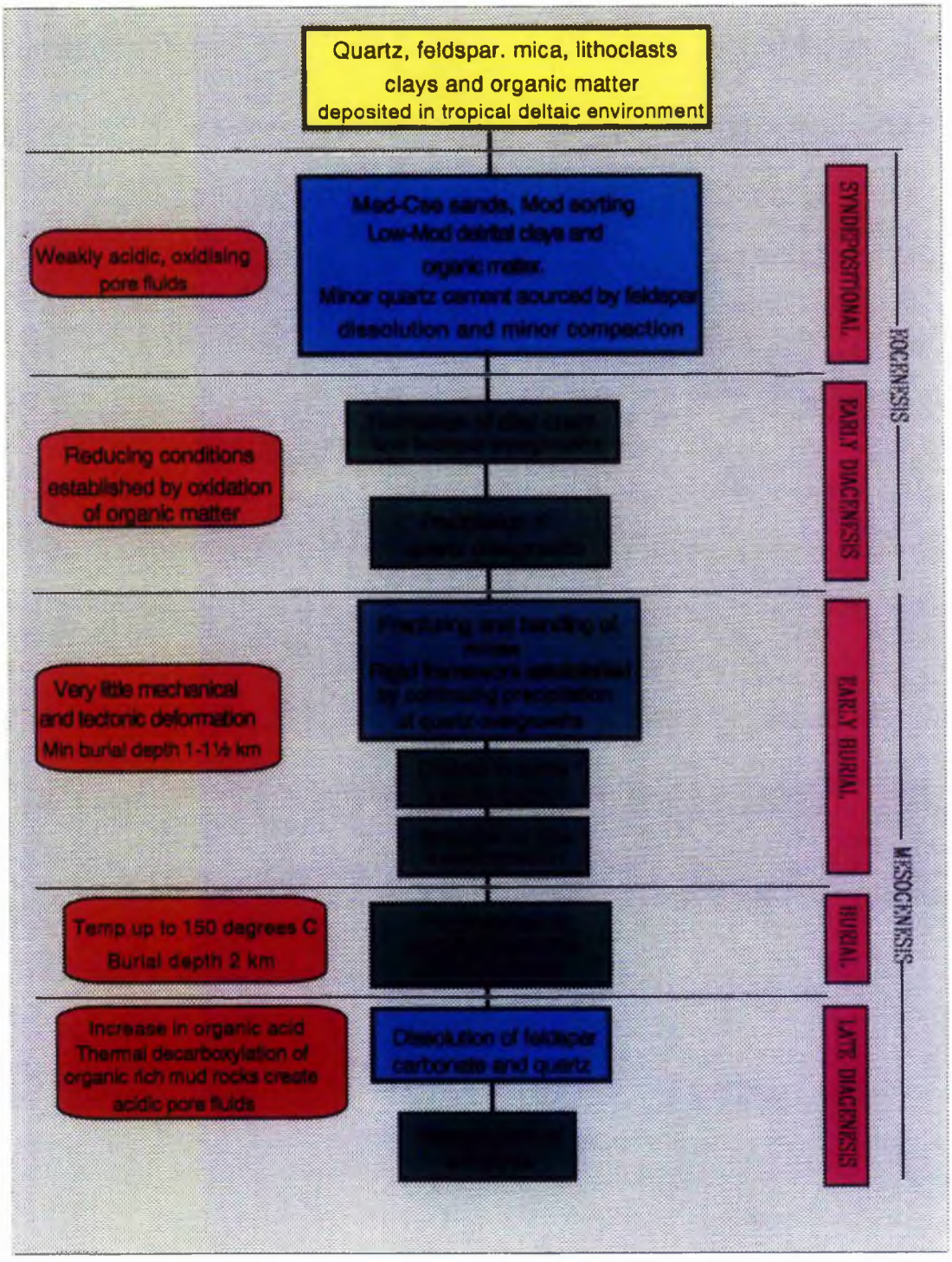

Fig. 8.2 Flow chart showing principal diagenetic reactions in the Elk Point sandstones.

down as shallow water fluvial-dominated deltaic deposits; Granite Wash lithology was deposited by a fan-delta system. The Elk Point Group is interpreted as a *sequence* mainly deposited as a Highstand Systems Tract with deposition under retrogradation. The individual sandstone formations are *parasequence sets*. Within the Watt Mountain Formation two flooding surfaces are represented by bioturbated shales.

The sandstones are quartz arenites, subarkoses and exceptionally sub-litharenite and litharenites, with feldspar contents greater in sandstones from the Granite Wash (varying between 5% and 30%). The sediments were derived from the igneous-metamorphic terrain of the Peace River Arch.

Diagenesis is dominated by quartz overgrowths, clay and carbonate (Fig. 8.2). A repetitive sequence of diagenetic episodes up to the formation of carbonate can be seen amongst the four formations of the Elk Point Group. It is suggested that this cyclicity was controlled by episodes of marine flooding between the formations. Pore filling anhydrite is the last diagenetic mineral. It was deposited in a single episode through the entire sequence due to remobilisation of Devonian evaporitic anhydrites by Cretaceous seawaters.

In addition, porosity in the sandstones has been considerably reduced by other minerals. Illite and chlorite are the dominant clays with small amounts of smectite and corrensite. Kaolinite is scarce. Fluid inclusion temperatures from quartz overgrowths give a temperature of 147-161°C, while isotopic analysis of carbonate cements give a temperature of 65-100°C for calcite and 50-110°C for dolomite. The temperatures for carbonate could be higher by 50% if the brines were highly saline. The temperatures derived from quartz overgrowths are very high and may suggest a temperature of maximum burial rather than that at the time of formation of the overgrowths.

8.2 CONCLUSIONS:

The study shows that the course of diagenesis is not determined primarily by preburial, prediagenetic tectonic setting, provenance and depositional environments even though the Karoo deposits are entirely terrestrial, while the sediments of Elk Point Group are marginal, the petrology and diagenetic history of the two areas are remarkably similar (Fig. 8.3). Diagenetic reactions in sandstones, apart from those formed and buried exclusively in marine conditions follow similar trends irrespective of their depositional origin (fluvial/marginal).

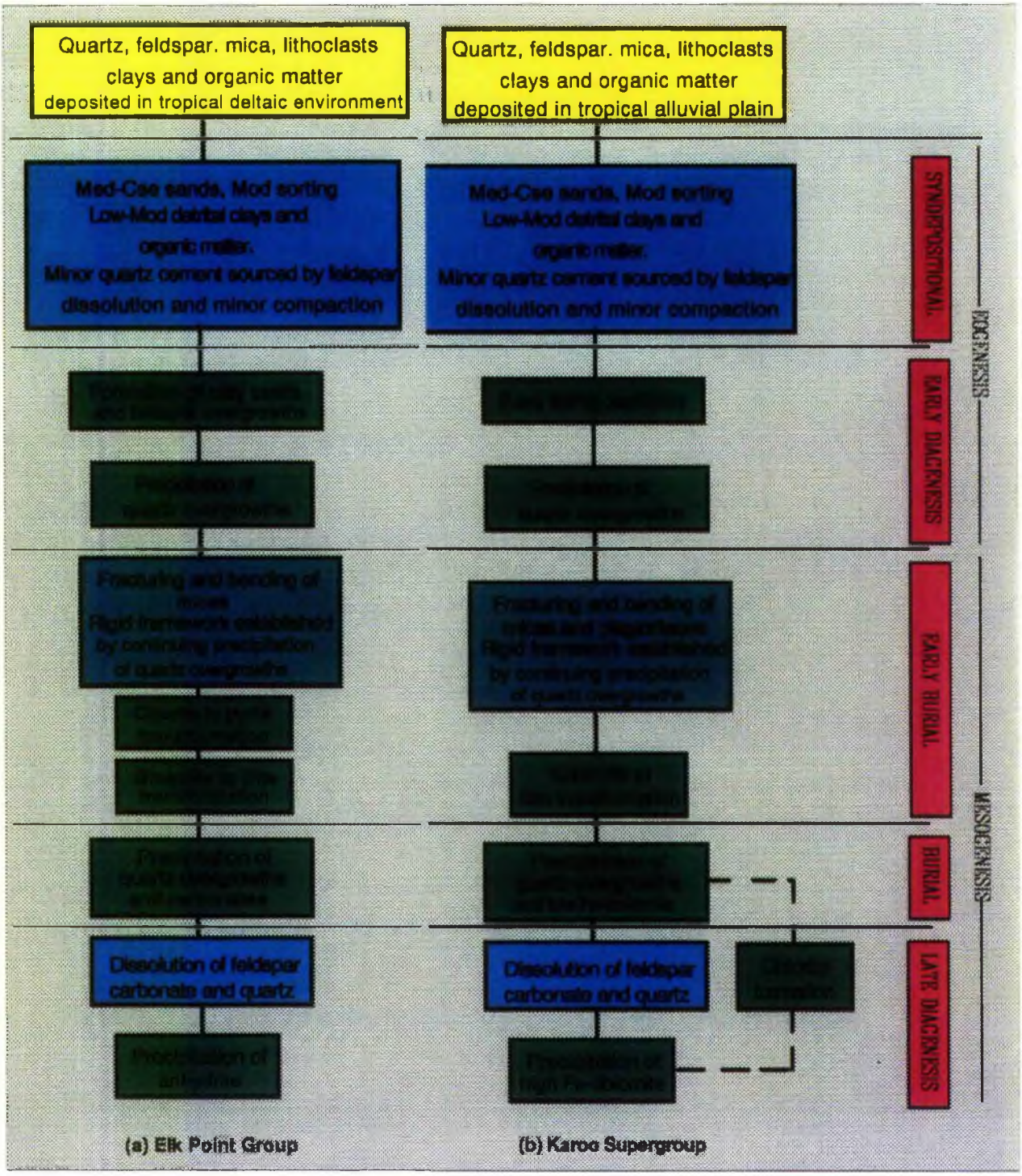

Fig. 8.3 Flow chart showing a comparasion of principal diagenetic episodes in the (a) Elk Point and (b) Karoo sandstones.

Petrological studies of both the sequences suggest that diagenesis was influenced by initially weakly acidic/neutral pore waters. The sediments of the two successions were deposited in tropical well-vegetated environments and eogenesis (early diagenesis) was influenced significantly by bacterial degradation of organic matter. In both cases feldspar, lithoclasts and mica were available from a granitic-metamorphic terrain for break-down to give a supply of silica. Fresh-water admixture in the sandstones of both the areas led to the formation of clays and quartz overgrowths.

No feldspar overgrowths have been seen in the Karoo sandstones, while Elk Point sandstones show varying thicknesses of overgrowth rims around detrital grains of feldspar.

Clays in the Karoo are dominated by kaolinite at shallow depths transforming into illite at greater depths. Chlorite is also present in the sandstones from greater depths. Elk Point sandstones largely have illite and chlorite with minor amounts of corrensite as clay; kaolinite is negligible. In both the cases some clays were formed prior to the formation of quartz overgrowths.

Late stage diagenesis was affected by marine flooding in the two areas; mid-Jurassic in case of the Karoo sandstones and upper Devonian in case of the Elk Point Group. With burial and increasing temperatures both silica and feldspars became unstable and were corroded. This led to the formation of carbonates. Further development of evaporitic conditions in the Elk Point Group study area gave rise to the anhydrite; a stage lacking in the diagenesis of the Karoo sandstones.

The differences of i) kaolinite vs illite and chlorite, ii) anhydrite, and iii) feldspar overgrowths in the Elk Point Group are due to i) depth of burial, ii) evaporitic environment, and iii) retention of pore fluids in the Elk Point Group forming a closed system as a result of intercalating impermeable marine shales.

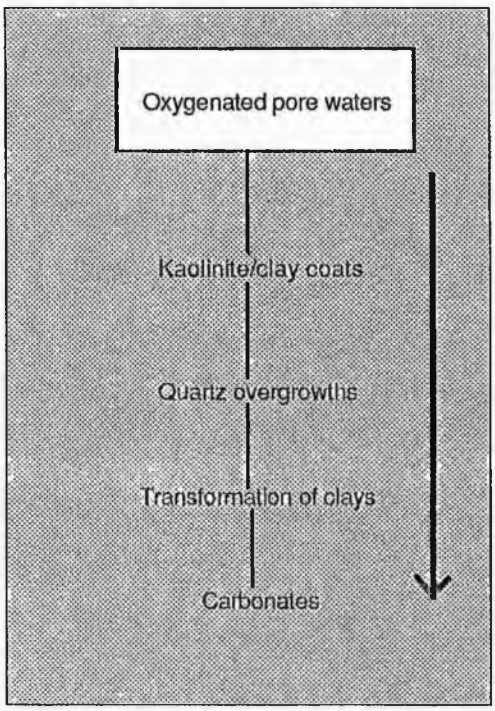

Fig. 8.4 Schematic diagenetic pathways in sandstones (modified form Burley *et al.*, 1985).

This study has led us to the development of a diagenetic paradigm based on Burley *et al.* (1985) for sandstones (fig. 8.4). Petrological work by other workers (Hemingway, 1968; Hawkins, 1978; Staub & Cohen, 1978; Almon & Davies, 1979; Edwards, 1979; Storey, 1979; Keighin & Fouch, 1981; Huggett, 1984; Cowan & Shaw, 1991) on sediments from various formations in Midlands (U.K.), Powder River Basin (U.S.A.), Belly River Formation in Central Alberta (Canada), Unita Basin (Utah), Trumfleet Field (West Yorkshire, U.K.), suggest that the eogenetic processes are dominated by the relatively rapid dissolution and reaction of amorphous and unstable components resulting in the formation of kaolinite or chlorite clay coats and the precipitation of quartz overgrowths. Initial diagenesis is influenced by acidic pore waters. Bacterial degradation of organic matter significantly influences the diagenesis.

The framework established by the eogenetic processes controls the mesogenesis. Continued compaction and the establishment of a rigid framework is dominant during mesogenesis. Transformation of various clays (phyllomorphic stage of Dapples, 1962), continued precipitation of quartz overgrowths and the formation of carbonates constitute an essential part of burial and late diagenetic features of mesogenesis.

8.3. Scope of Future Work:

A comprehensive sedimentological study of the Karoo Succession of Western Shelf, Seychelles has been made, subject to the limitation of complete core availability. Further confirmation and elucidation of the proposed model of Karoo sedimentation and paleogeographic reconstruction can be carried out if complete core (rather than cuttings) were made available. New material, if obtainable from future bore holes for study, would also help in the determination of stable isotopic composition and fluid inclusions of diagenetic minerals.

Wider correlation with bore holes in Madagascar and Africa will also be of immense use to strengthen the interpretation of the depositional environment for the Karoo Succession of Western Shelf, Seychelles. Such a correlation might also help confirm the probable unconformity between Member 3 and Member 4 occuring at Reith Bank-1 over a wider area.

A study of post-Karoo marine sediments should be undertaken to improve the division of the successions with a view to interpretation in terms of Sequence Stratigraphy (Van Wagoner *et al.*, 1988) and to test a Global Cyclostratigraphic Model (Perlmutter & Matthews, 1989). However, the samples available for study would only include side wall cuttings, which do not help in

determining the diagenetic sequences and their effects on reservoir quality.

The possibility of developing a detailed sedimentological model and paleogeographical reconstruction for the Elk Point Group of Alberta, Canada would be possible if complete cores and more petrophysical logs were available for study.

The most significant outcome of the present study is the similarity in the sequence of diagenetic episodes found in the sandstones from the fluvial (Karoo) and the deltaic (Elk Point) sequences. Further research into this aspect of sandstone diagenesis from a wider variety of depositional setting should be carried out to refine the existing paradigm for the diagenesis of sandstones in general.

BIBLIOGRAPHY

AAGAARD, P. 1979. Thermodynamic and kinetics analyses of silicate hydrolyses of low temperatures and pressures: Ph.D. dissertation, Berkley University of California, 126p.

ALCOCK, F.G. & BENTEAU, R.I. 1976. Nipsi Field- a middle Devonian clastic reservoir. In: *The sedimentology of selected clastic Oil & Gas reservoirs in Alberta.*ed. Lerland, M.M. *Canadian Society of Petroleum Geology* Spec Pub, 1-24.

ALMON, W.R. & DAVIES, D.K. 1979. Regional diagenetic trends in the Lower Cretaceous Muddy Sandstone, Powder River Basin. *In: Aspects of Diagenesis,* eds. Scholle, P.A. & Schluger, P.R., *Soc. Econ. Paleontol. & Mineral.*, Spec Pub. **26**, 379-400.

AM. ASSOC. PETROLEUM GEOLOGISTS & U.S. GEOLOGICAL SURVEY, 1976. Geothermal gradient map of North America. *United States Geological Survey.* Scale 1:5,000,000. 2 sheets.

ANON. 1908. The development of the resources of Seychelles. *Bull. Impl Inst.*, **6**, 121-126.

ANON. 1911. Guano deposits of Assumption island, Seychelles. *Bull. Impl Inst.*, **9**, 39-44.

AULSTEAD, K.L. & SPENCER, R.J. 1985. Diagenesis of the Keg River formation, northwestern Alberta: A fluid inclusion evidence. *Bull. Can. Petroleum Geology*, **33** (2), 167-183.

AYERS, F.M. 1952. Geology of the Wajir Mandera district, north-east Kenya. *Geol. Surv. Kenya Report,* **48**, 65p.

BAILLIE, A.D. 1953. Devonian system of Williston Basin area. *Manitoba Department of Mines and Natural Resources, Mines Branch*, Pub. 52-5.

BAKER, B.H. 1963. Geology and mineral resources of the Seychelles Archipelago. *Geol. Surv. Kenya Mem.*, **3**, 140.

BAKER, B.H. & MILLER, J.A. 1963. Geology and geochronology of the Seychelles islands and structure of the floor of the Arabian sea. *Nature,* **199**, 346-348.

BASU, A. 1985. Reading provenance from detrital quartz. In: *Provenance of Arenites,* ed. Zuffa, G.G. NATO ASI Series, **148**, 231-248.

BASU, A. YOUNG, S.W., SUTTNER, L.J., JAMES, W.C. & MACK, G.H. 1975. Re-evaluation of the use of undulatory extinction and polycrystallinity in detrital quartz for provenance interpretation. *Jour. Sed. Petrology,* **45**, 873-882.

BAUER, M. 1898. Beitrage Zur Geologie der Seychellen, insbesondere zur Kenntniss des Laterits. *Neues Jahrb. Min.*, Bd **2**, 163-219.

BELTRANDI, M.I. & PYRE, A. 1973. Geological evolution of southwest Somalia. In: *Bassins Sedimentaries du Littoral Africain, 2, Littoral Austral et Oriental. Assoc. Services Geol. Africaine, Paris.* 159-178.

BELYEA, H.R. 1952. Notes on the Devonian system of the north central plains of Alberta. *Canadian Geological Survey*, paper 52-27, 66p.

BELYEA, H.R. 1959. Devonian Elk Point group, central and southern Alberta. *Canadian Geological Survey*, paper 59-2, 14p.

BERNER, R. A. 1978. Rate controls of mineral dissolution under Earth surface conditions. *Am. J. Sci.*, **278**, 1235-1252.

BIEN, G.A., CONTOIS, D.E. & THOMAS, W.H. 1959. The removal of soluble silica from fresh water entering the sea. In: *Silica in Sediments-Soc. Econ. Paleontol Mineral., Spec. Pub.*, 7, 20-35.

BJORLYKKE, K. 1984. Formation of secondary porosity: How important is it? In: *Clastic diagenesis,* eds. David, A. & Surdam, R.C., *Am. Assoc. Petroleum Geologists Mem.*, **37**, 277-286.

BLISSENBACH, E. 1954. Gelogy of alluvial fans in semiarid regions. *Geol. Soc. Amer.Bull*, **65**, 175-190.

BLUCK, B.J. 1964. Sedimentation of an alluvial fan in Southern Nevada. *J. Sedim. Petrol.*, **34**, 395-400.

BOLES, J.R. & FRANKS, S.G. 1979. Clay diagenesis in Wilcox sandstones of Southwest Texas: implications of smectite diagenesis on sandstone cementation. *J. Sedim. Petrology,* **49**, 55-70.

BRAUN, W.I. 1966. Stratigraphy and microfauna of Middle and Upper Devonian formations, Norman Wells area, Northwest territories, Canada. *N. Jb. Geol. palaeont. Abh.*, **125**, 247-264.

BRIGGS, I.C. 1974. Machine contouring using minimum curvature. *Geophysics.* **39** (1), 39-48.

BROWNLOW, A.H. 1979. Geochemistry. *Prentice-Hall, Englewood Cliffs.*298p.

Bull, W.B. 1964. Alluvial fans and near-surface subsidence in Western Fresno County California. *United States Geol. Surv.*, Professional paper 437-A, 71p.

Bull, W.B. 1972. Recognition of alluvial-fan deposits inthe stratigraphic record. In: *Recognition of ancient sedimentary environments*, eds., Hamblin, W.K. & Rigby, J.K., *Soc. Econ. Paleontol. Mineral.*, Spec. Pub. 16, 63-83.

Buller, J.V. 1958. The sub-Ashern stratigraphy of north-west Saskatchewan. *Oil in Canada*, **10** (23), 34-52.

Burley, S.D., Kantorowicz, J.D. & Waugh, B. 1985. Clastic diagenesis. In: *Sedimentology: Recent developments and applied aspects*, eds., Brenchley, P.J. & Williams, B.P.J., *Geological Society London*, 189-226.

Burley, S.D., Mullis, J. & Matter, A. 1989. Timing diagenesis in the Tartan Reservoir (U.K. North Sea): constraints from combined cathodoluminescence microscopy and fluid inclusion studies. *Mar. Pet. Geol.* **6**, 98-120.

Burns, L.K. & Ethridge, F.G. 1979. Petrology and diagenetic effects of lithic sandstones: Paleocene and Eocene Umpqua Formation, southwestern Oregon. In: *Aspects of diagenesis*, eds. Scholle, P.A. & Schluger, P.R. *Soc. Econ. Paleontol. & Mineral.*, Spec. Pub. 26, 141-152.

Burwash, R.A. 1957. Reconnaissance of subsurface Precambrian of Alberta. *Am. Assoc. Petroleum Geologists Bull.*, **41**, 70-103.

Burwash, R.A., Baadasgaard, H., Peterman, Z.E. & Hunt, G.H. 1964. Precambrian. In: *Geological History of Western Canada*, eds. McGrossan, R.G. & Glaister, R.P., *Alberta Soc. of Petroleum Geologists*, 14-19.

Buschendorf, F., Nielsen, H., Puchelt, H. & Ricke, W. 1963. Schwefel- Isotopen-Untersuchungen am Pyrit-Sphalerit- Baryt-Lager Meggen/Lenne (Duetschland) und an verschieden Devon-Evaporiten. *Geochim. Cosmochim. Acta*, **27**, 501-523.

Carothers, W.W. & Kharaka, Y.K. 1980. Stable isotopes of HCO_3 in oil-field waters-implications for the origin of CO_2. *Geochim. Cosmochim. Acta*, **44**, 323-332.

Choquette, P.W. & Pray, L.C. 1970. Geologic nomenclature and classification of porosity in sedimentary carbonates. *Amer Assoc Petroleum Geologists Bull*, **54**, 407-450.

Christie, H.H. 1971. Mitsue oil field: a rich stratigraphic trap. *Eigth World Petroleum Congress*, Proc., **2**, 269-274.

Claypool, G.E., Holser, W.T., Kaplan, I.R., Sakai, H. & Zak, I. 1980.The age curves of sulfur and oxygen isotopes in marine sulfate and their mutual interpretation. *Chem. Geol.*, **28**, 199-260.

Corrigan, A.F. 1975. The evolution of a Cratonic Basin from a Carbonate to Evaporitic Deposition and the Resulting Stratigraphic and Diagenetic Changes, Upper Elk Point Group, Northwestern Alberta. *The University of Calgary*,Unpub. Ph.D. thesis.

Cowan, G & Shaw, H. 1991. Diagenesis of Namurian Fluvio-deltaic sandstones from the Trumfleet Field, South Yorkshire. *Mar. Pet. Geol.*, **8**, 212-214.

Craig, H. 1957. Isotopic standards for carbon and oxygen and correction factors for mass-spectrometric analysis of carbon dioxide. *Geochim. Cosmochim. Acta*, **12**, 133-149.

Craig, H. 1961. Standards for reporting concentrations of deuterium and oxygen-18 in natural waters. *Science*, **133**, 1833-1834.

Crickmay, C.H. 1954. Palaeontological correlation of Elk Point and equivalents. In: *Ralph Leslie Rutherford Memorial volume, Western Canada Sedimentary Basin, a symposium*, ed. Clark, L.M. *Am. Assoc. Petroleum Geologists*, 143-158.

Curtis, C.D. 1977. Sedimentary geochemistry; environments and processes dominated by involvement of an aqueous phase. *Phil. Trans. R. Soc.*, **A286**, 353-371.

Coffin, M.F. 1990. The East African and Madagascan Margins: Stratigraphy, structure and tectonics. *Proc. First Regional Seminar on Petroleum Exploration, Seychelles* (in press).

Dapples, E.C. 1962. Stages of diagenesis in the development of Snadstones. *Geol. Soc. Amer. Bull.*, **73**, 913-934.

Davies, D. 1968. When did the Seychelles leave India?, *Nature*, **220**, 5173, 1225-1226.

Donaldson, A.C., Martin, R.H. & Kanes, W. H. 1970. Holocene Guadalupe Delta of Texas Gulf Coast. In: *Deltaic sedimentation: Modern and Ancient*,

eds., Morgan, J.P. & Shaver, R.H., *Soc. Econ. Paleontol. & Mineral.*, Spec. Pub. 15, 107-137.

Doveton, J.H. 1986. Log analysis of subsurface geology. *John Wiley & Sons, New York.* 273p.

Du Toit, A. 1937. Our wandering continents. *Oliver & Boyd*, Edinburgh, 366.

Dunoyer de Segonzac, G. 1970. The transformation of clay minerals during diagenesis and low grade metamorphism: a review. *Sedimentology,* **15**, 281-376.

Dupont, P.R. 1907. On a visit of investigation to St. Pierre, Astove, Cosmoledo, Assumption and the Aldabra Group of Seychelles Islands. *Unpub. report to the Governor of the Seychelles.*

Dupont, P.R. 1916. Aldabra, its Guano deposits and other resources. *Unpub. report to Government of Seychelles.*

Dupont, P.R. 1928. Seychelles Guano deposits. *C.R. 14th Int. Geol. Congr.*, 2, 609-610.

Ecklemans, V. 1968. Variations du rapport isotopique $^{32}S/^{34}S$ dans des anhydrites d'evaporites du devonien moyen superieur de Tournai et de Leuze. *Univ. Liege Fac. Sci.*, Annee Acad. 1967-1968, 45p.

Edwards, M.B. 1979. Sandstone in Lower Cretaceous Helvetiajellet Formation, Svalbard. Bearing on reservoir potential of Barents Shelf. *Am. Ass. Petrol Geol. Bull.* **63**, 2193-2203.

Elliot, T. 1986. Siliciclastic shorelines. In: *Sedimentary Environments & Facies,* ed. Reading, H.G. *Blackwell Scientific Publication,* 2ndn Ed., 155-189.

Fisher, R.L., Johnson, G.L. & Heezen, B.C. 1967. Mascarene plateau, Western Indian Ocean. *Geol. Soc. Amer. Bull.*, **78**, 10, 1247-1260.

Fontes, J-C. & Pierre, C. 1978. Oxygen 18 changes in dissolved sulphate during sea water evaporation in saline ponds (abs). In: *10th Int. Congr. on Sedimentology,* Jerusalem, 215-216.

Folk, R.L. 1964. Petrology of sedimentary rocks. *Hemphill Book Store*, Austin, Texas. 154p.

Forster, R. 1975. The geological history of the sedimentary basins of southern Mozambique, and some aspects of the origin of the Mozambique channel. *Paleoogeogr. Paleoclimatol. Paleoecol.*, **17**, 267-287.

Francis, T.J.G., Davies, D. & Hill, M.N. 1966. Crustal structure between Kenya and the Seychelles. In: *A discussion concerning the floor of the northwest Indian Ocean. Royal Soc. London Phil. Trans.*, ser. A, 259, 1099, 240-261.

Frankel, J.J. 1969. A mega-porphyritic dolerite on Long Island, Seychelles archipelago. *Geol. Mag.*, **106**, 3, 260-268.

Frankel, J.J. & Kent, L.E. 1964. On rocks from the Seychelles Islands. *22nd Intn. Geol. Congr.*, New Delhi, **10**, 161-190.

Frazier, D.E. 1967. Recent deltaic deposits of the Mississippi River; their development and chronology. *Trans. Gulf-Cst. Ass. geol. Socs.*, **17**, 287-315.

Friedman, I. & O'Neil, J.R. 1977. Compilation of stable isotope fractionation factors of geochemical interest. In: *Data of Geochemistry,* ed. Fleischer, M. 6th ed., *U.S. Geological Survey* Professional Paper 440-KK, 12p.

Fryer, J.C.F 1911. The structure and formation of Aldabra and neighbouring islands with notes on their flora and fauna. *Trans. Linn. Soc. Zool.*, **14**, 11, 397-441.

Galloway, W.E. 1974. Deposition and diagenetic alteration of sandstone in Northeast Pacific arc-related basins: implications for graywacke genesis. *Geol. Soc. Amer. Bull.*, 85, 379-390.

Galloway, W.E. 1977. Catahoula Formation of the Texas Coastal Plain-depositional systems, mineralogy, structural development, ground-water flow history, and uranium distribution. *University of Texas Bureau of Economic Geology Report of investigations*, **87**, 59p.

Galloway, W.E. & Hobday, D.K. 1983. Terrigenous Clastic Depositional Systems. *Springer, New YorK.*

Gardiner, J.S. 1906. Investigations in the Indian Ocean. *Proc. Brit. Assoc.*, 1-9.

Giles, M.R. & De Boer, R.B. 1989. Secondary porosity: creation of enhanced porosities in the subsurface from the dissolution of carbonate cements as a result of cooling formation waters. *Mar. Pet Geol.* **6**, 261-269.

Giles, M.R. & De Boer, R.B. 1990. Origin and significance of redistributional secondary porosity. *Mar. Pet Geol.* **7**, 378-397.

GRAYSTON, L.D., SHERWIN, D.F., & ALLAN, J.F. 1964. Middle Devonian. In: *Geological history of Western Canada*, Mc Crossan, R.G., & Glaister, R.P. eds. *Alberta Society of Petroleum Geologists*, 49-59.

GROSS, M.G. 1964. Variations in the O^{18}/O^{16} and C^{13}/C^{12} ratios of diagenetically altered limestones in the Bermuda Islands. *Jour. of Geol.*, **72**, 170-194.

GREENWALT, W.A. JR. 1956. Granite Wash of the Peace River area. *J. Alberta Soc. Petroleum Geologists*, **4**, 204-205.

GUTHRIE, D.D. 1956. Gilwood sandstone in the Giroux Lake area, Alberta. *J. Alberta Soc. Petroleum Geologists*, **4**, 227-231.

HACQUEBARD, P.A. 1977. Rank of coal as an index of organic metamorphism for oil and gas in Alberta. In: *The origin and migration of petroleum in the Western Canada Sedimentary Basin, Alberta*, eds. Deroo, G., Powell, T.G., Tissot, B. & McCrossan, G. *Geological Survey of Canada Bulletin* 262, 11-22.

HAWKINS, P.J. 1978. Relationship between diagenesis, porosity reduction and oil emplacement in late Carboniferous andstone reservoirs: Bothamsall OilField, East Midlands. *J. geol. Soc. London*, **135**, 7-34.

HEMINGWAY, J.E. 1968. Sedimentology of coal bearing strata. *In: Coal and coal bearing strata*, eds., Murchison, D. & Westoll, T.S. *Oliver & Boyd, Edinburgh*, 43-69.

HITCHON, B. 1984. Geothermal gradients, hydrodynamics, and hydrocarbon occurrences, Alberta, Canada. *Am. Assoc. Petroleum Geologists Bull.*, **68**, 713-743.

HOFFMAN, J. & HOWER, J. 1979. Clay mineral assemblages as low grade metamorphic geothermometers. In*: Application to thrust faulted disturbed belt of Montanna, U.S.A.*eds. Schole, P.A. & Schluger, P.R. *Soc. Econ. Palaeontol. Mineral.*, Spec. Pub. 26, 35-79.

HOOKE, R.L.B. 1967. Processes on arid-region alluvial fans. *Jour. of Geol.*, **75**, 438-460.

HOWER, I., ESLINGER, E.V., HOWER, M.E. & DERRY, E.A. 1976. Mechanism of burial metamorphism of argillaceous sediments, mineralogical and chemical evidence. *Geol. Soc. Amer. Bull.*, **87**, 725-735.

HRISKEVICH, M.E. 1966. Stratigraphy of Middle Devonian and older rocks of the Banff-Aquitaine Rainbow West 7-32 discovery well, Alberta. *Bull. Can. Petroleum Geology*, **14**, 523-527.

HUDSON, J.D. 1977. Stable isotopes and limestone lithification. *Jour. Gelogical Society London*, **133**, 637-660.

HUGGETT, J.M. 1982. The growth and origin of authigenic clay minerals in sandstones. *University of London*, Unpub PhD dissertation.

HUGGETT, J.M. 1984. Controls of mineral authigenesis in Coal Measures Sandstones of the East Midland, U.K. *Clay Min*, **19**, 343-357.

HURST, A. & IRWIN, H. 1982. Geological modelling of clay diagenesis in sandstones. *Clay Min*, **17**, 5-22.

HUTCHEON, I. 1981. Applications of thermodynamics to clay minerals and authigeniuc mineral equilibria. In: *Short course handbook 7. Clays and the Resource Geologist*, ed. Longstaff, F.J. *Mineral Association of Canada.*

HUTCHEON, I., OLDERSHAW, A. & GHENT, E.D. 1980. Diagenesis of Cretaceous sandstones of the Kootenay Formation at Elk Valley (Southeastern British Columbia). *Geochim. Cosmochim. Acta*, **44**, 1425-1436.

IRWIN, H., CURTIS, C. & COLEMAN, M. 1977. Isotopic evidence for source of diagenetic carbonates formed during burial of organic-rich sediments. *Nature*, **269**, 209-213.

JANSA, L.F. & FISCHBUCH, N.R. 1974. the evolution of a Middle and Upper Devonian sequence from a clastic coastal plain - deltaic complex into overlying carbonate reef complexes and banks, Sturgeon-Mitsue area, Alberta. *Geol. Surv. Canada Bull.*, **234**, 105p.

KAMENKAYE, M. 1978. Permian to Tertiary faunas and paleogeography: Somalia, Kenya, Tanzania, Mozambique, Madagascar and South Africa. *Jour. Petrol. Geol.*, **1**, 1, 79-101.

KAMENKAYE, M. & MEYERHOFF, A.A. 1980. Petroleum geology of the Mascarene Ridge, Western Indian Ocean. *Jour. Petrol. Geol.*, **3**, 2, 123-138.

KEIGHIN, C.W. & FOUCH, T.D. 1981. Depositional environments and diagenesis of some non-marine Upper Cretaceous reservoir rocks. Uinta Basin, Utah. *In: Recent and Ancient No-marine Depositional Environments: Models for*

Exploration, eds. Ethridge, F.G. & Flores, R.M. *Soc. Econ. Miner. Paleont.,* Spec Pub. **31**, 109-125.

KENT, P.E. 1974. Continental margin of East Africa- aregion of vertical movements. In: *The Geology of Continental Margins,* eds. Burk & Drake, *Springer Verlag,* 313-320.

KENT, P.E., HUNT, J.A. & JOHNSTONE, D.H. 1971. The geology and geophysics of coastal Tanzania. *Inst. Geol. Sci. Lon.,* Geophysics Paper, **6**, 101p.

KHANNA, M. 1990. Diagenesis & Palaeogeography of Karroo sandstones, Western Shelf, Seychelles: A potential for hydrocarbon exploration (abs). *Sediments 1990, 13th International Sedimentological Congress,* Nottingham, 270.

KHANNA, M. & WALTON, E.K. 1990. Provenance and diagenesis of Karoo sandstones, Western Shelf, Seychelles (abs). *British Sedimentological Research Group,* Reading.

KHANNA, M. & WALTON E.K. 1990. Petrological studies of Karroo sandstones, Western shelf, Seychelles. *Proc. First Regional Seminar on Petroleum Exploration, Seychelles* (in press).

KHANNA, S.N. & PILLAY, G.E. 1986. Seychelles: Petroleum potential of this Indian Ocean paradise. *Oil & Gas J.* (Mar. 1986), 136-139.

KHANNA, S.N. & PILLAY, G.E. 1987. Seychelles geology, hydrocarbon potential. *Oil & Gas J.* (Feb 1987), 43-44.

KHANNA, S.N. & PILLAY, G.E. 1988. Geology and petroleum prospects of Seychelles. Paper presented to *7th Offshore South East Asia Conference,* Singapore 1988.

KHARAKA, Y.K., CAROTHERS, W.W. & ROSENBAUER, R.J. 1983. Thermal decarboxylation of acetic acid: implications for origin of natural gas. *Geochim. Cosmochim. Acta,* **47**, 397-402.

KINDLE, E.M. 1914. The Silurian and Devonian section of western Manitoba. *Canada Geological Survey Memoir* 174, p 194E.

KRAMERS, J.W. & LERBEKMO, J.F. 1967. Petrology and mineralogy of Watt Mountain formation, Mitsue-Nipsi area, Alberta. *Bull. Can. Petroleum Geology,* **15** (3), 346-378.

KYLE, P.R., ELLIOT, D.H. & SUTTER, J.F. 1981. Jurassic Ferrar Supergroup tholeiites from the transantarctic mountains, Antarctica, and their relationship to the initial fragmentation of Gondwana. In: *Gondwana Five, Proc. Int. Gondwana Symp.*, 5th (Wellington, New Zealand, 11-16 February, 1980). Bakema, Rotterdam, eds. Cresswell M.M. & Vella D., 283-288.

LAND, L.S. 1983. The application of stable isotopes to studies of the origin of dolomite and to problems of diagenesis of clastic sediments. In: *Stable isotopes in sedimentary geology,* eds Arthur, M.A. *et al, Soc Econ. Paleontol. Mineral.,* Short Course No 10, Dallas, 4.1-4.22.

LAND, L.S. 1984. Frio Sandstone Diagenesis, Texas Gulf Coast: A Regional Isotopic Study. In: *Clastic Diagenesis,* eds. McDonald, D.A. & Surdam, R.C., *Am. Assoc Petroleum Geologists.,* 47-62.

LANE, D.M. 1959. Dawson Bay Formation in the Quile' Lakes- Qu' Appelle area, Saskatchewan. Saskatchewan *Department of Mineral Resources Report* 38, 49p.

LAW, JAMES 1955. Gelogy of north-west Alberta and adjacent areas. *Am. Assoc. Petroleum Geologists Bull.,* **39** (10), 1927-1978.

LAWRENCE, J.R. & TAYLOR, H.P. 1971. Deuterium and oxygen-18 correlation: clay minerals and hydroxides in Quaternary soils compared to meteoric waters. *Geochim. Cosmochim. Acta,* **35**, 993-1003.

LONGSTAFFE, F.J. 1986. Oxygen isotope studies of diagenesis in the basal Belly river sandstone, Pembina I-Pool, Alberta. *J. Sedim Pet.,* **56**, 1, 78-88.

MATTER, A. & RAMSEYER, K. 1985. Cathodoluminescence microscopy as a tool for provenance studies of sandstones. In: *Provenance of Arenites,* ed. Zuffa, G.G. NATO ASI Series, **148**, 191-212.

MCCAMIS, J.G. & GRIFFITH, L.S. 1967. Middle Devonian facies relationships, Zama Basin, Alberta. *Bull. Can. Petroleum Geology,* **20**, 187-237.

MCCREA, J.M. 1950. On the isotopic chemistry of carbonates and a paleotemperature scale. *J. Chem. Phys.,* **18**, 849.

MCGHEE, J.R. 1949. Pre-waterways Palaeozoic stratigraphy of Alberta plains. *Am. Assoc. Petroleum Geologists Bull.*, **33**, 603-613.

McGILL, P. 1966. Ostacods of probable late Givetian age from Slave Point formation, Alberta. *Bull. Can. Petroleum Geology,* **39** (10), 1927-1976.

MEYER, H. 1980. Preliminary evaluation of the mineral potential of the Silhouette Island. *Unpub. U.N. report.* 6p.

MIALL, A.D. 1984. Deltas. In: *Facies Models,* eds., Walker, R.G., *Geoscience Canada reprint series* 1, 105-118.

MIALL, A.D. 1984b. Principles of Sedimentary Basin Analysis. *Springer-Verlag, New York,* 490p.

MIALL, A.D. 1985. Architectural-Element Analysis: A new method of Facies Analysis applied to Fluvial Deposits. *Earth Scl. Rev.,* **22**, 261-308.

MINERALOGY INC. 1981. Discussion of porosity and permeability; thin section description; x-ray diffraction mineralogy and scanning electron microscopic analysis of core plugs from the Seychelles Reith Bank #1 and the Seychelles Seagull Shoals #1. *An unpub. report.*

MOLNAR, P., PARDO-CASAS, F. & STOCK, J. 1988. The Cenozoic and late Cretaceous evolution of the Indian Ocean Basin: uncertainties in the reconstructed positions of the Indian, African and Antarctic plates. *Basin Research,* **1**, 23-40.

NADEAU, P.H., WILSON, M.J., Mc HARDY, W.J. & TAIT, J.M. 1984a. Interstratified clays as fundamental particles. *Science,* **225**, 923-925.

NADEAU, P.H., WILSON, M.J., Mc HARDY, W.J. & TAIT, J.M. 1984b. Interparticle diffraction: a new concept for interstratified clays. *Clay Miner.* **19**, 757-769.

NADEAU, P.H., WILSON, M.J., Mc HARDY, W.J. & TAIT, J.M. 1985. The conversion of smectitie to illite during diagenesis: evidence from some illitic clays from bentonites and sandstones. *Mineral. Mag.* **49**, 393-400.

NADEAU, P.H. & BAIN, D.C. 1986. Composition of some smectites and diagenetic illitic clays and implications for their origin. *Clay & Clay Minerals,* **34**, 455-464.

NARAYANAN, K. & VOLLSET, J. 1987. Geological evolution of southern and eastern Africa before and after the break up of Gondwanaland. In: *Oil & Gas Exploration in SADCC Region,* eds. Southern Africa Development Coordination Conference Energy Sector, 85-128

NOPEC A.S. 1985. Study of the Basic Petroleum data in the Seychelles. I & II. 165p.

NORRIS, A.W. 1965. Startigraphy of Middle Devonian and older Paleozoic rocks of the Great Slave Lake region, Northwest Territories, *Geol. Surv. Canada Memoir* 322, 180p.

NORTON, I.O. & SCALTER, J.G. 1979. A model for the evolution of the Indian Ocean and the break-up of Gondwanaland. *J. Geophys. Res.* 84, 6803-6830.

OPEN UNIVERSITY, 1976. Sedimentary basin case study: The Western Canadian sedimentary basin. *The Open University Press, Milton Kynes,* 68p.

OSBORNE, M & HASZELDINE, S. 1990. Fluid inclusions in diagenetic quartz record oil fluid burial temperatures, not precipitation temperature (abs.). *British Sedimentological Research Group,* Reading.

PERLMUTTER, M.A. & MATTHEWS, M.D. 1989. Global Cyclostratigraphy-A Model. In: *Quantitative Dynamic Stratigraphy,* ed. Cross, T.A. *Prentice Hall,* 233-260.

PERRY, E.A. & HOER, J. 1970. Burial diagenesis in Gulf Coast peletic sediments. *Clay & Clay Minerals,* **18**, 165-177.

PIEL, K.M. 1971. Palynology of Oligocene sediments of central British Columbia. *Canadian Journal Botany,* 49, 1885-1920.

PIERRE, C. 1982. Teneurs en isotopes stables (^{18}O, ^{2}H, ^{13}C, ^{34}S) et conditions de genese des evaporites marines: application a quelques millieux actuels et au Messinien de la Mediterrannee. *University of South Paris, Orsay,* Thesis, 266p.

PIERRE, C. 1985. Isotopic evidence for the dynamic redox cycle of dissolved sulphur compounds between free and interstitial solutions in marine salt pans. *Chem. Geol.,* **53**, 191-196.

PIERRE, C. & FONTES, J-C. 1982. Etude isotopique des saumures et des gypses des marais salants de Salin-de-Giraud (Sud de la France). *Geol. Mediterr.,* 9, 4, 479-486.

PIERRE, C. & ROUCHY, J-M. 1986. Oxygen and sulfur isotopes in anhydrites from Givetian and Visean evaporites of Northern France and Belgium. *Chem. Geol.,* 58, 245-252.

PUGH, D.C. 1972. Subsurface lower Paleozoic stratigraphy in northern and central Alberta. *Geol. Surv. Canada*, Paper 72-12, 54p.

RABINOWITZ, P.D., COFFIN, M.F. & FALVEY, D. 1983. The separation of Madagascar and Africa. *Science*, **220** (4592), 67-69.

RAVELSON, E., ANDRIAMANANTENA, J, JEAN, R. & RAMANAMPISOA, L. 1990. The South Morondava Karroo and its petroleum potential. *Proc. First Regional Seminar on Petroleum Exploration, Seychelles* (in press).

REED, F.R.C. 1949. The geology of the British Empire. 2nd ed. *Edward Arnold & Co.*, London, 544-545.

RICHARDSON, S.M. & HANSEN, K.S. 1991. Stable isotopes in the sulfate evaporites from southeastern Iowa, U.S.A.: Indications of postdepositional change. *Chem. Geol.*, **90**, 79-90.

RIDER, M.H. 1986. The geological interpretation of well logs. *John Wiley & Sons, New York*. 175p.

RIDER, M.H. 1990. Gamma-ray log shape used as a facies indiactor; critical analysis of an oversimplified methodology. *Geol. Soc. London Spec. Pub.*, **48**, 27-37.

ROBERTSON RESEARCH INTERNATIONAL LTD. Nov., 1980. The Biostratigraphy and Palaeoenvironments of the interval 200' to 14340' with petrography of few selected field and cutting samples from the AMOCO Seychelles Petroleum Company Owen Bank-1A Well, Offshore Seychelles.

ROBERTSON RESEARCH INTERNATIONAL LTD. Aug., 1981a. The Biostratigraphy and Palaeoenvironments of the interval 1400' to 12,790' with petrography, X-ray diffraction and K/Ar age dating of selected samples from the AMOCO Seychelles Petroleum Company Reith Bank-1 Well, Offshore Seychelles.

ROBERTSON RESEARCH INTERNATIONAL LTD. Sept., 1981b. The Biostratigraphy and Palaeoenvironments of the interval 1181' to 8995' with petrography and K/Ar age dating of selected samples from the AMOCO Seychelles Petroleum Company Seagull Shoals-1 Well, Offshore Seychelles.

ROTTENFUSSER, B.A. & OLIVER, T.A. 1977. Depositional environments and petrology of the Gilwood member north of the Peace River Arch. *Bull. Can. Petroleum Geology*, **25** (5), 907-928.

ROYER, JEAN-YVES 1990. The opening of the Indian Ocean since Late Jurassic: An overview. *Proc First Regional Seminar on Petroleum Exploration*, Seychelles (in press).

SASS, B.M., ROSENBERG, P.E. & KITTRICK, J.A. 1987. The stability of illite/smectite during diagenesis: an experimental study. *Geochim. Cosmochim. Acta*, **51**, 2103-2115.

SAVIN, S.M. & EPSTEIN, S. 1970a. The oxygen and hydrogen isotope geochemistry of clay minerals. *Geochim. Cosmochim Acta*, **34**, 25-42.

SAVIN, S.M. & EPSTEIN, S. 1970a. The oxygen and hydrogen isotope geochemistry of ocean sediments and shales. *Geochim. Cosmochim Acta*, **34**, 43-63.

SCHLICH, R. 1974. Appendix I: bathymetric, magnetic and seismic reflection data, DSDP. *Natl. Sci. Fndt.*, DSDP Project 25, Washington, 763-829.

SCHLICH, R. 1974. Sea-floor spreading history and deep-sea drilling results in the Madagascar and Mascarene Basins, Western Indian Ocean. In: *Initial Reports of DSDP.*

SCHLICH, R. 1982. The Indian Ocean: aseismic ridges, spreading centres, and oceanic basins. In: *The Ocean Basins and Margins*, eds., Nairn, A.E.M. & Shehll, F.G. vol 6, The Indian Ocean, Plenum, New York, 51-147.

SCHMIDT, V. & McDONALD, D.A. 1979. Texture and recognition of secondary porosity in sandstones. *SEPM Spec. Pub.* **26**, 209-225.

SCHLUMBERGER, 1989. Log interpretation principles/applications. *Schlumberger Educational Services, Texas.*

SCOTESE, C.R., GAHAGEN, L.M. & LARSON, R.L. 1988. Plate tectonic reconstructions of the Cretaceous and Cenozoic ocean basins. *Tectonophysics.* **155**. 27-48.

SEAGOUFIN, J. & PATRIAT, P. 1981. Reconstructions de l'Ocean indien occidental pour les epoques des anomalies M21, M2 et 34. Paleoposition de Madagascar. *Bull. Soc. Geol. Fr.*, **23** (6), 603-607.

SERRA, O. 1985. Sedimentary environments from wireline logs. *Schlumberger Educational Services, Texas.* 211p.

Serra, O. 1986. Wellsite interpretation of wireline logs. *Schlumberger Educational Services, Texas.* 60p.

Shanmugam, G. 1985. Types of porosity in sandstones and their significance in interpreting provenance. In: *Provenance of Arenites*, ed. Zuffa, G.G. *NATO ASI Series*, **148**, 115-138.

Shawa, Monzer S. 1969. Sedimentary history of the Gilwood sandstone (Devonian), Utikuma Lake area, Alberta, Canada. *Bull. Can Petroleum Geology*, **17** (4), 392-409.

Shawa, Monzer S. 1987a. Elk Point Sandstone Reservoirs, Peace River Arch, Alberta, Part I: *Shawa Geoconsultants Report* #521-86.

Shawa, Monzer S. 1987b. Elk Point Sandstone Reservoirs, Peace River Arch, Alberta, Part II: *Shawa Geoconsultants Report* #522-86.

Sherwin, D.F. 1962. Lower Elk Point section in east-central Alberta. *Journal of Alberta Society of Petroleum Geologists*, **10** (4), 185-191.

Smith, G. le Blanc. 1980. Genetic stratigraphy of the Witbank Field. In: *Karoo Basin Symposium, Trans. Geol. S. Afr.*, **83**, 313-326.

Sommer, S.E. 1972. Cathodoluminescence of carbonates: 1-Characterisation of cathodoluminescence from carbonate solid solutions. *Chem. Geol*, **9**, 257-273.

Srodon, J., Morgan, D.J., Eslinger, E.V., Eberl, D.D. & Karlinger, M.R. 1986. Chemistry of illite/smectite and end member illite. *Clay & Clay Minerals*, **34**, 368-378.

Steel, R.J., Maehle, S., Hilsen, H., Roe, S.L. & Spinnangr, A. 1977. Coarsening-upward cycles in the alluvium of Hornelen Basin (Devonian) Norway: Sedimentary response to tectonic events. *Geol. Soc. Amer. Bull.*, **88**, 1124-1134.

Staub, J.R. & Cohen, A.D. 1978. Kaolinite enrichment beneath coals: a modern analog, Snuggedy Swamp, South Carolina. *J. sediment. Petrol.*, **48**, 203-210.

Stephens, W.E. & Devey, C.M. 1990. Seychelles and the fragmentation of Gondwana: Evidence from the igneous rocks. *Proc First Regional Seminar on Petroleum Exploration*, Seychelles (in press).

Storey, S.R. 1979. Clay-carbonate diagenesis of deltaic sandstones-Basal Belly River Formation (Upper Cretaceous) Central Alberta, Canada (Abs) *Am. Ass. Petrol. Geol. Bull.*, **63**, 534.

Surdam, R.C., Boese, S.W. & Crossey, L.J. 1984. The chemistry of secondary porosity. In: *Sandstone Diagenesis*, eds. McDonald D.A. & Surdam, R.C., *Amer Asooc Petroleum Geologists* Mem., **37**, 127-150.

Surdam,R.C., Crossy, L.J., Scen Hagen, E. & Heasler, H.P. 1989. Organic-inorganic interactions and sandstone diagenesis. *Amer Assoc petroleum Geologists Bull.*, **73**, 1-23.

Suska, M.M. 1963 Mid-Devonian Elk Point Group and Cambrian rocks of north-central Alberta. *University of Alberta*,Unpub. M.Sc. Thesis.

Suwa, K. Yanagi, T., Tokieds, K., Umemura, H., Asami, M. & Hoshino, M. 1983. Geology and petrology of the Seychelles Islands. In: *Eighth preliminary report of African studies; Nagoya University*, ed. Suwa, K., **8**, 3-21.

Thachuk, N.M. 1968. Gelogical study of the Middle Devonian Gilwood arkoses in the Nipsi area, Alberta. *J. Can. Petroleum Technology*, 7 (4), 181-194.

Tomkins, R.V. 1955. Potash in Saskatchewan. *Transactions of Canadian Institute of Minning and Metallurgy*, **58**, 38-41.

Trotter, Richard & Hein, Frances J. 1988. Sedimentology and depositional setting of the Granite Wash, northwestern Alberta. In: *Sequences, Stratigraphy, Sedimentology: Surface and Subsurface.* eds. James, D.P. & Leckie, D.A., *Can Soc. Petroleum Geologists, Memoir* 15, 475-484.

Tsui, P.C. 1982. Deformation, Ground Subsidence and Slope Movements along the Salt River Escarpment in Wood Buffalo National Park. *University of Alberta*, Unpub. M.Sc. thesis.

Tsui, P.C. & Cruden, D. 1984. Deformation associated with gypsum karst in the salt River Escarpment, northeastern Alberta. *Can. J. Earth Sci.*, **21**, 949-959.

Turner, B.R. 1983. Braid plain deposition of the Upper Triassic Molteno Formation in the main Karroo (Gondwana) Basin, South Africa. *Sedimentology*, **30**, 77-89.

Usdowski, H.E. 1968. The formation of dolomite in sediments. In: *Recent developments in carbonate*

sedimentology in Central Europe, eds Miller, G. & Friedman, G.M., *Springer-Verlag, Berlin,* 255p.

Van Hees, H. 1956. Elk Point group. Journal *Alberta Society of Petroleum Geologists*, **4**, 29-37.

Van Hees, H. 1958. The Meadow Lake Escarpment- Its regional significance to Lower Palaeozoic stratigraphy. *North Dakota Geological Society, Saskatchewan Geological Society, IInd International Williston Basin symposium*, 70-78.

Van Vuuren, C.J. 1987. Stratigraphy and sedimentology of the coal-bearing Ecca Group in the Karoo basin, South Africa. In: *Curr Res Afr. Earth Sci., Mathies & Schandelmeier (eds).* 235-238.

Van Wagoner, J.C., Posamentier, H.W., Mitchum, R.M., Vail, P.R., Sarg, J.F., Loutit, T.S., & Hardenbol, J. 1988. An overview of the fundamentals of sequence stratigraphy and key definitions. In: *Seal Level Changes: An Integrated Approach,* eds Wilgus, C.K. *et al, Soc. Econ Paleontol. Mineral.,* Spec. Publ. 42, 39-45.

Velain, C. 1879. Notes sur la constitution geologique des iles Seychelles. *Bull. Soc. Geol. France*, **7**, 278p.

Visher, G.S. 1965. Use of vertical profile in environmental reconstruction. *Am. Assoc. Petroleum Geologists Bull.*, **49**, 41-61.

Walton, E.K. & Khanna, M. 1989. The Karroo Succession, Western Shelf, Seychelles. *Unpublished Seychelles National Oil Co report.*

Walton, E.K. & Khanna, M. 1989. The Karroo Succession, Western Shelf, Seychelles (abs). *British Sedimentological Research Group*, Leeds.

Walton, E.K. & Khanna, M. 1990. The Karroo Succession, Western Shelf, Seychelles. *Proc First Regional Seminar on Petroleum Exploration,* Seychelles (in press).

Walker, C.T. 1957. Correlation of Middle Devonian rocks in western Saskatchewan. *Saskatchewan Department of Mineral Resources* report 25, 59p.

Walker, R.G. 1990. Facies modeling and sequence stratigraphy. *J. Sedim. Pet.*, **60**, 5, 777-786.

Walker, R.G. & Eyles, C.H. 1991. Origin of sequence-bounding erosion surface in Cardium Formation. *Jour. Sed. Petrology*, **61**(4), 473-496.

Walters, R. & Linton, R.E. 1973. The sedimentary basin of coastal Kenya. In: *Bassins Sedimentaries du Littoral Africain, 2, Austral et Oriental. Assoc. Services Geol. Africaine,* Paris, 133-158.

Wilson, R.C.L. 1991. Sequence stratigraphy: An introduction. *Geoscientist*, **1**, 1, 13-23.

Workman, L.E. 1953. Elk Point formation in the Peace River region. *J. Alberta Soc. Petroleum Geologists*, **1** (8). 7-8.

Yanagi, T., Wakizaka, Y. & Suwa, K. 1983. Rb-Sr whole rock ages of granitic rocks from the Seychelles Is lands. *8th Prelim. Rept. Afrc. Studies, Nagoya University*, 23-36.

Yemane, K. 1987. Depositional environment of Lower Beaufort (Upper Permian) Karoo deposit of Northern Malawi and similar sequences in Southern Africa. *Curr Res Afr. Earth Sci.* (eds Mathies & Schandelmeier), 231-234.

APPENDICES

APPENDIX 1 - DATA BASE

1. KAROO SUPERGROUP:

1.1. Wire line Logs:

1.1.1. Reith Bank-1:

Caliper-gamma ray/Neutron Porosity-Bulk Density: 500' to 10,500'. Scale 1:500 & 1:200.
SP curve-gamma ray/Resistivity: 400' to 4700'; 7300' to 12,600'. Scale 1:500 & 1:200.
Caliper/Resistivity: 1300' to 4600'; 7300' to 10,400'. Scale 1:500 & 1:200.
Velocity log: 400' to 12,600'.
Cement Bond log: 3900' to 10,300'.
Coriband log: 4800' to 10,300'.
Air gun & well velocity survey: 3900' to 10,300'.

1.1.2. Seagull Shoals-1:

SP curve-gamma ray/Resistivity: 400' to 1100'; 1200' to 8900'. Scale 1:500 & 1:200.
Caliper/Neutron log: 300' to 1100'; 4400' to 8900'. Scale 1:500 & 1:200.
Velocity log: 400' to 9000'.
Air gun & well velocity survey: 400' to 9000'.
Formation evaluation log: 8900' to 9000'.
Coriband log: 4500' to 8900'.

1.1.3. Owen Bank-1A:

SP-gamma ray/Resistivity: 400' to 1200'; 1300' to 10,200'; 10,300' to 13,500'. Scale 1:500 & 1:200.
Caliper/Neutron log: 400' to 1200'; 1300' to 10,200'; 10,300' to 13,500'. Scale 1:500 & 1:200.
Caliper/Resistivity: 1300' to 10,300'. Scale 1:500 & 1:200.
Continuous dipmeter: 1400' to 13,500'.
Velocity log: 1300' to 13,500'.

1.2. Technical Reports:

1.2.1. Reith Bank-1:

Final well report.
Geochemical report.
Robertson Research International Ltd. (Aug., 1981): The Biostratigraphy and Palaeoenvironments of the interval 1400' to 12,790' with petrography, X-ray diffraction and K/Ar age dating of selected samples from the AMOCO Seychelles Petroleum Company Reith Bank-1 Well, Offshore Seychelles.

1.2.2. Seagull Shoals-1:

Final well report.
Geochemical report.
Robertson Research International Ltd. (Sept., 1981): The Biostratigraphy and Palaeoenvironments of the interval 1181' to 8995' with petrography and K/Ar age dating of selected samples from the AMOCO Seychelles Petroleum Company Seagull Shoals-1 Well, Offshore Seychelles.

1.2.3. Owen Bank-1A:

Final well report.
Geochemical report.
Robertson Research International Ltd. (Nov., 1980): The Biostratigraphy and Palaeoenvironments of the interval 200' to 14340' with petrography of few selected field and cutting samples from the AMOCO Seychelles Petroleum Company Owen Bank-1A Well, Offshore Seychelles.

1.3. Report by Mineralogy Inc., September 1981:

Discussion of porosity and permeability; thin section description; X-ray diffraction mineralogy and scanning microscope analysis of core plugs from Seychelles Reith Bank #1 and the Seychelles Seagull Shoals #1.

1.4. Reports & papers:

1.4.1. NOPEC a.s. (march, 1985). Study of Basic Petroleum Data in the Seychelles. Vol. I & II.

1.4.2. Khanna, S.N. & Pillay, G. (1986). Seychelles: Petroleum potential of this Indian Ocean paradise. Oil & Gas Journal, p. 136-139.

1.4.3. Khanna, S.N. & Pillay, G. (1987). Seychelles geology, hydrocarbon potential. Oil & Gas Journal, feb., p. 43-44.

1.5. Samples:

1.5.1. Core Samples:

Reith Bank-1: 10,429' to 10,451' at 2' intervals; 12,726' to 12,655' at 2' interval.
Seagull Shoals-1: 8973' to 8995' at 2' intervals.
Owen Bank-1A: 13,402' to 13,434' at 2' intervals.

1.5.2. Side wall cuttings:

Reith Bank-1: 4770' to 12,790' at 20' intervals.
Seagull Shoals-1: 4500' to 9000' at 20' intervals.
Owen Bank-1A: 1360' to 14,360' at 20' intervals.

1.5.3. Thin sections from Robertson Research International:

A total of 356 thin sections were supplied by Robertson Research International.

1.6. Exlogs:

A full set of exlogs for each of the three well was also been supplied,

1.6.1. Reith Bank-1:

Pressure analysis log: 440' to 12790'.
Temperature data log: 440' to 12790'.
Well progress log: 440' to 12790'.
Drilling data pressure log: 440' to 12790'.
Wireline data pressure log: 440' to 12790'.
Hole condition log: 440' to 12790'.
Mud log: 440' to 12790'.

1.6.2. Seagull Shoals-1:

Pressure analysis log: 335' to 9005'.
Temperature data log: 335' to 9005'.
Well progress log: 335' to 9005'.
Drilling data pressure log: 335' to 9005'.
Wireline data pressure log: 335' to 9005'.
Hole condition log: 335' to 9005'.
Mud log: 335' to 9005'.

1.6.3. Owen Bank-1A:

Pressure analysis log: spud to 14351'.
Temperature data log: spud to 14351'.
Well progress log: spud to 14351'.
Drilling data pressure log: spud to 14351'.
Wireline data pressure log: spud to 14351'.
Hole condition log: spud to 14351'.
Summary log: spud to 14351'.

2. ELK POINT GROUP:

The database for the Elk Point Group consists of core samples, lithologs and gamma-ray logs covering 118 wells. Not all wells had a complete set of data comprising samples, lithologs and gamma-ray logs.

APPENDIX 2 - LABORATORY STUDIES

2.1. KAROO:

2.1.1. Robertson Research Thin sections:

Reith Bank Sections supplied by Robertson Research International. These sections were used for thin section optical microscopy.

No	Depth	No	Depth	No	Depth
1	6152'	35	7422'	69	8247'
2	6164'	36	7426'	70	8255'
3	6170'	37	7435'	71	8417'
4	6171'	38	7455'	72	8430'
5	6179'	39	7465'	73	8445'
6	6200'	40	7495'	74	8465'
7	6240'	41	7533'	75	8483'
8	6260'	42	7600'	76	8525'
9	6266'	43	7629'	77	8628'
10	6267'	44	7765'	78	8655'
11	6285'	45	7825'	79	8704'
12	6431'	46	7875'	80	8725'
13	6500'	47	7935'	81	8752'
14	6635'	48	7948'	82	8771'
15	6644'	49	7974'	83	8789'
16	6695'	50	7985'	84	8867'
17	6717'	51	8058'	85	8890'
18	6812'	52	8066'	86	8924'
19	6835'	53	8088'	87	9035'
20	6855'	54	8074'	88	9179'
21	6992'	55	8077'	89	9298'
22	7010'	56	8084'	90	9374'
23	7171'	57	8086'	91	9436'
24	7141'	58	8095'	92	9646'
25	7280'	59	8102'	93	9700'
26	7283'	60	8105'	94	9842'
27	7300'	61	8111'	95	9985'
28	7400'	62	8125'	96	10012'
29	7408'	63	8140'	97	10097'
30	7410'	64	8156'	98	10140'
31	7414'	65	8158'	99	10303'
32	7415'	66	8161'	100	10320'
33	7416'	67	8215'		
34	7420'	68	8235'		

2.1.2. Thin sections prepared at St Andrews University:

Following thin section were prepared at St Andrews University. S1-S13 were samples from Seagull Shoals-1 and R1-R28 from Reith Bank-1A wells. H/S:hand specimen study; T/S:thin section study; SEM: scanning electron microscope study; XRD: x-ray diffraction study; XRF: x-ray fluorescence; B/S: electron-microprobe and back-scatter study; C/L:cathodoluminescence; F/I: fluid inclusion study.

S.No	Sample	Depth	H/S	T/S	SEM	XRD	XRF	B/S	F/I	C/L
1	S1	8973	X	X	X	X	X			
2	S2	8975	X	X	X			X	X	X
3	S3	8977	X	X	X	X	X	X		X
4	S4	8979	X	X	X	X		X	X	X
5	S5	8980	X	X	X					
6	S6	8982	X	X	X	X				
7	S7	8983	X	X	X					
8	S8	8985	X	X	X	X	X			
9	S9	8987	X	X	X	X	X			
10	S10	8989	X	X	X	X	X			
11	S11	8991	X	X	X					
12	S12	8993·	X	X	X	X	X			
13	S13	8995	X	X	X	X	X			
14	R1	10429	X	X	X	X	X			
15	R2	10431	X	X	X					
16	R3	10433	X	X	X	X	X			
17	R4	10435	X	X	X	X	X			
18	R5	10437	X	X	X					
19	R6	10439	X	X	X					
20	R7	10441	X	X	X	X	X			
21	R8	10443	X	X	X	X	X			
22	R9	10445	X	X	X	X	X	X		X
23	R10	10447	X	X	X	X				
24	R11	10449	X	X	X	X	X	X		X
25	R12	10451	X	X	X	X	X	X		X
26	R13	12726	X	X	X			X	X	X
27	R14	12728	X	X	X			X	X	X
28	R15	12730	X	X	X	X	X	X		X
29	R16	12732	X	X	X	X	X	X		X
30	R17	12734	X	X	X					
31	R18	12736	X	X	X	X	X			
32	R19	12738	X	X	X					
33	R20	12740	X	X	X					
34	R21	12742	X	X	X					
35	R22	12744	X	X	X		X			
36	R23	12746	X	X	X	X	X			
37	R24	12748	X	X	X		X			
38	R25	12750	X	X	X	X	X		X	
39	R26	12752	X	X		X	X			
40	R27	12754	X	X		X	X			
41	R28	12755	X	X		X	X			

2.2. ELK POINT GROUP:

The details of all wells studied are given below. WM: Watt Mountain; KR: Keg River; CH: Chinchaga; GW: Granite Wash; LOG:litholog; PET LOG:petrophysical log; H/S:hand specimen study; T/S:thin section study; SEM: scanning electron microscope study; XRD: x-ray diffraction study; XRF: x-ray fluorescence; B/S: electron-microprobe and back-scatter study; C/L:cathodoluminescence; F/I: fluid inclusion study; I/A:isotope analysis; C:carbonate; A:anhydrite.

S.No.	Sample No.	Metres	Feet	WELL	FM	LOG	PET	H/S	T/S	SEM	XRD	XRF	I/A	B/S	F/I	C/L
1	8-35-68-3W5	1671.5	5516	68-3	WM	x	x	x	x	x						
2	8-35-68-3W5	1674.2	5525	68-3	WM	x	x									
3	4-15-70-2W5	1728.5	5704	70-2	CH	x	x	x	x	x						
4	4-26-70-4W5	1838.8	6068	70-4	WM	x	x									
5	4-26-70-4W5	1841.2	6076	70-4	WM	x	x	x	x	x						
6	11-22-70-9W5	2067.4	6822.5	70-9	WM	x	x	x	x	x						
7	12-28-71-3W5	1658.8	5474	71-3	WM	x	x	x	x	x						
8	4-8-71-4W5	1848.9	6101.5	71-4	WM	x	x									
9	4-8-71-4W5	1850	6105	71-4	WM	x	x	x	x	x						
0	4-8-71-4W5	1853.3	6116	71-4	WM	x	x									
11	10-26-71-5W5	1824.5	6021	71-5	WM	x	x									
12	10-26-71-5W5	1827	6029	71-5	WM	x	x	x	x	x						
13	10-26-71-5W5	1830.9	6042	71-5	WM	x	x									
14	6-11-71-8W5	2145	7142.9	71-8	WM	x	x	x	x	x						
15	6-11-71-8W5	2146.5	7147.8	71-8	WM	x	x									
16	10-11-71-12W5	2320.6	7658	71-12	WM	x	x	x	x	x						
17	10-11-71-12W5	2323.3	7667	71-12	WM	x	x	x	x	x						
18	10-11-71-12W5	2325.8	7675	71-12	WM	x	x									
19	2-4-72-3W5	1604.2	5294	72-3	WM	x	x	x	x	x						
20	8-12-72-5W5	1731.2	5764.9	72-5	WM	x	x	x	x	x						
21	10-33-72-9W5	1882.1	6211	72-9	WM	x	x	x	x	x						
22	4-4-73-4W5	1610.5	5314.5	73-4	WM	x	x	x	x	x						
23	10-8-73-5W5	1654.4	5459.5	73-5	WM	x	x	x	x	x						
24	10-8-73-5W5	1654.5	5460	73-5	WM	x	x	x	x	x						
25	10-8-73-5W5	1655.8	5464	73-5	WM	x	x									
26	10-8-73-5W5	1657	5468	73-5	WM	x	x	x	x	x						
27	10-8-73-5W5	1658	5471.5	73-5	WM	x	x									
28	10-8-73-5W5	1658.2	5472	73-5	WM	x	x	x	x	x						
29	10-8-73-5W5	1661.5	5483	73-5	WM	x	x	x	x	x						

S.No.	Sample No.	Metres	Feet	WELL	FM	LOG	PET	H/S	T/S	SEM	XRD	XRF	I/A	B/S	F/I	C/L
30	10-8-73-5W5	1662.1	5485	73-5	WM	x	x	x	x	x						
31	10-8-73-5W5	1664.4	5492.5	73-5	WM	x	x									
32	4-27-73-7W5	1732.1	5768	73-7	WM	x	x	x	x	x						
33	4-2-74-5W5	1638.1	5405.7	74-5	WM	x	x									
34	4-2-74-5W5	1642	5418.6	74-5	WM	x	x	x	x	x						
35	14-22-74-6W5	1789.6	5905.7	74-6	WM	x	x	x	x	x						
36	14-22-74-6W5	1793.2	5971.4	74-6	WM	x	x									
37	12-23-74-6W5	1687.3	5568	74-6	WM	x	x	x	x	x						
38	3-14-74-10W5	1839.4	6070	74-10	WM	x	x									
39	3-14-74-10W5	1844.2	6086	74-10	WM	x	x	x	x	x						
40	4-19-75-5W5	1824.1	6019.5	75-5	WM	x	x	x	x	x						
41	6-35-75-9W5	1777.3	5865	75-9	WM	x	x	x	x	x						
42	10-35-75-10W5	1811.1	5976.5	75-10	WM	x	x	x	x	x						
43	10-35-75-10W5	1815.5	5991	75-10	WM	x	x	x	x	x						
44	7-30-76-7W5	1849.1	6157.6	76-7	WM	x	x									
45	7-30-76-7W5	1851.2	6164.5	76-7	WM	x	x	x	x	x						
46	10-14-76-12W5	2000.8	6602.5	76-12	WM	x	x	x	x	x						
47	11-23-77-8W5	1798.2	5934	77-8	WM	x	x									
48	11-23-77-8W5	1800.6	5942	77-8	WM	x	x	x	x	x						
49	11-23-77-8W5	1806.7	5962	77-8	WM	x	x	x	x	x						
50	6-21-77-9W5	1860.5	6139.7	77-9	WM	x	x	x	x	x						
51	6-21-77-9W5	1862.5	6146.3	77-9	WM	x	x									
52	4-21-77-10W5	1906.3	6290.8	77-10	WM	x	x	x	x	x						
53	12-30-78-7W5	1722.3	5683.6	78-7	WM	x	x	x	x	x						
54	12-30-78-7W5	1728.5	5704.1	78-7	WM	x	x									
55	10-27-78-11W5	1849.4	6103	78-11	GW	x	x	x	x	x						
56	4-2-79-8W5	1725.9	5695.5	79-8	WM	x	x	x	x	x						
57	4-2-79-8W5	1728.3	5703.4	79-8	WM	x	x									
58	14-13-79-11W5	1792.1	5914	79-11	GW	x	x	x	x	x						
59	2-6-80-7W5	1702.7	5618.9	80-7	WM	x		x	x	x						
60	2-11-80-8W5	1705.2	5627.2	80-8	WM	x		x	x	x						
61	2-11-80-8W5	1709.8	5642.3	80-8	WM	x										
62	2-32-80-11W5	1798.4	5934.7	80-11	GW	x		x	x	x						
63	2-32-80-11W5	1799.8	5939.3	80-11	GW	x										

S.No.	Sample No.	Metres	Feet	WELL	FM	LOG	PET	H/S	T/S	SEM	XRD	XRF	I/A	B/S	F/I	C/L
64	16-14-68-21-W5	2936.1	9777.2	A22	WM	x	x	x	x	A2	x	x				
65	6-9-68-23W5	3175.4	10574	A33	WM	x	x	x	x	A3	x	x	C			
66	6-14-69-20W5	2829.9	9423.6	A55	WM	x	x	x	x	A5	x	x				
67	4-14-70-15W5	2486.5	8280	A66	WM	x	x	x	x	A6	x	x				
68	11-4-71-16W5	2488.9	8288	B17	WM	x	x	x	x	B1	x					
69	13-20-71-21W5	2793.4	9302	B28	WM	x	x	x	x	B2	x	x				
70	11-18-72-17W5	2504.2	8339	B39	KR		X	x	x	B3	x	x				
71	8-16-72-18W5	2554.8	8507.5	B410	WM	x	x	x	x	B4	x	x				
72	10-14-72-23W5	2943.8	9803	B511	GW	x	x	x	x	B5	x	x	C			
73	11-11-73-13W5	2218	7386	B612	GW	x	x	x	x	B6	x					
74	2-21-73-13W5	2137.5	7118	C113	WM	x	x	x	x	C1	x	x				
75	10-1-73-17W5	2323.7	7738	C214	WM	x	x	x	x	C2	x	x				
76	8-13-73-19W5	2517.7	8383.9	C416	WM	x	x	x	x	C4	x	x				
77	16-36-73-21W5	2582.3	8599.1	C517	WM	x	x	x	x	C5	x	x	C			
78	6-8-74-14W5	2371.8	7898.1	C618	WM	x	x	x	x	C6	x	x				
79	16-20-74-18W5	2358.6	7854.1	D119	WM	x	x	x	x	D1	x	x				
80	9-30-74-21W5	2556.5	8513.1	D220	GW	x	x	x	x	D2	x	x				
81	16-35-74-24W5	2728	9084.2	D321	GW	x	x	x	x	D3	x	x				
82	3-4-75-18W5	2349.5	7823.8	D422	GW	x	x	x	x	D4	x	x				
83	10-8-75-19W5	2401.3	7996.3	D523	WM	x	x	x	x	D5	x	x				
84	6-1-75-24W5	2733.6	9102.9	D624	GW	x	x	x	x	D6	x	x				
85	4-22-77-14W5	2088.2	6953.7	E125	GW	x	x	x	x	E1	x	x				
86	10-11-77-16W5	2249.2	7489.8	E226	GW	x	x	x	x	E2	x	x				
87	12-11-78-22W5	2313.5	7704	E529	GW	x	x	x	x	E5	x	x				
88	8-16-79-21W5	2405	8008.7	E630	GW	x	x	x	x	E6	x	x	C			
89	2-9-80-18W5	2142	7132.9	F131	GW	x	x	x	x	F1	x					
90	9-13-80-21W5	2367.5	7883.8	F333	GW	x	x	x	x	F3	x	x				
91	6-8-81-8W5	1673.3	5521.9	11	WM	X	X	X	X	11	X	t	CA			
92	6-8-81-8W5	1678.5	5539.1	12	WM	X	X	X	X	12	X	X		X	X	X
93	6-8-81-8W5	1681.2	5548	13	WM	X	X	X	X	13	X				X	
94	10-5-81-9W5	1685.7	5562.8	21	WM	X	X	X	X	14	X	X				
95	10-5-81-9W5	1744.8	5757.8	22	GW	X	X	X	X	15	X					
96	7-25-81-10W5	1717.9	5669	41	GW	X	X									
97	12-4-82-9W5	1702.1	5617	61	KR	X	X									

S.No.	Sample No.	Metres	Feet	WELL	FM	LOG	PET	H/S	T/S	SEM	XRD	XRF	I/A	B/S	F/I	C/L
98	8-10-82-10W5	1767.9	5834	71	GW	X	X									
99	6-31-84-7W5	1597.6	5272	111	GW	X	X	X	X	16	X	X			X	
100	16-3-84-14W5	1772.1	5847.9	133	WM	X	X	X	X	23	X	X				
101	5-17-85-8W5	1563.8	5160.5	161	CH	X	X	X	X	26	X					
102	5-17-85-8W5	1564.8	5163.8	162	CH	X	X	X	X	34		X	A			
103	5-17-85-8W5	1566	5167.8	163	CH	X	X	X	X	35	X					
104	4-9-85-9W5	1545.5	5100	171	GW	X	X	X	X	41	X	X		X	X	X
105	11-29-86-3W5	1585.2	5231	181	CH	X	X	X	X	42	X		C			
106	11-29-86-3W5	1585.8	5233	182	CH	X	X	X	X	43	X	X	CA			
107	1-22-86-8W5	1500	4950	191	KR	X	X	X	X	44	X	X				
108	1-22-86-8W5	1505.8	4969	192	CH	X	X	X	X	45	X	X	A			
109	1-22-86-8W5	1513.9	4996	193	GW	X	X	X	X	46	X	X				
110	6-27-86-9W5	1459.4	4816	211	KR	X	X	X	X	51	X	X	C	X	X	X
111	6-27-86-9W5	1463.9	4831	212		X	X	X	X	52	X					
112	10-15-86-10W5	1479.1	4881	221	GW	X	X	X		53	X	X				
113	10-15-86-10W5	1481.2	4888	222	GW	X	X	X	X	54	X					
114	16-31-86-12W5	1564	5161.2	231	WM	X	X	X	X	55	X	X				
115	16-31-86-12W5	1565	5164.5	232	WM	X	X	X	X	56	X		C		X	
116	2-21-87-5W5	1548	5108.4	241	CH	X	X									
117	10-7-87-7W5	1500.6	4952	251	CH	X	X	X	X	61	X	X	A	X	X	X
118	4-16-87-7W5	1516.4	5004	261	GW	X	X	X	X	62	X	X		X	X	X
119	4-3-87-8W5	1488.2	4911	271	KR	X	X	X	X	63	X	X		X	X	X
120	4-3-87-8W5	1489.1	4914	272	KR	X	X	X	X	64	X		A	X	X	X
121	9-11-87-9W5	1430.9	4722	281	KR	X	X	X	X	65	X			X		X
122	9-11-87-9W5	1434.2	4733	282	KR	X	X	X	X	66	X		C			
123	9-11-87-9W5	1435.2	4736	283	KR	X	X	X	X	71	X	X				
124	9-11-87-9W5	1438.2	4746	284	KR	X	X	X	X	72	X					
125	9-11-87-9W5	1442.4	4760	285	KR	X	X	X	X	73	X		C			
126	8-2-87-13W5	1576.8	5203.4	301	WM	X	X	X	X	74	X					
127	8-2-87-13W5	1578.5	5209.1	302	WM	X	X	X	X	75	X	X				
128	8-2-87-13W5	1581.6	5219.3	303	WM	X	X	X	X	76	X					
129	8-2-87-13W5	1583.4	5225.2	304	WM	X	X	X	X	81			A			
130	2-7-88-7W5	1485.2	4901	311	CH	X	X	X								
131	2-7-88-7W5	1486.7	4906	312	CH	X	X									

S.No.	Sample No.	Metres	Feet	WELL	FM	LOG	PET	H/S	T/S	SEM	XRD	XRF	I/A	B/S	F/I	C/L
132	10-14-88-9W5	1425.8	4705	331	KR	X	X									
133	10-14-88-9W5	1430.6	4721	332	GW	X	X									
134	12-36-88-11W5	1545.5	5100.2	341	GW	X	X	X	X	92	X					
135	12-36-88-11W5	1548.4	5109.7	342	GW	X	X	X	X	93	X	X				
136	12-36-88-11W5	1552.4	5122.9	343	GW	X	X	X	X	94	X					
137	11-36-88-12W5	1665.7	5496.8	351	GW	X	X									
138	1-5-90-10W5	1480.3	4885	371	KR	X	X									
139	1-5-90-10W5	1487.6	4909	372	KR	X	X									
140	1-5-90-10W5	1490.6	4919	373	GW	X	X									
141	1-5-90-10W5	1492.4	4925	374	GW	X	X	X	X	95	X	X				
142	5-25-90-11W5	1545.8	5101.1	383	KR	X	X	X	X	96	X	X				
143	9-35-91-6W5	1407.6	4645	401	GW	X	X	X	X	101	X				X	
144	9-35-91-6W5	1408.8	4649	402	GW	X	X	X	X	102	X	X			X	
145	12-25-91-10W5	1428.5	4714	421	CH	X	X	X	X	104						
146	12-25-91-10W5	1433	4729	422	GW	X	X	X	X	105	X					
147	4-34-91-7W5	1359.4	4486	431	CH	X	X									
148	4-34-91-7W5	1366.2	4508.5	432	CH	X	X									
149	4-34-91-7W5	1368.5	4516	433	CH	X	X									
150	4-34-91-7W5	1370.9	4524	434	CH	X	X	X	X	106	X	X			X	
151	12-23-92-16W5	1778.8	5870	461	GW	X	X	X	X	114	X	X				
152	10-5-92-19W5	1662.1	5485	471	WM	X	X	X	X	115	X					
153	10-5-92-19W5	1663.3	5489	472	WM	X	X	X	X	116	X					
154	10-5-92-19W5	1667	5501	473	WM	X	X	X	X	121	X					
155	12-9-93-18W5	1580.3	5215	481	WM	X	X	X	X	122	X					
156	12-9-93-18W5	1591.5	5252	482	WM	X	X	X	X	123	X					
157	12-9-93-18W5	1593	5257	483	WM	X	X	X	X	124	X			X	X	X
158	12-9-93-18W5	1594.2	5261	484	WM	X	X	X	X	125	X					
159	4-19-93-19W5	1558.5	5143	491	WM	X	X	X	X	126	X		C			
160	4-19-93-19W5	1562.1	5155	492	WM	X	X	X	X	131	X					
161	4-19-93-19W5	1563.6	5160	493	WM	X	X	X	X	132	X			X		X
162	4-19-93-19W5	1567	5171	494	WM	X	X	X	X	133	X					
163	4-19-93-19W5	1578.5	5209	495	WM	X	X	X	X	134	X					
164	10-17-94-15W5	1499.7	4949	501	WM	X	X	X	X	135	X	X	C	X	X	X
165	10-17-94-15W5	1667	5501	502	GW	X	X	X	X	136	X	X	C	X	X	X

S.No.	Sample No.	Metres	Feet	WELL	FM	LOG	PET	H/S	T/S	SEM	XRD	XRF	I/A	B/S	F/I	C/L
166	10-17-94-15W5	1668.2	5505	503	GW	X	X	X	X	141	X	X		X		X
167	10-17-94-15W5	1669.1	5508	504	GW	X	X	X	X	142	X	X	C		X	
168	10-17-94-15W5	1670.3	5512	505	GW	X	X	X	X	143	X	X		X		X

APPENDIX 3 -EXPERIMENTAL TECHNIQUES

1. XRD ANALYSIS:

Rock chips were coarsely crushed in a crusher, followed by fine crushing in an Agate mortar. The sample holders were packed with the powder. X-ray analysis was performed on these unoriented samples on Philips PW1010 Diffractometer using a Graphite Monochromator. The conditions of x-ray analysis are as follows;

Cu K at 36Kv and 18mA with a Divergence slit of 1° and a Receiving slit 0.2mm wide.
Samples run without treatment from 5° - 65° at 1°/min; Attenuation scale $4*10^2$.
Samples run after ethyl glycolation from 5° - 35° at 1°/min; Attenuation scale $4*10^2$.
Samples run after heat treatment from 5° - 35° at 1°/min; Attenuation scale $4*10^2$.

1.1 Ethyl-glycol Treatment

After they were analysed without any treatment powdered samples were glycolated overnight in an Ethyl-glycol bath at 60°. This glycolation helps in identifying illite and mixed layering in clays.

1.2 Heat Treatment

After glycol analysis, samples were heated in a furnace at 550° for one hour and re-analysed. The heating allows differentiation between kaolinite and chlorite.

2. ELECTRON MICROPROBE & BACK SCATTER:

The instrument used was a JEOL JCXA-733 Super Probe. The accelerating potential used for analysis was 10 KV and the beam current was 10 nA. The beam diameter used was approximately 1 um, and the samples were coated with carbon at 250 A°.

Spot analysis was carried out on carbonate cements for CaO, MgO, FeO and MnO; feldspar overgrowths for SiO_2, Al_2O_3, K_2O and Na_2O. Analysis was also carried out on anhydrite, clays and quartz. Photographs were taken using the back-scatter technique to study the zonnation in cements and feldspar.

3. FLUID INCLUSION TECHNIQUES:

The apparatus used for fluid inclusion studies was the Linkam Microthermometric Apparatus in conjuction with a Leitz Microscope. The TH 600 is a dual purpose heating-freezing stage for the microthermometric analysis of inclusions over the dynamic range -180°C to +600°C with a maximum resolution of 0.1°C. The system satisfies the following conditions;

1. Good thermal contact between the sample and heat exchange medium or block (i.e. vertical gradient).
2. Minimal gradient between the sample and temperature sensor.
3. Minimal thermal gradient within the sample across the field of view (i.e. horizontal gradient).
4. Compatibility between cell windows and external optics.
5. Fully automatic programmable temperature control during both heating and freezing with direct digital temperature display and optional print out.

A linear rate of temperature change improves operator efficiency and enables reversible phase changes to be repeatedly monitored.

The apparatus consists of;

1. A heating/freezing chamber which is mounted on the stage of a Leitz microscope.
2. A console with a digital temperature display and heating controls.
3. A console with automatic temperature print out linked to the above console.
4. A dewar flask for gas cooling.

4. CATHODOLUMINESCENCE:

The apparatus used for cathodolumuniscence studies was a Technosyn Cold Cathode Luminescence Model 8200 MKII attached to an Olympus, model POS, polarizing microscope. The accelerating voltage used was between 15 KV and 20 KV while the gun current varied from 250-300. Photographs were taken using a 200 ASA Kodakchrome film with exposure time between 30 secs - 5 mins.

5. ISOTOPE ANALYSIS:

5.1. Sulphur Isotope:

Five grams of whole rock powder was weighed and dissolved in de-ionised water in a 200 ml beaker. The mixture was then heated slowly to boiling while continuous stiring for 15 min.

A 10% solution of barium chloride was prepared by dissolving 25 gms of $BaCl_2$ in 250 ml of de-ionised water.

The mixture was allowed to cool for sometime and then filtered through a No. 44 Whatman paper. The residue was dried and run on XRD to compare the amount of anhydrite dissolved in the water.

To the filtrate excess of $BaCl_2$ was added till there was no occurrence of precipitate. After allowing the precipitate to settle a few drops of precipitant was further added to confirm that precipitation was complete. The solution was then filtered through a No. 44 Whatman Paper to collect the precipitate. The filtrate obtained was tested for any sulphate by adding $BaCl_2$. The filter paper was left overnight at room temperature to dry and then transferred into a previously weighed silica crucible. The crucible with the filter paper containing the precipitate was placed on the frontal plate of a muffle furnace, previously heated to a temperature of 800°C, and gradually introduced into the furnace until the paper begins to char. The paper should not catch fire! Finally, the crucible was placed in the hottest part of the furnace until incineration was complete. The crucible was then cooled in a dessicator and weighed to get the weight of the precipitate.

If it was suspected that reduction has occured owing to improper ignition, the precipitate was moistened with 1 ml of concentrated sulphuric acid. The crucible was then heated gently over a sand bath to remove the acid and then ignited for about 15 minutes in the hottest part of the furnace.

Reactions:

Calcium sulphate (anhydrite) in the solution is precipitated as barium sulphate due to ion exchange.

$$CaSO_4 + BaCl_2 \text{ -----> } \underset{\text{(ppt)}}{BaSO_4} + CaCl_2 \quad ...1$$

If the filter paper is ignited then reduction of barium sulphate occurs as follows;

$$BaSO_4 + 2C \text{ -----> } BaS + 2CO_2\uparrow \quad ...2$$

When the sulphide is treated with concentrated sulphuric acid then it converts to barium sulphate,

$$2BaS + \underset{\text{(conc.)}}{2H_2SO_4} \text{ -----> } 2BaSO_4 + 2H_2S\uparrow ...3$$

The extracted sulphate was ground with 200 mg of Cu_2O plus 600 mg of SiO_2 before heating to 1120°C (following Coleman & Moore, 1978). The resulting SO_2 was analysed using an 'ISOPEC' 64 spectrometer.

5.2. Carbon and Oxygen Isotopes:

Carbonate minerals were prepared for isotopic analysis by reacting organic-free, powdered rock samples (<44 µm) with 100% phosphoric acid using the method outlined by McCrea (1950). Samples with calcite were left in a hot water bath at 25° C for three hours to collect the CO_2. Dolomite samples were left in a water bath at 25° C for three days.

The resulting CO_2 was analysed on a VG SIRA 10/SIRA II spectrometer.

6. XRF ANALYSIS:

6.1. Method of Analysis:

The sample was prepared using small chips ground in a Tema swing mill with tungsten discs until the powder was less than 200 mesh.

Major Elements were determined using a fused glass bead prepared from 0.5g of rock powder and 2.5g of Spectroflux and ammonium nitrate as oxidant. The method used is essentially that of Norrish & Hutton (1968, Geochemica et Cosmochimica Acta). X-ray analysis was performed on a Philips PW1212 using a Rhodium tube for primary excitation. Calibration was done by reference to a monitor (H12) supplied by K. Norrish, and using 25 internatinal rock standards. The method uses a calculated regression line through apparent fluorescence values (AFV) as described by Harvey et al. (1973, X-ray Spectrometry). Matrix corrections were applied on an iterative basis using an on-line microcomputer and using coefficients for the Rhodium tube, supplied by K.Norrish. The methods and conditions were similar to those described by Norrish & Chappel (1977; in Zussman, J. "Physical methods in determinative mineralogy", Academic Press, p. 201-272). Iron was determined as total Fe_2O_3. FeO was not determined by wet methods due to lack of sample material.

6.2. Accuracy and Precision:

The precision estimates are based on six replicates each on six separate beads and the statistics are derived in the manner described by Harvey et. al. (X-ray Spectrometry, Vol. 2, p. 33-44, 1973). The apparently poor coefficient of variation (c.v.) for P_2O_5 is due to the original sample being deficient in this component.

Accuracy can only be estimated by reference to 'accepted' values based on well-known USGS reference standards. The six standards were run 'blind' in a normal analytical session. The 'accepted' values are those given by Abbey, Geological Survey of Canada (1977), Paper 77-34.

Spot No.	FeO Obsd	FeO %age	MgO Obsd	MgO %age	MnO Obsd	MnO %age	CaO Obsd	CaO %age
47	7.77	14.927	14.252	27.380	1.441	2.7683	28.512	54.775
48	7.656	15.103	13.845	27.312	1.384	2.7302	27.729	54.702
49	11.809	22.291	11.787	22.250	2.222	4.1944	27.081	51.120
50	12.679	22.771	12.477	22.408	2.213	3.9744	28.233	50.705
51	7.668	13.822	17.058	30.748	1.445	2.6047	29.227	52.684
52	7.201	12.443	18.587	32.119	1.364	2.3570	30.639	52.945
53	11.221	21.051	11.976	22.468	2.597	4.8722	27.432	51.465
54	11.895	21.732	11.713	21.399	2.997	5.4755	28.053	51.253
55	8.706	15.997	15.886	29.190	1.855	3.4085	27.897	51.260
56	9.752	17.165	16.221	28.552	2.167	3.8144	28.593	50.330
57	9.664	24.295	12.786	24.295	2.53	4.8073	27.571	52.388
58	9.407	17.537	14.142	26.364	2.181	4.0659	27.832	51.886
59	7.415	14.075	16.44	31.207	1.572	2.9841	27.173	51.582
60	8.944	15.042	18.681	31.419	1.511	2.5413	30.244	50.867
61	11.22	20.906	11.564	21.547	2.695	5.0217	28.111	52.380
62	11.084	20.687	12.027	22.448	2.918	5.4463	27.47	51.272
63	7.568	14.001	16.692	30.881	1.399	2.5882	28.314	52.383
64	7.218	13.169	17.302	31.567	1.197	2.1839	29.015	52.937
65	9.83	17.474	14.869	26.431	1.612	2.8655	29.866	53.090
66	10.166	17.718	15.106	26.328	1.612	2.8095	30.414	53.009
67	10.004	17.724	14.568	25.810	1.934	3.4265	29.859	52.902
68	10.8	18.518	15.115	25.917	2.112	3.6213	30.215	51.808
69	9.753	17.050	14.64	25.594	2.849	4.9807	29.881	52.239
70	10.979	19.089	14.599	25.383	2.6	4.5207	29.259	50.873
71	8.585	15.979	15.838	29.479	1.339	2.4923	27.887	51.372
72	9.146	16.770	15.623	28.647	1.673	3.0677	28.016	51.372
73	8.951	16.372	15.522	28.391	2.087	3.8173	28.034	51.276
74	8.4	15.283	16.204	29.481	1.984	3.6097	28.298	51.485
75	9.438	16.744	16.206	28.752	1.533	2.7533	29.089	51.609
76	9.063	16.077	16.457	29.194	1.622	2.8774	29.15	51.711
77	13.303	25.422	10.431	19.933	2.058	3.9328	26.459	50.563
78	12.516	23.698	10.756	20.366	1.966	3.7225	27.498	52.066
79	12.361	23.467	11.409	21.660	2.114	4.0135	26.71	50.710
80	14.613	26.402	10.733	19.392	2.115	3.8213	27.809	50.244
81	13.376	24.328	11.784	21.433	1.927	3.5049	27.816	50.592
82	12.166	22.790	11.542	21.621	2.228	4.1736	27.37	51.271

Table II. Composition of the carbonate cement in Karroo sandstones. (Obsd: observed values from machine; %age: recalculated percentages).

Spot No.	FeO		MgO		MnO		CaO	
	Obsd	%age	Obsd	%age	Obsd	%age	Obsd	%age
1	9.253	15.716	15.392	26.143	3.74	6.3524	30.49	51.787
2	10.176	17.254	15.652	26.539	2.67	4.5272	30.478	51.678
3	3.346	5.5755	22.126	36.869	2.302	3.8358	32.238	53.719
4	3.853	6.3479	21.472	35.375	2.556	4.2110	32.816	54.065
5	5.864	10.143	17.881	30.930	3.095	5.3536	30.971	53.572
6	7.796	13.173	18.539	31.326	3.153	5.3278	29.692	50.172
7	10.655	16.327	18.482	28.320	3.815	5.8459	32.307	49.505
8	12.69	21.002	14.242	23.571	4.466	7.3915	29.022	48.033
10	3.362	5.7748	21.755	37.368	2.391	4.1069	30.71	52.750
11	2.982	5.4277	19.417	35.342	2.056	3.7422	30.485	55.487
12	5.36	9.3580	17.25	30.116	2.792	4.8745	31.875	55.650
13	2.779	5.0027	19.554	35.200	1.83	3.2943	31.387	56.502
14	9.891	19.540	11.465	22.650	1.872	3.6982	27.39	54.111
15	5.017	9.8370	15.796	30.971	2.778	5.4469	27.41	53.744
16	3.655	6.4627	19.552	34.571	2.212	3.9112	31.136	55.054
17	10.341	18.797	11.993	21.799	3.846	6.9909	28.834	52.412
18	2.622	4.9797	18.57	35.268	1.82	3.4565	29.641	56.294
19	3.212	5.9933	18.058	33.694	2.096	3.9109	30.227	56.401
20	4.531	7.6155	18.803	31.603	2.893	4.8624	33.27	55.918
21	4.165	8.0990	16.53	32.143	1.965	3.8210	28.766	55.936
22	4.393	8.2763	16.465	31.019	1.951	3.6756	30.27	57.028
23	11.282	21.323	12.188	23.035	0.775	1.4647	28.664	54.176
24	9.913	19.353	12.142	23.704	1.935	3.7776	27.232	53.164
25	9.611	18.418	7.44	14.258	8.23	15.772	26.899	51.550
26	4.715	9.2977	15.77	31.097	1.881	3.7092	28.345	55.895
27	6.063	10.774	17.225	30.610	1.903	3.3818	31.08	55.232
28	1.74	3.4157	16.028	31.464	4.89	9.5995	28.282	55.520
27	0.591	1.1346	16.798	32.250	5.781	11.098	28.916	55.515
30	1.222	2.2207	19.934	36.226	4.064	7.3855	29.806	54.167
31	1.197	2.1571	16.907	30.468	6.805	12.263	30.582	55.111
33	11.63	21.152	11.178	20.330	2.678	4.8707	29.495	53.645
34	2.186	4.0790	17.896	33.393	3.989	7.4434	29.52	55.083
35	10.124	19.258	7.184	13.666	8.596	16.352	26.664	50.722
36	10.602	21.078	11.945	23.748	0.863	1.7158	26.887	53.456
37	3.145	6.1363	16.81	32.798	3.147	6.1402	28.15	54.924

APPENDIX 5 - EXAMPLES OF ENVIRONMENTS

LEGEND

STAINING

- ● HIGH
- ◒ MODERATE
- ○ LOW

POROSITY

- <1 DIVISION (0-5%)
- >1, <2 DIVISIONS (5-10%)
- >2, <3 DIVISIONS (10-15%)
- >3, <4 DIVISIONS (15-20%)
- >4 DIVISIONS (20%)

ROCK TYPES

- SHALE
- CLAYSTONE
- SILTSTONE
- SANDSTONE
- LIMESTONE
- DOLOMITE
- ANHYDRITE
- SIDERITE
- COAL
- MARLSTONE - CALC.
- MARLSTONE - DOL.
- SALT & SALT CRYSTALS
- METAMORPHIC ROCK
- IGNEOUS ROCK
- CALCAREOUS
- DOLOMITIC
- SIDERITIC
- SILICEOUS
- CHERT
- P PYRITE

GRAIN SIZE

- 1 DIVISION · VERY FINE
- 2, < 3 DIVISIONS · FINE
- 3, < 4 DIVISIONS · MEDIUM
- 4, < 5 DIVISIONS · COARSE
- 5, < 6 DIVISIONS · VERY COARSE
- 6, < 7 DIVISIONS · GRANULE
- < 7 DIVISIONS · PEBBLES

ROUNDNESS/SORTING

- A ANGULAR
- a SUBANGULAR
- r SUBROUNDED
- R ROUNDED

- P POORLY SORTED
- M MODERATELY SORTED
- W WELL SORTED

RELATIVE ABUNDANCE

		CEMENT	COMPONENTS
A	ABUNDANT	>15%	>30%
C	COMMON	5-15%	10-20%
R	RARE	1-5%	1-5%
T	TRACE	<1%	<1%

SEDIMENTARY STRUCTURES

- LAMINATION
- FLAT BED
- WAVY, CONTORTED LAMINATION
- SLUMPS
- CONVOLUTES
- RIPPLES
- TROUGH CROSS-BED (med,small)
- TABULAR CROSS-BED
- EROSIONAL CONTACT
- BIOTURBATION, CHURNED (intensity)
- HORIZONTAL BURROW
- VERTICAL BURROW
- LOAD CLAST
- MUD CRACK
- STYLOLITE (high angle)
- STYLOLITE (low angle)
- CONCRETION
- BURROWS (carbonates)
- FLASER BEDDING
- CHANNELING (med,small)
- HUMMOCKY CROSS STRAT.
- GB GRADED BED
- X-BEDS
- NODULAR ANHYDRITE

MINERALS or FOSSILS

- FELDSPAR
- MICA
- GLAUCONITE
- OOLITE, PISOLITE
- STROMATOLITES
- INTERCLAST (carbonates)
- PELLET
- PHOSPHATE or SIDERITE PELLETS
- CARBONACEOUS FLAKE
- RIP-UP CLAST
- FISH REMAINS
- ALGAE
- AMPH
- THAMNOPORA
- STROM
- B BIOCLAST
- BRACH
- BRYOZOA
- TENTAC
- CORAL
- PELECEPOD
- PLANT
- ROOTS
- CRINOID
- FORAM
- GASTROPOD
- OSTRACOD
- SPONGE SPICULE
- LENSOIDAL ANHYDRITE

CEMENT

- C · CALCITE
- D · DOLOMITE
- A · ANHYDRITE
- K · KAOLINITE
- SI · SILICA
- P · PYRITE
- S · SIDERITE

POROSITY TYPE

- P · INTERPARTICLE
- X · INTERCRYSTALLINE
- W · INTRAPARTICLE
- V · VUGGY
- M · MOLDIC
- F · FRACTURE

SHAWA GEOCONSULTANTS LTD.

SHAWA GEOCONSULTANTS LTD

PROJECT 522-86

LOCATION 6-15-82-16W5

DATE April 3 1987

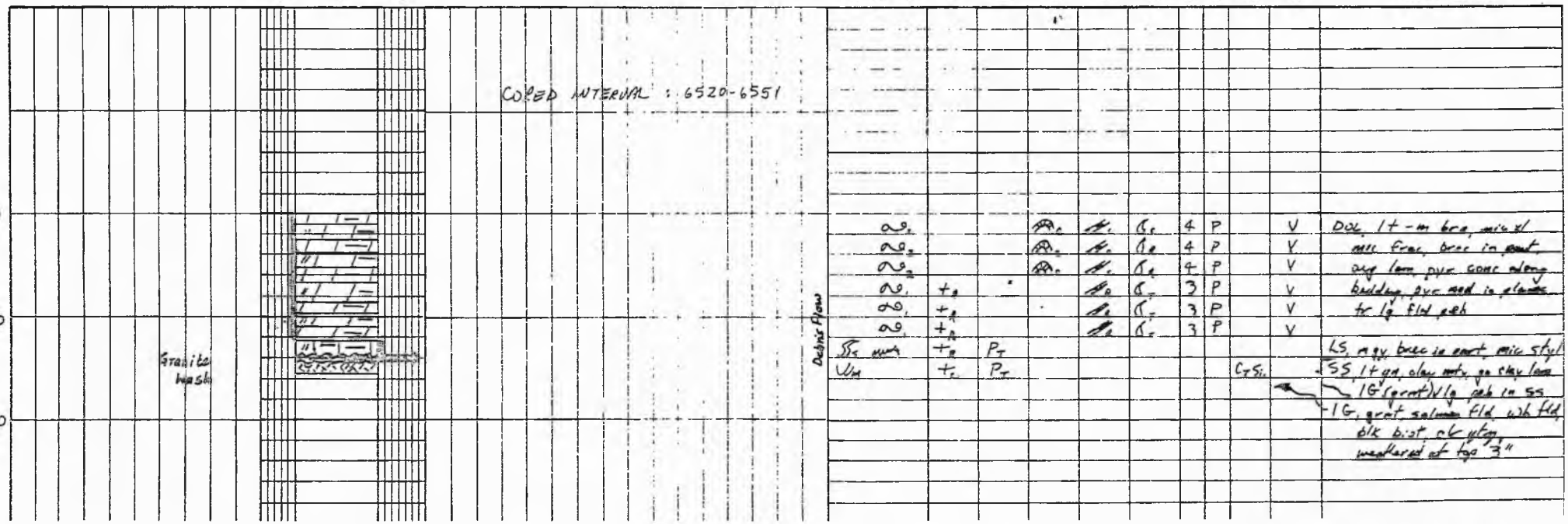

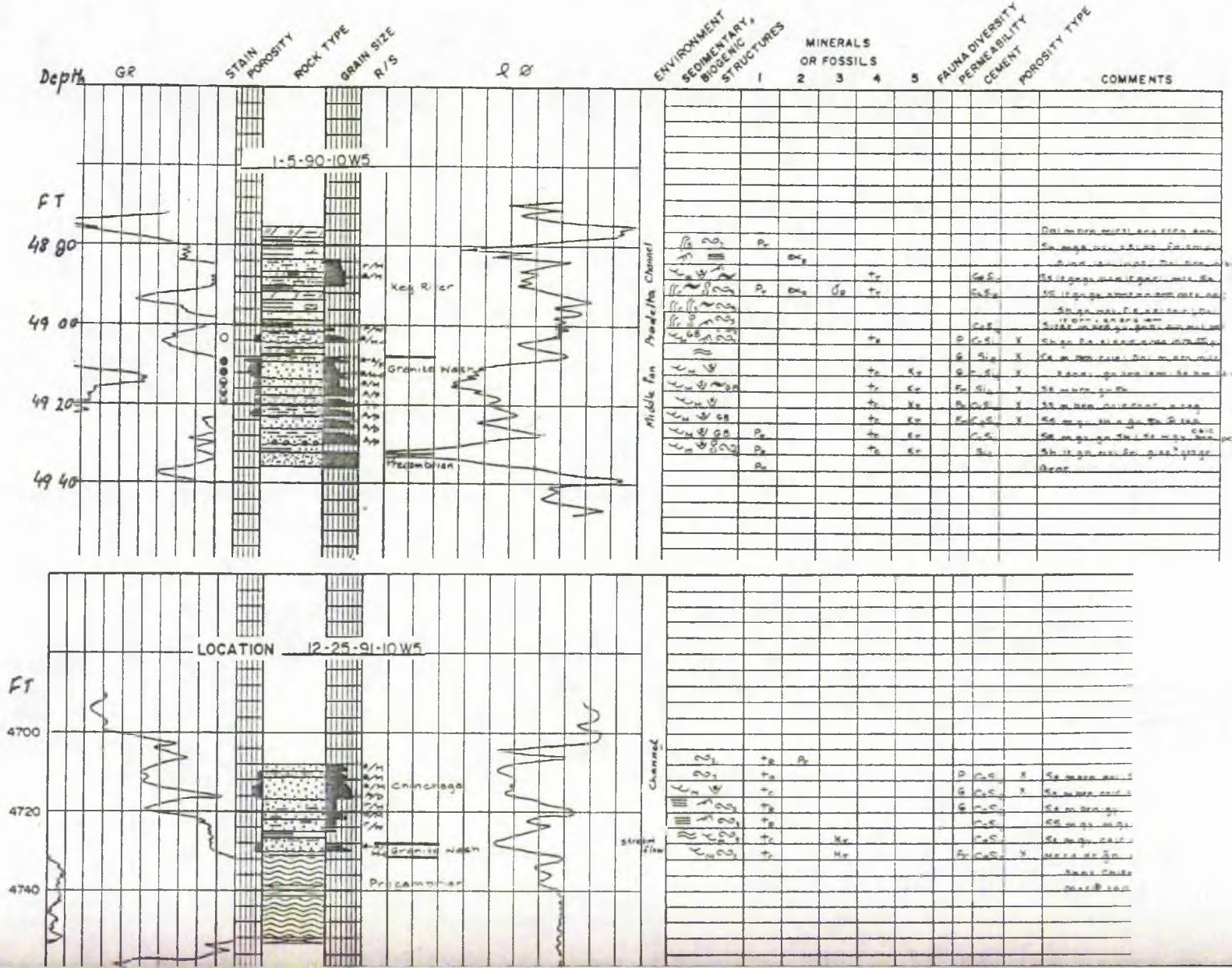
Depth
GR
STAIN
POROSITY
ROCK TYPE
GRAIN SIZE
R/S
ENVIRONMENT
SEDIMENTARY & BIOGENIC STRUCTURES
MINERALS OR FOSSILS
1
2
3
4
5
FAUNA DIVERSITY
PERMEABILITY
CEMENT
POROSITY TYPE
COMMENTS
1-5-90-10W5
FT
4800
4900
4920
4940
Keg River
Granite Wash
Precambrian
Middle fan
Prodelta
Channel
LOCATION 12-25-91-10W5
FT
4700
4720
4740
Chinchaga
Granite wash
Precambrian
Channel
sheet flow

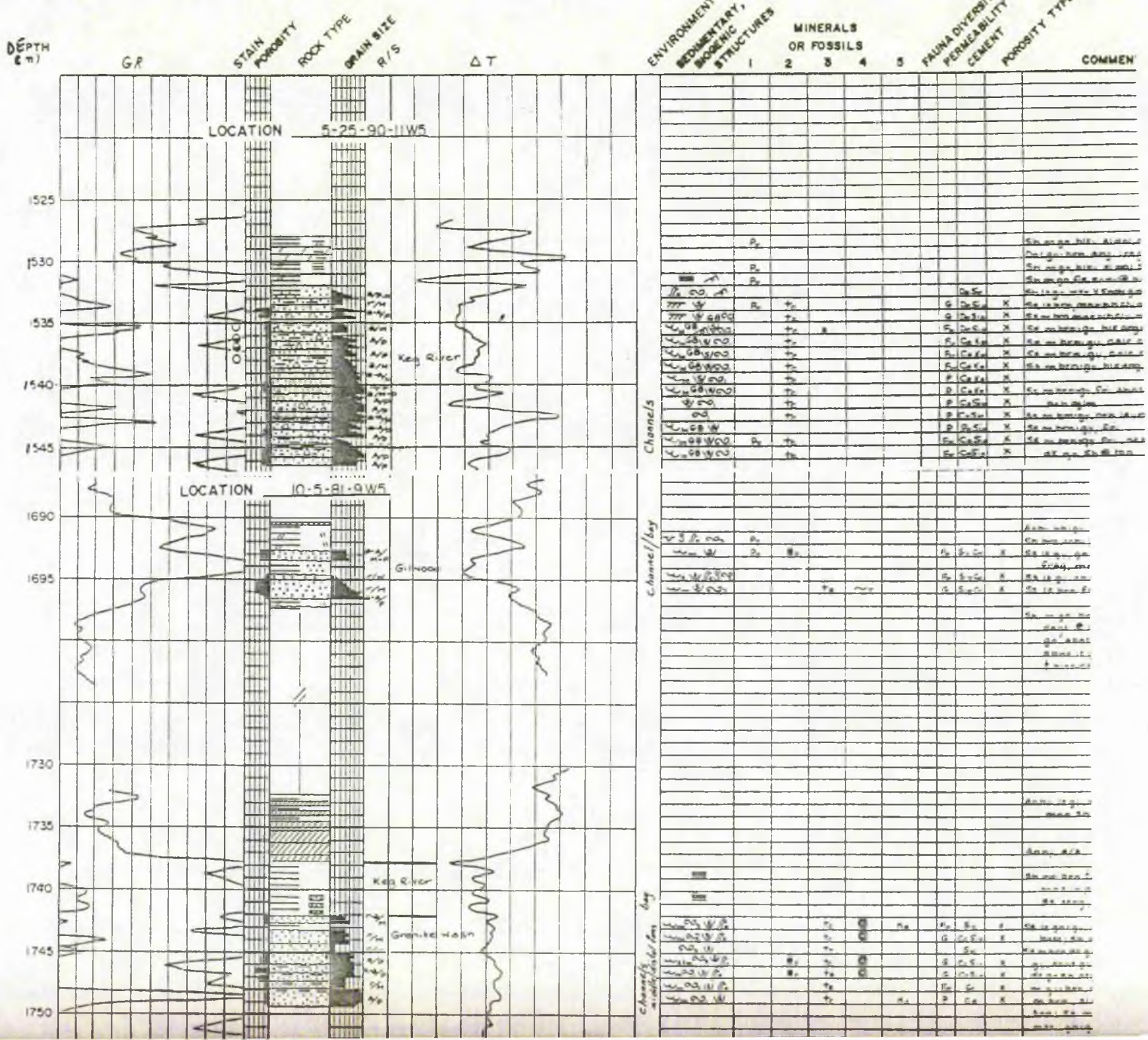
DEPTH (m)
GR
STAIN
POROSITY
ROCK TYPE
GRAIN SIZE
R/S
ΔT
ENVIRONMENT
SEDIMENTARY, BIOGENIC STRUCTURES
MINERALS OR FOSSILS
1
2
3
4
5
FAUNA DIVERSITY
PERMEABILITY
CEMENT
POROSITY TYPE
COMMEN
LOCATION 5-25-90-11W5
LOCATION 10-5-81-9W5
Key River
Gilmood
Key River
Grosmont Halite
1525
1530
1535
1540
1545
1690
1695
1730
1735
1740
1745
1750
Channels
c. channel/bay
bay
c. channels in middle/lower bay

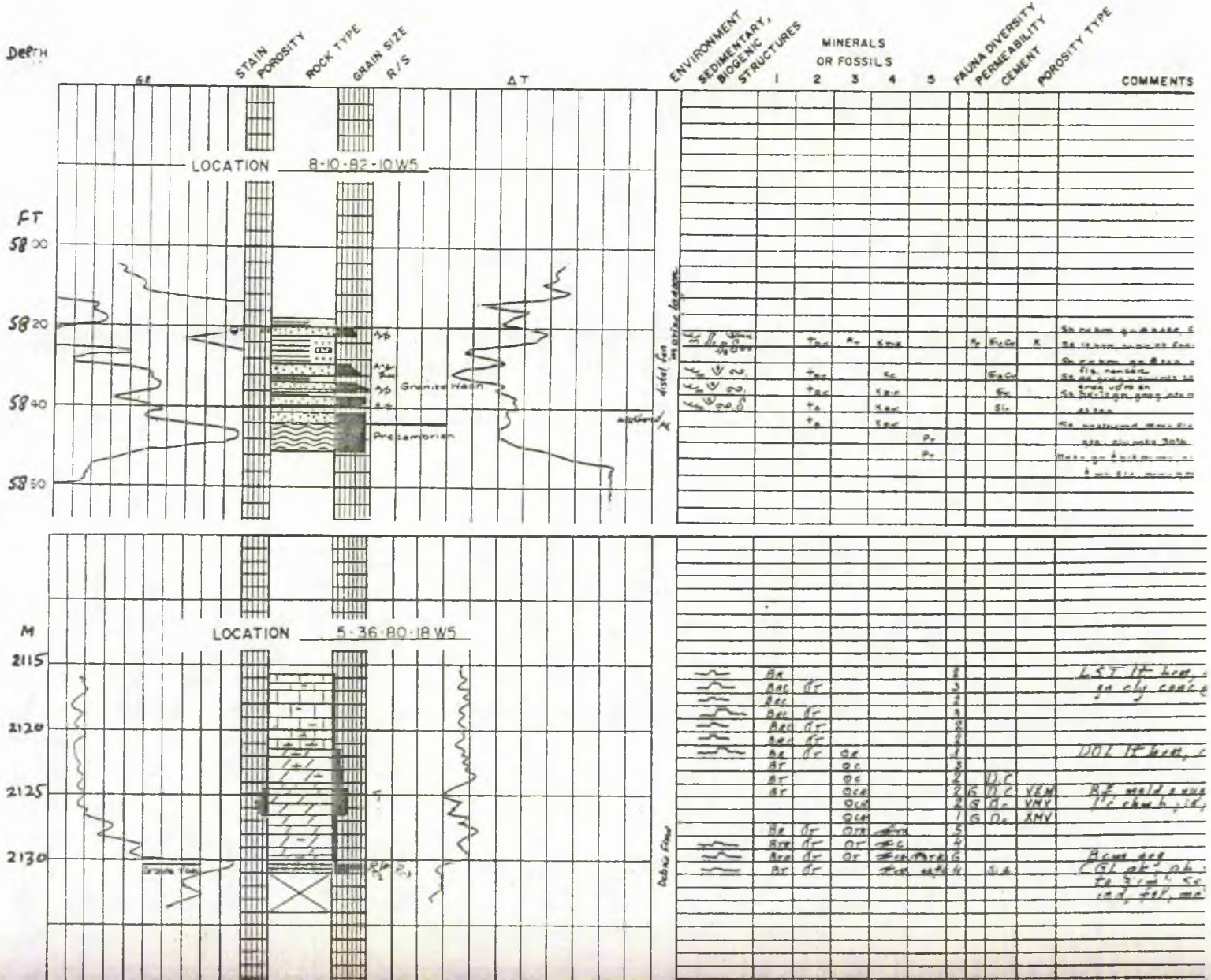
Depth
GR
STAIN
POROSITY
ROCK TYPE
GRAIN SIZE
R/S
ΔT
ENVIRONMENT
SEDIMENTARY, BIOGENIC STRUCTURES
MINERALS OR FOSSILS
1
2
3
4
5
FAUNA DIVERSITY
PERMEABILITY
CEMENT
POROSITY TYPE
COMMENTS
LOCATION 8-10-82-10W5
FT
5800
5820
5840
5850
Granite Wash
Precambrian
distal fan marine bodies
LOCATION 5-36-80-18W5
M
2115
2120
2125
2130
Debris Flow